Analysis of the physiological response of perivascular adipose tissue during cold exposure

Dissertation zur

Erlangung des Doktorgrades (Dr. rer. nat.)

der

Mathematisch-Naturwissenschaftlichen Fakultät

der

Rheinischen Friedrich-Wilhelms-Universität Bonn

vorgelegt von

Benjamin M. Freyter

aus

Slupsk, Polen

Bonn 2022

Angefertigt mit Genehmigung der Mathematisch-Naturwissenschaftlichen Fakultät

der Rheinischen Friedrich-Wilhelms-Universität Bonn

1. Gutachter: Prof Dr. Alexander Pfeifer

2. Gutachter: Prof. Dr. Gerd Bendas

Tag der Promotion: 13.01.2023

Erscheinungsjahr: 2023

Acknowledgements

I would like thank Prof. Alexander Pfeifer for his supervision and providing me the opportunity to shift my carrier by providing funds for my first sequencing project. I also would like to thank my second my second supervisor, Prof. Gerd Bendas and my committee members.

I extend my thanks to the members of the lab for their scientific and practical support, especially Deborah, Davide, Elena, Francesca, Gerburg, Hannah, Jaspal, Laia, Laura and Staffan.

Additionally, I would like to express my gratitude to my grandfather Romuald and my sister Ligia for their enthusiastic support throughout my education.

Table of Contents

Abbreviations

%	**Percent**
ø	Diameter
°C	Degree Celsius
µ	Micro
µl	Micro litre
AA	Aortic aneurysm
AAA	Abdominal aortic aneurysm
ABP	L-ascorbate, biotin, and pantothenate solution
ACE	Angiotensin-Converting Enzyme
ADIPOQ	Adiponectin
ADP	Adenosine diphosphate
ADRB3	Beta-3 adrenergic receptor
Akt	AKT Serine/Threonine Kinase
Akt1	AKT Serine/Threonine Kinase 1
ALPL	Alkaline Phosphatase, Biomineralization Associated
AMP	Adenosine monophosphate
ApoB	Apolipoprotein B
ApoE	Apolipoprotein E
APS	Ammonium persulfate
AS	Aortic stenosis
AT-1	Angiotensin II type 1 receptor
ATF2	Activating Transcription Factor 2
ATGL	Adipose Triglyceride Lipase
ATHS	Atherosclerosis
ATP	Adenosine triphosphate
AV	Aortic valves
AVD	Aortic valve disease
BA	Primary brown adipocytes
BAi	Immortalized brown adipocytes
BAT	Brown adipose tissue
BMP	Bone Morphogenic Protein
Braf	B-Raf Proto-Oncogene, Serine/Threonine Kinase
BSA	Bovine Serum Albumin
$CaCl_2$	Calcium chloride
cAMP	Cyclic adenosine monophosphate
Ccl11	C-C Motif Chemokine Ligand 11
Ccl12	C-C Motif Chemokine Ligand 12
Ccl17	C-C Motif Chemokine Ligand 17
Ccl2	C-C Motif Chemokine Ligand 2
Ccl5	C-C Motif Chemokine Ligand 5
Ccl6	C-C Motif Chemokine Ligand 6
Cd160	CD160 Molecule / Natural Killer Cell Receptor BY55
cDNA	Complementary DNA
Cebpd	CCAAT Enhancer Binding Protein Delta
Cmklr1	Chemerin Chemokine-like Receptor 1
Cst3	Cystatin C
Cx3cl1	C-X3-C Motif Chemokine Ligand 1
Cxcl1	C-X-C Motif Chemokine Ligand 1

Cxcl10	C-X-C Motif Chemokine Ligand 10
Cxcl13	C-X-C Motif Chemokine Ligand 13
Cxcl16	C-X-C Motif Chemokine Ligand 16
Cxcl2	C-X-C Motif Chemokine Ligand 2
Cxcl9	C-X-C Motif Chemokine Ligand 9
DAG	Diglyceride
DAP1	Death Associated Protein 1
DEG	Differentially Expressed Gene/Genes
DEPC	Diethyl pyrocarbonate
DMEM	Dulbecco's modified Eagle's medium
DNA	Deoxyribonucleic acid
EC50	Half maximal effective concentration
ECM	Extracellular matrix
EDTA	Ethylenediaminetetraacetic acid
Egfr	Epidermal Growth Factor Receptor
EGTA	Ethylene glycol-bis(β-aminoethyl ether)-N,N,N',N'-tetraacetic acid
EPAC1	Exchange Protein Directly Activated by cAMP, isoform 1
ERK	Extracellular Signal-Regulated Kinase
EtOH	Ethanol
$FADH_2$	Flavin adenine dinucleotide
FBS	Fetal Bovine Serum
FFA	Free fatty acids
FFA	Free Fatty Acid
FGF21	Fibroblast Growth Factor 21
Fos	FOS Proto-Oncogene, AP-1 Transcription Factor Subunit
G	Earth's gravitational constant
Gas 6	Growth Arrest Specific 6
GATA4	GATA Binding Protein 4
GATA5	GATA Binding Protein 5
Gdf10	Growth Differentiation Factor 10
Gdf-15	Growth Differentiation Factor 10
GDP	Guanosine 5'-diphosphate
Gm-Csf	Colony Stimulating Factor 2
GO	Gene Ontology
GOBP	Gene Ontology domain Biological Process
H2O	Dihydrogen oxide
HCl	Hydrogen chloride
HEPES	4-(2-hydroxyethyl)-1-piperazineethanesulfonic acid
Hgf	Hepatocyte Growth Factor
HGNC	HUGO Gene Annotation Committee
HMGB1	High-Mobility Group Box 1
HPRT	Hypoxanthine Phosphoribosyltransferase 1
HSL	Hormone-Sensitive Lipase
IBMX	3-isobuthyl-1-methylxanthine
IFN-γ	Interferon Gamma
Igf1	Insulin-like Growth Factor 1
Igfbp-2	Insulin Like Growth Factor Binding Protein 2
Igfbp-3	Insulin Like Growth Factor Binding Protein 3
Igfbp-5	Insulin Like Growth Factor Binding Protein 5
Igfbp-6	Insulin Like Growth Factor Binding Protein 6

Igfbp7	Insulin Like Growth Factor Binding Protein 7
IgG	Immunoglobulin G
Il-10	Interleukin 10
Il-11	Interleukin 11
Il12 p40	Interleukin 12 Beta
Il-13	Interleukin 13
Il-1ra	Interleukin 1 Receptor Antagonist
IL-1α	Interleukin 1 Alpha
IL-1β	Interleukin 1 Beta
Il-28A/B	Interleukin 28
IL-4	Interleukin 4
IL-6	Interleukin 6
IL-8	Interleukin 8
IRF4	Interferon Regulatory Factor 4
IRS2	Insulin Receptor Substrate 2
JAK	Janus Kinase
JNK	c-Jun Amino-Terminal Kinase
K2HPO4	Monopotassium phosphate
KCl	Potassium chloride
LDL	Low-Density Lipoprotein
LdlR	Low Density Lipoprotein Receptor
LDLR	LDL Receptor
Lep	Leptin
LIX	Cytokine LIX/C-X-C Motif Chemokine 5
MAG	Monoacylglycerol
Mapk	Mitogen Activated Kinase
Mapk8	Mitogen-Activated Protein Kinase 8
Mcp-1	Macrophage Chemoattractant Protein 1
$MgCl_2$	Magnesium chloride
Mgl	Monoglyceride Lipase
Mmp-12	Matrix Metalloproteinase 12
Mmp-2	Matrix Metalloproteinase 2
Mmp-3	Matrix Metalloproteinase 2
Mmp-9	Matrix Metalloproteinase 9
Mpo	Myeloperoxidase
mTOR	Mechanistic Target of Rapamycin Kinase
Na_2HPO_4	Disodium phosphate
NaCl	Sodium Chloride
NADH	Reduced nicotinamide adenine dinucleotide
$NADH_2$	Mitochondrially Encoded NADH:Ubiquinone Oxidoreductase Core Subunit 2
NaN_3	Sodium azide
NE	Noradrenaline
Nf1	Neurofibromin 1
NOTCH1	Notch Receptor 1
NP-40	Nonyl phenoxypolyethoxylethanol
NRG4	Neuregulin 4
O_2	Oxygen
oxLDL	Oxidized Low Density Lipoprotein
p38 or MAPK14	Mitogen-Activated Protein Kinase 14
PBS	Phosphate-buffered saline

PCR	Polymerase chain reaction
Pdgfra	Platelet Derived Growth Factor Receptor Alpha
PI3K	Phosphatidylinositol-4,5-Biphospate 3-Kinase
PKA	Protein Kinase A
Pon1	Paraoxonase 1
Ppara	Peroxisome Proliferator Activated Receptor Alpha
PPARγ	Peroxisome Proliferator Activated Receptor Gamma
Pref-1	Delta Like Non-Canonical Notch Ligand 1
PVA	Primary perivascular adipocytes
PVAi	Immortalized perivascular adipocytes
PVAT	Perivascular adipose tissue
R	R programming language
RAGE	Receptor for Advanced Glycation End Products
Rbp4	Retinol Binding Protein 4
Retn	Resistin
RIPA	Radioimmunoprecipitation assay buffer
RMT	Arginine Methyltransferase
RNA	Ribonucleic acid
RT-qPCR	Real-time polymerase chain reaction
RUNX2	Runt-Related Transcription Factor 2
SDS	Sodium dodecyl sulphate
Sfrp1	Secreted Frizzled Related Protein 1
SM22-Alpha or TAGLN	Transgelin
SMAD	SMAD Family Member
Smad3	SMAD Family Member 3
SMC	Smooth muscle cells
Sp1	Sp1 Transcription Factor
STAT	Signal Transducer and Activator of Transcription
Stat3	Signal Transducer and Activator of Transcription 3
SV40	Simian vacuolating virus 40
T3	Triiodothyronine
TAA	Thoracic aortic aneurysm
TAG	Triglyceride
TBS	Tris-buffered saline buffer
TEMED	N, N, N’, N’-Tetramethylethylenediamine
Tgfbp1	Transforming Growth Factor Binding Factor 1
TGF-β	Transforming Growth Factor β
Thbd	Thromboregulin
Timp3	TIMP Metallopeptidase Inhibitor 3
Timp4	TIMP Metallopeptidase Inhibitor 4
Tnf or TNF-α	Tumor Necrosis Factor
TRP	Transient Receptor Potential Channel
UCP1	Thermogenin
v/v	Volume to volume
VCAM-1	Vascular cell adhesion protein 1
VEC	Valvular endothelial cells
VEGF	Vascular Growth Factor
VIC	Valvular interstitial cells
VLDL	Very Low-Density Lipoprotein

WAT	White adipose tissue
WATg	Gonadal adipose tissue
WATi	Inguinal white adipose tissue
Wisp-1 or Ccn4	Cellular Communication Network Factor 4
WNT	Wnt Family Member
wt/v	Weight to volume

Table of Figures

1 INTRODUCTION

1.1 AORTIC DISEASES

Aorta is the largest and most central artery, which is directly connected to the heart and converts blood pulses from the left ventricle of the heart to a steadier flow in peripheral vessels: The aortic walls distend like a balloon during systole, recoil during diastole and, thus, maintain a constant flow of oxygenated blood through the whole body. During average lifespan, the aorta transports nearly 0.2 billion litres of blood. Therefore, the aorta is exposed to constant biomechanical stress from the aortic valve/aortic root to the aortic bifurcation, which causes structural weakening of the walls and changes depending on age, gender, lifestyle, and genetic factors[1–7]. These changes might even result in aortic diseases, for example aortic stenosis (AS), aortic aneurysms (AA), dissections or atherosclerosis (ATHS)[8]. AS, AA, and ATHS show similar pathogenetic mechanisms, and are the most common diseases of aorta in developed countries[9,10]. Their incidence and treatment costs are on the rise[11,12].

1.1.1 Aortic valve and diseases

The aortic valves are located in the aortic root connecting the left ventricle with the ascending aorta. Healthy aortic valves consist of three semilunar, thin leaflets that open and close about 100 000 times a day and around 3.7 billion times during an average human lifespan[13]. Aortic valves ensure one-directional blood flow from the left ventricle to aorta during left ventricle contraction (systole). In this process, the free edges of the leaflets join at an angle of 120°, preventing the backflow of blood. The thin lines of attachment of the three leaflets transfer the pressure of blood in aorta to the aortic wall. During systole, the blood pressure is higher in the left ventricle than in aorta, rapidly pushing the flattened leaflets open. Healthy aortic valves open in 20-30 ms and close after the pressure gradient reversal, letting back less than 5% of pumped blood into the aorta[13].

The leaflets are composed of two types of cells: valvular endothelial (VECs) and valvular interstitial cells (VICs). VECs cover all valves of the heart and are a non-thrombogenic barrier between blood and the valves. VECs align perpendicularly to the direction of shear stress[13]. VICs are embedded among collagen inside of the leaflets. VICs phenotypically are an intermediate form of fibroblasts and smooth muscle cells (SMC) with extracellular matrix synthetizing and contractile properties [13–17]. Healthy human aortic valves are thinner than a millimetre and are composed of VECs and three extracellular matrix layers: a collagen-rich fibrosa on the side of aortic lumen, the glycosaminoglycan-rich spongiosa in the middle, and elastin-rich ventricularis on the side of the left ventricle[18,19].

The function of the aortic valves may be impaired by diseases. The most known inborn valve disease is the incidence of bicuspid aortic valve instead of a tricuspid aortic valve. 1-2% of the population possesses congenitally abnormal bicuspid valve, which is a hereditable disease. Bicuspid aortic valve was described to be associated with mutations in Notch Receptor 1 (*NOTCH1*), GATA Binding Protein 4 (*GATA4*), and GATA Binding Protein 5 (*GATA5*) genes[20–24]. Bicuspid aortic valve changes the blood flow and the biomechanical stress compared to tricuspid aortic valve and is an innate risk factor for the development of AVD[25]. Over half of patients submitted for valve replacement were born with bicuspid aortic valve and almost every person born with this defect will require surgical treatment[25].

Aortic stenosis (AS) describes the narrowing of the left ventricle's exit, while aortic valve sclerosis (AVS) describes the thickening and calcification of aortic valve[26]. Together, they are a condition known as aortic valve disease (AVD)[27]. AVS is a leading factor contributing to development of AS[26].

Research conducted at the end of the 1990s indicated that 2% of study cohort of 5201 people over 65 from four communities in United States suffered from AS, while about 30% of the population showed AVS in the United States[28,29]. Another study reported prevalence of any grade AVS in Mediterranean population of over 45% of the population at an age over 65 and more than 73% at an age over 85[30]. The proportion of moderate to severe cases are also increasing with age: from 5.5% in ages 65-75 and 26.2% in ages over 85. Developed aortic stenosis was detected in 0.5% of population in a Mediterranean area in ages 65-75, and 7.1% in ages above 85[30]. The symptoms of AS are angina pectoris, fainting, and heart failure[31]. The symptoms vary greatly depending on the stage of the disease and begin subtly[26].

Studies showed that Apolipoproteins B and E accumulate in the morphologically early lesions of degenerative AVS[32]. Oxidized Low-Density Lipoprotein (oxLDL) was detected in deeper parts of fibrosa, and close to calcium deposits[33]. The authors of the article suggested that this accumulation may play a role in the disease progression[33]. Very Low-Density Lipoproteins (VLDL) are produced and released by the liver and are step-wisely degraded to Low-Density Lipoproteins (LDL) by lipoprotein lipases expressed by the endothelial cells covering the luminal surface of the blood vessels. Both VLDL and LDL transport cholesterol and other hydrophobic lipids through the bloodstream to the different organs, mainly to the liver. The shell of LDL contains apolipoprotein B-100, which is expressed mostly in the liver as a product of *APOB* gene[34]. LDL interacts with LDL receptors (LDLR) in peripheral tissues and induces its receptor-mediated endocytosis[35,36]. Following, the cholesterol carried by the LDL is hydrolysed in lysosomes and degraded to products that may easily cross the lysosomal membrane. The cholesteryl ester is hydrolysed by acid cholesteryl esterase and the excess of free cholesterol is transported to the endoplasmic reticulum, where it is stored and further hydrolysed over time[37]. The increase of LDL in the blood is a risk factor for calcific aortic valve disease and aortic aneurysm[28,38–40]. An increased level of plasma LDL causes endothelial dysfunction, enhanced adherence of monocytes to arterial endothelial cells, and increased LDL uptake into the intima, the vascular layer of endothelial cells[41]. SMCs and macrophages overloaded with cholesterol may transform into foam cells, which in turn is a contributing factor in development of AA, AS, and ATHS[42–45]. However, cholesterol accumulation in the macrophages cannot be increased by native LDL due to LDL receptor downregulation upon cholesterol build-up in cells and is instead caused by the uptake of modified forms of LDL like oxLDL, possibly involving scavenger receptor Class A-I/II and CD36[37,46–49]. OxLDL activates antiapoptotic signalling and induces proinflammatory responses[50,51]. The oxLDL attract macrophages, which may transform into foam cells[52]. This mechanism was described in ATHS resulting in necrosis of atherosclerotic plaque[53]. OxLDL has also been found to promote osteoblastic differentiation of VICs *in vitro* through RAGE and MAPK pathways[54]. More on that topic is described in the chapter 1.1.3 of this thesis.

In aortic valves, valvular interstitial cells, endothelial cells, mesenchymal, and circulating progenitors may transdifferentiate into myofibroblasts or osteoblasts, initiating calcification[55,56,57]. The trigger for the transdifferentiation may be cytokines, growth factors, hypertension, altered mechanical stress or reactive oxygen species[58,59,60,61,62,63,64]. Immunohistochemistry of human aortic valvular lesions suggest that Angiotensin-Converting Enzyme (ACE) may contribute to the development of aortic stenosis by increasing the expression of Macrophage Chemoattractant Protein-1 (MCP-1), which stimulates monocytes accumulation within lesions. Other possible mechanisms include reduction of cholesterol efflux and increasing modified LDL uptake in macrophages[65–67]. O'Brien *et al.* described colocalization of ACE and ApoB in aortic lesions and associations of ACE with LDL in blood plasma[68]. The authors also detected expression of AT-1 receptor in subset of cells in stenotic valves and suggested investigation of ACE inhibitors for future experimental treatments of AVD[68]. An ACE inhibitor, Ramipril, showed beneficial effects in treatment of other cardiovascular diseases, including ATHS, which may have been only partially attributed to minor blood pressure reduction[69]. ACE inhibition may lead to endothelial function restoration and decrease of SMC proliferation[69,70].

Currently there is no therapy available to treat AVD besides aortic valve replacement[13,71]. Available aortic valve replacements consist of mechanical, bioprosthetic, tissue-engineered and polymeric valves. Mechanical valves are durable, lasting approximately 25 years, but require constant anti-coagulation treatment. Additionally, mechanical valves may generate noise heard by the patient. Bioprosthetic valves are replacements of patient's own aortic valve with pulmonary valve, a transplant from a deceased donor or a porcine or a bovine xenograft. The bioprosthetic valves have superior haemodynamics compared to mechanical valves, but they are prone to calcification, and have shorter lifespan. Bioprosthetic valves originating from donors or animals are fixed for example in glutaraldehyde or decellularized. Tissue-engineered valves may use decellularized natural or biocompatible polymeric, biodegradable scaffolds, which can serve to grow tissue-like valve replacement using patient's own cells or be coated with bioactive substance. Tissue-engineered valves promise quality of a native valve, but they still require additional research. The final replacement possibility are polymeric valves, which should combine the durability of mechanical valves with advantages of bioprosthetic valves. Polymeric valves are not popular due to poor historical properties and the possibility to stiffen at higher heart rates[13].

1.1.2 Aortic aneurysms

The aortic wall consists of the three layers *tunica intima*, *tunica media* and *tunica adventitia,* which are separated by the membrana elastica interna and membrana elastica externa, respectively. *Tunica intima* is one layer of endothelial cells, which are in direct contact with the blood. *Tunica media* is a thick composite of elastic fibres sheets, collagen fibres, and SMCs. *Tunica adventitia* is the outermost part of a blood vessel, and consists mostly of collagen fibres, a network of smaller blood vessels supporting the artery, and lymphatic vessels. *Tunica adventitia* also anchors the vessels to nearby organs and tissues[7,72]. Diameter of healthy aorta is between 16-18 cm in women and 19-21 cm in men[73].

One of many abnormalities of aorta is AA, which is a permanently localized fragment of aorta with at least an increased diameter of 50% [74]. The prevalence of aortic aneurysm was estimated at 1.3-8.9% in men and 1.0-2.2% in women[75,76]. It is the tenth cause of death in men over an age of 55, responsible for over 1% of total deaths in this age group in 1986 in the United States[77]. Abdominal aortic aneurysms (AAA) occur close to the aortic bifurcation, while thoracic aortic aneurysms (TAA) affect the ascending and the descending aorta located in the thorax. Both kinds of AA seem to have distinct pathogenesis[78]. AAA are partly linked to atherosclerosis and mostly associated with men at an age over 65 and smoking [76,79].

In contrast, the rarely occurrent TAA is mostly inherited and associated with a degeneration of elastic fibres and loss of vascular SMC in the media, the middle layer of aorta[80]. Besides other factors, this effect may be connected to higher occurrence of extracellular matrix metalloproteinases 2 (MMP-2), and 9 (MMP-9) in degenerated areas of TAA[81]. Several pro-inflammatory cytokines Il-1β, IL-6, IL-8, IFN-γ, MCP-1, TNF-α were detected in AAA[82,83,84]. IL-1β, IL-6, and TNF-α were also found to be elevated in the serum of AAA patients[85]. Another study described that IL-4 induces severe AAA formation and increased levels of MMP-9, and MMP-12, while blockade or inborn absence of IL-4 reduced its formation[86].

AAs are progressing slowly and mostly asymptomatic. Pre-ruptured aneurysms may manifest with neglectable symptoms like back pain, chest and abdominal pain, cough, or hoarseness[87,88,89]. Current management of aortic aneurysms include control of blood pressure, aortic wall reinforcement by placement of an expandable stent graft inside of the aorta or replacement of the diseased aorta fragment with a synthetic graft[90,91,92]. A prospective study reported elevated cardiovascular, and all-cause mortality that increases with the size of aneurysms[93]. The cardiovascular mortality risk possibly rises by 4-6% per mm increase over an aortic diameter over 23 cm[73]. Aortic aneurysms may result in ruptures, which have 80% mortality of the patients that reach the hospital and 50% of the patients who undergo a surgery[2].

1.1.3 MAPK, RAGE pathways, and senescence in aortic diseases

MAPK pathways regulate multiple cellular processes, like mitosis, gene expression, survival, apoptosis, and differentiation[94]. Five groups of MAPKs have been found in mammals: extracellular signal-regulated kinases (ERKs) 1 (HUGO Gene Nomenclature Committee (HGNC) symbol MAPK3) and 2 (HGNC symbol MAPK1), c-Jun amino-terminal kinases (JNKs) 1, 2 and 3, p38 (HGNC gene symbol MAPK14) isoforms α, β, and γ, ERKs 3 (HGNC gene symbol MAPK6) and 4 (HGNC symbol MAPK4), and EKR5 (HGNC symbol MAPK7)[94]. ERK1 and ERK2 are activated by growth factors and phorbol esters. The JNK and p38 kinases react to stress stimuli like osmotic shock, temperature changes or cytokine stimulation[94].

The mitogen-activated protein kinase (MAPK) pathways play major roles for osteoblast differentiation and mineralization[95,96]. ERK positively regulates calcification and osteoblastic differentiation in osteoblastic precursor cells and in vascular SMC[97–10097]. In VICs, which show a similar phenotype compared to SMCs, inhibition of MAPK/ERK pathway reduced calcification in vitro[97]. In endothelial cells, native and modified LDL induces p38 upregulating cell adhesion molecules

E-selectin, vascular cell adhesion protein 1 (VCAM-1), and monocyte-chemoattractant protein 1 (MCP-1). VCAM-1, MCP-1 and p38 have pro-inflammatory effects and recruit immune cells from the blood stream to the vascular wall. p38 might also be involved in endothelial cells migration associated with angiogenesis, which is observed in ATHS and AVD[101]. In vascular SMCs, OxLDL induces p38 activity and increases cytotoxicity, calcification and apoptosis[101]. p38 is also activated by bone morphogenic protein 2 (BMP2) as part of the non-Smad-signalling, which induces the BMP-dependent SMAD signalling and the expression of runt-related transcription factor 2 (RUNX2), an osteogenic transcription factor necessary for osteoblast differentiation[101].

SMAD proteins are also transcription factors, which transduce the signals of transforming growth factor β (TGF-β) family from the TGF-β receptors located in the plasma membrane into the nucleus. Thus, the TGF-β/BMP-Smad-signalling regulates proliferation, transdifferentiation (e.g., EC to mesenchymal cells) and senescence[102].

Senescence describes a permanent cellular cell cycle arrest and can be activated as a stress response creating a defence mechanism against tumorigenesis and proliferation of damaged cells. Senescence is one cause of aging and age-related disorders. Senescent cells may negatively impact neighbouring cells by secreting senescence-associated cytokines[103]. Senescent SMCs were found in aortas of patients with bicuspid aortic valves and within calcified aortic valves. Senescent SMCs in aortas were enriched with surface localized MMP1 and secreted substantially higher amounts of MMP1 and TGFβ1[104,105].

The activation of p38 by oxLDL may be mediated by the receptor for advanced glycation end products (RAGE). RAGE has multiple ligands and is expressed among others in ECs, SMCs and mononuclear cells[54]. RAGE was demonstrated to have a pro-osteogenic role and its downregulation by pioglitazone attenuated progression of aortic valve calcification[106].

1.2 Adipose tissue types

Fat tissue is classically categorized as white adipose tissue (WAT) or brown adipose tissue (BAT), mainly because of their clear localizations and different functions[107,108]. WAT is the primary tissue storing energy in form of large, unilocular lipid droplets, whereas BAT dissipates energy as heat, and contain multiple, small lipid droplets, and plenty of mitochondria[109,110]. Adipose tissue is organized in multiple depots in mammalian bodies. Main human WATs are subcutaneous (WATi) – abdominal and gluteofemoral -, and visceral adipose tissues surrounding organs in omental, mesenteric, retroperitoneal, and gonadal (WATg) regions. WAT can be also found intramuscularly[111].

Murine WAT are dominantly located in subcutaneous and visceral parts of the body[112]. Posteriorly, murine WAT is in inguinal region (WATi), and anteriorly in cranial, and axillo-thoracic regions. Visceral depots are in mesenteric, perirenal, retroperitoneal, and perigonadal (WATg) regions[113].

In mice, the biggest and most active depot of BAT is in interscapular region[112,114], while in human infants BAT exists in interscapular, supraclavicular, and neck areas. In human adults, active BAT depots are present in supraclavicular, and neck areas[115,116].

Adipose tissue is mainly composed of adipocytes – brown in BAT, and white or beige in WAT[117]. In addition to WAT and BAT, islets of beige adipocytes appear in mammalian WAT after cold exposure via β-adrenergic receptor stimulation or other stimuli, e.g., cytokines, natriuretic peptides, or lactate produced during excercise[118].

Uncoupling Protein 1 (UCP1), or Thermogenin is a mitochondrial protein that enables adaptive thermogenic process, resulting in heat generation, by uncoupling respiratory chain[119]. UCP1 levels are high in brown adipocytes (BA), even when they are unstimulated, while beige adipocytes are easily detected in WAT only after exposure to cold or other adipose tissue inducers[118]. After three weeks of exposure to 10°C, beige adipocytes isolated from WATi had similar UCP1 content and thermogenic ability as brown adipocytes[120]. Induction of beige adipocytes is depot specific and takes place mostly in murine WATi, whereas WATg is resistant to beige-ing[118].

Recently, the fat tissue located around blood vessels, the perivascular adipose tissue (PVAT) started to gain recognition beyond only mechanical support. Thoracic PVAT has been found to show BAT-like characteristics, including the expression of UCP1[121–123]. Of note, most of PVAT was found to originate from Transgelin (Sm22, SM22-Alpha or TAGLN) positive cells, differently from BAT and WAT. This was demonstrated by mice lacking PVAT due to the knockout of Peroxisome Proliferator Activated Receptor Gamma (PPARγ) in SM22α-expressing cells leaving both BAT and WAT unaffected [123,124]. SM22-Alpha is expressed in smooth-muscle-cells, SMC-like cells and pre-adipocytes [125,126].

1.3 Adipose tissue activation by cold exposure

Cold exposure stimulates transient receptor potential (TRP) channels in peripheral sensory neurons, which is detected by the sympathetic nervous system, which in turn releases the catecholamine noradrenaline (NE) from nerve fibres in, among others, adipose tissue[110,127,128]. NE activates βadrenoceptors on the surface of adipocytes, which results in G_s-protein dependent activation of adenylate cyclase, increasing levels of a secondary messenger cAMP, and stimulation of protein kinase A (PKA)[128]. There are three β-adrenoreceptors: 1,2, and 3, whereas the β_3 adrenoceptor is expressed predominantly in adipocytes[129]. PKA phosphorylates, among others, mitogen-activated protein kinase 14 (P38 or MAPK14) and hormone-sensitive lipase (HSL). P38 phosphorylates multiple transcription factors, such as activating transcription factor 2 (ATF2) and interferon regulatory factor 4 (IRF4), which bind to enhancers or promoter regions of UCP1, activating its transcription[124]. HSL is described in chapter 1.4 and UCP1 in 1.5. β_3 stimulation modulates secretion of various cytokines, for example was linked to the release of Interleukin 6 (IL6) via P38 in white adipocytes[128], acute secretion of adiponectin (ADIPOQ) via exchange protein directly activated by cAMP, isoform 1 (EPAC1)[130], and inhibition of leptin secretion[131].

1.4 Lipid storage and lipolysis

Lipids are biomolecules soluble in non-polar solvents[132]. Their biological functions are structural support, signalling and energy storage[133,134]. The energy density of lipids is twice as high as of carbohydrates[135]. Probably all mammalian cell types may store some lipids intercellularly, whereas adipocytes are highly adapted for lipid storage[107].

In non-mammals and in some cases of mammalian metabolic diseases, lipids are not only produced but also be stored in the liver[136,137]. Lipids are stored in form of droplets, encapsulated in proteins protecting the droplets' core from degradation[137]. White and abdominal perivascular adipocytes store lipids as a single, big droplet[138,139], whereas brown and thoracic perivascular adipocytes contain many small, multilocular droplets[108,140].

Lipolysis is a catabolic process, in which triglycerides (TAG) are hydrolysed into glycerol and free fatty acids (FFA)[141]. Lipolysis mostly takes place in adipocytes and - to smaller extent - in all other cell types[141]. Three enzymes are participating in the hydrolysis of TAG in cellular lipid droplets. First, adipose triglyceride lipase (ATGL), selectively hydrolyses TAG into diacylglycerols (DAG) and FFA. Second, HSL, can hydrolyse, among others, TAG, DAG, and monoacylglycerol (MAG), and finally monoglyceride lipase (MGL), which catalyses hydrolysis of MAG into glycerol and FFA. ATGL and HSL are activated by β_3-adrenoreceptor stimulation[141].

1.5 Cellular respiration, oxidative phosphorylation and non-shivering thermogenesis

Cellular respiration is a series of reactions and results in generating ATP in mitochondria by transferring electrons from NADH or $FADH_2$ to O_2 along the respiratory chain [142].

At the beginning, acetyl-CoA, which was produced by utilizing carbohydrates, lipids and proteins, is oxidized in the citric acid cycle (Krebs cycle) to generate electrons with high transfer potential, which is converted into phosphoryl transfer potential. The electric potential energy is utilized by a cascade of proton pumps, which are part of the respiratory chain complexes: NADH-Q oxidoreductase, Q-cytochrome c oxidoreductase, and cytochrome c oxidase. Electrons are carried from NADH-Q oxidoreductase by utilizing NADH to Q-cytochrome c oxidase by the reduced form of coenzyme Q. The same coenzyme also may carry electrons from FADH2, that is generated from the oxidation of succinate to Q-cytochrome c oxidase[142].

The process leads to pumping the protons out of the mitochondrial matrix, generating a pH gradient and a transmembrane potential. The last step – the production of ATP – is conducted by ATP synthase, that channels protons back into the mitochondrial matrix employing energy of proton gradient and phosphorylates AMP and ADP to ATP[142]. This last step is called oxidative phosphorylation. This phenomenon is the coupling of fuel oxidation and the phosphorylation of ADP by a proton gradient across the inner mitochondrial membrane[142].

Oxidative phosphorylation is uncoupled by activated UCP1, a transmembrane protein, which can introduce proton leak from mitochondrial intermembrane space into the mitochondrial matrix. UCP1 "wastes" that potential of electrical energy, which would be used for ADP phosphorylation, and induces heat generation instead. The resulting process of heat generation by UCP1 is the non-shivering thermogenesis, which enables to maintain body temperature and survival on low protein diet[143]. The UCP1-mediated non-shivering thermogenesis takes place in mitochondria-rich adipose tissues as BAT, PVAT and beige adipocytes in WAT[144].

UCP1 is activated by external stimuli[145]. Among others, NE release by the nervous system upon cold exposure activates lipolysis via β_3 adrenoreceptor, increasing intracellular cAMP. Lipolysis leads to increased availability of FFA, which are energy source for UCP1[146]. Additionally, long-chain fatty acids increase the conductance of inner mitochondrial membrane by activating UCP1[147].

Non-shivering thermogenesis may have a crucial role for prevention or severity reduction of aortic diseases. BAT activation by β_3-adrenoreceptor agonism or cold exposure showed to reduce plasma lipids and may protect from development of ATHS. However, BAT is unable to clear cholesterol remnants from the blood stream, which is cleared by the liver[148].

1.6 ENDOCRINE AND PARACRINE ROLES OF ADIPOSE TISSUES IN AORTIC DISEASES

1.6.1 Cytokines

Adipose tissue has endocrine and paracrine functions and secretes adipokines, extracellular vesicles, lipids, peptide hormones, and miRNAs[112]. Adipokines are cytokines derived from adipocytes[149]. Cytokines are small, secreted proteins mediating communication between cells[150]. The secretion profile differs among fat depots and conditions[117]. Adipokines play a role in multiple processes, like regulation of glucose and lipid metabolism, immune responses, blood pressure, or arterial elasticity[151,152].

A well-studied example of adipokines is leptin, which is secreted by adipocytes and in smaller amounts by stomach, intestine, mammary epithelium, placenta, or skeletal muscles[153]. Leptin was discovered because of a spontaneous mutation in a mouse colony in Jacksons Laboratory in 1950, causing obesity in mice[154]. 41 years later, researchers discovered the location of the responsible gene in mice and correctly predicted the approximate location of the human gene[155].

Leptin was firstly described as a food intake and energy expenditure regulator[156]. It binds the long form of the leptin receptor and activates downstream cascades as IRS2, MAPK, ERK, PI3K/Akt, mTOR, and JAK/STAT[157]. Leptin deficiency or defective leptin/leptin receptor signalling protects against ATHS in mice[158].

Another circulating adipokine is ADIPOQ[151], which can reach plasma concentrations in the size of µg/mL levels[159]. ADIPOQ deficiency induces insulin resistance, vascular injury, and ATHS[152,160,161]. Leptin and ADIPOQ are adipose tissue-derived, endocrine hormones, affecting target tissues[162].

Adipose tissue's secretion of various cytokines, e.g., Neuregulin (NRG4), Fibroblast growth factor (FGF21), Vascular endothelial growth factor (VEGF), Bone Morphogenic Proteins (BMPs) or Interleukin 6 (IL6) can be increased by cold exposure [163].

1.6.2 Extracellular vesicles

Extracellular vesicles (EVs) are small, secreted lipid envelopes with diameter ranging from 40 to 500 nm[164,165]. These vesicles are released by most of cell types and may transport lipids, nucleic acids, and proteins to acceptor cells[165], and are found in every body fluid[166,167]. Adipose tissue is one of the largest secreting organs[168], and proteins transported by EVs are a substantial part of adipose tissue secretome[169]. EVs released to extracellular space may can reach recipient cells, dock at their plasma membrane, and be internalized by the target cells, delivering their cargo[167]. EVs may be specifically recognized by the target cells thanks to specific interactions between proteins on the surface of EVs and receptors present on the recipient cells[167]. Once internalized, the content of EVs may trigger specific responses in the acceptor cells[167]. The transmitted signal may vary in disease states, disrupting homeostasis, and even promote cancer metastasis[165,170].

1.6.3 Adipose tissue-derived miRNAs in aortic diseases

miRNAs are about 18-24 nucleotide long non-coding RNAs, playing a role in the post-transcriptional regulation[171,172]. Canonical miRNAs are transcribed by RNA polymerase II in longer form of hairpin loop-containing pri-miRNAs, which are capped and polyadenylated in humans[173,174], and can encode clusters of different miRNA genes[175]. pri-miRNAs hairpins are enzymatically cleaved by Drosha to pre-miRNAs[176]. pre-miRNAs are then exported from the nucleus to the cytoplasm by the GTP-dependent Exportin-5[177], where they are processed by Dicer resulting in miRNA duplexes[178]. miRNAs regulate the transcription of mRNAs by repression or degradation within the cell of origin or in an endocrine manner in distant cells via extracellular vesicles transport and endocytosis[172]. The importance of adipose tissue-derived miRNAs was shown in a study published by Thomou et al., which investigated adipose tissue-dependent knock-out of Dicer[179]. The affected mice were unable to produce mature miRNAs, which lead to 3-fold increase of FGF21 in the circulation, as well in muscles, liver, and pancreas. The Dicer-KO also resulted in the reduction of WAT mass, whitening of BAT, and insulin resistance[179]. Over half of miRNAs detected in circulating exosomes were downregulated more than 4-fold emphasizing, that adipose tissue is a major source of circulating miRNAs. Application of extracellular vesicles from Dicer KO mice supplemented with miRNA-99b partially re-induced FGF21 suppression[179]. FGF21 has been identified as an anti-inflammatory cytokine with cardioprotective effects[180] and is increased in patients with AVD[181]. FGF21 is also increased after myocardial infarction, oxidative stress, or diabetes and seems to be part of protective mechanism after these malfunctions/diseases occur[181].

There are more than 1200 murine and almost two thousand human miRNAs in miRbase database[182]. It is predicted that most of human genes are targeted by at least one miRNA[183–185]. The number of validated miRNA targets varies greatly, and some miRNAs target over two hundred mRNAs[186]. Adipose tissue-derived miRNAs have the potential to regulate an enormous variety of processes.

2 AIM AND OBJECTIVES

The aim my thesis was to characterise PVAT and elaborate functional roles of PVAT on transcriptional level in comparison to BAT, and additionally WATi, and WATg, to investigate putative, cold-responsive factors that may affect the development or progression of AA and AVD.

Therefore, I established the isolation, differentiation, and immortalization of PVA and characterized them in vitro. To analyse the impact of PVAT in vivo, I exposed wild type mice to cold to activate adipose tissues, and breed the strains *Pparg* floxed with *Sm22-α* Cre mice to prevent the formation of PVAT.

3 MATERIALS AND METHODS

3.1 COMMON SOLUTIONS

Materials

- Disodium phosphate, Na_2HPO4 (Carl Roth, Cat. No. P030)
- Monopotassium phosphate, K_2HPO_4 (Carl Roth, Cat. No. 3904)
- Potassium chloride, KCl (Carl Roth, Cat. No. 6781)
- Sodium chloride, NaCl (Carl Roth, Cat. No. 3953)

PBS solution

Component	Concentration
KH_2PO_4	1.4 mM
KCl	2.7 mM
NaCl	137 mM
Na_2HPO4	8 mM
Solvent for the solution was H2O, and pH was set to 7.4. Product was autoclaved	

3.2 ISOLATION OF MURINE TISSUES

Equipment

- Decapitation scissors
- Fine straight dissecting forceps x2
- Small tweezers

- Scissors
- Mini scissors
- Curved scissors
- Fine straight dissecting forceps
- Stereo microscope (Leica® Microsystems)

Materials

- DMEM Glutamax™-I (4.5 g Glucose/l medium) (-) Pyruvate (Gibco™, Cat. No. 61965)
- 70% Ethanol
- innuSOLV RNA Reagent (Analytik Jena AG Cat. No. 845-SB-2090100)

Prior to tissues isolation, 8-10 weeks old male C57BL6J mice were sacrificed by decapitation. Tissues were isolated in following order: Aortic Valves, Perivascular Adipose Tissue, Inguinal White Adipose Tissue, Gonadal Adipose Tissue, and finally Brown Adipose Tissue. Before dissection, fur was wetted with 70% EtOH. All frozen tissues were stored in -80°C until further processing.

3.2.1 Aortic Valves

Decapitated mice were immobilized by pinning the limbs into a Styrofoam layer, thorax was opened, ribs, lungs, esophagus, inferior vena cava were removed, and the blood was cleaned with tissue paper. Next, the aorta was cut out of the spine, starting from diaphragm up to above the heart (to isolate the heart with aorta) using curved scissors, gently pulling the aorta using non-pointy tweezers. The aorta with heart and thymus were put in ice-cold PBS, shaken to remove blood, and transferred to a transparent dish with a gel, allowing to immobilize the organs. The aorta was pinned down from the side of the thymus, which was the orientation point for further isolation. Next, the aorta was cut above the pin in ascending part and put into PBS on ice, queuing for PVAT isolation. Thymus and all leftover tissues blocking the view were removed. The heart was cut in half horizontally, and the bottom part was disposed. Mini curved dissecting scissors were used to cut the upper part up to few mm into the aorta. The walls of the heart were spread and pinned down to the gel, exposing aortic valves' leaflets, which were then carefully removed using mini tweezers, and placed directly into ice-cold innuSOLV RNA reagent. The aortic valves from 6 mice were pooled in one reaction tube, grinded and processed further as described in3.3.4.2.

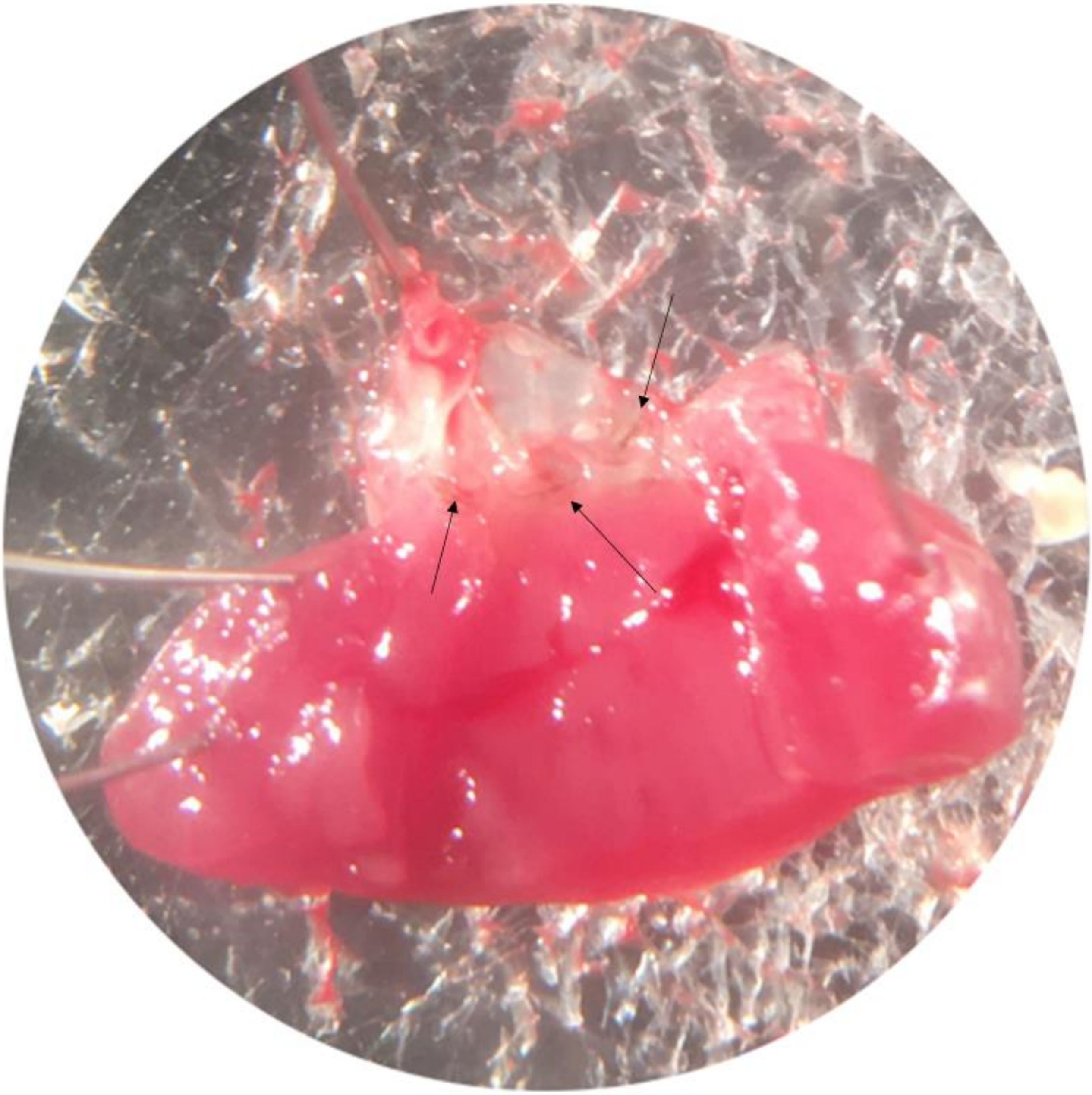

Figure 1. Open heart exposing aortic leaflets

3.2.2 Thoracic Perivascular Adipose Tissue

The thoracic aorta, left after aortic valves isolation, was pinned on both sides into the gel on a dish, gently stretching it to ease the PVAT-pulling process. Next, PVAT was cautiously pulled out from aorta using two pointy tweezers, removing blood vessels. The PVAT pieces were processed as following for different purposes:

For Perivascular Preadipocytes isolation:

PVAT pieces were placed into DMEM on ice, pooling tissues from 4 mice per biological replicate and further processed as described in 3.3.2.1.

For Sequencing:

PVAT pieces were placed directly into ice-cold innuSOLV RNA reagent in a reaction tube, and flash-frozen after tissues collection from 6 mice. Tissues were further processed as described in 3.3.4.2 and 3.3.4.

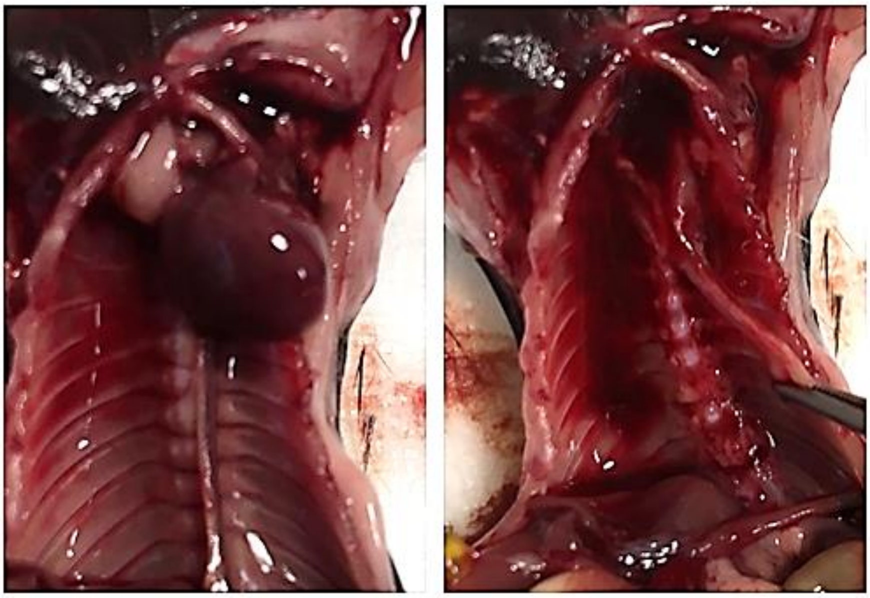

Figure 2. Exposed aorta in murine thorax (left), and partially cut-out aorta from the surface of the spine (right), heart removed.

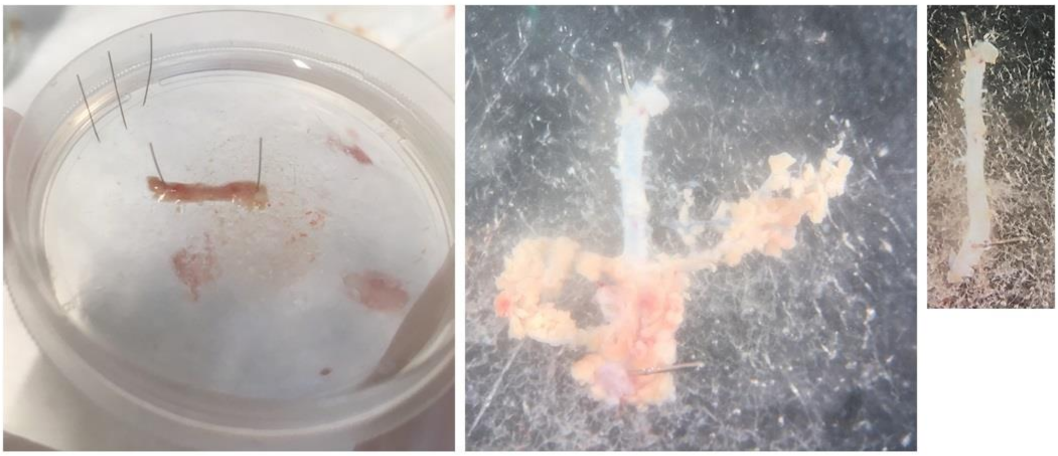

Figure 3. PVAT dissection process.

From left to right: Aorta with PVAT pinned to gel on isolation dish, middle of PVAT pulling process, and aorta after PVAT isolation.

3.2.3 Inguinal White Adipose Tissues

Skin was cut vertically on the side of the mouse, from the leg up to the level of the ribs and pulled out to expose subcutaneous adipose tissue. The skin was stretched and pinned down to the Styrofoam, the fat pads dissected, and their lymph nodes removed. Fat pads were put in a reaction tube and flash-frozen.

3.2.4 Gonadal White Adipose Tissues

The abdominal skin of the mouse was cut vertically from the bottom up to the diaphragm, and the testicles were pulled out from the cavity. The attached gonadal white adipose tissue was dissected and cleared from possible remains of other tissues. The gonadal fat pads were put in a reaction tube and flash-frozen.

3.2.5 Brown Adipose Tissue

Mouse was turned over and skin was removed from the interscapular area. Brown fat pads were lifted with fine straight dissecting forceps and cut out of the mouse. Brown Adipose Tissue core was dissected from the fat pads, placed in a reaction tube and flash frozen.

3.3 CELL CULTURE

Equipment

- Countess Automated Cell Counter (Invitrogen, Cat. No. C10227)
- Stereo microscope (Leica® Microsystems)
- Laminar air flow, Herasafe™ (Heraeus)
- Incubator, HERAcell® 150 (Heraeus)
- Water bath

Materials

- 3,3’,5-Triiodo-L-thyronine sodium salt (Sigma-Aldrich, Cat. No. T6397)
- 10 cm^2 TC dishes, Standard (Sarstedt, Cat. No. 83.3902)
- 30 µm and 100 µm nylon meshes (Millipore, Cat. No. NY3002500, NY1H00010)
- 6-well plates (Sarstedt, Cat. No. 83.3920)
- 12-well plates (Sarstedt, Cat. No. 83.3921)
- 8-Bromoguanosine- 3', 5'- cyclic monophosphate (8-Br-cGMP) (Biolog Life Science Institute GmbH & Co. KG)

- Collagenase, Type II (Worthington, Cat. No. CLS2)
- Cryogenic vials (Sarstedt, Cat. No. 72.379.992)
- D(+)-Biotin (Novabiochem, Cat. No. 58-85-5)
- Dexamethasone (Sigma Aldrich, Cat. No. D4902)
- DMEM Glutamax™-I (4.5 g Glucose/l medium) (-) Pyruvate (Gibco™, Cat. No. 61965)
- Fetal Bovine Serum, FBS (Biochrom AG, Cat. No. S0015)
- Insulin solution human (Sigma-Aldrich, Cat. No, I9278)
- Pantothenate (Sigma Aldrich, Cat. No. P5155)
- Penicillin/streptomycin (P/S; Merck, Cat. No. A2213)
- Rosiglitazone (Sigma-Aldrich, Cat. No. R2408)
- Sodium ascorbate (Carl Roth, Cat. No. 3149)
- Syringes 5 ml (BD Discardit II, Cat. No. 309050)
- Trypan Blue Stain (Gibco, Cat. No. 15250)
- PBS

3.3.1 Media compositions

Growth medium (GM)

Component	Volume
DMEM Glutamax™-I (4.5 g Glucose/l medium) (-) Pyruvate	445 ml (55 ml removed)
Pen-Strep (1%)	5 ml
FBS heat-inactivated	50 ml

Differentiation medium (DM)

Component	Volume/Concentration
DMEM Glutamax™-I (4.5 g Glucose/l medium) (-) Pyruvate	445 ml (55 ml removed)
Pen-Strep (1%)	5 ml
FBS heat-inactivated	50 ml
Insulin	1 nM
T3	20 nM

Induction medium (IM)

Component	Volume/Concentration
Differentiation medium	50 ml (37°C)
Dexamethasone	1 µM
IBMX	0.5 mM
Rosiglitazone (only for PVA)	2 µM for PVA or none for BA

3.3.2 Isolation of murine preadipocytes

Media

Isolation Buffer

Component	Concentration/ Volume
$CaCl_2$	1.3 mM
Glucose	5 mM
HEPES	100 mM
KCl	5 mM
NaCl	123 mM
H_2O	Desired volume
Set pH to 7.4 and filter sterile	

BA Digestion Buffer

Component	Concentration
BSA	1.5% wt/v
Collagenase II	2 mg/ml
Dissolve BSA and Collagenase II in Isolation Buffer and filter sterile	

PVA Digestion Buffer

Component	For 50 ml
DMEM Glutamax-I (4.5 g Glucose/l medium) (-) Pyruvate	50 ml
Collagenase II	0.2 g
BSA	0.32 g

BA Isolation Medium

Component	Concentration/Volume
DMEM Glutamax-I (4.5 g Glucose/l medium) (-) Pyruvate	50 ml
FBS heat-inactivated	10% v/v
HEPES	10 nM
Insulin	4 nM
Pen-Strep	1% v/v
Sodium Ascorbate	25 µg/ml
T3	4 nM

Growth medium

Component	Concentration/Volume
DMEM Glutamax-I (4.5 g Glucose/l medium) (-) Pyruvate	445 ml
FBS heat-inactivated	50 ml
Pen-Strep	1% v/v

3.3.2.1 Perivascular Preadipocytes Isolation Procedure

PVAT pieces from four 8-weeks old male C57BL6/J mice were prepared according to PVAT isolation protocol (3.2.2) and were transferred from ice-cold DMEM to gentleMACS™ falcon with 1.25 ml of PVA Digestion Buffer for PVA. Following, collected PVAT pieces were dissociated using gentleMACS™ for ca 42 min. Next, growth media was added to reach 5 ml of volume in the falcon. The digested tissue mixture was centrifuged in the same falcon for 10 min under centrifugal force of 300 G, the supernatant with floating fraction was carefully removed and the supernatant was resuspended in 2 ml of growth media, following uptake into a syringe and filtrated through 100 µl nylon mesh attached to the tip of the syringe. Finally, the cellular suspension was evenly distributed over the surface of a well in 6-well plate and left in an incubator at 37°C and 5% CO_2 for one day for further handling. Where possible, the procedures were performed under laminar flow in sterile environment.

3.3.2.2 Brown Preadipocytes Isolation Procedure

BAT pieces from three newborn mice were chopped thoroughly using surgical scissors in 2.5 ml of BA Digestion Buffer, followed by 30 min digestion in water bath at 37°C, forcefully shaking every 5 min. Subsequently, the suspensions were filtered through 100 µm nylon mesh and incubated on ice for 30 min. Middle phase was taken using syringes and needles and was filtered through 30 nm nylon mesh. Afterwards, the suspensions were centrifuged by 700 G at 23°C. Next, the supernatant was carefully aspirated, and the pellet resuspended and seeded onto a well in 6-well plate and left in an incubator at 37°C and 5% CO_2 for one day for further handling. Where possible, the procedures were performed under laminar flow in sterile environment.

3.3.2.3 Immortalization of Preadipocytes

The preadipocytes were infected with a lentivirus containing the SV40 large T antigen dispersed in 800 µl of Growth Medium. The medium containing the lentivirus was gently distributed over the surface of previously, gently aspirated surface of a well, containing attached preadipocytes. The well plate with the lentivirus was distinctly labelled and put into an incubator and left overnight at 37°C in atmosphere of 5% CO_2. Next morning, 2.4 ml of Growth Medium was added to the well. Media was changed every second day and the cells were split at 90% of confluency.

3.3.2.4 Expansion of Immortalized Preadipocytes

Cellular expansion was performed by 90% confluency starting from immortalized primary preadipocytes. Cells were washed with autoclaved PBS at room temperature, following by incubation with 0.05% Trypsin-EDTA (1X) until complete cellular detachment. Afterwards, Trypsin was deactivated by adding Growth Medium. The first passaging was performed transferring the cellular suspension from one well in 6-well plate into two 10 cm petri dishes. Higher passaging was performed with similar expansion ratio of 1 to 10, up to passage no 4.

3.3.2.5 Cryopreservation of Preadipocytes

Cells were washed with autoclaved PBS at 23°C at 90% confluency and incubated with 0.05% Trypsin-EDTA (1X) until complete cellular detachment. Afterwards, the suspension was mixed with Growth Medium in ratio of 1:1 and centrifuged at 600 G for 5 min. Next the supernatant was carefully aspirated, and pellet was resuspended and diluted to achieve 1 million cells per mL in case of PVA and 3 million cells per mL in case of BA, using filtered Trypan Blue Stain and Countess Automatic Cell Counter, taking into consideration that 10% of the volume will be filled with DMSO. Subsequently the suspensions were transferred into pre-labelled cryogenic vials and placed in pre-cooled cell freezing container - Mr. Frosty™ - with appropriate volume of isopropanol. Finally, Mr. Frosty™ with filled cryogenic vials was placed for at least 90 min in -80°C. For longer periods, the cryo-conserved cellular suspensions were stored in -150°C.

3.3.3 Cellular differentiation protocols

Cells in all three protocols were seeded on well plates with density of alive 1 million cells per full plate or 22800 cells/cm^2. Cells were incubated through the entire process at 37°C and 5% CO_2 atmosphere. All medium changes and treatments were performed sterile under laminar flow. Medium volume for BA was 1 and 2 ml for wells in 12- and 6-well plates, respectively. In case of PVA, the volume was double the volume, starting from first differentiation medium after induction.

BAi differentiation protocol

Figure 4. BAi differentiation protocol

BAi were seeded on day -4 using growth medium and left in the incubator for two days. On day -2 the cellular layer on the surface of the wells should be almost confluent. The medium was aspirated, and the wells were filled with differentiation medium +/- treatment. Two days later the medium was changed to induction medium for BA +/- treatment. Following, every two days the medium was changed to differentiation medium +/- treatment until harvest on day 7.

PVAi 2 ID differentiation protocol

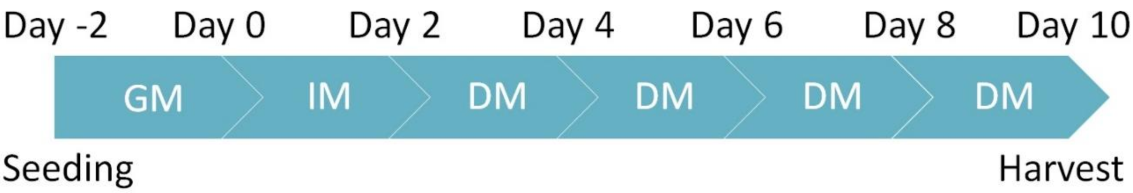

Figure 5. PVAi differentiation protocol with 2 days of induction

In two induction days protocol for PVAi (PVAi 2 ID), the cells were seeded on day -2 in growth medium and left in the incubator for two days. Next, the cells were induced with induction medium for PVAi (with Rosiglitazone) +/- treatment. Medium was aspirated after two days, and the wells were filled with differentiation medium +/- treatment. The media was changed to differentiation medium every second day, four times in total until day 10.

PVAi 4 ID differentiation protocol

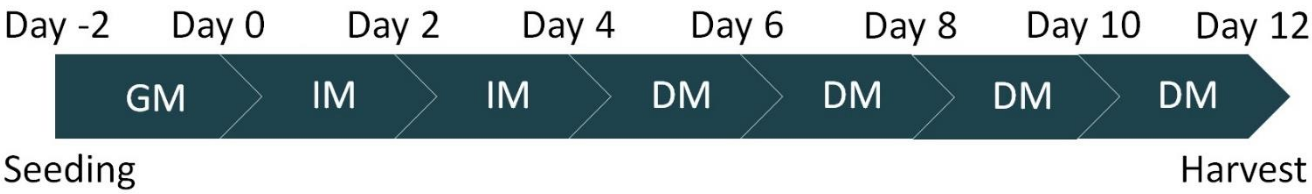

Figure 6. PVAi differentiation protocol with 4 days of induction

In four induction days protocol for PVAi (PVAi 4 ID), the cells were seeded on day -2 in growth medium and left in the incubator for two days. Next, the cells were induced with induction medium for PVAi (with Rosiglitazone) +/- treatment, which was replaced after 2 days. Medium was aspirated after additional 2 days and the wells were filled with differentiation medium +/- treatment. The medium was changed to differentiation medium every second day until day 12.

RNA Analysis

Equipment

- 7900HT Fast Real-Time PCR System with 384-Well Block Module (Applied Biosystems™, Cat. No. 4329001)
- Eppendorf® Centrifugal Vacuum Concentrator 5301 (Eppendorf®)
- QuantStudio™ 5 Real-Time PCR System, 384-Well (Applied Biosystems™, Cat. No. A28140)
- NanoDrop™ 2000 spectrophotometer (Thermo Scientific™)
- Bullet Blender® 24 (Biostep®)

Materials

- Chloroform (Carl Roth, Cat. No. Y015)
- DEPC (Carl Roth, Cat. No. K028.1)
- Ethanol (Carl Roth, Cat. No. 9065)
- innuSOLV RNA Reagent (Analytik Jena AG Cat. No. 845-SB-2090100)
- Isopropanol (Carl Roth, Cat. No. AE73)
- ProtoScript® II First Strand cDNA Synthesis Kit (New England Biolabs® Inc., Cat. No. E6560L)
- Sodium acetate, 3M (Sigma-Aldrich, Cat. No. 71196)
- Sterile 1.5 ml reaction tube (Sarstedt Cat. No. 72.690.001)
- SYBR™ Green PCR Master Mix (Applied Biosystems™, Cat. No. 4364346)

3.3.4 RNA isolation

3.3.4.1 Isolation from cells

Medium was aspirated from wells and cells were washed with sterile PBS, which was aspirated again, leaving no visible liquid in on the surface with adherent cells. Well plates were frozen in -80°C immediately after previous process.

At the day of isolation, the well plates were kept on ice and 1 ml of refrigerated innuSOLV RNA reagent was added to each well with sample cells. The cells were scrapped with 1 ml pipette tips and transferred into 1.5 ml sterile reaction tubes. Subsequently, 200 µl of chloroform was added to each sample and each tube was manually shacked for 15 seconds. The tubes were left for 5 min on ice, followed by centrifugation for 10 min at 13000 rpm and 4°C. The upper phase was transferred to new 1.5 ml sterile reaction tubes and mixed with 500 µl of isopropanol. Next the RNA was pelleted by centrifugation at 13000 rpm and 4°C for 10 min. Afterwards the supernatant was removed, and RNA was washed three times with 75% EtOH with 5 min centrifugation at 13000 rpm and 4°C. At the end, the RNA was dried using the Eppendorf® Centrifugal Vacuum Concentrator 5301 for 30 min. The samples were then dissolved in 20 µl DEPC H_2O and RNA was quantified using NanoDrop™ spectrophotometer.

3.3.4.2 Isolation from tissues for sequencing

Aortic valve samples were pooled from 6 mice during tissue isolation by inserting the valves directly to ice-cold innuSOLV RNA reagent. The valves were grinded in the reaction tube. Afterwards, innuSOLV RNA was added to reach 1 ml and RNA was isolated following the same protocol as for cells, described above.

Adipose tissues from 6 mice were pooled by cutting similar mass of tissues from frozen tissues, around 2 mg from BAT, 5 mg from WATi and WATg. PVATs were pooled during isolation, putting tissues directly in innuSOLV RNA reagent and keeping it on ice, until 6 mice were pooled. Afterwards the reaction tube with pooled PVAT samples and innuSOLV RNA reagent were flash-frozen. All tissue samples for sequencing were kept in -80°C before and after RNA isolation.

In order to dissociate tissues from pooled BAT, WATi and WATg, Bullet Blender® 24 with zirconium oxide and iron oxide beads was used, following the protocol below:

Firstly, a mixture of diameter zirconium oxide (⌀ 1 mm) and iron oxide (⌀ 0.5 mm) beads were mixed in proportion 1:2, up to a total volume similar to volume of the tissue to be grinded. Pooled tissue samples in reaction tubes were put on ice. Next, 500 µl of ice-cold innuSOLV RNA reagent and grinding bead mix were added to each pooled tissue sample. Afterwards the tissues were dissociated in the Bullet Blender® 24, inserting max 6 reaction tubes with tissues and running it for 4 min on level 9. The tubes were checked and if not dissociated properly, were returned to the Bullet Blender® and run for another 1-2 min. The reaction tubes with samples were put back directly into ice and rest of the samples were dissociated in the same way. Subsequently, 500 µl of innuSOLV RNA reagent was added into each reaction tube and briefly vortexed. Following, 200 µl of chloroform was added into each reaction tube and vortexed for 5 seconds, checking, if the liquids look homogenous. Every sample was left at room temperature for 5 min and centrifuged for 10 min at 4°C and 13000 rpm. The upper, clear phases were transferred into new, sterile reaction tubes. Next steps were as described by the RNA isolation from cells above.

3.3.5 RNA purification

For RNA preparation for sequencing, the samples had to meet rough quality criteria. To improve NanoDrop™ purity ratios, samples were purified following protocol described below.

15-20 µl of RNA samples were mixed with 60 µl of ice-cold 100% ethanol, 2 µl of 3M sodium acetate, vortexed thoroughly, and left overnight at -80°C. Day after, the samples were centrifuged at 13000 rpm and 4°C for 30 min. RNA pellet was washed twice with ice-cold 80% ethanol, centrifuging as before for 10 min each time. Following, the ethanol was thoroughly removed and dried using Eppendorf® Centrifugal Vacuum Concentrator 5301 for 30 min. Finally, the pellet was mixed with 15-20 µl DEPC H_2O and measured again in NanoDrop™.

3.3.6 Complementary DNA synthesis

RNA concentration was measured using NanoDrop™, following manufacturer's instructions. 1000 ng of RNA was transcribed using First Strand cDNA Synthesis Kit with a three-steps program: 25°C for 300 seconds, 42°C for 3600 seconds and 80°C for 300 seconds.

3.3.7 Real-time PCR (RT-qPCR)

mRNA expression levels were measured using HT7900 Fast Real-Time PCR System or QuantStudio™ 5 Real-Time PCR System, both using 384-Well Blocks. The reactions were performed using SYBR™ Green PCR Master Mixes from Applied Biosystems™, following manufacturer's guidelines, with following program:

Step	Temperature (°C)	Time (s)	Cycles
1	95	600	
2	95	15	
3	60	60	Back to step 2, 40 times
4	95	1	
5	65	15	
6	95	∞	

Quantification of mRNA levels was performed based on the crossing point values of the amplification curves using the second derivative maximum method. As internal control and for normalization Hypoxanthine-guanine phosphoribosyltransferase (*Hprt*) was used.

3.3.7.1 Primers

Primer sequences used in Real-time PCR target gene amplification are listed in the table below:

Primer	Primer sequence (5'->3')
***Adrb3* forward**	CCT TCA ACC CGG TCA TCT AC
***Adrb3* reverse**	GAA GAT GGG GAT CAA GCA AGC
***Hprt* forward**	ACA TTG TGG CCC TCT GTG TGC TCA
***Hprt* reverse**	CTG GCA ACA TCA ACA GGA CTC CTC GT
***Pparg* forward**	TCC GTA GAA GCC GTG CAA GAG ATC A
***Pparg* reverse**	CAG CAG GTT GTC TTG GAT GTC CTC G
***Ucp1* forward**	GGT GAA CCC GAC AAC TTC CGA AGT G
***Ucp1* reverse**	GGG TCG TCC CTT TCC AAA GTG TTG A
***Fabp4* forward**	GCG TGG AAT TCG ATG AAA TCA
***Fabp4* reverse**	CCC GCC ATC TAG GGT TAT GA

3.4 PROTEIN ANALYSIS

Equipment

- BioPhotometer® D30 (Eppendorf)
- Centrifuge 5430R (Eppendorf)
- Consort EV 202 power supply (Sigma Aldrich)
- Flat-tipped tweezers
- Image Quant LAS 4000 mini (Life sciences, Cat. No. 28-9558-10)
- Mini-PROTEAN® Tetra Cell electrophoresis system (BioRad Laboratories, Inc.)
- Odyssey® Fc Imaging System (LI-COR Biosciences)
- Stuart® Analog Tube Rollers SRT6 (Cole-Palmer®)
- Trans-Blot® Turbo™ Transfer System (BioRad Laboratories, Inc.)

Materials

- Ammonium Persulphate, APS (GE Healthcare, Cat. No. GE17-1311-01)
- 2-Mercaptoethanol (Sigma Aldrich, Cat. No. M6250)
- Bromophenol blue (Carl Roth, Cat. No. 6558)
- Complete protease inhibitor cocktail (Roche, Cat. No. 04693116001)
- Milk powder (Sigma Aldrich, Cat. No. 70166)
- N, N, N′, N′-Tetramethylethylenediamine, TEMED (Sigma Aldrich, T9281)
- Nitrocellulose membrane, Amersham Protran 0.45 NC (GE Healthcare Life Sciences, Cat. No. 10600002)
- PageRuler Prestained Protein Ladder (Thermo Scientific, Cat. No. 26616)
- Phosphate-Buffered Saline (as described at 3.1)
- Phosphoric Acid (Carl Roth, Cat. No. 9076)
- Proteome Profiler Mouse XL Cytokine Array (R&D Systems®, Inc., Cat. No. ARY028)
- Rotiphorese®Gel 30 “Acrylamide” (Carl Roth, Cat. No. 3029)
- Sodium deoxycholate (Sigma Aldrich, Cat. No. D6750)
- Sodium fluoride, NaF (Carl Roth, Cat. No. 4530)
- Sodium orthovanadate, Na_3VO_4 (Carl Roth, Cat. No. 0735)
- Syringe filter 0.22 µm (VWR, Cat. No. 514-0061)
- Tween® 20 (Carl Roth, Cat. No. 9127)

Primary and secondary antibodies:

Calnexin	Novus Biologicals, Cat. No. NB300-518
Tubulin	Dianova, Cat. No. MS-719-P0
PPARγ	Santa Cruz® Biotechnology Cat. No. sc-7273
Anti-mouse IgG (H+L) (DyLight™ 800 4X PEG Conjugate)	Cell Signaling Technology®, Cat. No. 5257
Anti-rabbit IgG (H+L) (DyLight™ 800 4X PEG Conjugate)	Cell Signaling Technology®, Cat. No. 5151

3.4.1 Protein Isolation

Cells were washed with cold PBS, soaked with RIPA Plus buffer, scrapped with a 1 ml tip and transferred into 1.5 ml reaction tube, followed by centrifugation for 30 min at 4°C by 13000 rpm. The formed clear phase was transferred into a new, sterile 1.5 ml reaction tube, stored at -20°C or used immediately, keeping it constantly on ice.

RIPA Buffer

Component	**Concentration/Volume**
Sodium deoxycholate	0.1% wt/v
Sodium chloride	150 mM
NP-40	1% wt/v
Sodium dodecyl sulphate	0.1% wt/v
Tris-HCl (pH 7.5)	50 nM
Millipore H_2O	98.8% of the total volume
Addons to make RIPA Plus	
Complete protease inhibitor cocktail	40 µl/ml
Sodium fluoride	10 mM
Sodium orthovanadate	1 mM
Those addons were freshly mixed with RIPA before use	

3.4.2 Protein Quantification

Coomassie solution

Component	**Concentration**
Coomassie Brilliant Blue G-250	0.01% wt/v
EtOH	5% v/v
Phosphoric acid	8.5% v/v
Millipore H_2O	86.5% of the total volume
Stored at 4°C	

To perform protein quantification, 2 µl of a sample was added to 98 µl of 0.15 M NaCl solution, blank consisted of 100 µl 0.15 M NaCl. Further, 1 ml of Coomassie solution was added to each sample, the blank, and incubated for 2 min prior to measurements. The absorbance of those solutions was measured using Eppendorf BioPhotometer® D30 and protein concentration was calculated using BSA standard calibration curve prepared with standard BSA dilutions.

3.4.3 SDS-Page

Gel preparation

Gels for protein separation consisted of 10% resolving fraction at the bottom and stacking layer with a 15-chambered comb at the top. The gels were left at room temperature until solidification.

Component	10% resolving gel	Stacking gel
H_2O	4 ml	3.4 ml
Acrylamide	3.3 ml	0.83 ml
Tris-HCl	2.5 ml, pH = 8.8	0.63 ml, pH = 6.8
20% APS	50 µl	25 µl
TEMED	4 µl	5 µl

After protein concentration measurements, samples were diluted in RIPA buffer and mixed with 3x Lämmli buffer to obtain final protein concentration of 1.4 µg/µl. Subsequently the samples were denatured at 97°C for 5 min and applied onto acrylamide gels. Electrophoresis was performed at 120 V using Mini-PROTEAN® Tetra Cell and electrophoresis buffer.

3.4.4 Western blotting

Proteins were transferred onto a nitrocellulose membrane by semi-dry western blotting with Trans-Blot® Turbo™ Transfer System (BioRad Laboratories, Inc.) for 30 min at 25 V, 1 A using Standard SD protocol.

Towbin buffer

Component	Concentration/Volume
Tris-HCl	25 mM
Glycine	192 mM
Methanol	20% v/v
H_2O	Ca. 80% of total volume
pH was adjusted to 8.3	

Afterwards, the membranes were washed in TBST and incubated with 5% fat-free milk solution in TBST under continuous, low frequency tilting at room temperature. Subsequently, the membranes were washed again in 3 times for 5 min in TBST and incubated overnight with appropriate primary antibody in 5% BSA solution at 4°C.

TBS 10x

Component	Concentration/Volume
Tris-HCl	100 mM
NaCl	1.4 M
SDS	0.1% wt/v
H_2O	Ca. 99.9% of total volume
pH was adjusted to 8.0	

TBST

Component	Concentration/Volume
TBS 10x	10% of total volume
Tween-20	0.1% of total volume
H_2O	Ca. 90% of total volume
Stored at room temperature and protected from light using aluminium foil	

5% fat-free milk solution

Component	Weight/Volume
Fat-free milk powder	5 g
TBST	100 ml

5% BSA solution

Component	Weight /Volume
BSA	5 g
TBST	100 ml

After overnight incubation with first antibody, the membranes were washed 3 times for 10 min in TBST and incubated with secondary fluorescent antibody in TBST for 1 hour at room temperature under continuous tilting. Next, the membranes were washed again 3 times for 5 and developed using Odyssey® Fc Imaging System (LI-COR Biosciences).

In case of Tubulin, the membrane after detection of PPARγ was washed 3 times for 10 min in TBST and incubated for 2 hours with primary Tubulin antibody and after another round of 3 washes in TBST for 5 min, was incubated with secondary antibody for 1 hour and subsequently washed 3 times for 10 min in TBST and developed using Odyssey® Fc Imaging System (LI-COR Biosciences).

3.4.5 Detection of Secreted Cytokines

PVAi was seeded one day before BAi. Both cell types were seeded with density of 1 million cells per 6-well plate in duplicates for each biological replicate. PVAi was differentiated according to 4 days induction protocol for PVAi and BAi according to standard BAi differentiation protocol. All cells were confluent prior to induction. On last day, the media were aspirated, and the cells were washed thrice with DMEM Glutamax™-I (4.5 g Glucose/l medium) (-) Pyruvate. After the last aspiration, 0.5 ml of DMEM Glutamax™-I (4.5 g Glucose/l medium) (-) Pyruvate was added to each well and the cells were incubated in this FBS-free condition for 6 hours. Finally, the supernatants of each biological duplicates were pooled together and frozen in -80°C. Arrays were performed following manufacturer's protocol and signals were detected using Image Quant LAS 4000 mini.

3.5 NE DOSE-RESPONSE CURVE

Equipment

- EnSpire™ Multimode Plate Reader (Perkin Elmer)

Materials

- Direct cAMP ELISA kit (ENZO Life Sciences, Inc., Cat. No. ADI-901-066)
- Norepinephrine, NE (Sigma Aldrich, Cat. No. A9512)3-Isobutyl-1-methylxanthine, IBMX (Sigma Aldrich, Cat. No. I5879)
- 12-well plates (Sarstedt, Cat. No. 83.3921)

Three biological replicates of PVAi and BAi were seeded onto 12-well plates. PVAi and BAi were differentiated according to the according protocols. On the last day of differentiation, cells were pre-treated for 30 min with 0.5 mM IBMX, following by 30 min treatment with series of NE concentrations: 10 nM, 100 nM, 1 µM, 10 µM, 50 µM and 0.1 mM, all containing 0.5 mM IBMX. Immediately after the treatments, supernatants were aspirated and washed with PBS, and the well plates were put on liquid nitrogen for flash-freezing and stored in -80°C.

The cells were lysed in 300 µl of 0.1 M HCl. Additionally, the control samples were diluted 4 times, samples treated with 10 to 100 nM, 5 times, samples treated with 1 to 100 µM, 30 times with 0.1 M HCl. Next, the cAMP ELISA was performed following manufacturer's protocol. After finishing the kit's procedure, the absorbance of each sample was measured using 405 nm wavelength by EnSpire™ Multimode Plate Reader.

3.6 HIGH-RESOLUTION RESPIROMETRY

Equipment

- Oxygraph O2k (Oroboros Instruments, Cat. No. 10002-03)
- Hamilton syringes (Hamilton Company, Series 600, 700 and 800)

Materials

- Mitochondrial respiration buffer, MIR05

- Egtazic acid, EGTA (Sigma-Aldrich, Cat. No. E4378)
- $MgCl_2$ x 6 H_2O (Scharlab, Cat. No. MA00360500)
- Lactobionic acid (Sigma-Aldrich, Cat. No. 153516)
- Taurine (Sigma-Aldrich, Cat. No. T 0625)
- KH_2PO_4 (Supelco, Cat. No. 104873)
- HEPES (Sigma-Aldrich, Cat. No. H7523)
- D-Sucrose (Carl Roth®, Cat. No. 4621.1)
- BSA, essentially fatty acid free (Sigma-Aldrich, Cat. No. A-6003)
- Digitonin (Sigma-Aldrich, Cat. No. 37008)
- Octanoyl-L-carnitine (TOCRIS Bioscience, Cat. No. 0605)
- Pyruvate (Sigma-Aldrich, Cat. No. P2256)
- Malate (Sigma-Aldrich, Cat. No. M1296)
- Glutamate (Sigma-Aldrich, Cat. No. G1626)
- Succinate (Sigma-Aldrich, Cat. No. S2378)
- GDP (Sigma-Aldrich, Cat. No. 51060)
- NaN_3 (Sigma-Aldrich, Cat. No. S2002)

Before the measurement, the Oxygraph O2k was switched on for more than one hour, the mitochondrial respiration buffer (MIR05) was warmed-up to 37°C, and all needed materials and substrates were prepared. Ethanol from measurement chambers was aspirated and the chamber was washed 3 times with water, 1 time with 70% ethanol, again 3 times with water, once with MIR05 buffer, and finally filled with 2 ml of MIR05 buffer. When oxygen concentration and oxygen flux were steady, 2-3 mg of PVAT and BAT were inserted to separate chambers, which were afterwards carefully closed, and air bubbles were removed. Next, the following substances were injected into the chambers: Digitonin, Octanoyl-L-carnitine, Pyruvate, Malate, Glutamate, Succinate, GDP and NaN_3.

Mitochondrial respiration buffer

Compound	**Final concentration**
Egtazic acid	0.5 mM
$MgCl_2$	3 mM
Lactobionic acid	60 mM
Taurine	20 mM
KH_2PO_4	10 mM
HEPES	20 mM
D-Sucrose	110 mM
BSA, essentially fatty acid free	1 g/l

Substances used for analysis

Compound	Final concentration
Digitonin	25 µg/ml
Octanoyl-L-carnitine	1 mM
Pyruvate	5.2 mM
Malate	2 mM
Glutamate	10 mM
Succinate	10 mM
GDP	200 mM
NaN_3	100 mM

3.7 *Ex vivo* Measurement of Lipolysis

Equipment

- EnSpire™ Multimode Plate Reader (Perkin Elmer)

Materials

- 24-well plates (Sarstedt, Cat. No. 83.3922)
- 96-well plates (Sarstedt, Cat. No. 83.3924)
- Bovine serum albumin, fatty acids free, Fatty acid-free BSA (Sigma Aldrich, Cat. No. A7030)
- Free glycerol reagent (Sigma-Aldrich, Cat. No. F6428)
- Glycerol standard (Sigma-Aldrich, Cat. No. G7793)
- DMEM, high glucose, HEPES, no phenol red (Gibco™, Cat. No. 21063029)

Fat tissues were isolated as described in 3.2. For each sample, approximately 2 mg of PVAT, 5 mg of BAT and 20 mg of WATi was taken and incubated in 12-well plate with 200 µl in case of PVAT or 400 µl of lipolysis medium in case of BAT and WATi, with or without 1 µM NE for 2 hours. Afterwards, 40 µl of lipolysis medium out from the sample mixes into wells in 96-well plate. Subsequently, 60 µl of free glycerol reagent was added into each well of the samples.

Lipolysis reagents

Component	Concentration/Volume
Fatty acid-free BSA	2% wt/v
DMEM, high glucose, HEPES, no phenol red	Ca. 100% of total volume

The standard was prepared by combining 5 µl of glycerol standard solution and 95 µl of free glycerol reagent. Blank consisted of 40 µl of unused lipolysis medium and 60 µl of free glycerol reagent. Next, the prepared 96-well plate was incubated at 37°C, 5% CO_2 atmosphere for 5 min and were measured with EnSpire™ Multimode Plate Reader (Perkin Elmer) using 540 nm, with a reference measured using 600 nm wavelengths. Total glycerol release was calculated using the values obtained from the blank and the standard. The values were normalized to the weight of the tissue and volume of lipolysis medium used for each measurement.

3.8 Cold exposure for RNA sequencing

Male, 8 weeks C57BL6/J mice old mice were acclimatized for 3 days at 16°C and kept at 4°C for 7 days. Mice were fed with chow diet ad libitum and had constant access to water. In total, 30 mice were cold exposed in 5 rounds of 6 mice each. Control mice were kept at 23°C for 10 days in parallel.

3.9 Sequencing Analysis

Equipment

- Personal Computer with AMD Ryzen 9 3900X 12-Core Processor and 64 GB DDR-4 SDRAM

Software and packages

Programming languages	**Version**	**Reference**
Python3	3.8.3	[187]
R	4.0.1	[188]
Integrated Development Environment	**Version**	**Reference**
RStudio	1.1.456	[189]
Spyder	4.1.4	[190]
Software/Package	**Version**	**Reference**
AnnotationHub	2.22.0	[191]
biomaRt	2.46	[192]
Bokeh	2.1.1	[193]
ClusterProfiler	4.2.2	[194]
Cutadapt	2.10	[195]
DESeq2	1.28.1	[196]
enrichR	2.1	[197]
fgsea	1.20.0	[198,199]
HTSeq	0.12.4	[200]
multiMiR	1.12.0	[201]
org.Mm.eg.db	3.12	[202]
Pandas	1.0.5	[203]
pheatmap	1.0.12	[204]
rWikiPathways	1.14.0	[205]
STAR Aligner	2.7.6a	[206]
tidyverse	1.3.0	[207]
VennDiagram	1.6.20	[208]
reactome.db	1.77.0	[209]

3.9.1 RNA-Sequencing, Data Processing and Analysis

Library preparation and sequencing was performed by NGS Core Facility, Life & Brain Center, 53127 Bonn. For 3'mRNA-Seq, the library was prepared using QuantSeq 3' mRNA-Seq Library Prep Kit FWD for Illumina and sequencing was performed on HiSeq2500 V4 (High Output Mode, 1x50bp), following manufacturers' guidelines. RNA from aortic valve samples provided to NGS Core Facility consisted of 20 µl with concentration of 20 ng/µl. RNA samples from adipose tissues consisted of 22 µl with concentration of ranging from 117 ng/µl to 227 ng/µl. Same samples were used to perform mRNA- and miRNA-Sequencing.

The generated reads were single-end and of length of 50 nucleotides and were processed on personal computer with AMD Ryzen 9 3900X 12-Core Processor and 64 GB DDR-4 SDRAM, according to Quant™Seq User Guide. First 12 nucleotides, poly(A) tails, and nucleotides with Phred quality score below 30 were trimmed by Cutadapt[195]. Additionally, minimum read length was set to 20 nucleotides. Next, the reads were aligned to a reference genome of a C57BL6/J mouse GRCm38.p6[210] using STAR Aligner[206]. Afterwards, reads per gene were counted with HTSeq software[200]. Until this point, each step was performed on Ubuntu 20.04 LTS operating system[211]. All commands were programmed in and executed from a bash script[212]. Further, the differential expression analysis was performed using DESeq2[196]. Data filtering was performed using Python's[187] package Pandas[203] or dplyr[213] for R[188]. GO terms lists for heatmaps[204] and volcano plots were downloaded from The Mouse Genome Database[214]. Volcano plots were created with Bokeh package[193] for Python[187], Venn diagrams with package VennDiagram[208] for R[188], other graphs with GraphPad Prism 9 or ggplot2 [207]package for R[188]. Pathway enrichment analysis was performed using reactome.db[209] in combination with org.Mm.eg.db[202] and fgsea[198,199] R packages. GO terms enrichment analysis was done using ClusterProfiler[215], and org.Mm.eg.db[202].

miRNA targets were obtained with multiMiR[201] package and the obtained MGI gene symbols were converted to HGNC[216] symbols using biomaRt[192] to be compatible with DisGeNET database[217]. Next, disease terms containing target genes were queried from DisGeNET database using enrichR[197] package. Following, disease terms matching patterns (case insensitive) "valve sten", "valve calc", "valve dis" for aortic valve stenosis group and "aneurysm", "dissection", "aortic dis", "aortic rupt", "aortic root dilat" for aortic aneurysm were filtered from the terms, and each target gene was assigned to one or both groups. Subsequently, the number of miRNA targets falling into groups of aortic valve diseases and aneurysms were counted for each miRNA.

3.10 Statistical analysis

Data with error bars is represented as mean ± standard error of the mean (S.E.M.). Statistical analyses for qPCR, WB, microscopic lipid droplets comparison, and cAMP response to NE treatment were performed using one-way or two-way analysis of variance (ANOVA) with Tukey post-hoc test for multiple comparison correction, and for tests, where multiple comparison was not applicable, unpaired or ratio-paired, two-tailed t-test was performed. Statistical analysis for adipokine abundance in conditioned media of PVAi and BAi was performed using unpaired t-tests with Benjamini and Hochberg adjustment for multiple comparisons. For sequencing data, statistical analysis was performed using Wald test with Benjamini and Hochberg adjustment for multiple comparisons.

4 RESULTS

4.1 ESTABLISHMENT OF IN-VITRO MODEL OF PERIVASCULAR ADIPOCYTES

To characterise perivascular adipocytes (PVA) and study their role without freshly isolating cells from increasing numbers of mice and always achieving reproducible results, I established isolation, immortalization, and differentiation procedure of PVA. Isolation of cells from PVAT was a challenging process due to scarce mass of the tissue around the murine thoracic aortas and the impossibility to isolate the cells from newborn mice due to the size of the animal and limited mass of their PVAT. Additionally, PVAT isolation requires to use a microscope in contrast to BAT, WATg, and WATi. I used immortalized brown adipocytes (BAi) as a reference for immortalized PVA (PVAi) characterisation.

4.1.1 Media and protocol establishment for PVAi

Initially, I investigated optimal growth and differentiation media composition, and culture duration, since PVAi did not form any lipid droplets when standard differentiation and induction protocol for BAi was used. Therefore, four different media (*Table 1*) and two periods of differentiation were tested (*Figure 4*, *Figure 5*, and *Figure 6* in 3.3.3 Cellular differentiation protocols part of the Materials and Methods).

Medium/Ingredient	DM	DM + pyr	PVATM1
Differentiation			
Insulin	1 nM		1 nM
T3	20 nM		20 nM
Rosiglitazone	-		0.2 µM
ABP	-		L-ascorbate 0.284 mM, biotin 1 nM, pantothenate 17 nM
cGMP	-/+ 200 µM		-/+ 200 µM
Pyruvate	-	1 mM	1 mM
Induction (additionally to differentiation media)			
3-isobutyl-1-methylxanthine	0.5 mM	0.5 mM	0.5 mM
Dexamethasone	1 µM	1 µM	1 µM
Rosiglitazone	-	-	2 µM

Table 1. Evaluated media compositions for PVAi differentiation establishment

To assess the adipogenic induction potency, cell cultures were visually inspected every day during the whole differentiation procedure. The first lipid droplets were observed in both PVAi and BAi cultured in the media "PVATM1", and in BAi cultured in DM + cGMP (Appendix *Figure 42*).

Four days after the induction, lipid droplets were only formed in PVAi cultivated in PVATM1 using the two-day induction (2 ID) protocol and in BAi under each condition. When the induction period was repeated for additional two days (4 ID), lipid droplets were discovered in BAi and with the highest density in BAi cultivated in "PVATM1". In contrast, sparse islands of lipid droplets were observed in PVAi cultivated in PVATM1 (*Figure 7*).

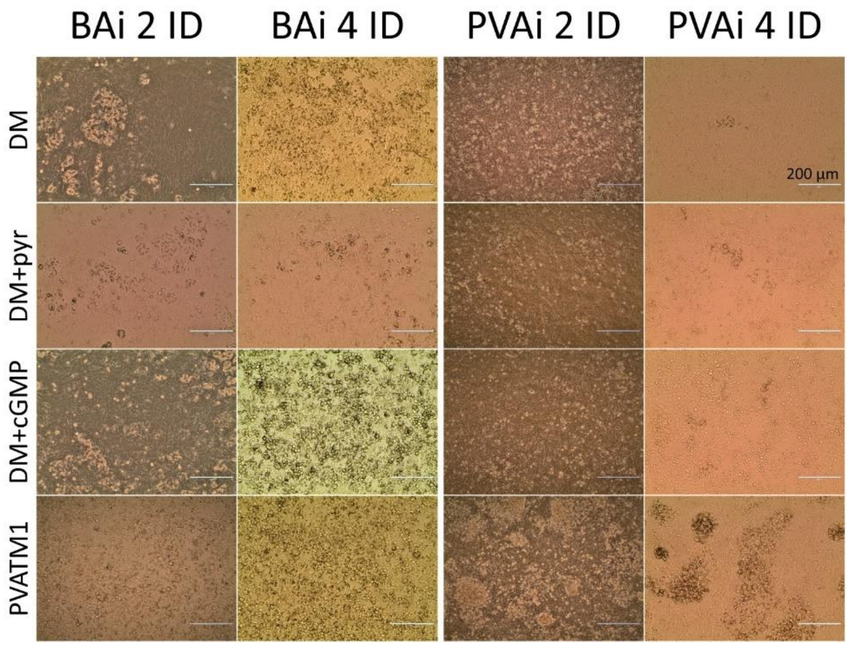

Figure 7. Microscopic comparison of differentiation of immortalized brown (BAi) and perivascular adipocytes (PVAi) cultivated as indicated for four days after the first induction

Therefore, PVATM1 was selected for further differentiation procedure development for PVAi, and the optimal differentiation and induction durations were further investigated. Additionally, further variations of differentiation and induction media were tested. Here, a prolonged culture period and a new approach of supplementing Rosiglitazone only during the induction were investigated.

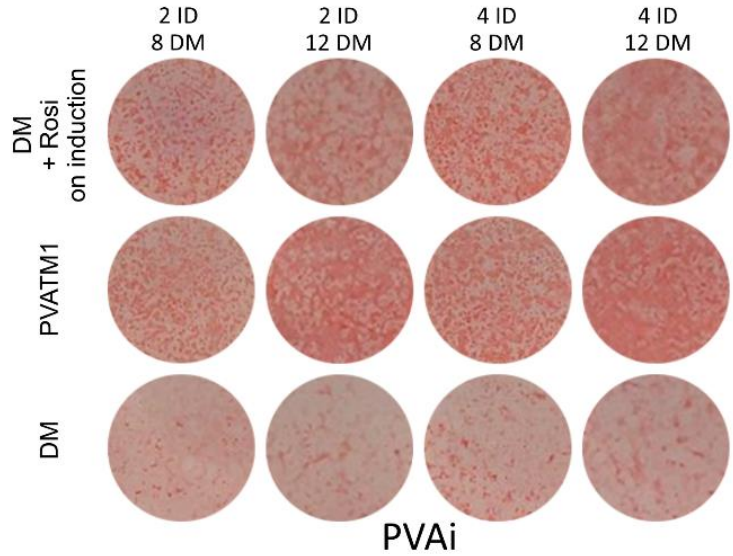

Figure 8. Representative Oil Red-O comparison of 8 and 12 differentiation days with three types of differentiation media and two induction periods for immortalized perivascular adipocytes (PVAi)

The density of lipid droplets was slightly higher in the four-day induction protocol than in two-day induction protocol for PVAi. The addition of Rosiglitazone only during induction was sufficient to reach the lipid density that was obtainable using PVATM1. The culture period prolongation until twelve days after the first induction seemed not to be needed since the ORO staining was already optimal in the approach with 4 ID following with eight-day culture in DM (*Figure 8*). Additionally, the cellular layers were easily detaching from the growth surface in the cell culture in case of the prolonged growth duration.

Due to satisfying results, I chose to focus on supplementing induction media with Rosiglitazone, and eight-day cultivation with BAi differentiation media (DM) with two-, and four-days induction approaches for PVAi differentiation protocol.

4.1.2 BAi accumulates more lipid droplets than PVAi but their average size remains equal

After choosing optimal differentiation protocol, I started characterisation of PVA by comparing lipid droplet sizes and number between differentiated PVA and brown adipocytes (BA) under a microscope (*Figure 9*). PVA and BA are both multilocular, and visually indistinguishable, which is consistent with the description for BA[218]. While the mean diameter of lipid droplets was the same in PVA and BA, the overall number of lipid droplets was about 37% higher in BA (Figure 9).

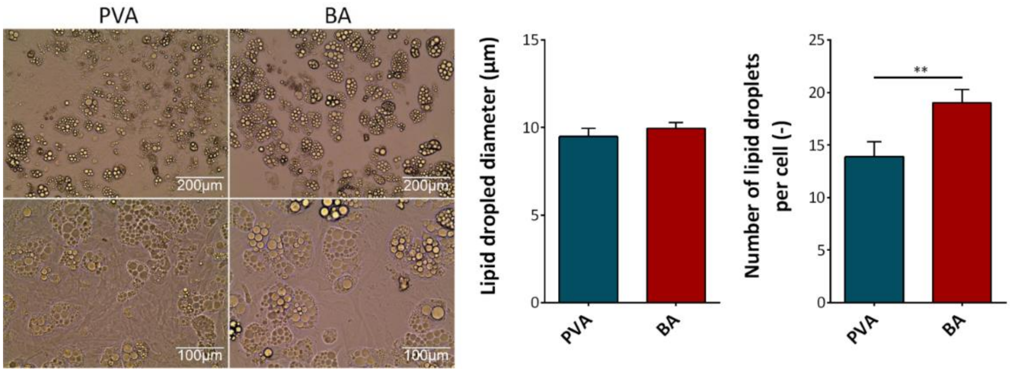

Figure 9. The morphology of primary perivascular adipocytes (PVA) is like primary brown adipocytes (BA). BA have more lipid droplets than PVA.

*Morphology of primary PVA and BA (left), and mean lipid droplets diameter and number of lipid droplets per cell (right). Data is shown as mean ± SEM. Unpaired t-test. ** p ≤ 0.01. n = 34*

4.1.3 PVAi presents lower expression levels of adipogenic markers than BA

To assess if differentiated PVAi would present brown adipocyte-like features on molecular level, four brown adipocytes hallmark genes were tested. Peroxisome Proliferator Activated Receptor Gamma (PPARG) is the master adipogenic transcription factor[219] and is also most abundant in adipocytes[220]. Adrenoreceptor Beta 3 (ADRB3) is expressed in mature adipocytes, but not in preadipocytes[221], and mediates noradrenaline signal to PPARG[222]. Fatty Acid Binding Protein 4 or Adipocyte-type fatty acid-binding protein (*Fabp4* or AP2) is highly expressed in adipocytes[223]. Mitochondrial uncoupling protein 1 (UCP1) is responsible for unique function of brown adipose tissue[143] and its main marker. Therefore, relative gene expression levels of *Pparg*, *Adrb3*, *Fabp4*, and *Ucp1* between PVAi and BAi were investigated via qRT-PCR. Additionally, the ability to respond to cGMP was evaluated as a control, since adipocytes respond to cGMP by increasing expression of the chosen genes[219]. On transcriptional level, PVAi 2 ID and 4 ID, and BAi, were all responsive to media supplementation with cGMP (*Figure 10*).

Gene expression levels for all four tested markers were not significantly different between PVAi 2 and 4 ID, and expression of all tested markers was always higher in BAi than in PVAi (*Figure 10*).

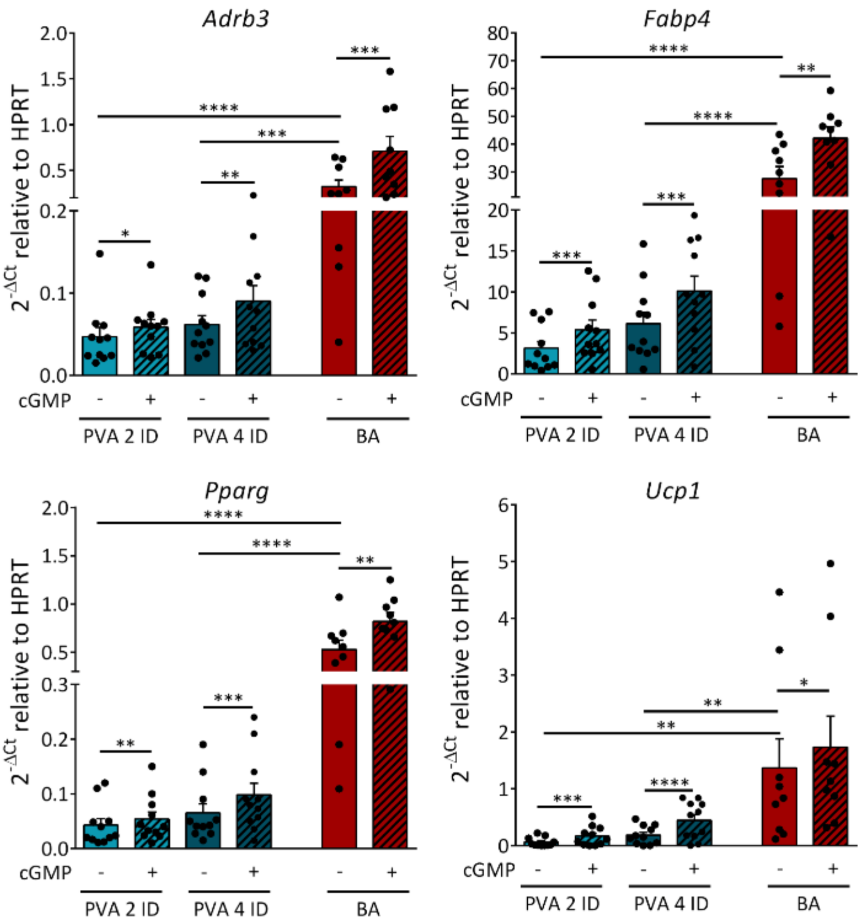

*Figure 10. Transcriptional levels of adipocyte-specific markers are lower in PVAi than in BAi. Transcriptional comparison using qPCR of adipocyte-specific markers in immortalized perivascular adipocytes induced for 2 and 4 days (PVAi 2, and 4 ID), and immortalized brown adipocytes (BAi). PVAi vs BAi n = 9 - 11. Ratio paired T-test to test cGMP effect, and ordinary one-way ANOVA with Tukey post hoc test to compare PVAi 2, 4 ID, and BAi. * $p \leq 0.05$, ** $p \leq 0.01$, *** $p \leq 0.001$, **** $p \leq 0.0001$.*

Consistently with the gene expression analysis, PPARG protein expression was higher in BAi in comparison to PVAi differentiated with 2 and 4 ID (*Figure 11*).

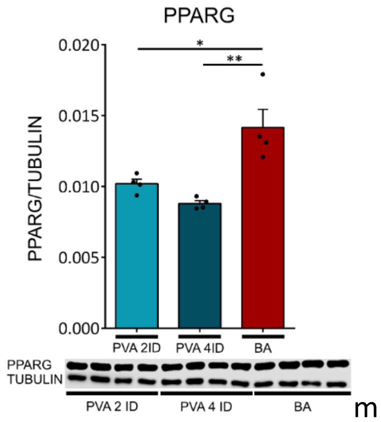

Figure 11. Protein expression levels of PPARG is higher in BAi than in PVAi

*PPARG expression in immortalized perivascular adipocytes induced for 2 and 4 days (PVAi 2, and 4 ID), and immortalized brown adipocytes (BAi). n = 4. Ordinary one-way ANOVA with Tukey post hoc test. * $p \leq 0.05$, ** $p \leq 0.01$.*

4.1.4 PVAi 4 ID show similar response to NE as BAi in terms of cAMP production after NE stimulus

Noradrenaline interacts with $\beta_{1\text{-}3}$, and $\alpha_{1\text{-}2}$ receptors in murine mature brown adipocytes, where β_3-adrenoreceptor is the most significant, and induces cAMP production[143]. cAMP is a second messenger produced by activated adenylate cyclases. cAMP stimulates downstream effectors, which activate lipolysis, glucose uptake, and thermogenesis[224]. To investigate how PVAi respond to NE stimulus and compare it to BAi, cAMP concentration was measured using ELISA assay. Dose-response curves were calculated along with the maximal cAMP response, and half-maximal effective concentration of NE using data from 30 min NE treatments with concentrations ranging from 10 nM to 0.1 mM NE.

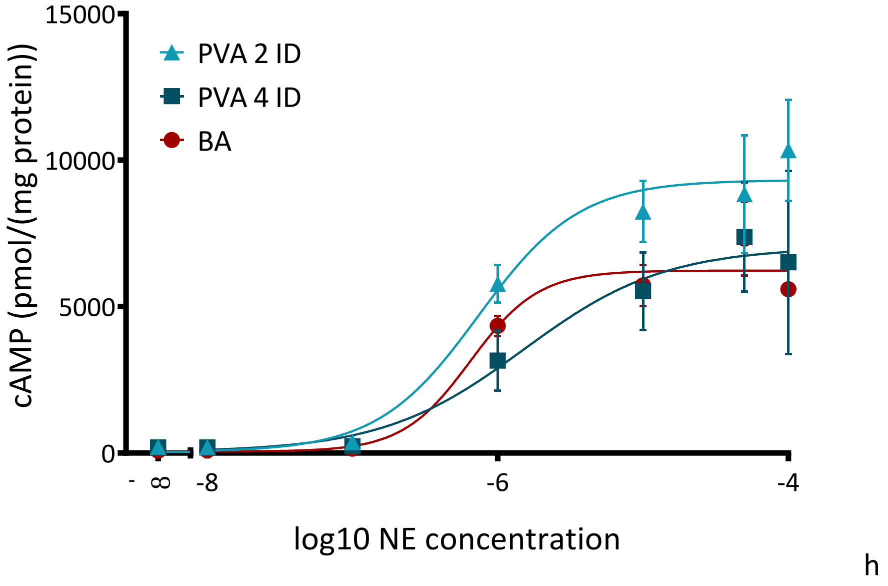

Figure 12. cAMP response to NE stimulation is similar in PVAi 4 ID and BAi

*NE-cAMP dose-response curves of immortalized perivascular adipocytes induced for two and four days (PVAi 2 ID, and 4 ID), and immortalized brown adipocytes (BAi). Two-way ANOVA with Tukey post hoc test. * $p \leq 0.05$.*

Half-maximal effective concentrations (EC50) and maximal cAMP responses of all tested groups were not significantly different.

Sample	Maximal response (pmol cAMP/mg protein)	EC50 (µM)
PVAi 2 ID	9320 [7808 to 10832]	0.7345 [0.276 to 1.876]
PVAi 4 ID	7029 [3717 to 10340]	1.505 [0.137 to 16.47]
BAi	6230 [5469 to 6991]	0.6481 [0.237 to 16.47]

Table 2. Maximal cAMP response to NE treatment and EC50 values for PVAi 2 ID, PVAi 4 ID and BAi. 0.95 confidence intervals are represented as [from, to].

The increase in cAMP levels in both PVAi 2 ID, PVAi 4 ID, and BAi was concentration dependent. EC50 of NE were 0.73 µM for PVAi 2 ID, 1.5 µM for PVAi 4 ID and 0.65 µM for BAi. Maximal cAMP response was reached in all conditions after stimulation with 50 µM NE (*Figure 12*, *Table 2*).

4.1.5 Adipokines' secretion profile varies between PVAi and BAi

The secretion profile of adipose tissue-derived cytokines, called adipokines, varies in each adipose tissue depot and may play roles, among others, in cardiometabolic diseases[225]. The secretory profile of PVAi and BAi was examined, quantified, and compared. Array used for this experiment provided simultaneous detection of 111 murine cytokines, out of which 47 were detected in cell culture media (DMEM without FBS) after 6 h incubation of BAi, and 50 in media of PVAi. (*Figure 13*).

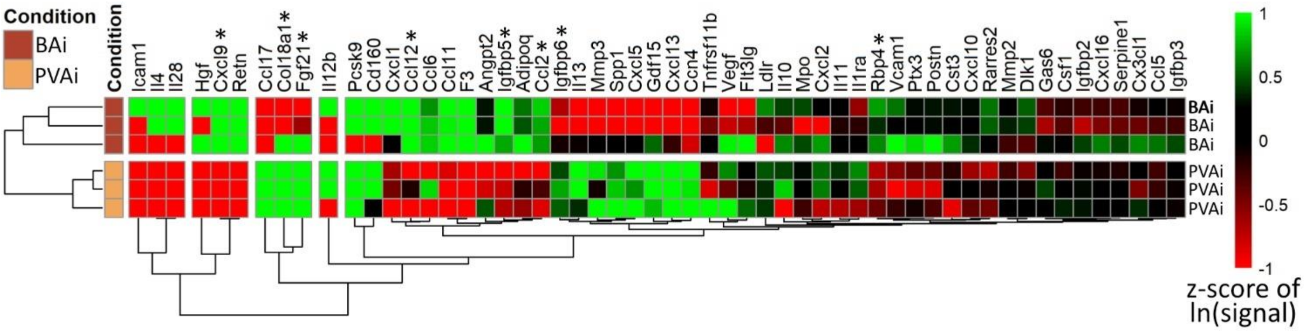

Figure 13. Differentially secreted cytokines detected in supernatants of PVAi, and BAi.

*Data shown as z-scores of natural logarithms of cytokines' signals. Colours capped at z-score = +/- 1. Unpaired t-tests with Benjamini and Hochberg correction. * p.adj ≤ 0.05, n = 3*

Among detected cytokines in both cell lines, secretion of Endostatin (*C*OL18A1), FGF21, and IGFBP-6, was higher in PVAi than in BAi supernatants, while CXCL9, CCL12, and RBP4 were considerably decreased in supernatants of PVAi. Resistin, IL-28A/B, IL-4, HGF, and CXCL9 were undetected in supernatants of PVAi, but were present in supernatants of BAi (*Figure 13*). Thus, PVAi and BAi presented clear distinguishable secretory profiles, where around half of the adipokines were differentially secreted or undetected in one of the cell lines.

To find functions of secreted adipokines in terms of adipocyte differentiation and homeostasis, the detected cytokines were filtered using Gene Ontology terms adipocyte cell differentiation (GO:0045444) and adipogenesis (GO:0060612) from Mouse Genome Informatics website[226] (*Table 3*).

Gene symbol	Protein name or symbol	Signal from PVAi (AU)	Signal from BAi (AU)	Function
Adipoq	ADIPONECTIN	98876.25	377897.83	Positive regulator of adipocyte differentiation[227]
Ccn4	WISP-1	318342.92	16176.17	Negative regulator of adipocyte differentiation[228]
Csf1	M-CSF	152559.58	120614.50	Positive regulator of adipogenesis[229]
Dlk1	PREF-1	50342.92	79231.17	Negative regulator of adipocyte differentiation[230,231]
Rarres2	CHEMERIN	39209.58	92414.50	Positive regulator of adipocyte differentiation[232]
Retn	RESISTIN	below threshold	128831.17	Negative regulator of adipocyte differentiation[233]

Table 3. Adipokines secreted from PVAi and BAi influencing adipocytes differentiation.

Subsequently, the detected cytokines from PVAi and BAi were converted to human gene symbols and checked, if they appear in genes associated with AVD or AA. 19 of detected cytokines were indeed found in DisGeNET disease terms for AVD and AA (Table 4). The analysis of secretory profiles of PVAi and BAi indicated existing influence of those cells on development and progression of aortic diseases, and regulation of adipose tissues homeostasis. These results suggest possible involvement of PVA and BA adipokines in progression and/or development of aortic diseases.

Gene symbol	Protein name or symbol	Signal from PVAi (AU)	Signal from BAi (AU)	Role in aortic diseases
Adipoq	Adiponectin	98876.25	377897.8	Attenuates Ang-II-induced AAA formation in mice[234]
Angpt2	Angiopoietin 2	169842.90	459564.50	Attenuates Ang-II-induced AA in mice[235]
Ccl2	MCP1	45526.25	202564.50	Induces AA[236–239], promotes AVD[240,241]
Col18a1	Endostatin	194676.30	9781.67	May aggravate aneurysm formation[242]
Cst3	Cystatin C	35359.58	below threshold	Deficiency promotes AA[243,244], may attenuate AVD[245]
Cx3cl1	Fractalkine	327676.30	369231.20	May potentiate AAA[246]
Il13	IL13	7969.58	below threshold	Induces MMPs, promoting AA[247]
Il4	IL4	below threshold	16299.50	IL-4 deficiency protects from AAA[248]
Mmp2	MMP2	53959.58	56614.5	Deficiency protective against AAA[249,250], might be involved in AVD progression[251]
Mmp3	MMP3	401842.9	88997.83	May promote formation of AA[252–255]
Mpo	Myeloperoxid	6454.58	6737.83	Implicated in AAA pathogenesis[256]; may contribute to AVD progression[257]
Postn	Periostin/OSF-2	52842.92	157564.50	Maintains inflammation in AAA[258], lack of Periostin leads to AVD[259]
Retn	Resistin	below threshold	128831.20	Enhances inflammatory cytokine production, serum levels associated with aortic diameter, increased levels in patients with

				AAA[260,261], Resistin inhibition is beneficial for patients with AVD[262–264]
Serpine1	Serpin E1/PAI-1	284342.90	261731.20	Overexpression proportional to AV calcification degree[265], attenuates AA[266–268]
Spp1	Osteopontin	218009.60	40540.00	Promotes AA and AVD[269–272]
Tnfrsf11b	Osteoprotegerin	369942.90	177897.80	Protective against AA[273,274], protective against AVD[275–278]
Vcam1	VCAM1	31259.58	102264.50	VCAM1 levels are associated with calcific AS[279], recruits macrophages to arterial walls, involved in pathogenesis of AA[280,281]

Table 4. Cytokines detected in PVAi or BAi supernatants found to play roles in AVD or AA in DisGeNET database

4.2 CHARACTERISATION OF ADIPOSE TISSUES' RESPONSE TO COLD EXPOSURE

Adipose tissue is divided into two main categories – BAT and WAT. PVAT shares characteristics of both, mostly depending on its location in the body. It remains unclear, if one should recognize PVAT as a separate adipose tissue or rather to associate it depot-specific with one of the main types[108]. To reveal the differences and similarities between fat tissues, 8-weeks old mice were cold exposed for three days at 16°C and seven days at 4°C with control mice held in 23°C for ten days. AV, BAT, thoracic PVAT, WATg, and WATi were isolated to investigate transcriptional profiles of four cold-exposed fat tissue depots. Additionally, the influence of cold exposure of AV was in investigated.

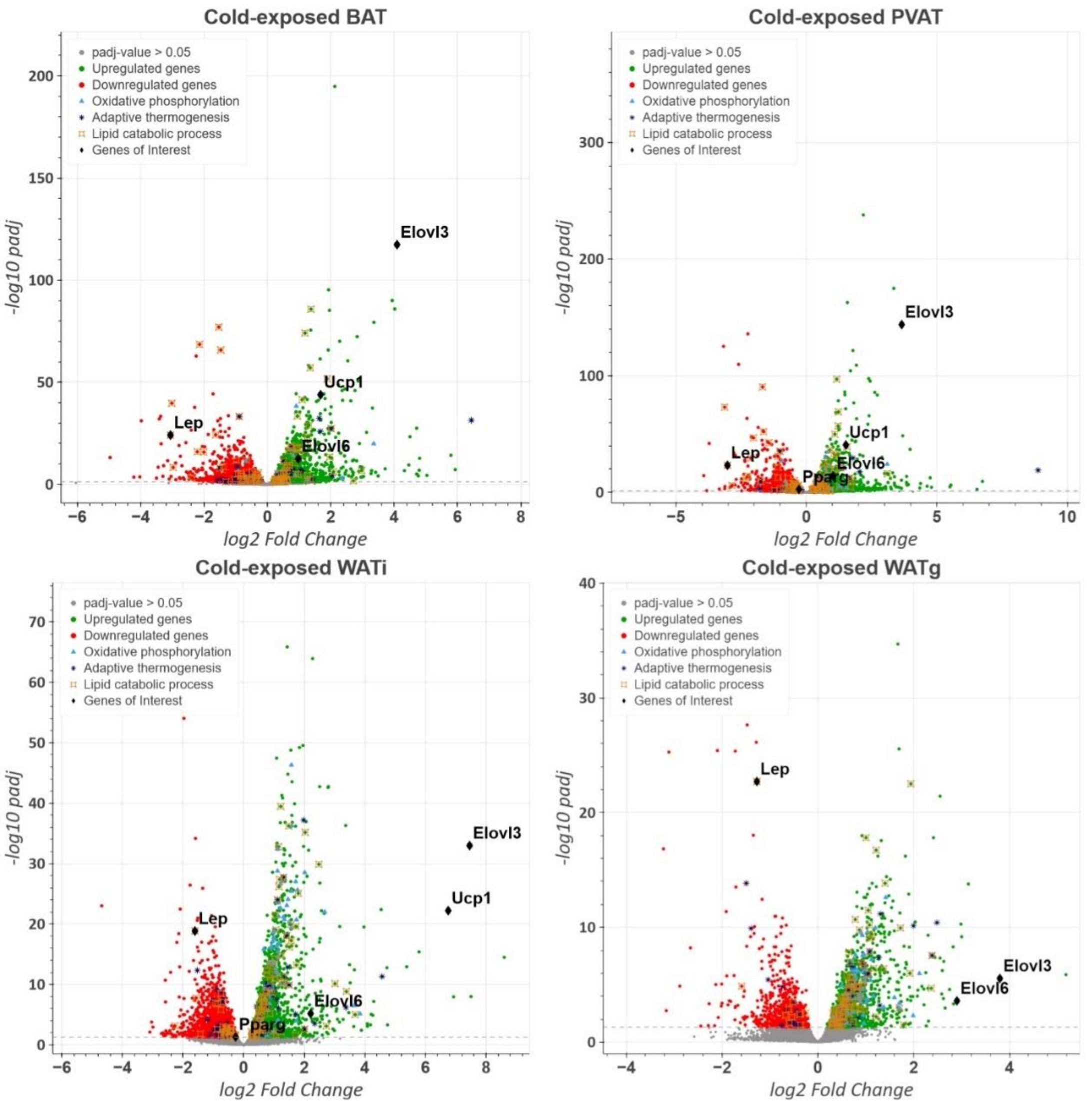

Figure 14. Effect of cold exposure on the expression of protein-coding genes in adipose tissues.

Volcano plots visualising DEG in cold-exposed BAT (top left), PVAT (top right), WATi (bottom left), and WATg (bottom right). Gray points: genes with unchanged expression following cold exposure (padj > 0.05). Green points: upregulated, cold-responsive genes. Red points: downregulated, cold-responsive genes. Blue triangles: DEG involved in oxidative phosphorylation. Black asterisks: DEG involved in adaptive thermogenesis. Orange stars: DEG involved in lipid catabolic process.

Four adipose tissues, PVAT, BAT, WATi, and WATg (Figure 14), isolated from cold-exposed male mice responded to the cold stimulus and presented over 2500 differentially expressed genes (DEG) below adjusted p-value of 0.05. The upregulation of known cold-responsive genes like Elovl3, Elovl6, and Ucp1 (unchanged in WATg) served as a quality control of the cold exposure and is consistent with literature[282–285]. In contrast, cold-exposed AVs isolated from the same mice, showed only 11 DEG.

The DEG of each tissue were compared and visualized with a Venn diagram (Figure 15 left). From four adipose tissues, WATi showed the highest number of unique DEG, while WATg showed the lowest number of DEG. PVAT and BAT shared the most DEG that were not differentially expressed in WATi or WATg, while both BAT and PVAT shared the least DEG only with WATg.

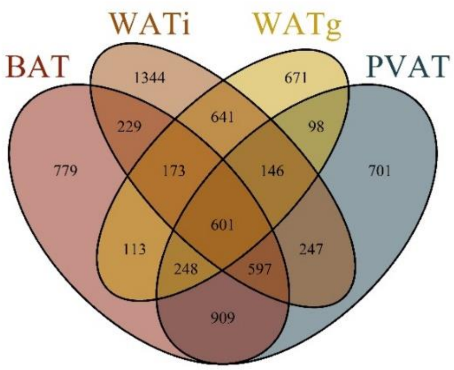

Figure 15. Overlap of differential expression between BAT, PVAT, WATi, and WATg following cold exposure.

Venn diagrams of all significantly differentially expressed genes in response to cold exposure in four adipose tissues.

The comparison of DEG in adipose tissues revealed that each fat depot has unique, cold-responsive genes. In terms of shared cold-responsive gene number, thoracic PVAT was most similar to BAT, showing 2355 shared DEG and least to WATg, showing only 995 shared DEG. Meanwhile WATg and WATi shared 1561 cold-responsive genes (Figure 15). Genes that were cold-responsive only in one tissue are shown in tables in chapter 7.1.

4.2.1 Functional analysis of adipose tissues' response to cold

Gene Ontology Analysis of cold-responsive genes (adjusted p value below 0.05 after cold exposure) and their affected pathways was investigated for each tissue. This approach helps to investigate adipose tissues response to cold in a simplified, functional way, and compare the responses of each adipose tissues.

Gene Ontology Analysis from domain of Biological Process (GOBP) revealed high similarities of adipose tissue groups BAT-PVAT and WATi-WATg in the most affected biological processes. The most significant, affected processes activated by cold in every adipose tissue is related to energy utilization, mitochondrial organization, and ribonucleotide metabolic process. Additionally, only BAT showed increased expression of genes responsible for carbohydrate metabolism. The observations are consistent with literature[286] but it was unknown for PVAT that it does not have a substantial expression increase for genes responsible for carbohydrate metabolism (*Figure 16*).

On the other hand, functional analysis using downregulated genes showed more diverse roles of those genes in adipose tissues. WATi and WATg showed highest similarities in functions of downregulated genes, whereas PVAT and BAT presented similar responses in downregulation of genes controlling histone lysine methylation, proliferation of epithelial cells, and rhythmic process (Figure 16).

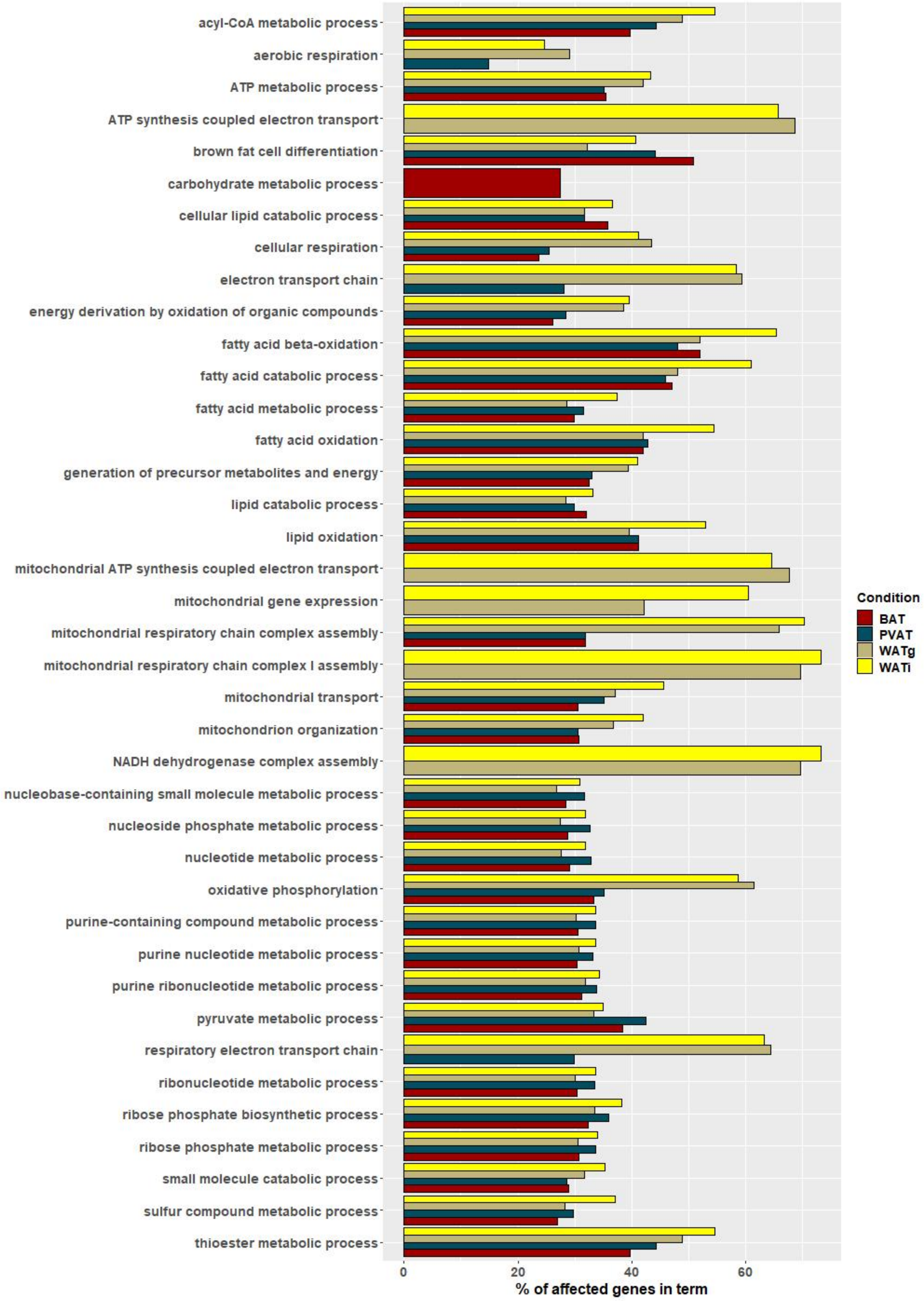

Figure 16. Fast Gene Ontology Analysis[287] from domain Biological Process of cold-responsive genes in BAT (red), PVAT (green), WATi (yellow), and WATg (brown). Bar graph presents top 20 most significant GOBP using cold-responsive genes of each analysed tissue.

Furthermore, reactome[209] pathway enrichment analysis was performed using cold-responsive genes from each adipose tissue. In case of BAT, only three pathways were found to be affected, which belonged to metabolism fatty acids or lipids, and no enriched pathway was found in BAT only. PVAT presented many positively enriched pathways related to DNA repair processes, proliferation and epigenetic proliferation regulation, while it only shares fatty acid metabolism with other adipose tissues. WATi and WATg presented the highest overlap in cold-responsive, enriched pathways among adipose tissues, which play role mostly in energy production for positively enriched pathways, and ECM synthesis and organization in the negatively enriched group (*Figure 17*).

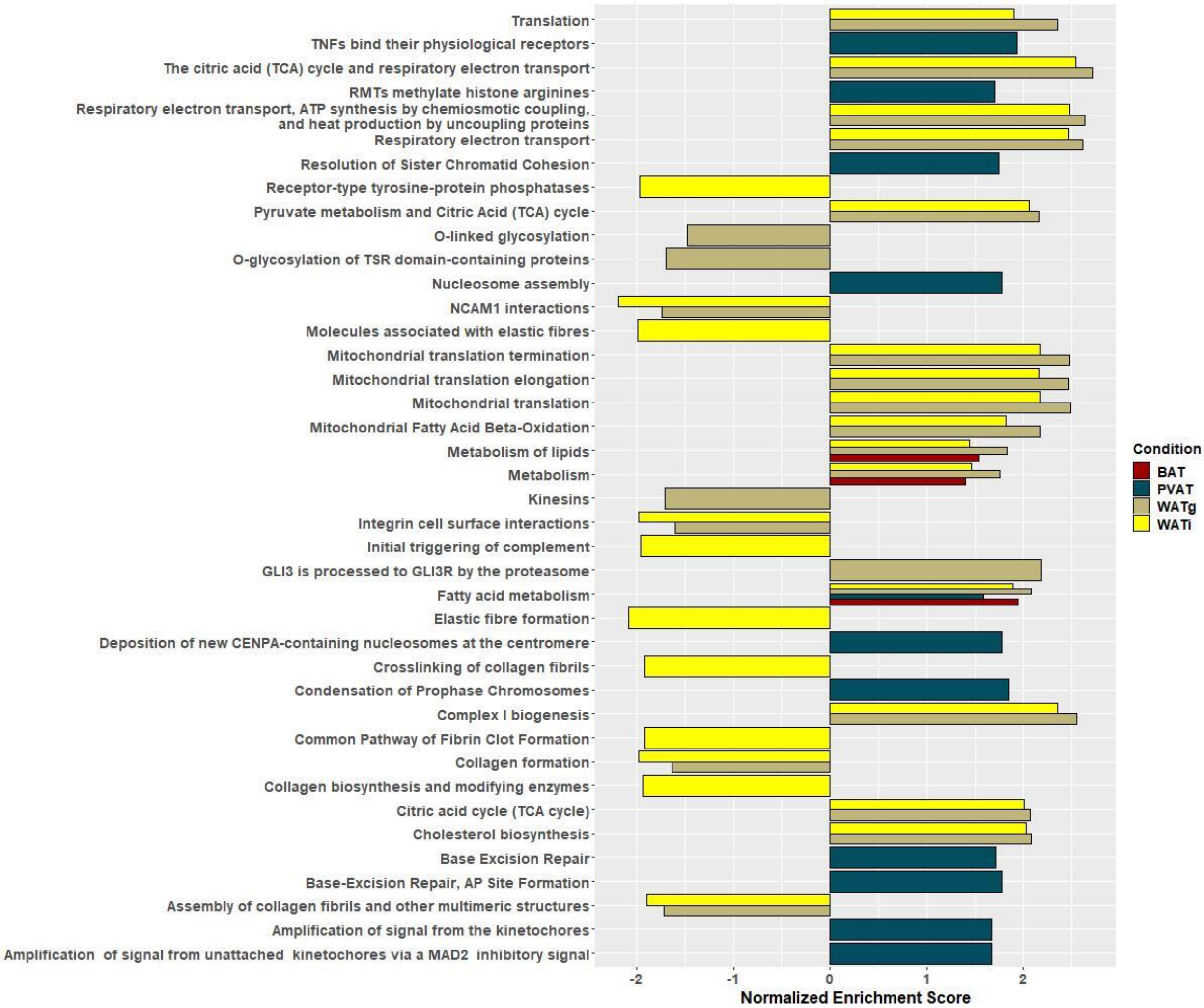

Figure 17. Gene Set Enrichment Analysis (GSEA) of differentially expressed genes using reactome pathways database[209] in cold-exposed adipose tissues.

Results show top 10 positively, and negatively affected terms from BAT (red), PVAT (green), WATi (yellow), and WATg (brown).

4.2.2 Cold-responsive genes unique to PVAT suggest PVAT-muscle interactions

In previous GOBP and GSEA analysis, the focus was on general response to cold of each adipose tissue, and previous results suggested additional functions of PVAT. Consequently, the subset of unique DEG for each adipose tissue was investigated for enriched GOBPs and pathways to reveal functions specific to each adipose tissue. Only PVAT and WATg was found to have significantly enriched GOBP terms in the unique subset of their cold-responsive DEG, although for WATg there were only three enriched GOBP terms: glycolipid biosynthetic process, negative regulation of protein dephosphorylation and negative regulation of phosphoprotein phosphatase activity.

In case of PVAT, the enriched GOBP terms in the subset of unique, cold-responsive genes revealed additional functions of PVAT related to muscle contraction or muscle regulation with 89 muscle-related DEG (Figure 18 top). The protein products of those 89 DEG localize intercellularly and are mostly associated with actin or tropomyosin binding or cation channels activity. Pathway enrichment analysis showed that only muscle contraction pathway was positively enriched (Figure 18 bottom).

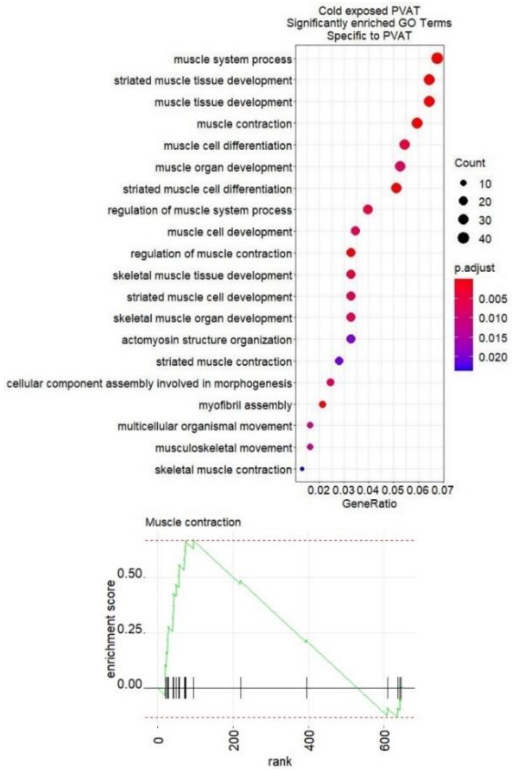

Figure 18. Gene Ontology and Fast Gene Set Enrichment Analysis[287] obtained from unique subset of DEG for PVAT following cold exposure.

Significantly enriched Gene Ontology Terms (top), and reactome[209] pathway (bottom) of genes that were differentially expressed in cold-exposed PVAT but not in other adipose tissues.

The unique response to cold of PVAT may suggest different tissue origin and additional, vascular system-related functions as PVAT feature, differentiating it from other adipose tissues.

4.2.3 Adipose features of PVAT are mostly similar to the features of BAT

The classification of PVAT is not yet clear, as literature describes clear differences between PVAT, BAT, and WAT[108]. RNA sequencing of four adipose tissues from mice held in cold, and normal temperature environments gave me the first opportunity to add clarity to the adipose tissue classification discussion.

For this purpose, I started with exploratory analysis using mRNA sequencing data of cold-exposed and room temperature-exposed BAT, PVAT, WATg, and WATi. Using regularized logarithmic transformation of normalized sample count data of each tissue in both conditions, I performed hierarchical clustering, and Principal Component Analysis (PCA) to investigate adipose tissues' similarities on a transcriptional level. Both hierarchical clustering (*Figure 19* top), and PCA (*Figure 19* bottom) revealed clear similarities of BAT-PVAT, and WATg-WATi groups, basically dividing them into two main groups. The exploratory analysis clearly shows greater differences between the tissues than the effect of cold exposure on each tissue. The analysis also revealed that there are smaller differences between BAT and PVAT, than WATg and WATi. Dendrogram lines connecting BAT and PVAT present lower differences than between WATg and WATi (*Figure 19* top). Also, BAT, and PVAT samples are located on almost the region of the first Principal Component (PC1 on *Figure 19* bottom), whereas WATi is shifted towards BAT and PVAT. Additionally, room temperature-exposed WATi is closer to BAT, and PVAT than cold-exposed WATg, meaning colloquially that room temperature-exposed WATi is more "brown" than cold-exposed WATg.

Next, to investigate adipose tissue-specific features, I clustered and compared the expression of genes playing role in adaptive thermogenesis, oxidative phosphorylation, lipid catabolic process, adipocyte cell differentiation, and lipid localization between BAT, PVAT, WATi, and WATg in cold exposure and room temperature. I clustered around 50 genes from each term with highest expression in BAT, PVAT, WATg, or WATi in order to depict adipose-specific relationships between those tissues.

Hierarchical clustering of gene expression levels on subsets of genes belonging to above mentioned terms revealed that the adipose tissue-specific transcription profile of PVAT is almost equal to BAT and less like WATi and WATg in these processes (*Figure 20*, *Figure 23*).

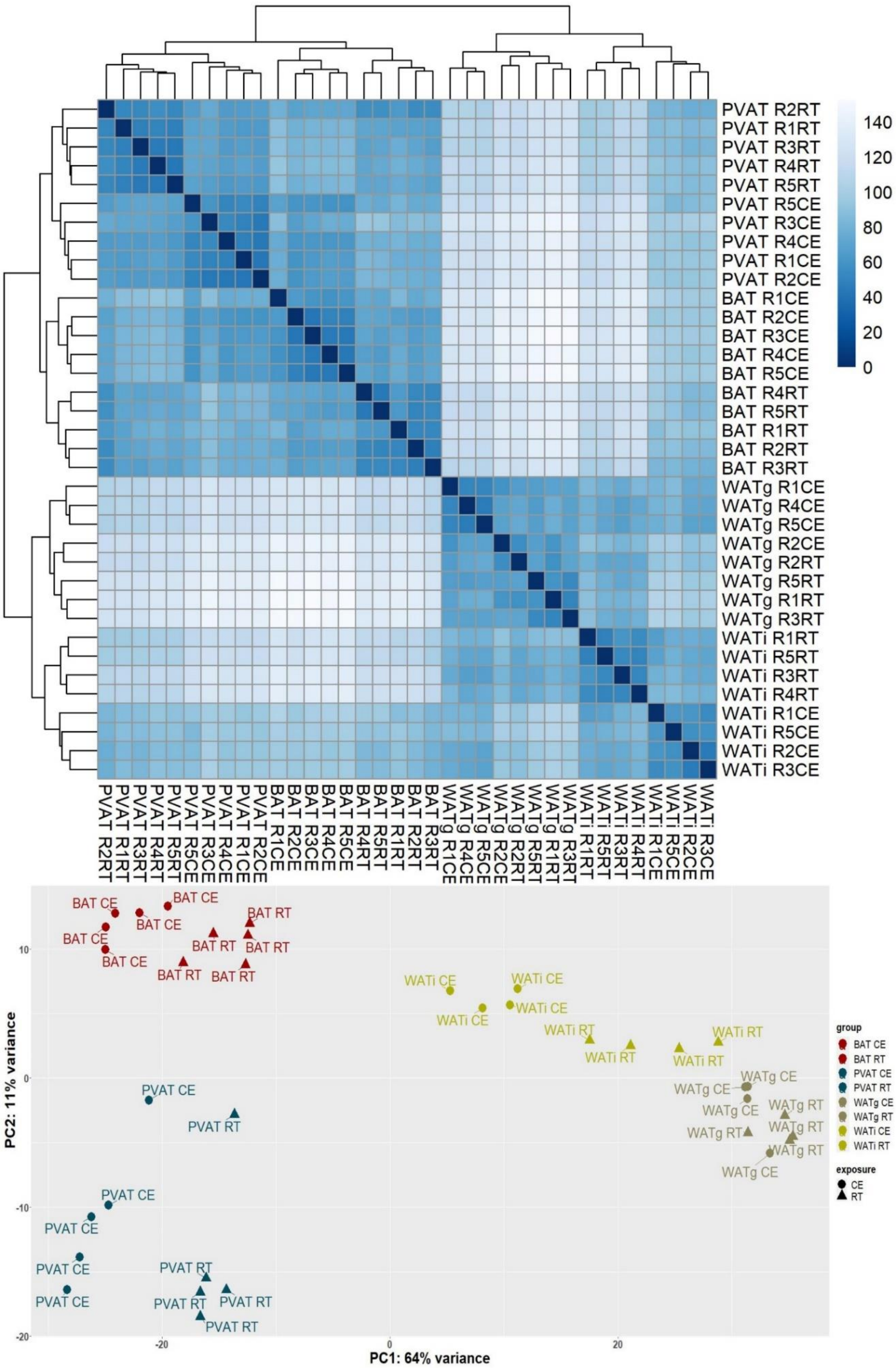

Figure 19. Hierarchical clustering of mRNA sequencing data shown as a heatmap of Euclidean distances between cold-exposed and room temperature-exposed BAT, PVAT, WATg, and WATg (top) and results of Principal Component Analysis for these tissues (bottom).

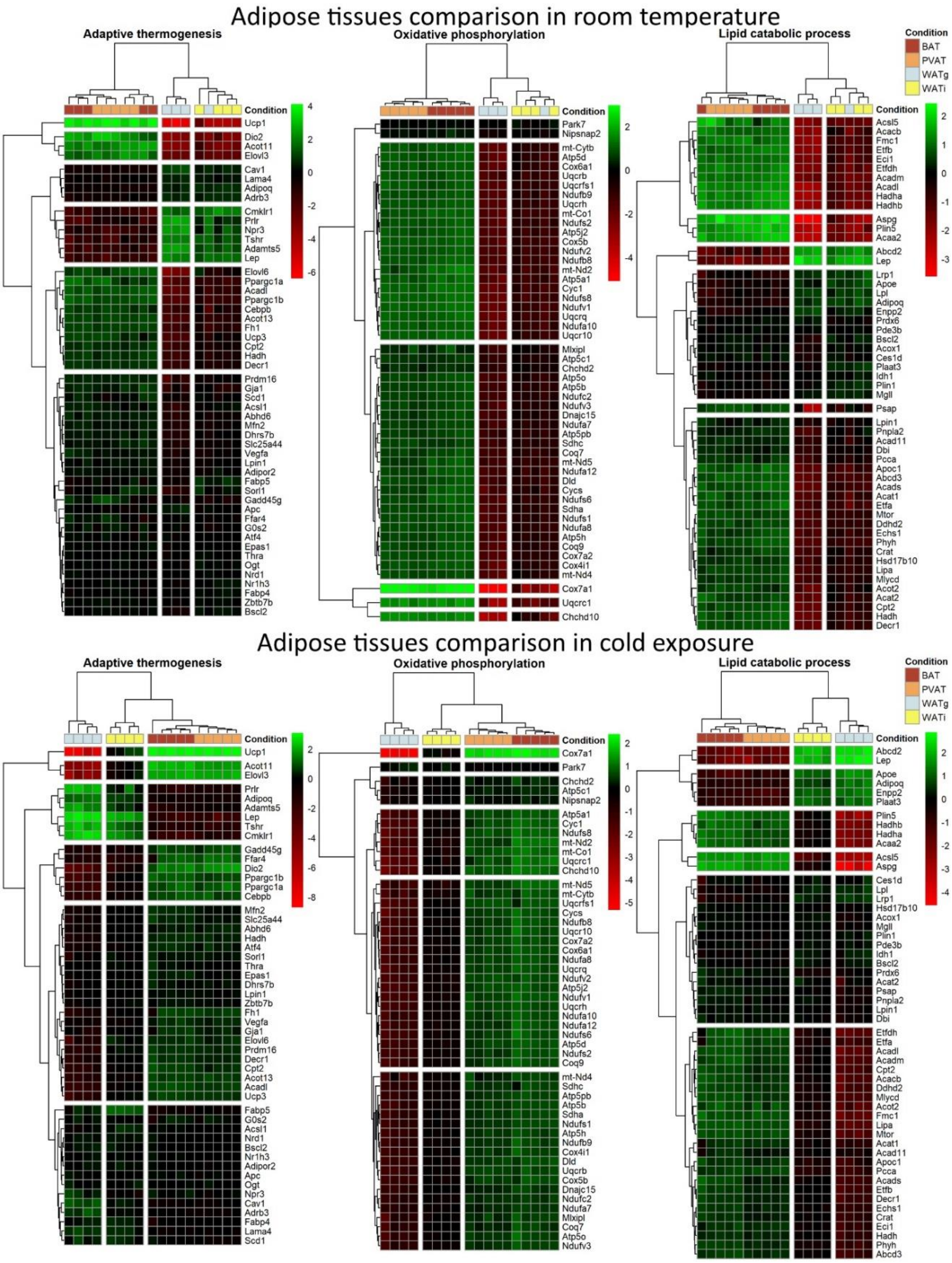

Figure 20.Transcriptional differences in adipose tissue from mice held in room temperature (top row), and in cold (bottom row).

Heatmaps depicting similarities and differences in differentially expressed genes belonging to terms adaptive thermogenesis (left), lipid catabolic process (middle), and oxidative phosphorylation (right) in room temperature (top row), and cold exposed (bottom row) PVAT, BAT, and WATi. Differences are shown as z-scores. Black colour depicts no or low changes in expression. Red colour depicts expression below average among all shown tissues. Green colour depicts expression above average among all shown tissues.

In room temperature, BAT and PVAT were identical in terms of lipid localization, adaptive thermogenesis, and lipid catabolic process, and the hierarchical clustering did not even distinguish between the two tissues. Additionally, BAT and PVAT were nearly identical in terms of oxidative phosphorylation in room temperature. Those similarities in room temperature were higher than between WATi and WATg, that were also very similar in the same terms (*Figure 20*, *Figure 23*).

In cold exposure, BAT and PVAT were nearly identical in every five of analysed terms, whereas WATi and WATg showed higher differences between each other than in room temperature. In terms of adaptive thermogenesis, and oxidative phosphorylation in cold exposure, WATi was more similar to BAT, and PVAT than to WATg (*Figure 20*).

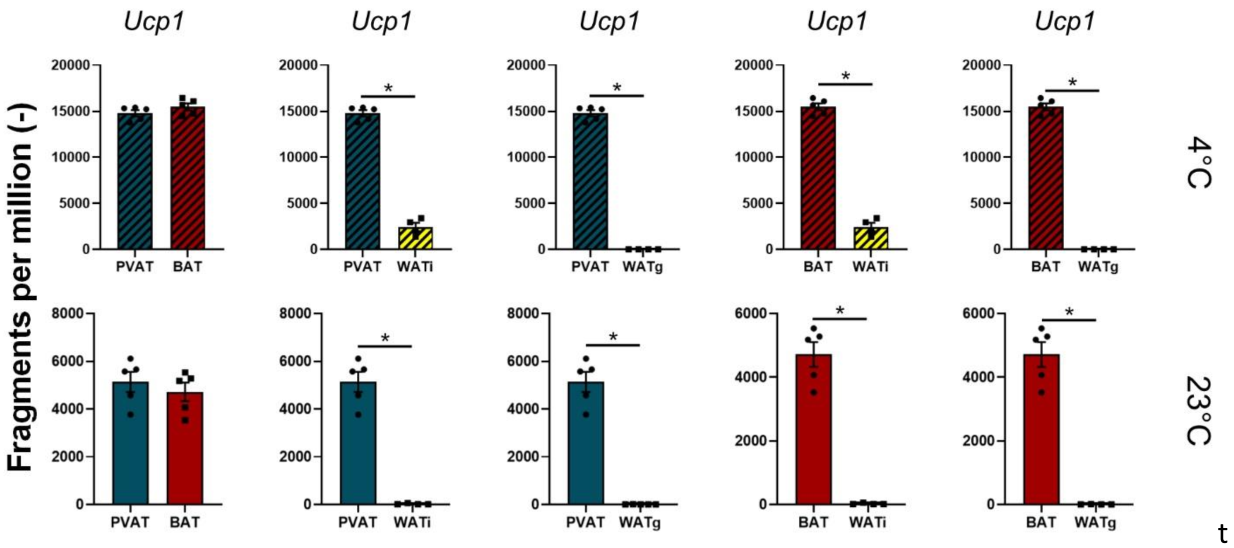

Figure 21. Pairwise Ucp1 expression levels comparison in cold-exposed (top) and room temperature-exposed (bottom) perivascular (PVAT), brown (BAT), white inguinal (WATi), and white gonadal (WATg) adipose tissues.

*Data shown as mean ± SEM. Wald test corrected for multiple testing by the Benjamini and Hochberg method. * adjusted $p \leq 0.05$. n = 4-5.*

Analysis of expression levels of genes belonging to adaptive thermogenesis revealed that *Ucp1*, *Dio2,* and *Elovl3* levels were almost identical in PVAT, and BAT (*Figure 22*). *Cidea and Acot 11* were slightly lower in PVAT and BAT before and after cold exposure (*Figure 22*). *Ucp1* levels in WATi and WATg was over 200-fold lower than in PVAT or BAT (*Figure 21*). Over half of the genes regulating adaptive thermogenesis showed nearly equal expression throughout all analysed adipose tissues. Around one third of the genes presented mild differences between BAT or PVAT and WATg or WATi (*Figure 20*, *Figure 23*).

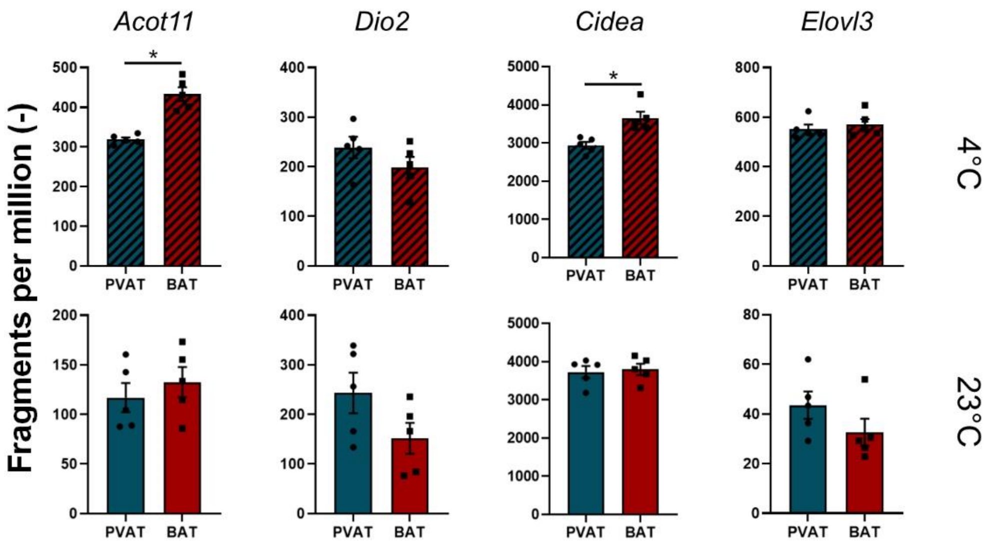

Figure 22. Pairwise Acot11, Dio2, Cidea, and Elovl3 expression levels comparison in cold-exposed (top) and room temperature-exposed (bottom) perivascular (PVAT), brown (BAT) adipose tissues.

*Data shown as mean ± SEM. Wald test corrected for multiple testing by the Benjamini and Hochberg method. * adjusted $p \leq 0.05$. n = 4-5.*

The terms lipid catabolic process and oxidative phosphorylation differed mildly in room temperature, showing major expression differences in levels of *Cidea* for lipid catabolic process and *Cox7a1* for oxidative phosphorylation. Again, the levels of Cox7a1 were nearly identical for PVAT and BAT and severely reduced in WATg. In cold exposure, the transcriptional differences between adipose tissues increased (*Figure 20*).

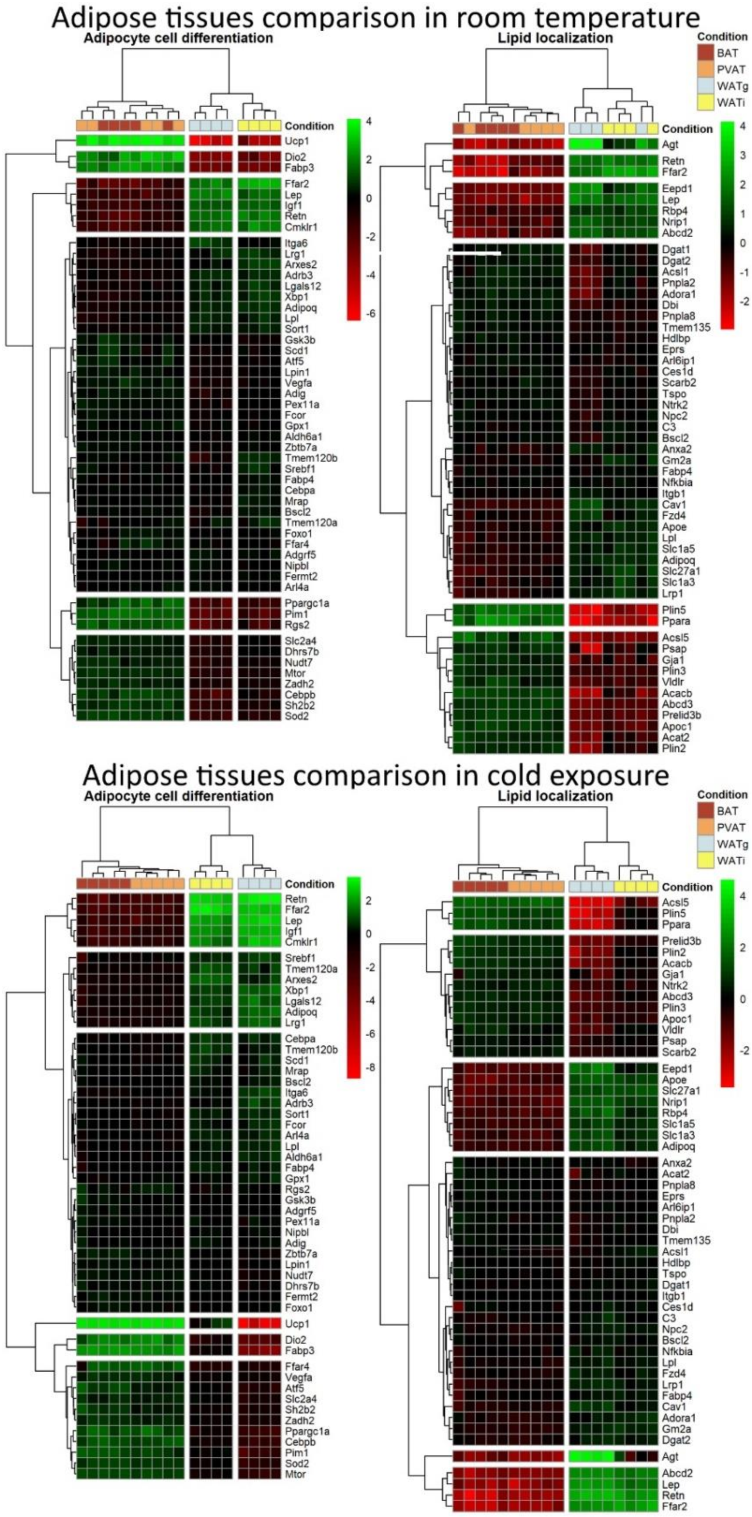

Figure 23. Transcriptional differences in adipose tissue from mice held in room temperature (top row), and in cold (bottom row) in terms of adipocyte cell differentiation, and lipid localisation.

Heatmaps depicting similarities and differences in differentially expressed genes belonging to terms adipocyte cell differentiation (left), and lipid localization (right) in room temperature (top row), and cold exposed (bottom row) PVAT, BAT, WATi, and WATg. Differences shown as z-scores. Black colour depicts no to low changes in expression. Red colour depicts expression below average among all shown tissues. Green colour depicts expression above average among all shown tissues.

Subsequently, I wanted to confirm my findings about similarities of PVAT and BAT with in-house available methods, therefore I tested the ability of PVAT, BAT, and WATi to break down lipids using lipolysis assay (Figure 24). Lipolytic capabilities of each of those tissues increased in response to NE, which increases lipolytic activity of adipose tissue[288] and served as a positive control. BAT produced 7.2-fold more glycerol than WATi, whereas no significant difference could be observed between PVAT and BAT. A trend was seen in form of increased lipolysis of PVAT in comparison to WATi (padj = 0.11).

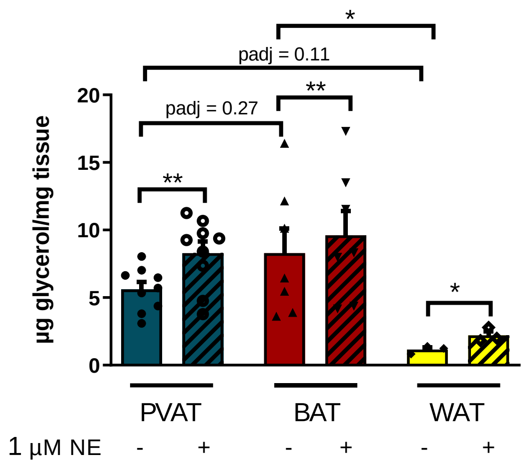

Figure 24. Lipolytic activity of BAT, PVAT, and WATi.

*Ex vivo lipolytic activity measured as a release of glycerol release normalized to the mass of tissue used for the assay. The tissues were incubated with or without 1 µM NE. Data is shown as mean ± SEM. One-way ANOVA wit Tukey post-hoc test for comparison between tissues and paired t-test for evaluating the effect of NE. * p ≤ 0.05, ** p ≤ 0.01. n = 3-9*

Besides the lipolytic activity, I wanted to confirm the findings about oxidative phosphorylation GOBP. For that reason, I analysed PVAT and BAT *ex vivo* with high resolution respirometry to investigate mitochondrial respiration and metabolic activity. Oxygen consumption of the PVAT and BAT were similar, with a trend in increased mitochondrial basal respiration (p = 0.0517) in PVAT. No differences were found in maximal respiration, ATP production, proton leak and non-mitochondrial respiration between PVAT and BAT (Figure 25).

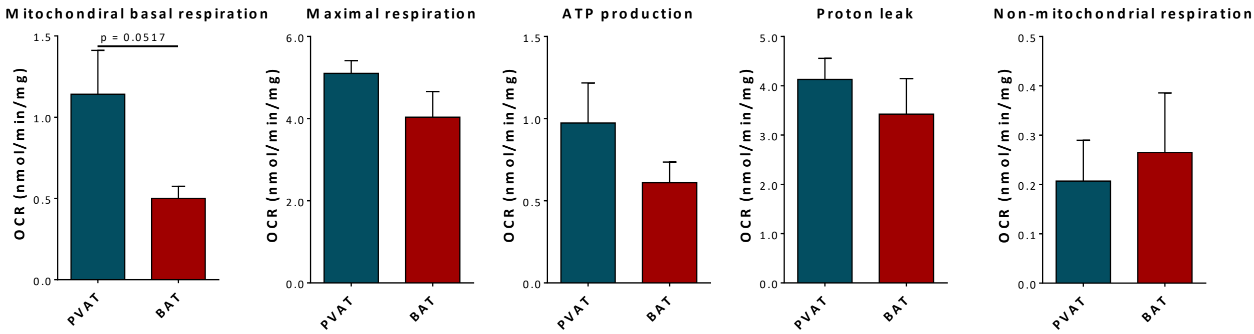

Figure 25. PVAT resembles BAT in mitochondrial respiration.

Measurement of ex vivo mitochondrial respiration in PVAT and BAT normalized to the masses of used tissues. From left mitochondrial basal respiration, maximal respiration, ATP production, proton leak, and non-mitochondrial respiration. Data shown as mean ± SEM. Unpaired t-test. n = 5

Previous analyses clearly showed that BAT, and PVAT are highly similar, and to highlight differences, I performed further analysis, focusing only on those two tissues or brown adipose tissue depots.

In the first steps, I focused on functional analysis of transcriptional profiles in conditions PVAT versus BAT in cold exposure and in room temperature.

The functional analysis in form of GOBP revealed that the main differences between PVAT and BAT from cold-exposed mice are related to immune and nervous systems, which suggests substantial differences in innervation and immune cells number between PVAT and in cold exposure (*Figure 26* top).

Further, pathways analysis pointed on positive enrichment of neuronal system, and ion channels pathways in PVAT. On the other side, citric acid cycle and sulphur amino acid metabolism pathways were negatively enriched in PVAT (*Figure 26* bottom two rows).

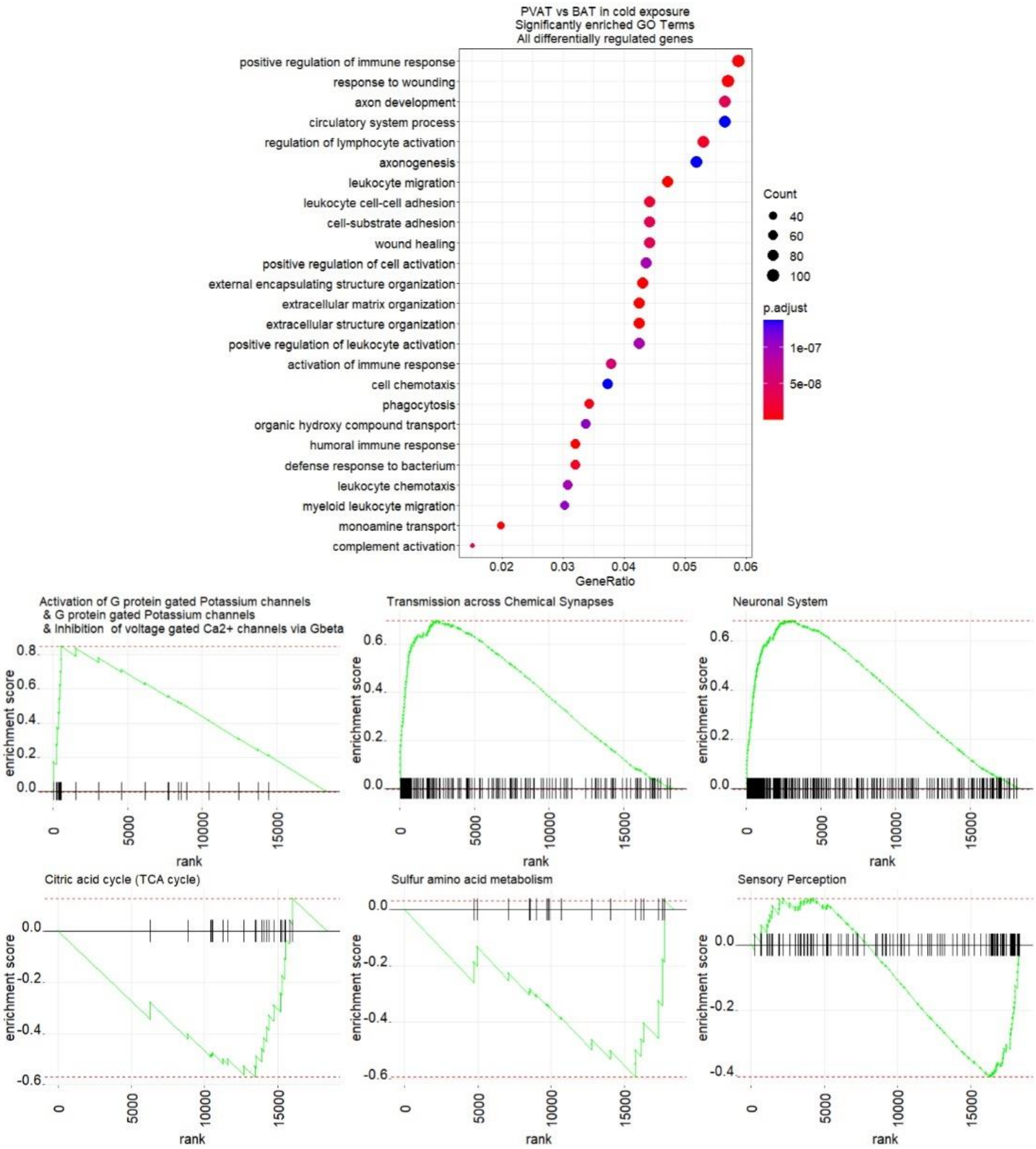

Figure 26. Fast Gene Ontology Analysis[287] from domain of Biological Process (top) and Gene Set Enrichment Analysis (GSEA; bottom two rows) using reactome pathways database[209] of cold-exposed PVAT vs BAT.

In room temperature, the GOBP top terms between PVAT and BAT were related to innervation and circulatory system (*Figure 27* top). Pathway enrichment analysis revealed positive enrichment of neuronal system-related pathways, and negative enrichment of pathways related to RNA II Polymerase, citric acid cycle, and cellular response to heat stress (*Figure 27* bottom two rows).

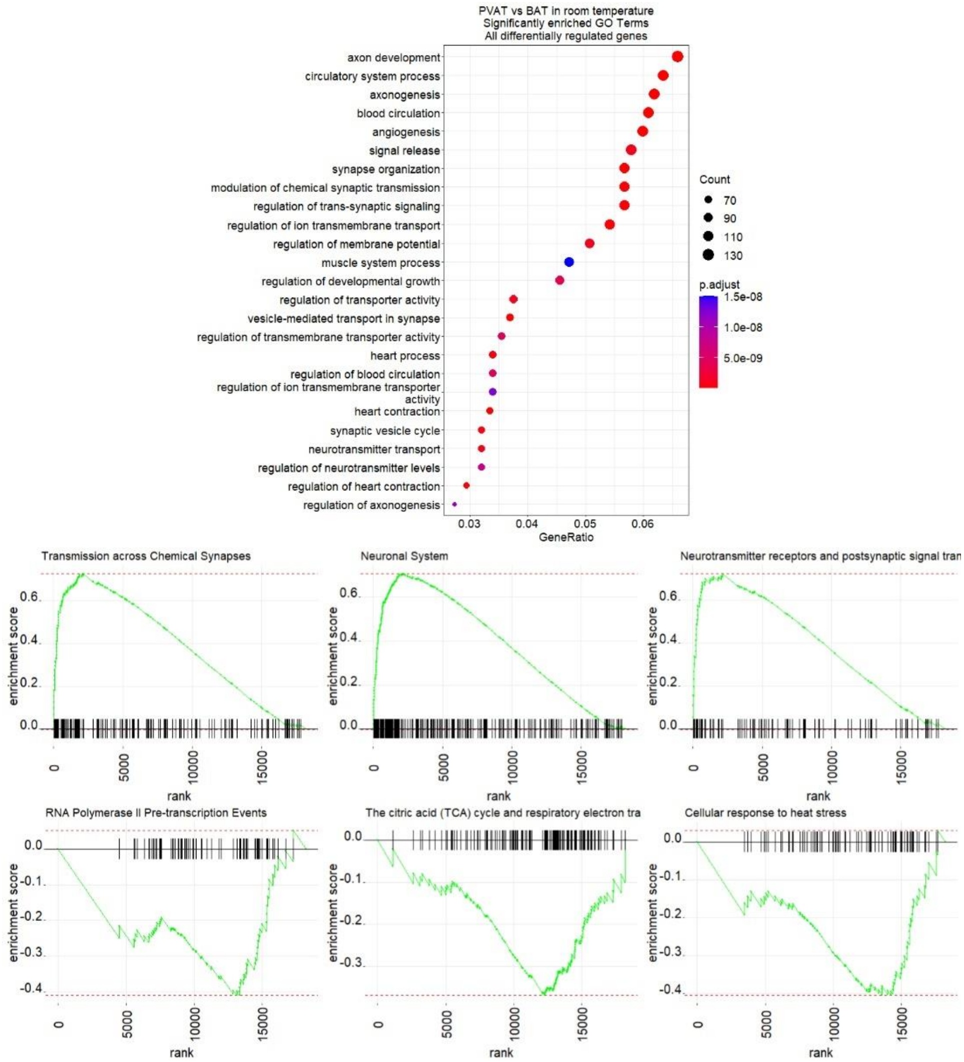

Figure 27. Fast Gene Ontology Analysis[287] from domain of Biological Process (top) and Gene Set Enrichment Analysis (GSEA; bottom two rows) using reactome pathways database[209] of room temperature-exposed PVAT vs BAT.

4.3 Cold-responsive adipokines present diverse transcription profile

4.3.1 Diverse transcription profile of secreted proteins in cold-exposed adipose tissues

Adipose tissue is a secretory organ capable of influencing other tissues and organs, e.g., the cardiovascular system, including the aorta. Dysfunctional adipose tissue as observed e.g., in obese individuals has detrimental effect on the cardiovascular system[108,289–291]. Less is known about the effect of cold-exposed adipose tissue-derived cytokines on AA and AVD. Therefore, cytokine expression was investigated in cold-exposed adipose tissues using mRNA sequencing.

In the first step, gene symbols from GO Term Extracellular Space (GO:0005615)[214] were utilized to subset extracellular space encoding genes from DEG of each, cold-exposed adipose tissue. The GO

Term Extracellular Space contains genes, of which products are secreted from the cell, excluding extracellular matrix[214]. Next, the differentially regulated extracellular space encoding genes were organized in form of a Venn diagram, to illustrate the number of shared and unique cold-responsive genes encoding secreted proteins in each adipose tissue (Figure 28).

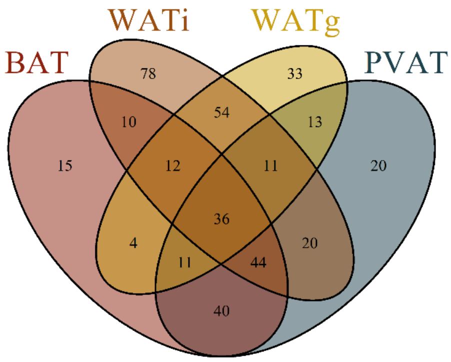

Figure 28. Overlap of differentially expressed cytokines between BAT, PVAT, WATi, and WATg following cold exposure.

The Venn diagram depicts the number of cold-responsive genes (padj < 0.05) belonging to GO Term Extracellular Space (GO:0005615) ([214]) in PVAT, BAT, WATi and WATg. Genes with FPM at least 10 were considered as transcribed

Each tissue presented unique subset of cold-responsive cytokines' genes. WATi showed the highest number of total and unique, cold-responsive cytokines' genes, while BAT, PVAT, and WATg had similar numbers of total and unique cold-responsive cytokines (Table 5). miRNA that were cold-responsive only in one tissue are shown in tables in chapter 7.2.

Tissue	Total number of cold-responsive cytokines	Cold-responsive cytokines only in one tissue
PVAT	195	20
BAT	172	15
WATi	265	78
WATg	174	33

Table 5. Unique and total numbers of cold-responsive cytokines from adipose tissues

4.3.2 Most expressed, cold-responsive adipokines play various roles in adipose tissue homeostasis, inflammation, and insulin sensitivity

To investigate the most prevalent adipokines that additionally strongly responded to cold exposure, the basal expression datasets were filtered using GO term "extracellular space" (GO:0005615)[214] (*Figure 29*).

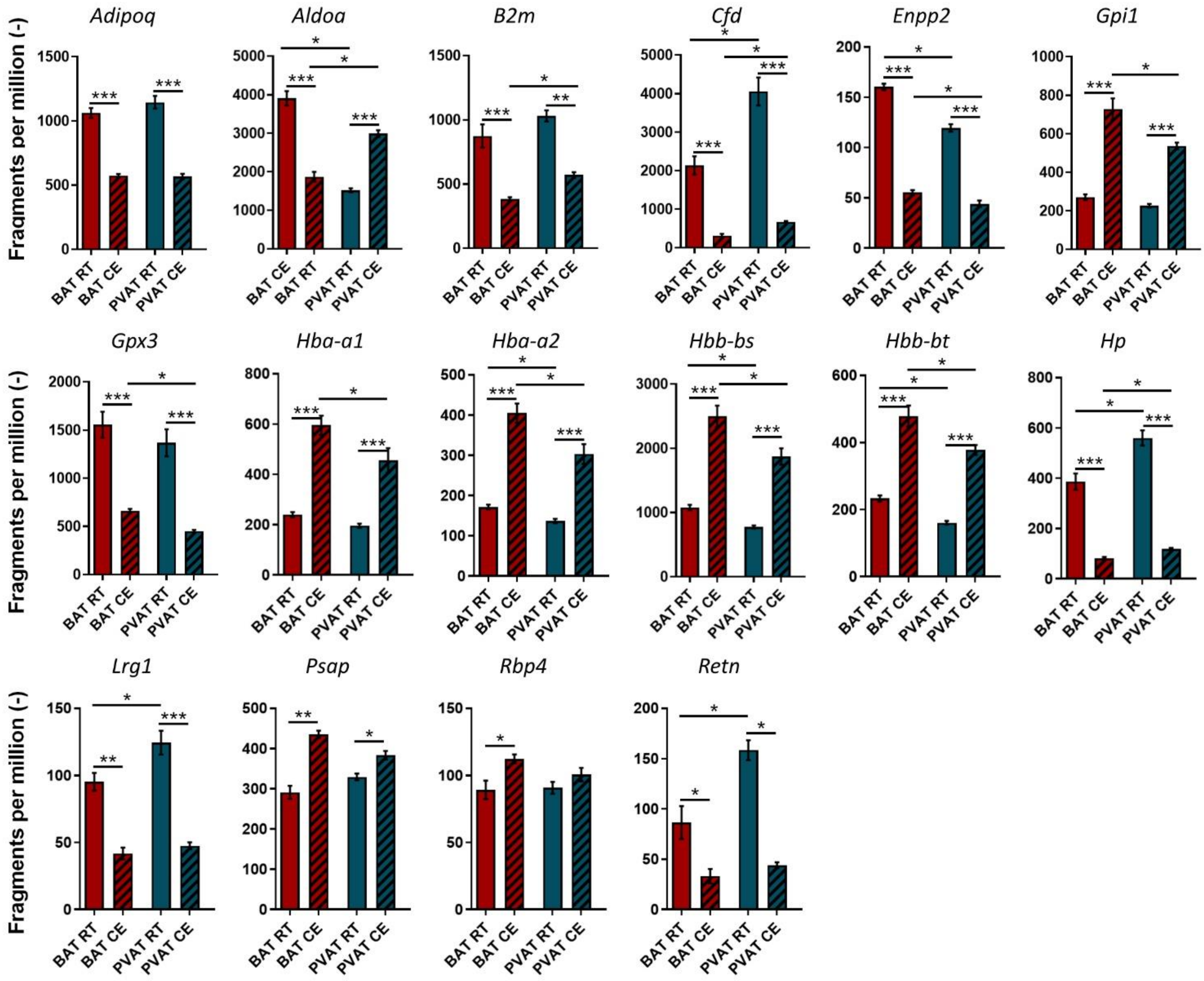

Figure 29. Most highly expressed, cold-responsive cytokines in BAT, and PVAT.

*CE = Tissue was exposed to cold, RT = Tissue was exposed to room temperature. Data shown as mean ± SEM. Wald test corrected for multiple testing by the Benjamini and Hochberg method. * adjusted $p \leq 0.05$, ** adjusted $p \leq e^{-10}$, *** adjusted $p \leq e^{-20}$. n = 4-5.*

Following, the role of those adipokines was researched in literature focusing on roles in adipogenesis, adipocyte differentiation, AA, and AVD (Table 6).

Gene symbol	Protein name or symbol	Roles
Adipoq	Adiponectin	Positive regulator of adipocyte differentiation[227], attenuates AAA formation in mice[234]
B2m	Beta-2-Microglobulin	Risk factor for coronary artery disease, predicts aortic stiftness[292,293]
Cfd	Complement factor D	Regulates insulin secretion[294]
Enpp2	Ectonucleotide Pyrophosphatase/Phosphodiesterase 2	Contributes to adipose tissue expansion[295], directs osteogenic differentiation of VICs[296]

Gpi1	glucose-6-phosphate isomerase 1	Putative biomarker for predicting TAA in bicuspid aortic valve disease patients[297]
Gpx3	Glutathione Peroxidase 3	Increases Insulin Receptor expression and adipocyte differentiation[298]
Hba-a1	Haemoglobin alpha, adult chain 1	Haemoglobin component
Hba-a2	Haemoglobin alpha, adult chain 2	Haemoglobin component
Hbb-bs	Haemoglobin, beta adult s chain	Haemoglobin component
Hbb-bt	Haemoglobin, beta adult t chain	Haemoglobin component
Hp	Haptoglobin	Free haemoglobin scavenger, antioxidant, anti-inflammatory[299]. Hp2-2 genotype mice form larger aneurysms[300]. Patients with Hp2-2 are more likely to develop cardiovascular disease[301]
Lrg1	Leucine-rich alpha-2-glycoprotein 1	Promotes insulin sensitivity and suppresses inflammation[302,303]
Psap	Prosaposin	Mediates inflammation in atherosclerosis[304] and promotes muscle differentiation[305]
Rbp4	Retinol Binding Protein 4, plasma	Positively correlates with blood pressure and cardiovascular disease[306,307], required for browning and thermogenesis[308]
Retn	Resistin	Promotes adipogenesis[309]

Table 6. Most highly expressed, cold-responsive cytokines in BAT, and PVAT adipokines involved in adipose tissue homeostasis

4.3.3 Cytokines influencing aortic valve stenosis and aortic aneurysms

To identify potential interactions of adipose tissue's cytokines and AVD and AA (Table 7), DisGeNET database was queried for the cold-responsive cytokines from each tissue, and the resulting data frames were filtered for disease terms related to aortic valve diseases, aortic aneurysms, and atherosclerosis. Next, gene symbols were extracted from selected diseases terms, the publication of origin reviewed, and presented for both diseases.

Among detected cold-responsive cytokines in all four investigated adipose tissues, eight were found to have published interactions with development or progression of AA or AVD (Table 8).

Cytokine	Regulation upon cold exposure	Tissue	Possible action
Adipoq	Downregulated	BAT, PVAT	Attenuates AAA formation in mice[234]
Apoe	Downregulated	BAT, PVAT	ApoE-deficiency enhances AS in senile mice[310]
Igf1	Downregulated	BAT, PVAT	Igf1 inhibition in VICs induces AV calcification[311], IGF-1 levels are reduced in calcified AVs[312]
Lep	Downregulated	BAT, PVAT, WATg, WATi	Leptin induces osteoblast differentiation of VICs[313].

			Leptin levels are increased in AVD patients[157]. Leptin applied locally induces aortic wall degeneration[314]. Leptin antagonist applied locally attenuates AT-II-induced TAA[315]
Serpine2	Downregulated	BAT, PVAT, WATg, WATi	Serpine2 inhibits ECM degradation, may be protective against AA[316]
Thbd	Upregulated in BAT, and PVAT, downregulated in WATg, and WATi	BAT, PVAT, WATg, WATi	Protects against AAA by indirect inhibition of RAGE pathway. Potential gene therapy against AAA[317]
Timp4	Downregulated	BAT, PVAT, WATg, WATi	Downregulated in AAA[318], may be protective against AAA[319]

Table 7. Differentially expressed cytokines found in DisGeNET disease terms related to AVD or AA.

The expression of Apolipoprotein E (*Apoe*) was found to be reduced upon cold exposure 4.4-fold in BAT, and 3.1-fold in PVAT (Figure 30). ApoE is essential for normal catabolism of triglyceride-rich lipoprotein components[320]. A study published in the Journal of the American College of Cardiology revealed more severe AVD in ApoE-deficient mice, suggesting altered lipid metabolism as one of the causes of the disease[310].

Another adipokine, leptin, which was found to induce osteoblasts differentiation of human VICs[313]and aortic wall degeneration when applied locally[314], was strongly downregulated in all four adipose tissues upon cold exposure – 8.3-fold in BAT, and 8.1-fold in PVAT (*Figure 30*).

The transcription levels of Insulin Like Growth Factor 1 (*Igf1*) after cold exposure were also reduced in each investigated adipose tissue, being almost 4-fold downregulated in BAT, and 3.2-fold in PVAT (Figure 30). Interestingly, the levels of Igf1 are reduced in human calcified AVs[312] and its inhibition by Dipeptidyl Peptidase 4 (DPP-4) was found to induce AV calcification in vitro and in vivo[311].

Thrombomodulin (Thbd), which prevents High-Mobility Group Box 1 (HMGB1) to bind to the RAGE, what in turn is protective against AAA[317], was upregulated 1.6 fold in BAT and 1.4 fold in PVAT after cold exposure (*Figure 30*). HMGB1 is a DNA-binding protein, released following cytokine stimulation and after cell death[321]. RAGE is one of the receptors for HMGB1, and additionally faciliates a trasport route for HMGB1 and its partner molecule complexes by endocytosis to endolysosomal compartments. HMGB1 acts as a detergent in the lysosomal membrane and therefore its partner molecules will not be degraded in lysosomes but reach to the cytosol to induce inflammation.

Thrombomodulin assists in degradation of HGMB1, and was successfully used in japaneese clinical trials to treat disseminated intravascular coagulation in sepsis[322].

Two proteinase inhibitors – *Serpine2* and *Timp4* were downregulated after cold exposure in BAT and PVAT (*Figure 30*). These proteinase inhibitors were usually twofold, and each one of them may be protective against AAA by preventing the ECM from degradation[316,319,323].

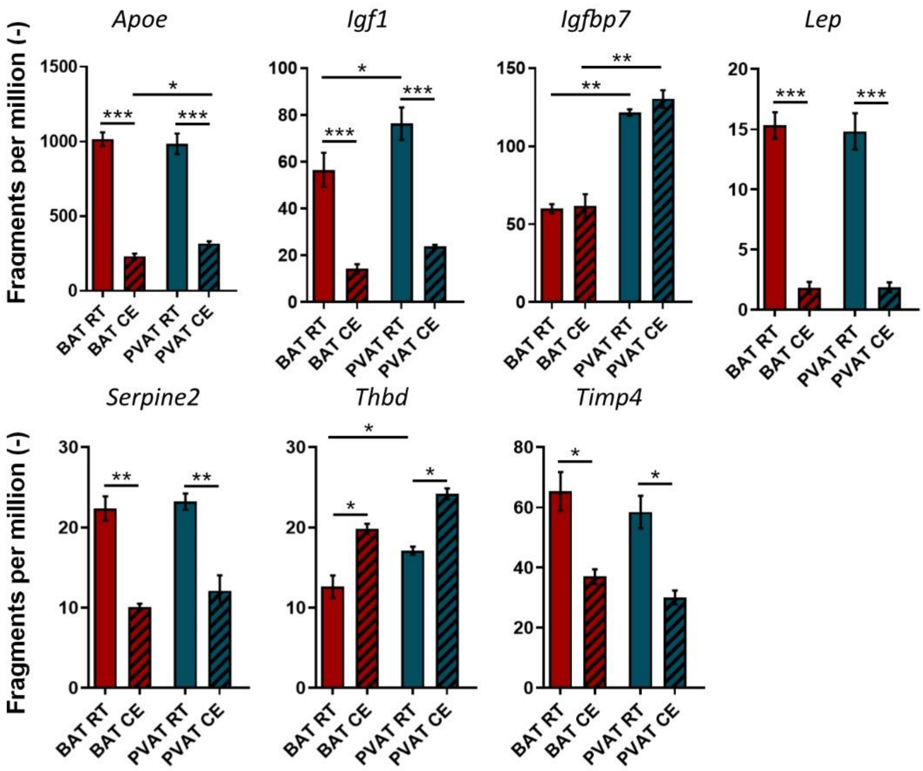

Figure 30. Expression of cold-responsive cytokines related to AA or AVD in BAT, and PVAT.

*CE = Tissue was exposed to cold, RT = Tissue was exposed to room temperature. Data shown as mean ± SEM. Wald test corrected for multiple testing by the Benjamini and Hochberg method. * adjusted $p \leq 0.05$, ** adjusted $p \leq e^{-10}$, *** adjusted $p \leq e^{-20}$. n = 4-5.*

4.4 Regulatory roles of cold-responsive miRNAs

miRNAs play role in transcriptional regulation of gene expression by interacting with mRNA and driving them into degradation. They may work inside of the cells of origin or be secreted into extracellular space as free miRNAs or be transported with extracellular vesicles. Therefore, they mediate intracellular communication[324] and may influence processes and diseases in other tissues[325]. In this chapter, I present analysis of miRNAs derived from cold exposed adipose tissues with focus on possible involvement of cold-responsive miRNAs in aortic valve disease and aortic aneurysm.

4.4.1 Cold-exposed adipose tissues and aortic valves present mostly unique cold-responsive miRNAs

To analyse miRNAs expression profiles in four adipose tissues in response to cold, miRNA sequencing of cold-exposed BAT, PVAT, WATi, and WATg was performed. The tissues were isolated from 8-weeks old mice, that were cold-exposed for three days at 16°C, followed by seven days at 4°C. The control mice were held at 23°C for 10 days. The most responsive tissues to cold exposure in terms of differential regulation of miRNA were BAT, PVAT, and WATg, which presented 71, 67, and 62 differentially regulated miRNAs, respectively. WATi showed only 20 miRNAs of differentially regulated miRNAs (*Figure 31*, *Figure 32*). Those numbers are comparable to results found in literature for BAT and WATi[326].

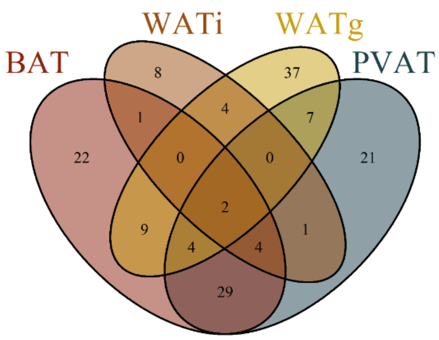

Figure 31. miRNA cold responsiveness is mostly unique in adipose tissues

Most cold-responsive (adjusted p value < 0.05 under cold exposure) miRNAs in WATg, and WATi were found to be cold-responsive only in those tissues. BAT and PVAT presented almost equal unique number of cold-responsive miRNAs and shared even more cold-responsive miRNAs, which made them the most similar tissues in terms of miRNA differential expression in response to cold. Additionally, PVAT and BAT presented the highest number of cold-responsive miRNAs, followed by WATg. miRNAs that were cold-responsive only in one adipose tissue are in tables in the Appendix part 7.2.

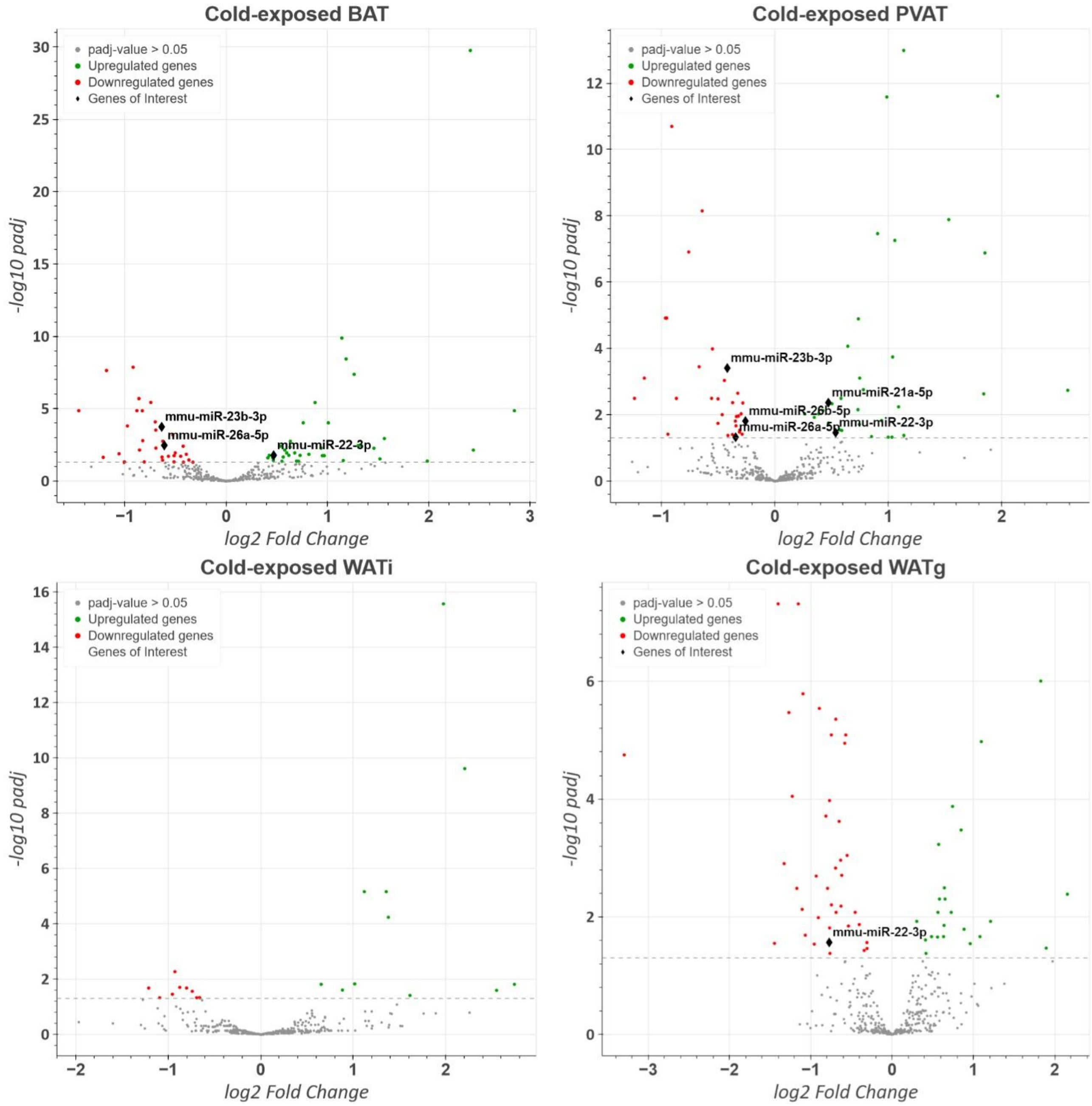

Figure 32. Effect of cold exposure on the expression of miRNA in brown adipose tissue (BAT), thoracic, perivascular adipose tissue (PVAT), gonadal white adipose tissue (WATg), and inguinal adipose tissue (WATi).

4.4.2 Cold-responsive miRNAs from adipose tissues and aortic valves target variety of genes associated with aortic valve stenosis and aortic aneurysms

Besides cytokines, adipose tissue-derived miRNAs may influence other tissues and organs[179]. I investigated general involvement of cold-responsive adipo-miRNAs in regulation of pathways and diseases. To achieve that, I performed miRNA validated target analysis using multiMiR package[201]. DisGeNET database contains one of the largest collections of genes and variants related to human diseases [217]. Unfortunately, no equivalent of this database exists for murine diseases. Therefore, I converted MGI gene symbols to HGNC symbols to subsequently query DisGeNET disease database [217]. Following, I divided results of miRNA sequencing to up- and downregulated, cold-responsive miRNAs' targets. Subsequently, I used WikiPathways[327] database to obtain an overview of cold-responsive adipo-miRNAs target pathways.

The majority of the most highly enriched pathways by cold-responsive, up- and downregulated adipo-miRNAs play role in metabolism, cellular proliferation, migration, and differentiation, cancer-related processes, and in signalling pathways of multiple interleukins (*Figure 33*).

Further, I analysed which diseases the cold-responsive adipo-miRNAs may affect by performing terms enrichment using DisGeNET[217] and database. Most of enriched disease terms of both up- and downregulated miRNAs are related to cancer, mental disorders, red blood cell count and haemoglobin changes (*Figure 34*).

The enriched pathways and disease terms are only an overview of the most significantly affected fraction of every enriched term or pathways from these analyses. One of the aims of this thesis was to investigate possible interactions of adipokines and miRNAs from cold-exposed adipose tissues, and therefore further analysis will be focusing on AA and AVD

To investigate roles of cold-exposed adipose tissues in AA and AVD, I filtered DisGeNET[217] enrichment results to match following patterns "valve sten", "valve calc", "valve dis" for aortic valve diseases, and "aneurysm", "dissection", "aortic dis", "aortic rupt", "aortic root dilat" for aneurysms.

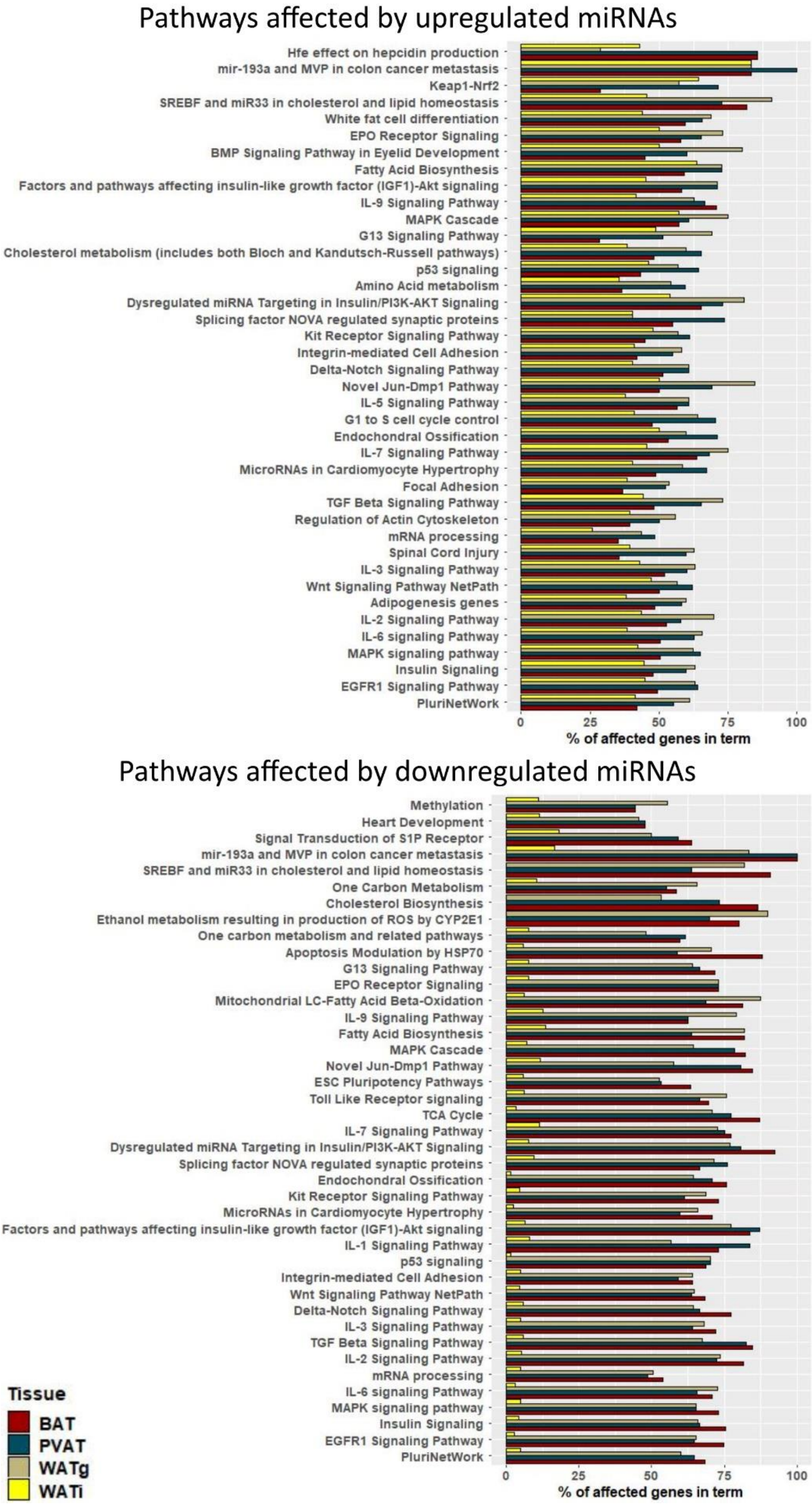

Figure 33. Most significantly affected pathways by up- and downregulated adipo-miRNAs

WikiPathways[327] enrichment analysis using targets of upregulated, cold-responsive miRNAs from brown (BAT), perivascular (PVAT), gonadal (WATg), and subcutaneous (WATi) adipose tissues using enrichR package[197].

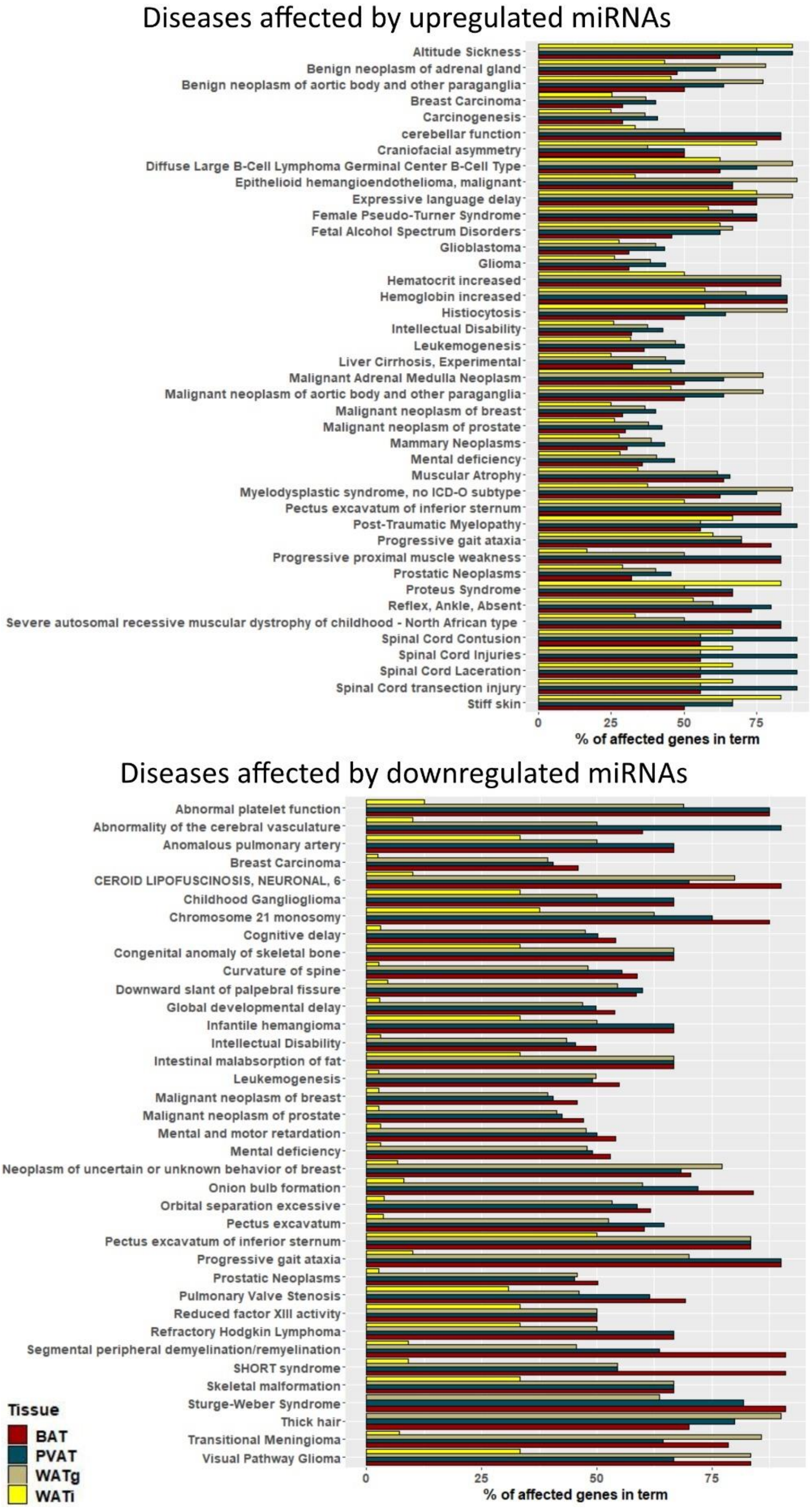

Figure 34. Most significantly affected disease terms by adipo-miRNAs, in which target genes of up- (top), and downregulated (bottom) miRNAs play roles.

DisGeNET[217] enrichment analysis using targets of upregulated, cold-responsive miRNAs from brown (BAT), perivascular (PVAT), gonadal (WATg), and subcutaneous (WATi) adipose tissues using enrichR package[197].

In general, upregulated miRNAs targeting genes related to AA and AVD had their expression moderately elevated, ranging from 27 to 100% increase (*Figure 35*). Downregulated miRNAs targeting genes related to AA and AVD were also moderately underexpressed (*Figure 35*).

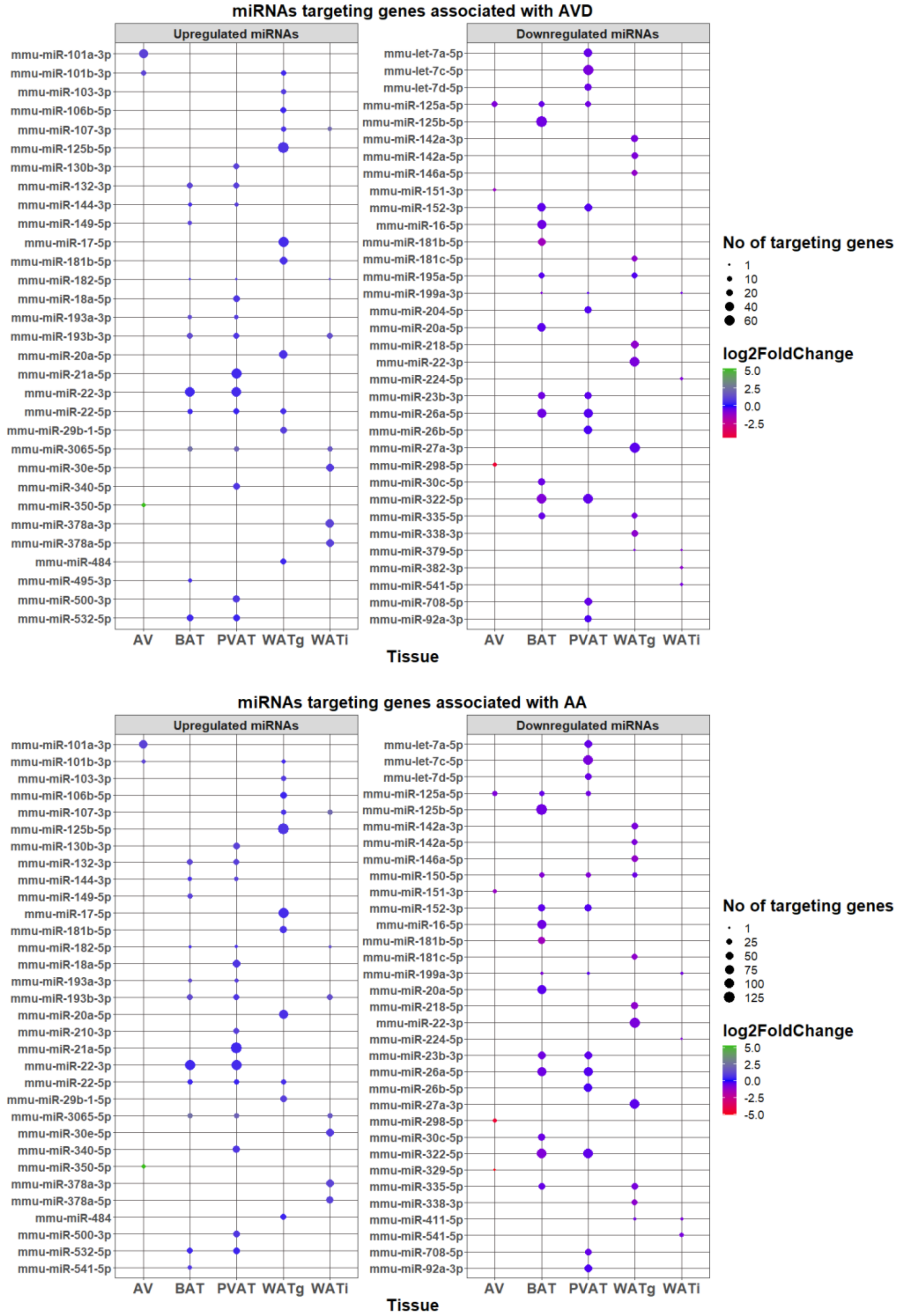

Figure 35. Cold-responsive miRNAs expressed in AV, BAT, PVAT, WATg, and WATi targeting genes associated with AVD (top) and AA (bottom).

Graphs show maximum top 10 miRNAs according to number of targeting genes for each tissue, and corresponding values of miRNAs that were found in top 10 in each other tissue. Missing dot means that the miRNA was not significantly, differentially regulated in given condition (padj > 0.05) or not detected.

miR-21a-5p and miR-22-3p were found to target the most of genes related to AVD or AA, according to previously stated search criteria. Their relative expression was in top 5 relevant miRNAs for aortic diseases in each tissue (*Figure 36*). miR-21a-5p was found to target 64 genes related to AVD and 128 genes related to AVD, while miR-22-3p was found to target 51 genes related to AVD and 111 related to AA.

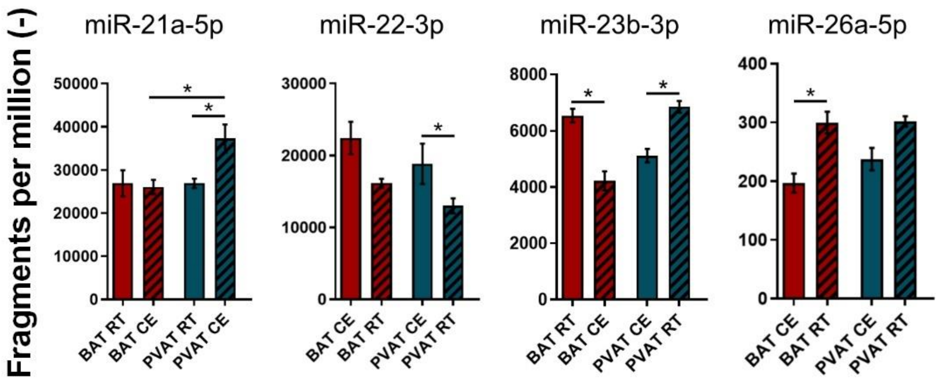

Figure 36. Expression of miR-21a-5p, miR-22-3p, miR-23b-3p, and miR-23a-5p in cold-exposed and control BAT, and PVAT.

*CE = Tissue was exposed to cold, RT = Tissue was exposed to room temperature. Data shown as mean ± SEM. Wald test corrected for multiple testing by the Benjamini and Hochberg method. *adjusted p ≤ 0.05. n = 3-5.*

miR-21a-5p targets 32 of 159 members of MAPK signalling pathway and 11 of 76 members of RAGE pathway, while miR-22-3p targets 48 of 159 and 17 of 76 members of MAPK signalling, and RAGE pathways, respectively. Together, miR-21a-5p and 22-3p target unique 70 of 159 members of MAPK signalling pathway and 25 of 76 of RAGE pathway.

miR-23b-3p and miR-26a-5p after cold exposure were downregulated in PVAT and BAT, while miR-26b-5p was only downregulated in PVAT. mir-23b-3p was found to target 23 genes related to AVD, and 50 genes related to AA, while miR-26a-5p was found to target 46, and 81 genes related to AVD and AA, respectively. miR-26b-5p was found to target 39 genes related to AVD, and 69 genes related to AA.

In total, differentially regulated miRNAs from cold-exposed BAT, PVAT, WATg, and WATi were found to target respectively 443 (BAT), 374 (PVAT), 428 (WATg), and 231 (WATi) genes related to AA or AVD. The most common targeted genes' transcripts related to AVD or AA by cold-responsive miRNAs from AV, BAT, PVAT, WATg, and WATi are shown in Figure 37.

In the list of most targeted genes related to AA and AVD (*Figure 37*), nine genes (*Egfr*, *Fos*, *Akt1*, *Braf*, *Nf1*, *Tgfb1*, *Tnf*, *Mapk8*, and *Tgfbr1)* belonged to the MAPK pathway, and seven (*Egfr*, *Akt1*, *Mmp9*, *Stat3*, *Sp1 Mapk8*, and *Smad3)* to the RAGE pathway.

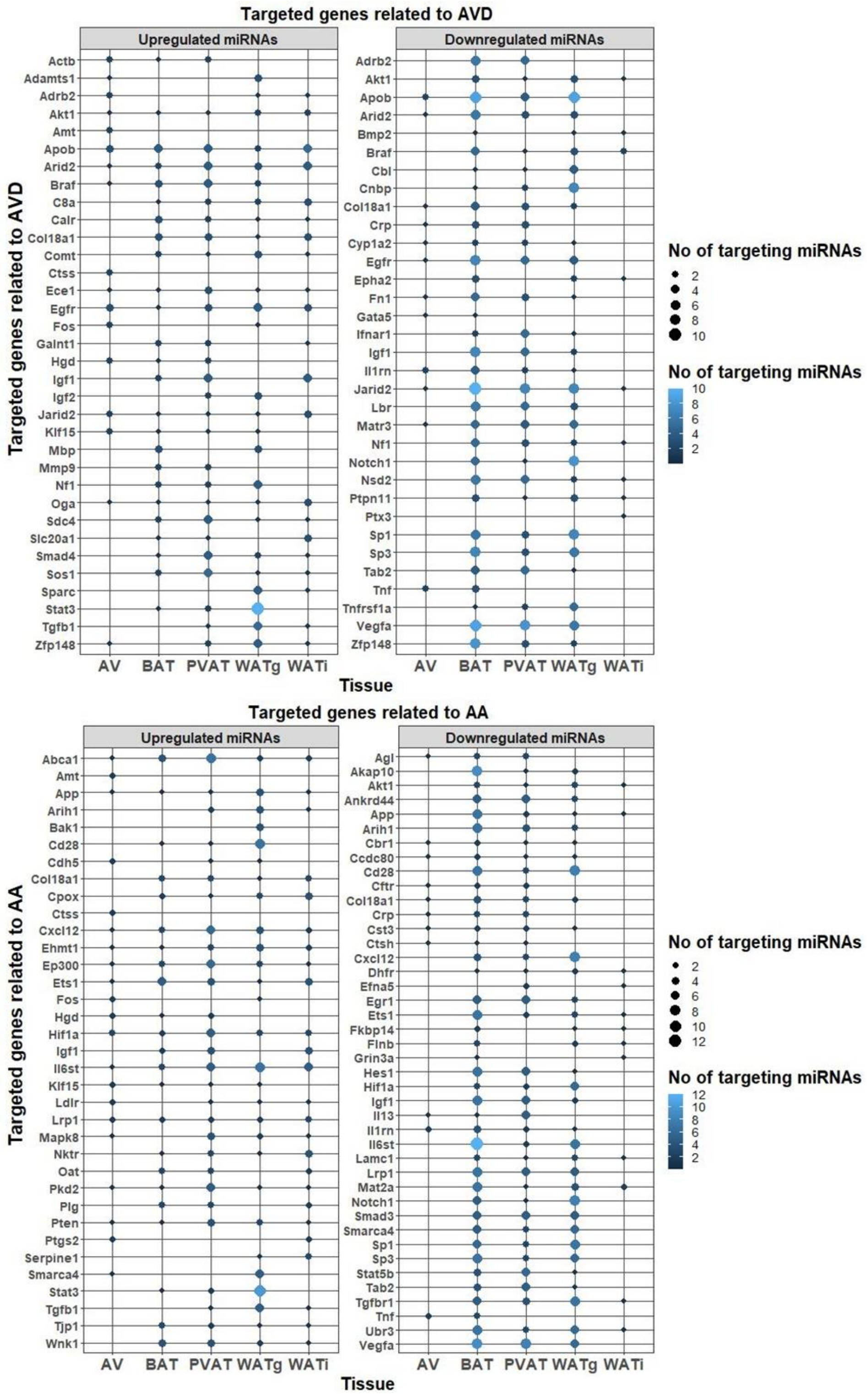

Figure 37. Combined top 10 most frequently targeted genes related to AVD (top) and AA (bottom) in AV, BAT, PVAT, WATg, and WATi by upregulated, cold-responsive miRNAs in those tissues.

4.4.3 Extracellular vesicles from mature BAi inhibit differentiation of acceptor BAi

Intercellular communication, besides cell-to-cell contact, include secretion, and release with membranous extracellular vesicles (EV), which may contain adipokines and miRNAs[328]. Therefore, I tested adipocytes' ability to communicate via EV, and to influence the adipogenic development in acceptor cells. Adipogenic development test was chosen because of adipogenesis-modulatory functions pf cytokines and miRNAs identified in chapters 4.1.5, 4.3.2, and 4.4.2.

To test the influence of secretory factors contained in EV on adipocytes differentiation, BAi were selected because the cell line isolation and development protocol were standardized and commonly used. Prior to extracellular vesicle treatments, the influence of extracellular-vesicles-free FBS was investigated with Oil Red O staining of intracellular lipids. Additionally, the cellular differentiation was stimulated with cGMP and inhibited for additional differentiation controls with Endothelin-1 (ET-1), which is adipocytes' differentiation inhibitor. The application of EV-depleted FBS for cell culture media has already resulted in reduction of lipid accumulation in BAi in every tested condition (*Figure 38*).

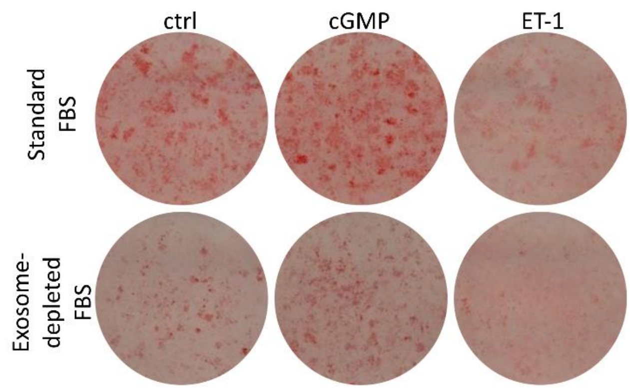

Figure 38. Growth of BAi in EVs-depleted FBS reduces cellular lipid accumulation.
Top row: BAi grown in standard FBS; bottom row: BAi grown in EVs-depleted FBS. From left: non-treated control BAi, cGMP-stimulated BAi, and differentiation-inhibited BAi.

Extracellular vesicles (EV) were isolated from supernatants of differentiated BAi, which were subsequently added to the cell cultures of differentiating, accepting BAi. Both donor and acceptor cells were grown in cell culture media supplemented with EV-depleted FBS to exclude the influence of EV originating from cell culture media. The addition of EV to the media of differentiating pre-adipocytes from day -2 to day 2 negatively impacted the differentiation potential of those pre-BAi. The treatment resulted in substantial, transcriptional downregulation of adipocyte-specific genes, that is *Pparg*, *Ucp1*, and *Fabp4*. The effect was similar to treatment with ET-1. Same trend was observed on protein level (*Figure 39*).

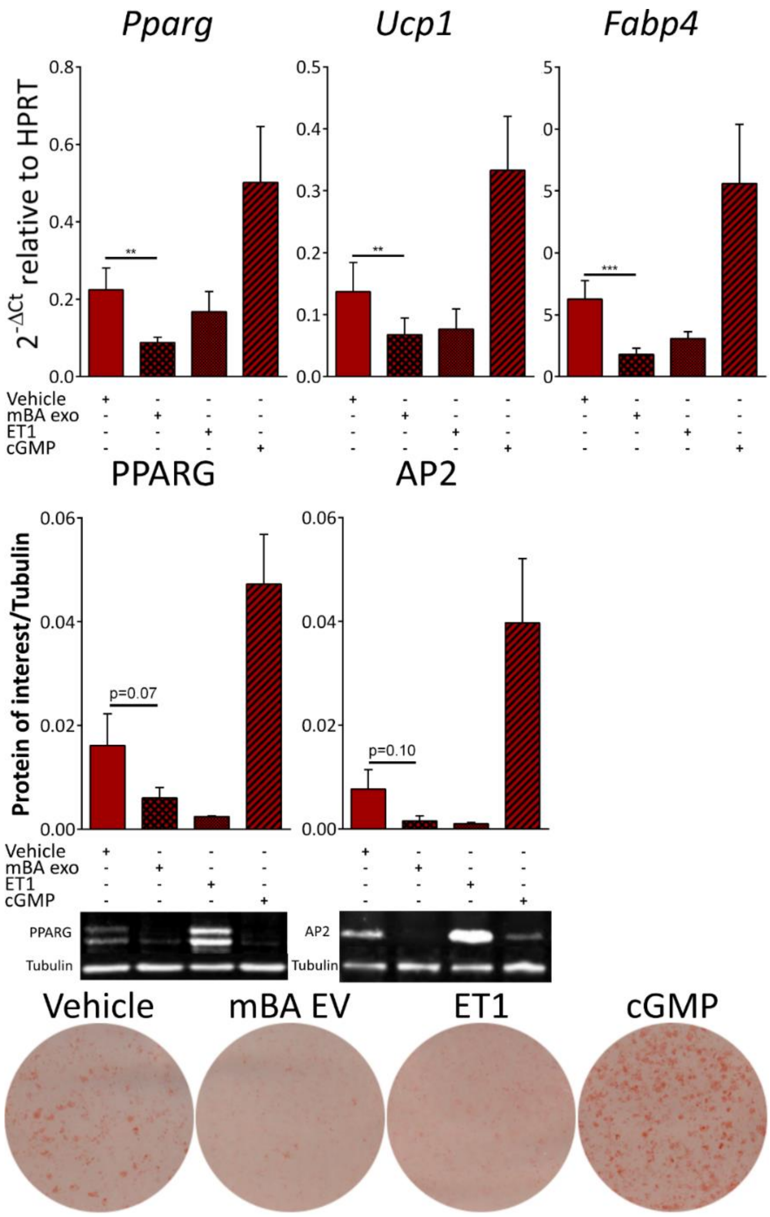

*Figure 39. Extracellular vesicles (EVs) from differentiated, immortalized brown adipocytes (BAi) inhibit acceptor BAi differentiation. Ratio paired T-test. * $p \leq 0.05$, ** $p \leq 0.01$, *** $p \leq 0.001$.*

This experiment demonstrated that secretory factors are needed for cellular differentiation, and that secretory factors contained in EV modulate processes in cells not directly connected with each other.

5 Discussion

Adipose tissue has been long considered as energy storing tissue. An additional function of brown adipose tissue, called thermogenesis, was first observed in the 1960s[329]. UCP1 was discovered in 1978[330]. An endocrine role of adipose tissue was identified by Siiteri in 1987[331,332]. In following years, adipose tissue was recognized as a secretory organ[333]. Multiple studies showed detrimental effects of adipose tissue disfunction[290,291,334–336], but less is known about the influence of adipose tissue activation by cold exposure on the development and progression of aortic diseases.

Therefore, this thesis investigated the effect of cold exposure on adipose tissues, with focus on secretory factors and their putative interaction with development and progression of AA and AVD.

5.1 First established model of immortalized perivascular adipocytes

My work resulted in the first *in vitro* model of immortalized perivascular adipocytes and their characterization. The isolation and differentiation of PVAi was complicated because of the scarcity and location of PVAT. It was also impossible to isolate the tissue from newborn mice due to the scarcity of the tissue. PVAi did not differentiate under the same conditions as BAi. Therefore, specific media composition needed to be found, along with optimal growth and differentiation conditions. The differentiation was achieved by induction media supplementation with the PPARγ agonist Rosiglitazone. To achieve the best results, the induction should be started two days after seeding and should take 4 days. My established model of PVAi induced for 4 days develops intercellular lipid droplets with the same mean size as BAi, expresses similar levels of UCP1, and reacts to NE stimulation as BAi. On the other hand, PVAi expresses lower levels of PPARG. Still, PVAi is a different brown cell type than BAi, which is clearly visible in different secretory profile, especially when 13% of analysed cytokines were detected only in PVAi or BAi, and 50% of cytokines were differentially secreted from PVAi and BAi. PVAi may be used in further research on importance of PVAT for vascular system and its involvement in disease occurrence, development, and progression. Additionally, loss of PVAT enhances atherosclerosis[337] and carries most probably further complications. Therefore, PVA may be needed for future replacement organs, for example as one of the cell types used in 3D organ and body parts printing.

5.2 PVAT IS MOSTLY SIMILAR TO BAT

Chronic cold exposure resulted in high transcriptional response in BAT, PVAT, WATg, and WATi, which resulted in over 2500 DEG per cold exposed adipose tissue. Most of enriched GO terms and pathways in every adipose tissue were metabolism-related, but each analysed fat depot revealed substantial unique subsets of differentially regulated genes. PVAT also shared the highest number of cold-responsive genes with BAT. On transcriptional level in adipocyte-related terms of adipocyte differentiation, adaptive thermogenesis, lipid localization, oxidative phosphorylation, and lipid catabolic process, BAT is more similar to PVAT than WATi to WATg. Hierarchical clustering for entire datasets, and adipose-related terms, and mitochondrial respiration measurements presented high similarities of BAT and PVAT, while lipolytic capabilities positioned PVAT between BAT and WATi. Transcriptional hierarchical clustering confirms, that PVAT is mostly similar to BAT, whereas WATi is closer to WATg, which is consistent with literature[108]. Additionally, functional comparison showed that PVAT is a BAT-like tissue. Ucp1 transcription, the marker for activated BAT and thermogenesis, is almost identical in both PVAT and BAT after exposure to room temperature or cold, which is consistent with previous non-cold exposed comparison of PVAT and BAT by Fitzgibbons et al[122]. PVAT and BAT responded very similarly to cold exposure in the subset of genes belonging to adaptive thermogenesis, lipid catabolic processes, and oxidative phosphorylation. Up to my knowledge, my study is the first study depicting striking transcriptional similarities of BAT and thoracic PVAT in response to chronic cold exposure.

The cellular morphology revealed that both PVA and BA contained multilocular lipid droplets. However, BA possesses higher number of lipid droplets and an increased droplet surface area, which might enhance the accessibility for lipases and catalases and explain the observed increased lipolytic capabilities of BAT *ex vivo*. The maximum levels of cAMP following NE stimulation were identical in PVAi and BAi, whereas EC50 was 2x higher in PVAi, probably due to reduced expression of *Adrb3*. The reduced levels of *Adrb3* in PVAT may be helpful in the recently described feature of PVAT to be able to take up and store NE[338,339].

These results suggest that thoracic PVAT should be rather considered as one of BAT depots with additional functions rather than a separate group of adipose tissue - similar to WATi and WATg considered as depots of white adipose tissue[340,341]. Moreover, PVAT is more similar to BAT that WATi to WATg. On transcriptional level, BAi presents higher levels of specific adipocyte markers compared to PVAi: *Adrb3*, *Fabp4*, *Pparg*, and *Ucp1*, which was not the case between PVAT and BAT in cold exposure or room temperature.

5.3 PVAT HAS ADDITIONAL VASCULAR REGULATORY FUNCTIONS

mRNA sequencing revealed additional functions of PVAT in response to cold related to muscle system process and muscle contraction (Figure 18). It is important to highlight, that PVAT was dissected using the microscope, so that no visible impurities were left in the sample.

Cold exposure causes peripheral vasoconstriction[342] and this effect might be partially caused by paracrine functions of PVAT. A study from 2020 showed that PVAT assists in arterial stress relaxation but was unable to conclude, if the effect was mechanical or paracrine[343]. Enrichment of GO Terms from domain biological process by downregulated genes from cold-exposed PVAT suggest that processes of cholesterol efflux are reduced, H_2S production may be suppressed (*Figure 45*), which would lead to vasoconstriction[344].

Adipose tissue is a source of stem cells, which may differentiate into SMCs[345–348]. Many DEG unique to cold-exposed PVAT typically belong to terms of muscle cell development and differentiation, which is triggered by cold exposure and indicates that PVAT may act as a donor of SMCs, and therefore may play an additional role in vascular regeneration. Indeed, vascular regeneration by resident and circulating stem cells was already shown in several pre-clinical studies[349–351]. Additionally, functional analysis of PVAT revealed that PVAT is the only adipose tissue with enhanced expression of genes responsible for cellular proliferation and vascular regeneration. My results show that cold exposure may enhance PVAT-mediated vascular regeneration.

5.4 ADIPOCYTES, ADIPOSE TISSUES AND AORTIC VALVES MAY COMMUNICATE WITH OTHER ORGANS AND TISSUES

Adipocytes need extracellular signals to differentiate *in vitro*, which I demonstrated in an experiment comparing differentiation levels of adipocytes grown in media using EV-depleted FBS (*Figure 38*). Moreover, fat cells communicate via extracellular vesicles with each other to remain in adequate differentiation status. Treatment of pre-adipocytes with extracellular vesicles isolated from fully differentiated BAi reduces differentiation level of the treated cells. As demonstrated, PVAi and BAi secrete plenitude of cytokines, which among others have been shown to influence adipogenesis, adipocyte differentiation, and development or progression of aortic diseases. Notably, Resistin and Interleukin-4 were undetected in supernatants of PVAi, in contrast to BAi. Both adipokines were detrimental in terms of development and progression of aortic valve disease or aortic aneurysms. On the other hand, PVAi secreted double the amount of TNF Receptor Superfamily Member 11B

(Tnfrsf11b) than BAi. This receptor was found to be protective against AA, and AVD[273–278], and was reported to be a decoy receptor preventing arterial calcification, inhibiting osteoclastogenesis, and protect against apoptosis[352,353]. Therefore, Tnfrsf11b is an important PVAT-derived adipokine that may be further investigated as a possible treatment of AA or AVD.

Besides cytokines, cells secrete multiple miRNAs that may control processes in the organism[324]. I showed that cold-responsive miRNAs were linked to their targets and processes which they affect inter- and intracellularly. Cold-responsive miRNAs from BAT, PVAT, WATg, and WATi present the highest involvement in adipogenesis, apoptosis, differentiation, proliferation, and immune response processes. These findings encourage further research to use cold exposure and PVAT activation as treatment and prevention of various diseases.

5.5 Adipose tissues may influence development and progression of aortic diseases

Adipose tissue has endocrine and paracrine functions besides storing lipids and playing role in thermogenesis [332]. Disfunctions of fat tissues have been linked to diabetes mellitus[354], cancer[355], and vascular diseases[356]. One of the main focuses of my thesis was identifying cytokines and miRNAs derived from cold-exposed adipose tissues, PVAT in particular, that may play role in development, progression or attenuation of AVD and AA. The limitations of this study were the fact, that it is not possible to assess the final effect of these findings on actual disease, and the number of cytokines or miRNAs being actually secreted and reaching the desired target tissue. However, the comparison of my results received from RNA sequencing with the DisGeNET database enabled me to highlight plenty of putative endocrine and paracrine interactions of fat tissues and aortic diseases.

Each adipose tissue presented between 192 to 314 cold-responsive cytokines' transcripts (Figure 28), at which the smallest number belongs to WATg, and the highest to WATi. Each fat depot had also a subset of differentially regulated cytokines' genes that were not found in other depots. From hundreds of genes, only a few were found to be described to play a role in AVD or AA. This may have been caused by low sequencing depth or ambiguous reads obtained as a result of 3'mRNA sequencing, which may have hidden significant differences in genes with low expression, e.g., part of cytokines. Another possibility may be that cytokines in DisGeNET database were not cold-responsive in adipose tissues or that many roles of cytokines in aortic diseases were not yet discovered.

Since adipose tissue does not contain adipocytes only, the secretion profile of PVAi and BAi was analysed. The cytokine assay revealed multiple secretory differences between these two cell types, especially visible in CCL, CXCL, and IGFBP protein families. Additionally, detected cytokines were compared with AVD and AA disease terms in DisGeNET database[217]. Many cytokines were linked to the selected diseases of aorta, suggesting that adipocytes may play a role in aortic valve and aorta homeostasis.

Leptin has been reported to induce AAA[357,358] and osteoblast differentiation of VICs via Akt and ERK signalling[313]. Chronic leptin stimulation of VICs was found to enhance ALPL activity and increase the expression of BMP-2 and RUNX2. Both proteins participate in development of AVD and AA[359–362]. Leptin transcription was severely reduced upon long-term cold exposure in all investigated adipose tissues, accounting for over 8-fold reduction in BAT and PVAT, over 3-fold in WATi, and 2.4-fold in WATg. This reduction of leptin production in adipose tissues may be beneficial in putative therapies against AVD or AA, of course in assumption that the body weight does not increase.

Thrombomodulin prevents HMGB1 from binding to RAGE by its degradation and, thus, RAGE pathway activation and $CaCl_2$-induced AAA[317]. Additionally, Thrombomodulin inhibits TNF-α production and therefore reduces inflammation. TNF-α also activates macrophages to produce HMGB1[363]. Thrombomodulin is mildly upregulated in cold-exposed PVAT and BAT, but severely downregulated in WATi and WATg. However, the direct contact of PVAT with aorta and its expression of thrombomodulin may play a more important, beneficial role on AAA than the protein derived from other adipose tissues.

ApoE was downregulated in BAT, PVAT, and in WATi following cold exposure. ApoE deficiency was reported to have a detrimental effect on severity of AVD in senile mice[56], presenting a probable negative effect of cold exposure caused *ApoE* downregulation on AVD development. *Igf1*, *Serpine2*, *and Timp4* were downregulated in every analysed adipose tissue upon cold exposure, which again could play negative role for development of AVD.

In summary of cytokine expression in cold exposed adipose tissues, downregulation of *Lep*, and upregulation of *Thbd* was found to be most beneficial for preventing the development or progression of AA and AVD.

Another type of intracellular interactions between fat tissues and aortic valves or aorta are secreted miRNAs. To identify possible miRNAs released in adipose tissues that may influence the development, progression or regression of aortic diseases, miRNA sequencing of whole adipose tissues and aortic valves was performed. It enabled me to identify important candidates for AA and AVD treatment, although miRNA sequencing of whole tissues cannot distinguish which miRNA and in what extent is being secreted.

The most upregulated or downregulated miRNAs from adipose tissues did not target a substantial number of genes' transcripts related to AVD or AA. miRNAs that were mildly affected by cold exposure, were described to target sometimes over a hundred transcripts of different genes belonging e.g., to the RAGE or MAPK/ERK signalling and associated to AVD or AA.

In vitro studies indicate involvement of receptor for advanced glycated end-products pathway (RAGE) to promote the development of calcific AVD via osteoblastic differentiation of VICs in the aortic valve[54,364]. Another study demonstrates participation of MAPK/ERK in the process of VICs calcification[97]. Multiple studies indicate involvement of RAGE pathway also in aortic aneurysm[365]. Inhibition of MAPK-ERK pathway or RAGE were suggested as a treatment against AA and AVD[366–368]. Hence, RAGE and MAPK pathways' members were investigated as potential targets of cold-responsive, adipose tissue-derived miRNAs, and indeed targeted by cold-responsive adipo-miRNAs.

This study revealed a substantial overlap of adipose tissue-derived, cold-responsive miRNAs' targets with members of both above mentioned pathways (Figure 40, Figure *41*). RAGE pathway[327] consists of 76 members, whereas 49 of them are validated targets of cold-upregulated adipo-miRNAs, and 55 of them are validated targets of cold-downregulated adipo-miRNAs.

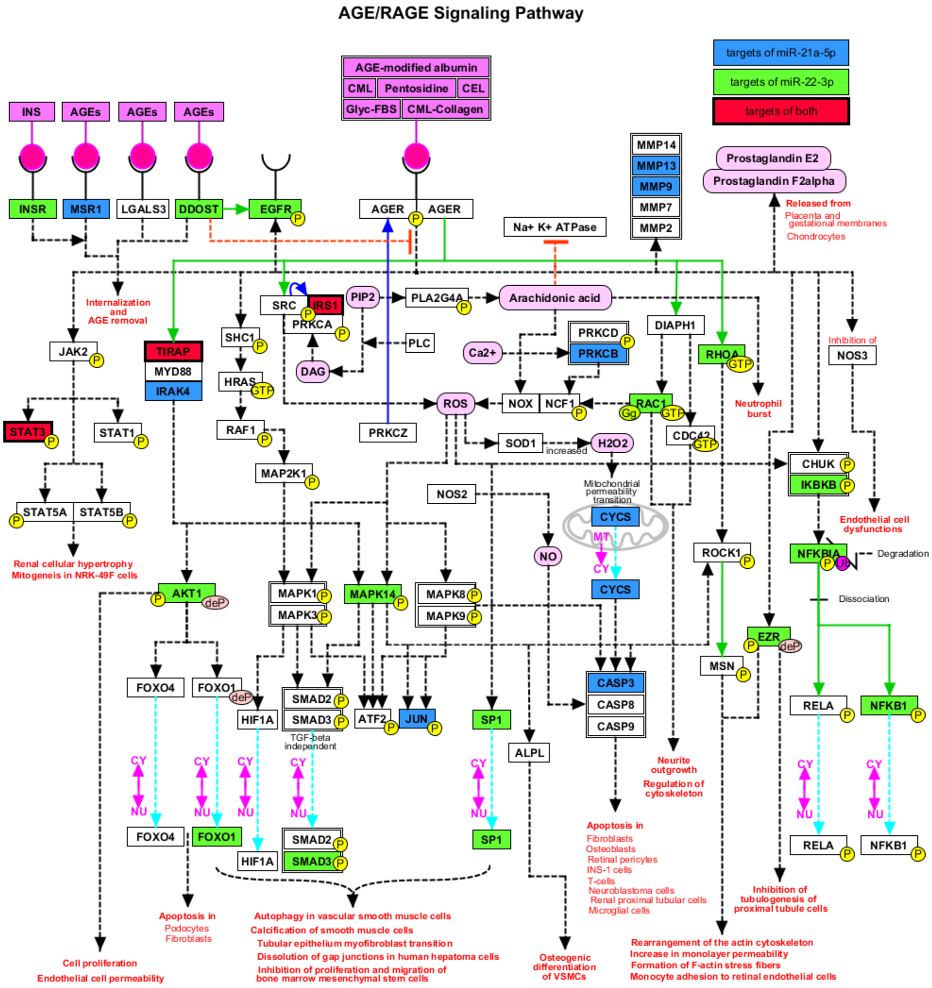

Figure 40. RAGE pathway members targeted by miR-21a-5p and miR-22-3p.

Targets of miR-21a-5p are marked in blue, targets of miR-22-3p are marked in green, and targets of both are marked in red. Original pathway maintained by NetPath, Alexander Pico, Christine Chichester, et al. was downloaded from wikipathways.org[327]

The MAPK pathway[327] has 159 members, from which 124 and 126 are validated targets of cold-up-, and downregulated adipo-miRNAs, respectively. Targeted members of the MAPK pathways are shown on Figure *41*.

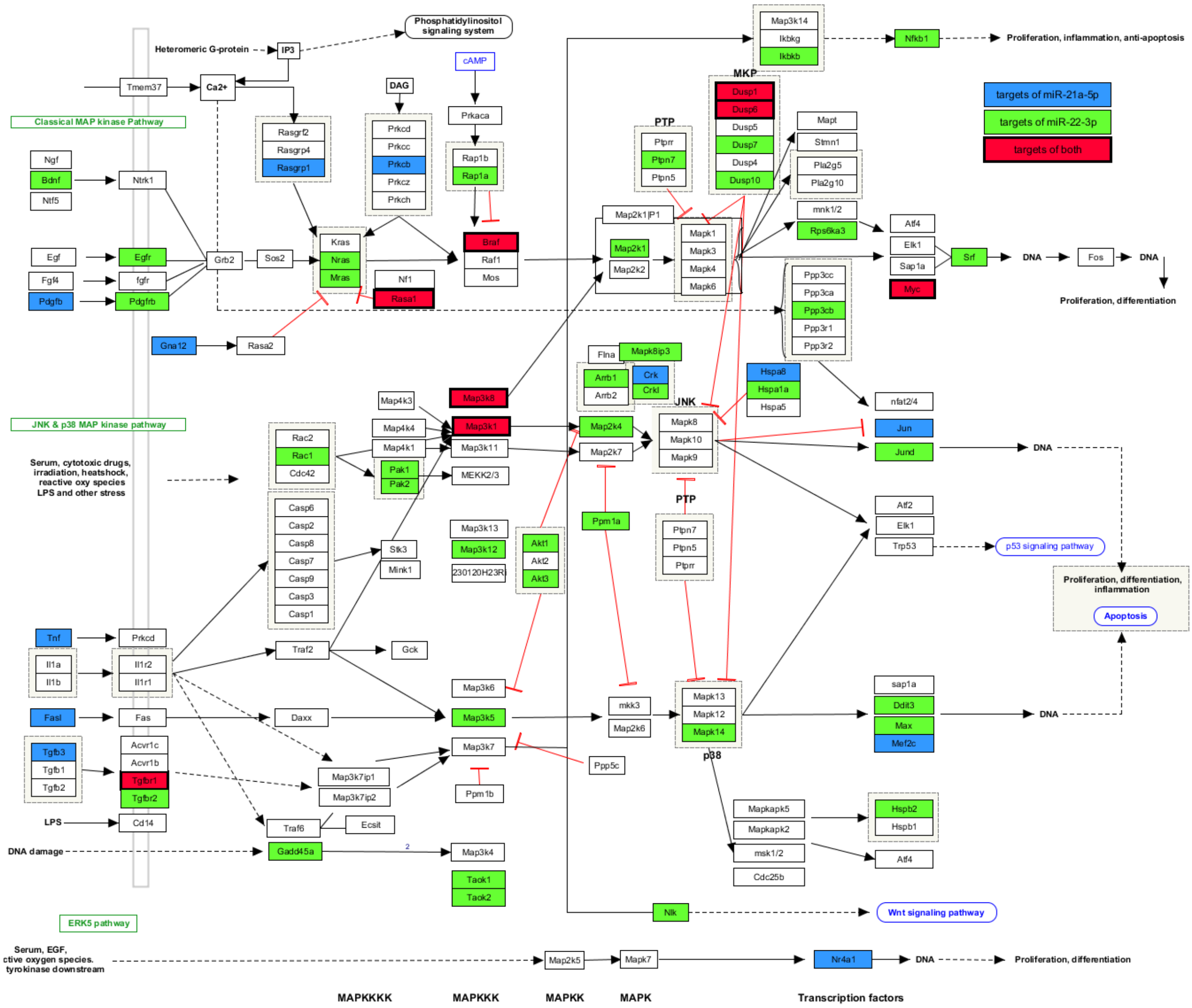

Figure 41. MAPK pathway members targeted by miR-21a-5p and miR-22-3p.

Targets of miR-21a-5p are marked in blue, targets of miR-22-3p are marked in green, and targets of both are marked in red. Original pathway maintained by Sebastien Burel, Kristina Hanspers, Martina Kutmon, Denise Slenter, et al. was downloaded from wikipathways.org[327]

Two most promising miRNAs from cold-exposed PVAT, miR-21a-5p and miR-22-3p were found to target 64, and 51 genes' transcripts associated with AVD and 128 and 111 genes' transcripts associated with AA. miR-21a-5p was upregulated 1.39-fold, and miR-22-3p, 1.45-fold in cold exposure PVAT. Intriguingly, miR-21a-5p and miR-22-3p belong to the top 10 miRNAs with the highest expression in PVAT. Additionally, miR-21a-5p was found to be cold-responsive in PVAT only. miR-21a-5p alone was found to target 32 out of 172 members of MAPK pathway and 11 out of 80 members of RAGE pathway. miR-22-3p targets 17 from 76 members of RAGE and 49 of 159 members of MAPK pathways.

Both miR-21-3p and miR-22-3p were among the miRNAs with the highest expression from miRNAs targeting AVD and AA associated genes in every analysed tissue, although they were not always cold-responsive. Number of targets and their relative expression is a valid reason to prioritize them in further study of cold-responsive, adipose-derived miRNAs against aortic diseases. The degree of upregulation may not be as important as the total number of targeted RAGE and MAPK pathways members, as the miRNAs would downregulate substantial numbers of these two pathways.

Many of validated targets of cold-responsive miRNAs that were associated with AVD or AA, were members of MAPK and RAGE pathways. This may have been caused not only by the importance of those pathways for AVD and AA but also the fact that those pathways were most studied in relation to those diseases. Since the analysis focused on validated miRNA targets and known genes listed in AVD- and AA-related terms in DisGeNET database, additional, potential players not being present in this database might have been missed. Additionally, the global cold-induced miRNA transcription profile and its effects needs *to be* validated *in vivo*. Both RAGE and MAPK pathways are targeted by up-, and downregulated miRNAs, which creates more complexity to the mechanism of action of the miRNAs. RAGE itself was not a validated target of any miRNA investigated in this study. Soluble RAGE plays a protective role in cardiovascular diseases, acting as a scavenger receptor in the circulation[365]. Combined action of cold-induced, adipo-miRNAs suggests beneficial effect against development and progression of AVD and AA. Moreover, cold-induced lipid clearance, substantial reduction of leptin transcription, and increased transcription of ADIPOQ may reinforce possible protective paracrine and endocrine functions of adipose tissues.

One of the major risk factors of aortic diseases is obesity. Therefore, it is reasonable to suspect that the levels of cytokines and miRNAs circulating in obese organism is dysregulated, which in turn could promote the development and progression of aortic diseases. Hence, it would be worthwhile to repeat the analysis in obese models. The regulatory processes of organisms are enormously complex, especially via miRNAs. With dozens of cold-responsive, adipose tissue-derived miRNAs targeting sometimes over hundred transcripts associated with aortic diseases, the final protective or detrimental effect of adipose tissue activation is most probably caused by combined action of secretory factors. The proximity of PVAT to aortic valves and aorta potentially makes PVAT the most important adipose tissue that may influence the progression and development of AA and AVD via secreted miRNAs and cytokines.

6 SUMMARY

Aortic valve disease (AVD) is common for people over 65 and its severity increases with age. Aortic aneurysm (AA) is the tenth cause of death for men above 55. Its prevalence was estimated to be up to 8.9% for men and up to 2.2% for women. There is no pharmaceutical treatment for both diseases. The only treatment for the patients suffering from AVD or AA is surgery.

In the last two decades, adipose tissues gathered more attention due to discoveries that shows that adipose tissues serve as an energy storage and play important endocrine, paracrine and thermoregulatory roles. It has been found that adipose tissues secrete cytokines and miRNAs that influence other tissues and organs. Dysfunctional adipose tissue may be causing major diseases.

Recently, perivascular adipose tissue gained more interest due to its location around blood vessels and new discoveries, which show that it regulates processes within vasculature and affects the development of atherosclerosis.

To analyse secretory factors derived from adipocytes in PVAT, I have established a model of immortalized perivascular adipocytes (PVAi). Analysis of adipokines from PVAi and immortalized brown adipocytes (BAi) led to identification of substantially different secretory profile of those two cell types. Moreover, my work highlighted the additional vascular regulatory and regenerative function of PVAT. In addition, it provided high-throughput transcriptome analysis of cold-responsive, adipose tissue-derived cytokines and miRNAs and connected them with vast amount of data in DisGeNET database, emphasizing adipose-derived cytokines and miRNAs as prevention or treatment for AVD and AA. This work identified two most promising, cold-upregulated miRNAs in PVAT that together target 33% of RAGE, and 44% of MAPK pathways members. Up to my knowledge, my thesis describes for the first time cold-responsive, perivascular adipose tissue-derived miRNAs that inhibit RAGE and MAPK pathways and might be utilized to treat aortic valve disease and aortic aneurysm.

7 APPENDIX

7.1 COLD-RESPONSIVE GENES FOUND ONLY IN ONE ADIPOSE TISSUE

Cold-responsive protein-coding genes (also predicted), and lncRNA genes found in BAT but not in PVAT, WATg, or WATi:

SYMBOL	log2(fold change)	Ratio	padj	Mean FPM BAT 4°C	Mean FPM BAT 23°C
1500004A13Rik	-1.607	0.328	0.03397482	0.383	1.168
1600020E01Rik	-0.563	0.677	0.03143909	6.774	9.995
1700001K23Rik	-2.177	0.221	0.04261918	0.149	0.674
1700008J07Rik	0.767	1.702	0.00011483	9.99	5.842
1700018G05Rik	2.993	7.963	0.00021462	1.421	0.176
1700052K11Rik	0.568	1.482	0.03189497	7.424	5.025
1700056E22Rik	0.624	1.541	0.00412126	9.426	6.133
1700112H15Rik	2.558	5.887	0.02381366	0.757	0.126
1810041H14Rik	1.161	2.236	0.01763185	2.112	0.936
2010001A14Rik	0.77	1.705	0.00255518	7.128	4.194
2310001H17Rik	-0.641	0.641	0.02385871	3.998	6.255
2310015D24Rik	-2.022	0.246	0.02650351	0.241	0.964
2310058D17Rik	1.253	2.384	0.04352301	1.479	0.63
2500004C02Rik	-1.104	0.465	0.04949321	0.894	1.912
2610037D02Rik	-0.683	0.623	0.0028515	6.603	10.623
2610507I01Rik	-0.869	0.548	0.03599933	2.016	3.678
2700049A03Rik	-0.816	0.568	0.01349632	2.506	4.437
2810006K23Rik	-0.45	0.732	0.0171298	12.438	17.029
2900052N01Rik	-1.571	0.337	0.00294713	0.752	2.218
2900076A07Rik	-1.249	0.421	0.00456086	1.321	3.14
3110056K07Rik	-0.585	0.667	0.03952678	4.284	6.441
4631405J19Rik	4.855	28.94	7.9876E-05	1.028	0.026
4732419C18Rik	-1.761	0.295	0.00022936	0.775	2.621
4833420G17Rik	-0.345	0.788	0.03053943	12.509	15.883
4930438E09Rik	-1.077	0.474	0.00449799	1.78	3.759
4930465I24Rik	3.349	10.19	0.03400306	0.538	0.044
4930556M19Rik	1.184	2.271	0.04161857	2.147	0.947
4930572G02Rik	2.52	5.734	0.04924925	0.593	0.105
4930597O21Rik	4.067	16.76	0.00482931	0.591	0.026
5430420F09Rik	-2.226	0.214	0.03246636	0.182	0.833
5830444B04Rik	-1.196	0.436	0.02789203	0.847	1.966
9430085M18Rik	1.168	2.247	0.0414921	1.717	0.759
9630013K17Rik	2.158	4.463	0.03608218	0.807	0.182
A230072C01Rik	-1.147	0.452	0.03360009	0.88	1.969
A430019L02Rik	-1.298	0.407	0.03911557	0.598	1.464
A430027C01Rik	-0.859	0.551	0.04939712	1.552	2.794

A530010L16Rik	2.323	5.005	0.01872638	0.885	0.173
A530041M06Rik	-0.674	0.627	0.00521431	4.34	6.911
A630072L19Rik	-1.863	0.275	0.03911971	0.236	0.856
A930004D18Rik	-2.233	0.213	0.00553052	0.29	1.376
Aatk	0.705	1.63	0.00299931	46.989	28.85
Abcc1	-0.426	0.744	0.02485477	12.77	17.138
Abcc8	3.289	9.772	1.606E-07	2.756	0.282
Abcc9	0.521	1.435	2.0767E-05	35.248	24.569
Abr	0.647	1.566	0.01539654	6.794	4.367
Abtb2	0.79	1.729	0.02164729	4.491	2.599
Accs	-0.569	0.674	0.04265025	3.618	5.373
Acp2	-0.325	0.798	0.02406586	23.648	29.676
Adamtsl3	-2.218	0.215	6.4471E-07	0.898	4.16
Adcy4	0.769	1.704	0.00081422	14.631	8.626
Adrb2	-1.309	0.404	0.04488015	0.759	1.913
Adssl1	-0.507	0.704	0.00842604	14.596	20.769
Agap3	0.335	1.262	0.03761831	17.66	14.03
Agk	-0.785	0.581	0.01395922	2.792	4.827
Akap8l	-0.55	0.683	0.02475106	10.224	15.005
Akip1	-0.548	0.684	0.00415481	9.099	13.287
Akt1	0.511	1.425	0.00257963	65.768	46.223
Akt3	0.671	1.592	0.03407487	5.983	3.76
Aldh16a1	0.597	1.512	0.00050328	15.189	10.072
Alms1	-1.571	0.337	0.00642985	0.658	1.943
Als2cl	0.526	1.44	0.00654825	12.36	8.548
Amotl1	-0.551	0.683	0.00018663	78.976	115.697
Angel2	0.275	1.21	0.02060975	44.271	36.599
Angptl1	-1.334	0.397	0.00256685	1.904	4.775
Angptl3	-0.808	0.571	0.01575661	2.755	4.816
Ankrd12	-0.558	0.679	9.8162E-05	80.955	119.264
Anxa7	0.341	1.266	0.00208834	48.906	38.588
Aplf	-1.141	0.453	0.04668541	0.946	2.096
Apold1	1.095	2.136	0.04228019	21.657	10.157
Appbp2os	2.317	4.984	0.00970985	1.003	0.194
Appl1	-0.498	0.708	2.4821E-05	22.943	32.371
Arc	-1.695	0.309	0.01251727	0.448	1.448
Arfip2	0.365	1.288	0.04224293	29.035	22.564
Arhgap19	-1.42	0.374	0.02200489	0.618	1.659
Arhgap27	0.686	1.609	0.01485703	7.348	4.589
Arhgdia	0.317	1.245	0.00742672	42.076	33.839
Arhgef15	0.422	1.34	0.01193754	25.532	19.104
Arhgef6	-0.831	0.562	2.9245E-05	6.495	11.529
Arid5b	-0.277	0.825	0.03542834	36.965	44.866
Arl1	-0.312	0.805	0.02104767	28.218	34.962
Arl5a	0.474	1.389	0.04875638	11.202	8.074
Armc6	1.323	2.502	9.1171E-07	6.016	2.397
Arntl2	-0.984	0.506	0.01596969	1.414	2.8

As3mt	0.669	1.59	0.01496026	7.816	4.922
Atad2b	-0.395	0.76	0.00180657	33.16	43.618
Atat1	0.648	1.567	2.7694E-07	33.842	21.653
Atm	-0.427	0.744	0.02835477	9.804	13.182
Atp6ap2	0.307	1.237	0.01038323	42.715	34.526
Atp6v0a1	0.307	1.237	0.03526389	31.395	25.396
Atp9a	0.304	1.235	0.02648363	90.09	72.965
AU040320	0.64	1.559	6.6074E-06	22.239	14.236
Axin1	0.526	1.44	0.01007309	11.715	8.102
Azin1	-0.392	0.762	0.00045509	27.238	35.744
B130021K23Rik	-1.086	0.471	0.04587496	0.797	1.702
B230377A18Rik	1.406	2.65	0.00500786	2.397	0.915
B3galt6	0.586	1.502	0.03770154	5.271	3.515
B4galt1	0.459	1.374	0.00278465	84.294	61.407
B9d2	0.674	1.595	0.00226	8.456	5.291
Babam2	0.439	1.356	0.00046918	45.332	33.499
Bach2	0.993	1.99	0.04434167	2.43	1.239
Baz2b	-0.397	0.759	0.00013065	77.353	101.873
Bbx	-0.452	0.731	0.00208781	19.816	27.076
BC060293	-1.781	0.291	0.00037953	0.868	2.982
Bcl2l12	-1.079	0.474	0.00691601	1.441	3.066
Bcl3	0.738	1.668	7.5286E-08	24.108	14.448
Bcorl1	-0.532	0.691	0.01013741	12.848	18.613
Bhlha9	5.278	38.8	1.3399E-05	0.918	0
Bnc2	-1.66	0.316	0.00611423	0.655	2.078
Bnip1	0.532	1.446	0.01033383	10.968	7.582
Bop1	0.555	1.469	0.007648	11.874	8.094
Bphl	0.364	1.287	0.01879887	32.833	25.454
Brap	0.413	1.331	0.00277722	44.581	33.557
Brca2	-0.852	0.554	0.03000001	2.065	3.749
Brf1	0.394	1.314	0.02784296	13.517	10.319
Brox	0.403	1.322	0.03738661	14.854	11.281
Brwd1	-0.288	0.819	0.03143909	27.224	33.306
Btbd11	-2.841	0.14	0.01498909	0.122	0.85
Cables2	0.464	1.379	0.03547805	10.369	7.526
Cacna1d	1.33	2.514	0.03593174	1.631	0.658
Calr3	-1.158	0.448	0.01077237	1.072	2.388
Camk2n2	1.767	3.404	5.7026E-06	3.686	1.09
Camkmt	-0.896	0.537	0.04135204	1.537	2.862
Cbx4	-0.294	0.815	0.00200603	46.723	57.31
Ccdc142os	1.662	3.164	0.04111993	1.478	0.473
ccdc198	2.803	6.978	0.0009228	1.447	0.213
Ccdc34	-0.995	0.502	4.3514E-09	8.189	16.342
Ccdc71	0.387	1.308	0.04840202	13.04	9.958
Ccdc77	-0.868	0.548	0.00036609	4.414	8.074
Ccdc85c	0.547	1.461	0.01940354	8.079	5.535
Ccl5	-1.692	0.309	0.0033373	0.833	2.701
Ccnh	-0.33	0.796	0.01960027	20.36	25.546

Ccni	-0.383	0.767	1.7366E-05	74.252	96.74
Ccny	0.224	1.168	0.0225125	53.475	45.748
Cct8	0.196	1.146	0.03977661	100.856	87.94
Cd247	-2.366	0.194	0.00084441	0.292	1.517
Cd52	-0.725	0.605	0.04657498	3.104	5.135
Cd55	-1.037	0.487	0.016087	1.43	2.957
Cdc123	-0.245	0.844	0.04996376	33.23	39.438
Cdc27	0.301	1.232	0.04763162	22.389	18.146
Cdc40	-0.372	0.772	0.01583066	19.264	24.913
Cdh2	-0.735	0.601	0.00161212	4.681	7.794
Cdhr5	-2.567	0.169	0.03414939	0.118	0.707
Cdk12	-0.492	0.711	5.5242E-05	30.626	43.11
Celsr1	-3.818	0.071	0.01575872	0.032	0.577
Cenpb	0.465	1.38	3.4695E-05	87.282	63.317
Cenpc1	-0.987	0.505	0.00025628	3.219	6.333
Cenpw	-1.367	0.388	0.00184878	1.158	2.989
Cep295	-0.507	0.703	0.03612296	5.595	7.971
Cep350	-0.276	0.826	0.01351889	32.99	39.914
Cep78	-1.187	0.439	0.0105152	1.037	2.365
Cfap54	-1.073	0.475	0.00359904	1.941	4.086
Chac1	1.097	2.139	0.03243937	2.146	1.016
Chchd6	-0.323	0.799	0.01155835	40.949	51.256
Chid1	0.379	1.3	0.01423558	21.262	16.35
Chrdl2	3.497	11.29	0.01068903	0.596	0.049
Cib4	-3.335	0.099	0.01923931	0.061	0.612
Cited1	1.969	3.914	0.0224404	1.01	0.26
Clasp2	-0.383	0.767	0.00225879	25.936	33.812
Clec2d	-1.133	0.456	0.00997036	1.343	2.94
Clec7a	-1.495	0.355	0.00309428	0.859	2.404
Clic5	-0.265	0.832	0.01620795	77.399	92.886
Cnot1	-0.461	0.726	0.00084824	19.855	27.317
Cnot6l	-0.278	0.825	0.02995862	38.827	46.987
Col12a1	-1.214	0.431	0.0010806	2.198	5.083
Comt	3.504	11.35	0.02265748	0.599	0.054
Coq4	0.399	1.318	0.02608272	14.766	11.241
Coro1c	0.521	1.435	0.04331337	9.93	6.885
Cptp	0.732	1.66	0.03306371	4.63	2.791
Cradd	0.732	1.661	0.0135794	7.227	4.383
Crim1	0.481	1.395	0.00011522	30.045	21.568
Crlf2	0.874	1.833	0.00459845	5.278	2.888
Crybg2	3.268	9.635	0.00220339	0.979	0.098
Cryl1	-0.613	0.654	0.00339335	6.765	10.355
Cspp1	-0.44	0.737	0.00079887	18.687	25.316
Ctcflos	0.392	1.312	0.01619416	55.513	42.391
Ctdsp1	0.399	1.319	0.04218821	20.108	15.276
Ctdspl2	-0.718	0.608	0.00047343	6.514	10.74
Ctnnbip1	0.496	1.411	0.00140631	57.097	40.502
Ctnnbl1	0.433	1.35	0.01019429	15.376	11.403

Cwf19l2	-0.417	0.749	5.5769E-06	48.914	65.3
Cxxc5	-0.568	0.675	0.00500863	14.834	21.929
Cyb561	1.718	3.289	0.00011653	2.703	0.822
Cyp2c70	3.161	8.942	0.01617073	0.686	0.075
Cyp4a10	1.87	3.656	0.02171241	1.04	0.288
Cyp4b1	0.827	1.774	0.00026325	17.046	9.608
Cytip	-1.563	0.338	0.00540528	0.623	1.838
D030028A08Rik	-0.928	0.526	0.04532182	1.282	2.444
D730044K07Rik	1.857	3.623	0.04998876	0.94	0.26
Daxx	0.372	1.294	0.02966972	16.967	13.119
Dbnl	0.634	1.551	1.3075E-06	27.873	17.95
Dchs1	1.077	2.109	0.0055114	4.448	2.104
Dclre1a	-0.889	0.54	0.01809236	2.263	4.195
Dctn6	-0.503	0.706	0.00149698	17.161	24.265
Ddhd1	-0.842	0.558	3.3548E-06	14.213	25.47
Ddx23	-0.501	0.707	0.04993402	5.939	8.435
Ddx6	-0.335	0.793	0.00116799	40.948	51.613
Defb42	-1.676	0.313	0.00430767	0.638	2.063
Dennd3	0.861	1.817	0.02788041	3.198	1.769
Dennd5b	-0.541	0.687	0.00071904	17.781	25.841
Dhcr24	1.451	2.733	0.00430767	1.971	0.721
Dhrs11	1.04	2.056	0.01346399	2.629	1.28
Dicer1	-0.296	0.815	0.01051701	33.23	40.806
Dlgap4	0.358	1.281	0.01876409	34.274	26.82
Dmtn	-0.345	0.787	0.03297072	18.543	23.531
Dnajc30	0.675	1.596	0.0049141	14.373	9.001
Dnase1l2	-1.513	0.35	0.04561377	0.434	1.258
Dnmt3a	-0.546	0.685	0.00015582	23.21	33.834
Dnph1	2.026	4.074	0.00066399	1.857	0.448
Dop1a	-0.463	0.725	0.01971533	10.577	14.578
Dph5	-0.388	0.764	0.04621158	9.7	12.696
Dpp9	0.576	1.491	0.00476718	12.867	8.616
Dpy19l4	-0.507	0.704	0.04777817	6.066	8.592
Dusp23	0.284	1.217	0.04575758	34.737	28.491
Dvl2	-0.631	0.646	0.03177034	4.257	6.573
E2f7	1.249	2.377	0.00742604	2.459	1.048
Ebpl	-0.485	0.715	0.04065241	6.012	8.423
Eef1g	-0.323	0.799	0.0166183	19.966	25.03
Efna2	-1.233	0.425	0.04684899	0.724	1.693
Eif2ak2	-1.129	0.457	3.2847E-05	3.197	6.977
Eif2b2	0.488	1.403	0.00184987	24.056	17.143
Eif3b	0.278	1.213	0.0141024	48.476	39.997
Elavl3	2.331	5.031	1.2006E-08	4.92	0.98
Eml5	-0.675	0.626	0.02415631	4.627	7.391
Epc1	-0.426	0.745	0.02438101	12.881	17.353
Epha4	0.903	1.87	0.00191425	5.712	3.049
Epn1	0.437	1.354	0.00103213	75.452	55.749
Ercc5	-0.362	0.778	0.04878575	14.665	18.802

Erf	0.659	1.579	0.0091173	9.481	6.011
Esf1	-0.259	0.835	0.01772908	45.544	54.473
Exoc3l	1.128	2.186	0.03000001	2.117	0.969
Fam102a	0.682	1.605	0.00022535	19.193	11.982
Fam110b	-0.745	0.597	0.04030478	1.982	3.322
Fam241a	-0.575	0.671	0.00313825	13.606	20.198
Fam50a	0.489	1.403	0.00806196	17.928	12.814
Fam53b	0.364	1.287	0.00164842	69.058	53.682
Fam53c	-0.371	0.773	0.04401045	12.324	15.954
Fam83g	1.016	2.022	0.01494603	2.886	1.413
Fam89a	0.797	1.738	0.01541274	4.497	2.606
Fbxl16	1.619	3.071	0.04338265	1.186	0.388
Fbxl2	1.048	2.068	0.01164708	3.137	1.525
Fbxo2	2.301	4.927	0.00135205	1.775	0.362
Fbxo28	0.431	1.348	0.01943934	18.863	14.01
Fer	-0.569	0.674	0.00045486	11.825	17.534
Fgf21	3.517	11.45	0.02497493	0.606	0.048
Fibin	-0.696	0.617	0.03944371	2.677	4.326
Fkbp7	-0.399	0.758	0.00950746	16.6	21.834
Fmnl2	-0.909	0.532	0.01669249	2.344	4.389
Fnbp4	-0.527	0.694	0.00107128	14.302	20.618
Fndc3a	-0.379	0.769	0.02516133	11.856	15.409
Foxc1	1.273	2.417	0.00714479	2.421	1.008
Foxn3	0.459	1.374	1.3634E-07	148.781	108.302
Fra10ac1	-0.386	0.765	0.02805891	18.054	23.504
Fubp1	-0.423	0.746	7.2977E-06	54.03	72.355
Fubp3	0.522	1.436	0.013367	9.519	6.613
Fut8	-0.559	0.679	0.00485115	12.094	17.839
Fzd3	1.287	2.44	0.01034061	3.072	1.263
Fzd8	-0.707	0.613	0.0299169	3.784	6.16
G2e3	-0.596	0.662	0.02080553	5.118	7.748
Galc	0.519	1.433	0.00430219	15.395	10.737
Galk1	0.478	1.393	0.03638064	9.712	6.981
Garnl3	1.19	2.282	4.1149E-05	5.198	2.268
Gba	0.448	1.364	0.03189497	12.204	8.933
Gcnt2	0.606	1.522	0.02926684	6.265	4.14
Gga1	0.358	1.281	0.02995205	22.417	17.502
Gga2	-0.686	0.621	0.02865927	3.113	4.985
Ggps1	-0.357	0.781	0.01030786	20.109	25.709
Gk5	-0.701	0.615	0.02504511	4	6.471
Gli3	-1.855	0.277	0.02526367	0.322	1.162
Gm10033	-1.16	0.448	0.00141275	1.911	4.228
Gm10616	-2.111	0.232	0.02523601	0.237	1.015
Gm11739	-1.773	0.293	0.00748194	0.44	1.516
Gm12786	2.934	7.645	0.0303549	0.598	0.082
Gm13341	0.586	1.501	0.00704612	60.923	40.549
Gm14286	-1.314	0.402	0.00612007	0.983	2.439
Gm15666	1.108	2.156	0.02835127	2.761	1.286

Gm15672	-1.608	0.328	0.00330173	0.647	1.974
Gm15675	-2.832	0.14	0.03410852	0.088	0.639
Gm15720	-0.912	0.531	0.01671927	2.08	3.916
Gm15893	0.832	1.78	0.02359004	4.026	2.28
Gm16053	-1.422	0.373	0.021852	0.54	1.435
Gm16559	-1.633	0.322	0.00465104	0.599	1.845
Gm17067	3.542	11.65	0.00415479	0.89	0.074
Gm17092	1.23	2.345	0.03112944	1.62	0.694
Gm17212	0.824	1.77	0.04887225	3.06	1.737
Gm17484	1.855	3.618	0.04391401	1.127	0.32
Gm20342	-0.919	0.529	0.00021108	4.024	7.616
Gm20632	-1.178	0.442	0.02611594	0.863	1.948
Gm22767	-4.279	0.052	0.00105649	0.057	1.175
Gm23442	-3.626	0.081	0.00430673	0.089	1.097
Gm2415	-0.837	0.56	0.00299931	2.864	5.135
Gm25394	-3.099	0.117	0.00235131	0.177	1.509
Gm25395	1.547	2.922	0.02725988	1.283	0.441
Gm25834	-1.933	0.262	0.03977661	0.234	0.892
Gm26560	2.576	5.964	0.00638586	1.094	0.192
Gm27010	-1.466	0.362	0.00029313	1.373	3.839
Gm32389	1.306	2.473	0.01849116	2.058	0.841
Gm32688	1.313	2.485	0.01184394	2.898	1.164
Gm36936	-1.353	0.391	0.0313827	0.656	1.673
Gm37019	-1.657	0.317	0.0002116	1.367	4.281
Gm37121	-0.897	0.537	0.02451804	1.727	3.195
Gm37238	-0.858	0.552	0.0179965	2.473	4.501
Gm37420	-2.312	0.201	1.5039E-08	1.004	5.013
Gm37589	-1.696	0.309	0.0121562	0.476	1.552
Gm37607	0.919	1.891	0.01986322	3.256	1.73
Gm37820	-2.774	0.146	0.00055623	0.231	1.62
Gm37906	-0.809	0.571	0.01779251	2.282	4.002
Gm38178	-1.478	0.359	0.04469771	0.53	1.49
Gm38366	-0.609	0.656	0.04638223	4.138	6.319
Gm38380	-0.554	0.681	0.04542684	4.973	7.301
Gm38387	-1.085	0.471	0.01137605	1.604	3.419
Gm39228	-1.143	0.453	0.0171298	0.966	2.152
Gm40377	2.374	5.186	0.01584486	0.935	0.184
Gm42559	-1.26	0.418	0.01461889	0.845	2.045
Gm42843	-3.216	0.108	0.02132175	0.057	0.565
Gm42967	-1.217	0.43	0.00738989	1.189	2.77
Gm43061	-0.832	0.562	0.04658399	1.601	2.856
Gm43071	-0.885	0.542	0.00028541	3.977	7.363
Gm43496	1.312	2.483	0.01100059	2.108	0.852
Gm43497	1.857	3.622	0.00559244	1.402	0.39
Gm43598	-1.602	0.329	0.01209489	0.568	1.703
Gm43773	-1.483	0.358	0.01962837	0.568	1.574
Gm43788	-0.619	0.651	0.0119754	5.203	8.014
Gm44164	-0.622	0.65	0.04088459	4.439	6.867

Gm44607	-2.044	0.242	0.00484982	0.617	2.552
Gm44694	-0.584	0.667	0.01344138	7.889	11.847
Gm44913	1.637	3.111	0.00738719	2.793	0.897
Gm45187	0.49	1.404	0.00147913	18.212	12.939
Gm45286	-1.586	0.333	0.01345543	0.479	1.425
Gm45486	1.708	3.268	0.02852662	1	0.306
Gm45537	-1.141	0.454	0.02262634	1.017	2.217
Gm45620	1.173	2.255	0.01193754	2.397	1.048
Gm45774	2.757	6.758	0.02019164	0.682	0.096
Gm45819	-1.962	0.257	0.00328844	0.477	1.837
Gm46404	-1.092	0.469	0.01693526	1.481	3.136
Gm47061	4.121	17.4	0.00107358	0.915	0.056
Gm47210	-2.06	0.24	0.02303572	0.272	1.108
Gm48146	-1.067	0.477	7.0457E-05	3.061	6.417
Gm48225	-2.749	0.149	0.001437	0.228	1.58
Gm48287	-1.126	0.458	9.6315E-05	2.407	5.258
Gm49124	-1.759	0.295	0.04247652	0.303	1.017
Gm49125	-1.429	0.371	0.02541733	0.599	1.611
Gm49204	-0.842	0.558	0.04251201	1.721	3.089
Gm5069	0.878	1.838	0.02530923	3.882	2.089
Gm6878	-1.747	0.298	0.00822935	0.443	1.494
Gnb1	0.301	1.232	0.00034252	132.152	107.293
Gnb1l	-1.101	0.466	0.04032183	0.948	2.026
Gpatch3	1.462	2.755	0.00714369	2.201	0.81
Gpr146	0.456	1.372	4.4302E-05	40.81	29.76
Grk2	0.371	1.293	0.00853426	29.173	22.576
Gsk3a	0.38	1.301	0.00463511	42.201	32.46
Guk1	-0.303	0.81	0.01701471	61.16	75.371
H2-Aa	-0.613	0.654	8.5643E-05	28.689	43.872
H2-DMa	-0.886	0.541	0.02802662	1.749	3.221
H2-DMb1	-1.015	0.495	0.02106647	1.802	3.625
H3c15	1.443	2.718	0.00808023	1.872	0.682
H3c4	1.274	2.419	0.00516909	3.067	1.26
H4c3	1.84	3.581	0.04340709	0.818	0.228
H6pd	0.367	1.29	0.00074111	77.025	59.732
Hdgfl3	-0.74	0.599	0.0120386	4.429	7.423
Herpud1	0.434	1.351	0.00191166	64.418	47.67
Hipk1	0.269	1.205	0.00292776	105.098	87.175
Hivep1	-0.517	0.699	0.00806457	8.502	12.182
Hltf	-0.64	0.642	0.00276888	6.613	10.293
Hmg20b	0.262	1.199	0.03777252	81.041	67.578
Hnrnpa1	-0.736	0.601	0.01901888	4.702	7.834
Hnrnpc	-0.245	0.844	0.01204978	48.856	57.912
Homer3	0.857	1.812	0.00338697	5.645	3.138
Hook3	-0.462	0.726	2.6774E-05	55.867	76.884
Hoxb3os	-1.242	0.423	6.8384E-05	2.422	5.744
Hoxc8	-0.918	0.529	0.01329026	8.548	16.165
Hsdl1	0.509	1.423	0.01632901	9.934	7.01

Hspa1a	-2.473	0.18	0.00431708	1.958	10.878
Hspb1	0.805	1.747	4.1077E-09	65.278	37.341
Hvcn1	-1.567	0.338	0.02042299	0.589	1.746
Idh2	-0.254	0.839	0.01670853	166.508	198.569
Ifi27l2b	-0.926	0.526	0.01241895	1.786	3.405
Ifih1	-0.531	0.692	0.04550784	5.326	7.679
Ifitm10	3.341	10.13	0.00995479	0.796	0.081
Ifnar1	-0.562	0.677	0.01939636	5.168	7.631
Ikzf3	-3.168	0.111	0.03145011	0.06	0.55
Ikzf5	-0.417	0.749	0.02784296	12.482	16.605
Il4ra	1.093	2.133	2.8087E-07	15.114	7.109
Il7	-2.027	0.245	0.03313143	0.209	0.849
Inafm1	0.651	1.57	0.00011053	21.765	13.88
Inip	-0.619	0.651	0.00424991	7.356	11.336
Ino80c	0.455	1.37	0.00298793	28.713	20.991
Ino80d	-0.38	0.769	0.01433629	15.292	19.904
Inpp5a	1.001	2.001	0.00547822	4.009	2.006
Ints2	-0.48	0.717	0.04009187	8.879	12.393
Ipmk	0.842	1.792	0.0018252	6.936	3.87
Iqce	-0.958	0.515	0.01228956	2.116	4.131
Ireb2	-0.328	0.797	0.0292739	19.649	24.593
Itga2b	1.132	2.192	0.03000001	2.488	1.141
Jag2	0.865	1.821	0.00085072	7.564	4.165
Kank4	2.954	7.751	0.00026295	1.381	0.176
Kat6a	-0.398	0.759	0.00842604	18.548	24.484
Kbtbd3	-0.829	0.563	7.4045E-05	4.977	8.852
Kcnd2	-2.89	0.135	0.01548119	0.119	0.875
Kdm5a	-0.353	0.783	4.7403E-05	66.977	85.542
Kdm6a	-0.47	0.722	0.00562595	12.265	16.935
Kif13a	0.444	1.36	0.00113852	25.339	18.65
Kif26a	0.41	1.328	0.02557796	14.583	10.985
Kifc2	-0.701	0.615	0.0250804	3.126	5.095
Kin	-0.405	0.755	0.00342406	23.338	30.934
Klc4	0.318	1.246	0.01311791	27.388	21.984
Krit1	-0.343	0.788	0.00649787	23.054	29.198
Ktn1	-0.451	0.731	1.818E-06	58.167	79.558
L3mbtl3	-0.623	0.649	0.00694505	6.182	9.503
Lamp2	0.226	1.17	0.00338622	114.903	98.22
Lancl3	1.343	2.538	0.02949176	1.766	0.704
Ldlr	0.637	1.555	0.00547822	48.756	31.269
Ldlrad4	0.73	1.659	0.04631672	3.647	2.208
Lgals1	-0.24	0.847	0.0424825	337.041	397.966
Lin37	0.474	1.389	0.04628094	7.617	5.486
Lmna	0.344	1.269	0.03799941	45.923	36.25
Lmnb2	-0.823	0.565	0.0171298	3.199	5.631
Lnpep	-0.283	0.822	0.02442427	49.424	60.125
Lnpk	-0.681	0.624	0.00860437	4.224	6.78
Ltbr	0.301	1.232	0.00434987	53.572	43.514

LTO1	-0.52	0.697	0.03620616	5.285	7.59
Luc7l	-0.354	0.782	0.00516481	32.816	41.935
Lyrm4	0.455	1.371	0.00118446	22.528	16.411
Lyve1	0.672	1.593	0.03205072	5.795	3.63
Madd	0.622	1.539	0.01663445	6.402	4.173
Magi1	-0.603	0.658	0.04410144	3.77	5.715
Magi3	-0.424	0.745	0.03731514	7.816	10.484
Mal2	-0.925	0.527	0.00055858	5.217	9.903
Malt1	-0.931	0.524	0.00291149	2.607	4.975
Manbal	-0.729	0.603	0.00062147	7.848	13.032
Mansc4	1.253	2.384	0.00732929	2.306	0.96
Map2	-1.068	0.477	0.01025755	1.374	2.881
Mapt	0.523	1.437	0.00256601	104.617	72.696
Marchf7	-0.296	0.815	0.01201628	36.709	45.039
Mark4	0.41	1.329	0.03145011	16.892	12.731
Maz	-0.766	0.588	0.0277364	2.144	3.63
Mc2r	-1.592	0.332	0.02317302	0.416	1.251
Mcm7	-0.704	0.614	0.00865732	4.279	6.943
Mcm8	-0.964	0.512	0.01155835	1.744	3.426
Mcu	0.462	1.377	0.00179543	32.404	23.556
Mdc1	-0.779	0.583	0.00742604	3.006	5.193
Megf6	2.95	7.73	0.01029294	0.776	0.092
Metrnl	0.762	1.696	0.02163729	5.695	3.331
Mettl6	-0.693	0.619	0.00032947	6.906	11.159
Mfsd2a	2.716	6.569	0.0163179	32.557	4.959
Mgat1	0.35	1.275	0.0262608	29.67	23.293
Mgrn1	0.236	1.178	0.02064703	75.468	64.121
Mia3	-0.226	0.855	0.04490837	49.477	57.888
Mib2	0.488	1.402	0.00081314	23.762	16.94
Micu1	0.48	1.395	2.9885E-05	33.908	24.252
Mier3	-0.387	0.765	0.01854143	15.088	19.768
Mipol1	-0.715	0.609	0.03169007	3.383	5.555
Mis12	-0.582	0.668	0.03410852	4.887	7.314
Mkrn1	0.639	1.557	2.8309E-07	26.054	16.716
Mnat1	-0.397	0.759	0.00487543	15.956	20.964
Morrbid	0.954	1.938	0.03160566	2.766	1.443
Mosmo	0.415	1.333	0.01142517	18.029	13.468
Mphosph8	-0.285	0.82	0.01198354	57.51	70.067
Mrfap1	0.279	1.213	0.00107164	132.366	109.101
Mrm1	0.449	1.365	0.04228019	13.1	9.597
Mrto4	0.628	1.545	0.01971249	10.679	6.892
Ms4a4b	-1.991	0.252	0.00179456	0.521	2.104
Msn	-0.331	0.795	0.00312242	61.482	77.399
Mtmr9	0.396	1.316	0.000447	39.458	29.935
Mttp	0.547	1.461	0.03203347	6.666	4.568
Mtx3	0.403	1.322	0.03464362	17.714	13.392
Mxd4	0.267	1.203	0.01345304	104.897	87.231
Mybbp1a	0.411	1.329	0.02042378	21.941	16.573

Myl6b	0.733	1.662	0.00142197	9.386	5.647
Myrip	1.316	2.49	0.02053469	2.69	1.068
N4bp1	0.313	1.242	0.03326281	25.135	20.233
N4bp2	-0.411	0.752	0.03748173	8.786	11.651
Nacc1	0.635	1.553	0.0127939	7.906	5.095
Naglu	0.635	1.553	0.02749522	9.695	6.286
Nasp	-0.444	0.735	0.03077776	10.935	14.942
Nav2	0.307	1.237	0.04333463	32.012	25.865
Ncapd3	-0.674	0.627	0.0002264	8.794	13.983
Ncdn	0.595	1.511	0.02359509	12.653	8.36
Ndel1	-0.305	0.809	0.01222644	47.464	58.712
Necap2	0.373	1.295	0.01397025	23.357	18.086
Neu1	0.432	1.349	0.01167805	19.543	14.498
Neurl2	0.898	1.864	0.02103328	3.233	1.754
Neurl4	0.43	1.347	0.00257647	22.254	16.571
Nfkbib	0.329	1.256	0.01434942	27.724	22.11
Ngdn	0.341	1.267	0.00553383	31.119	24.542
Nim1k	-0.686	0.622	0.01228956	4.65	7.448
Ninj1	0.337	1.263	0.01675483	38.674	30.62
Nkap	-0.301	0.812	0.02303572	20.388	25.072
Nkapd1	-0.572	0.673	0.00017643	17.586	26.196
Nkg7	-1.972	0.255	0.04119627	0.21	0.816
Nktr	-0.321	0.8	0.0321606	94.111	117.654
Noa1	0.417	1.335	0.01759464	15.537	11.58
Nono	-0.508	0.703	0.00713187	8.398	11.902
Npc1	-0.49	0.712	0.00038238	24.669	34.702
Nqo1	1.303	2.468	0.01879966	1.631	0.651
Nsd1	-0.274	0.827	0.00194354	72.423	87.633
Nsd2	-0.474	0.72	0.00759737	10.62	14.768
Nts	-1.598	0.33	0.00895029	0.732	2.176
Nubpl	0.619	1.536	0.00970799	9.345	6.06
Nudt2	-0.497	0.709	0.00982964	9.207	12.927
Nudt3	0.518	1.432	4.3383E-08	72.14	50.4
Ocstamp	1.351	2.551	0.01694719	1.861	0.715
Oip5os1	-0.244	0.845	0.01251727	139.318	164.882
Olfml2a	1.012	2.016	0.00651608	3.775	1.881
Oma1	0.37	1.292	0.0166183	19.143	14.805
Opcml	-1.404	0.378	0.02992406	0.542	1.425
Orc5	-0.453	0.73	0.0460064	7.358	10.105
Orc6	-0.57	0.674	0.04509866	5.261	7.781
Osbpl2	0.306	1.236	0.02806059	26.988	21.83
Ostf1	0.319	1.248	0.01402614	62.842	50.355
Otulin	0.354	1.279	0.02480887	16.867	13.193
Oxr1	-0.542	0.687	0.00030184	19.06	27.746
P2ry14	-1.167	0.445	0.04228019	1.058	2.345
Pafah1b2	0.371	1.293	0.01688726	29.427	22.772
Pappa	-1.212	0.432	0.01926729	1.008	2.348
Parp16	-0.781	0.582	0.0022532	5.381	9.223

Patz1	-1.204	0.434	0.01204425	0.949	2.192
Paxbp1	-0.628	0.647	0.00553516	7.602	11.74
Pbx2	0.401	1.321	0.00257982	34.297	25.994
Pcdh1	0.495	1.409	0.04599534	7.531	5.34
Pcdhb7	-3.145	0.113	0.01255575	0.089	0.783
Pcmtd2	-0.318	0.802	0.00995479	25.705	32.026
Pdcd6ip	0.305	1.236	0.01375292	56.515	45.724
Pde1a	-0.693	0.619	4.1188E-06	16.928	27.42
Pdgfd	-0.611	0.655	0.00872955	8.238	12.527
Pdlim2	0.82	1.766	0.03165751	5.583	3.139
Pdlim7	0.757	1.69	0.01468194	8.897	5.263
Pds5b	-0.468	0.723	0.00030381	25.736	35.518
Phc3	-0.423	0.746	0.00236728	20.455	27.372
Pi4ka	0.354	1.278	0.00164733	74.554	58.303
Pibf1	-0.828	0.563	0.00941678	2.843	5.036
Pih1d1	0.349	1.274	0.02981682	25.404	19.956
Pip5k1c	0.694	1.617	0.00030115	13.729	8.511
Pisd	0.438	1.355	0.00199385	24.888	18.392
Pitpna	0.29	1.223	0.01844189	45.099	36.923
Pla2g2d	-1.311	0.403	0.04827583	0.586	1.454
Plekha6	-1.365	0.388	0.0301237	0.728	1.901
Plpbp	0.296	1.227	0.01100059	48.561	39.488
Plxna2	0.578	1.493	1.7551E-05	31.472	21.098
Pms2	-1.411	0.376	0.00404282	0.888	2.366
Poli	-0.76	0.59	0.02609592	2.252	3.813
Porcn	-0.592	0.663	0.01661736	4.56	6.887
Ppil2	-0.536	0.69	0.02343192	5.546	8.068
Ppm1f	0.559	1.474	0.0053876	13.417	9.134
Ppp1r11	0.304	1.234	0.00980037	41.669	33.74
Ppp3ca	-0.213	0.863	0.02106647	109.294	126.668
Ppp4r2	0.332	1.259	0.0020994	47.669	37.848
Ppp5c	0.363	1.286	0.00568354	37.054	28.824
Ppwd1	-0.436	0.739	0.02178285	9.948	13.518
Pqlc3	-0.595	0.662	0.00640747	6.673	10.045
Praf2	1.155	2.228	0.00059798	4.793	2.163
Prdx4	-0.569	0.674	0.00506204	6.502	9.639
Prkd3	-0.535	0.69	0.00214954	11.005	15.903
Prkdc	-0.613	0.654	0.00650761	6.071	9.318
Prlr	1.425	2.684	0.00181403	2.944	1.096
Prpf40b	0.387	1.308	0.0410319	16.718	12.833
Prr14l	-0.67	0.629	0.00481736	5.993	9.54
Ptgis	-1.281	0.411	0.02985065	0.775	1.882
Puf60	0.37	1.293	0.0001138	72.64	56.276
Pxk	0.323	1.251	0.01638895	31.436	25.131
R3hdm2	0.266	1.202	0.00675593	67.762	56.39
Rab11fip5	0.4	1.32	0.01844189	15.52	11.748
Rab17	-4.026	0.061	0.00020363	0.09	1.445
Rab37	2.564	5.913	5.4217E-05	2.129	0.359

Rabl3	0.982	1.976	9.1948E-06	9.836	5.009
Rad50	-0.514	0.7	0.00556007	14.379	20.542
Rad54l2	-0.592	0.663	0.00418916	10.135	15.308
Ranbp6	-0.503	0.706	0.0344608	5.764	8.162
Ranbp9	0.545	1.459	0.01935761	12.898	8.852
Rap2b	-1.029	0.49	0.00327907	2.622	5.363
Rasa2	-0.482	0.716	0.0313661	6.538	9.155
Rbbp7	-0.474	0.72	0.00415481	23.119	32.09
Rbm25	-0.183	0.881	0.01758839	237.957	270.077
Rbm3	-1.672	0.314	0.01997032	0.437	1.407
Rbm4	-0.693	0.619	0.03908573	3.071	4.991
Rbm48	-0.579	0.669	0.00995479	6.237	9.319
Rbm4b	-0.555	0.681	0.00226379	9.718	14.33
Rbm8a	0.242	1.182	0.02023192	56.741	47.981
Rccd1	-1.069	0.477	0.0285858	1.174	2.476
Relch	-0.53	0.692	0.01266855	8.034	11.584
Retreg1	-0.888	0.54	1.514E-05	10.427	19.238
Rev3l	-0.691	0.619	0.0082911	7.665	12.398
Rfc1	-0.283	0.822	0.00828562	52.036	63.267
Rftn1	0.542	1.456	0.03264961	9.743	6.705
Rgl3	0.474	1.389	0.02869294	14.876	10.751
Rgs19	-0.733	0.602	0.00611278	4.387	7.277
Rhobtb1	0.656	1.575	0.00206763	10.911	6.948
Rictor	-0.452	0.731	0.0027141	13.813	18.895
Rinl	1.033	2.047	0.00734782	3.159	1.558
Rnase6	-1.892	0.269	0.0376559	0.232	0.877
Rnf157	1.571	2.971	0.00796808	1.685	0.575
Rnf169	-0.534	0.69	0.00749079	9.161	13.307
Rnf220	0.36	1.284	0.01877645	24.959	19.463
Rnps1	-0.774	0.585	0.00512177	4.248	7.258
Rpl11	-0.529	0.693	0.04203802	4.505	6.494
Rpl23	-0.424	0.746	0.00072427	35.434	47.564
Rpl3	-0.677	0.626	0.02648242	3.355	5.375
Rpl30	-0.445	0.734	0.04469771	10.946	14.946
Rpl34	-0.241	0.846	0.00680878	101.388	119.837
Rpl35a	-0.623	0.649	0.00162472	10.365	15.945
Rpl37a	-0.329	0.796	0.01696135	20.037	25.144
Rpl37rt	1.246	2.371	0.00162472	2.976	1.248
Rpl39l	2.01	4.028	1.3844E-11	8.184	2.018
Rpn1	0.308	1.238	0.00210086	52.382	42.343
Rreb1	-0.35	0.785	0.0317064	30.326	38.681
Runx1	-1.104	0.465	0.02770957	0.924	1.983
Runx3	-2.034	0.244	0.01557472	0.269	1.093
Rxrb	0.5	1.414	4.2828E-06	37.044	26.232
Ryr2	1.993	3.982	0.00028716	2.706	0.698
Sap18	0.393	1.313	0.02390902	16.932	12.863
Sar1a	0.244	1.184	0.01427496	67.666	57.174
Satb1	-0.831	0.562	2.3149E-05	5.847	10.443

Saysd1	0.629	1.546	0.0350518	5.48	3.546
Scaf1	0.476	1.391	0.02353725	10.403	7.479
Scpep1	0.35	1.275	0.03743054	101.607	79.755
Scrib	0.496	1.41	0.03731514	10.013	7.09
Sema3f	1.563	2.956	0.00033257	3.104	1.052
Sema4a	0.47	1.385	0.04015767	21.455	15.466
Septin6	-1.469	0.361	0.00025901	1.376	3.799
Serinc1	0.264	1.201	0.00569038	93.102	77.463
Setd2	-0.264	0.833	0.00459845	51.423	61.758
Setd6	0.593	1.508	0.00301791	11.482	7.624
Sez6l2	1.602	3.035	0.02648242	1.243	0.409
Sfn	1.06	2.085	0.02841558	2.618	1.263
Sh3rf1	0.645	1.563	0.0226176	8.13	5.194
Shroom1	1.152	2.221	0.00651608	2.876	1.28
Sin3a	-0.521	0.697	0.01120847	12.171	17.427
Sipa1l2	0.593	1.509	0.03616497	6.089	4.034
Slc13a2	2	4	0.02867339	0.935	0.242
Slc22a21	-2.709	0.153	0.00551598	0.147	0.966
Slc2a9	0.985	1.979	0.00672143	3.607	1.816
Slc44a2	0.43	1.347	0.04946355	12.035	8.947
Slc7a6os	-0.491	0.712	0.04241859	8.457	11.91
Slf1	-0.574	0.672	0.00364955	8.712	12.958
Slf2	-0.46	0.727	0.02235901	8.195	11.288
Smarcc1	-0.45	0.732	0.00191684	24.41	33.385
Smarcc2	-0.294	0.816	0.00432672	51.579	63.258
Smc4	-0.641	0.641	2.4913E-06	24.733	38.576
Smc5	-0.635	0.644	0.00108208	10.035	15.507
Smim7	-0.323	0.799	0.00296757	32.956	41.242
Snapc2	0.564	1.478	0.04199	8.03	5.455
Snhg14	-0.638	0.643	0.01630151	4.021	6.241
Snhg9	0.535	1.449	0.00055342	19.318	13.347
Snora20	-2.889	0.135	0.00463511	0.177	1.307
Snora21	-3.498	0.089	0.00085881	0.116	1.329
Snora47	-4.214	0.054	0.00025518	0.088	1.64
Snrnp48	-0.309	0.807	0.00432672	39.231	48.588
Snx27	0.254	1.192	0.04613506	38.905	32.567
Sod3	0.493	1.407	2.8984E-07	99.111	70.473
Sp1	-0.432	0.741	3.7281E-05	32.622	44.017
Spag9	-0.301	0.812	0.00245934	59.769	73.637
Sphk2	0.426	1.344	0.02068084	21.482	15.998
Spty2d1	-0.416	0.749	0.02459498	10.206	13.604
Srebf2	0.46	1.375	0.01590909	17.161	12.455
Ssc4d	1.142	2.206	0.01107777	2.538	1.151
Ssna1	-0.445	0.734	0.02967609	9.87	13.469
Stac2	3.755	13.5	0.00516481	0.71	0.049
Stag1	-0.535	0.69	0.00037118	12.059	17.453
Stag2	-0.264	0.833	0.01423558	40.757	48.928
Stap2	0.503	1.417	0.04987432	8.996	6.368

Stard4	0.684	1.607	0.03015994	6.667	4.134
Stat5b	0.326	1.254	0.0203036	25.604	20.46
Stbd1	0.812	1.755	0.00802756	6.036	3.416
Stk17b	-0.478	0.718	0.03590535	7.921	11.008
Stk36	1.466	2.762	0.01596969	1.624	0.588
Stmn2	0.981	1.974	0.00053239	5.494	2.813
Stx5a	-0.392	0.762	0.0303439	19.972	26.22
Sumf1	0.318	1.247	0.04202623	21.919	17.574
Svopl	-1.091	0.469	0.01135189	1.999	4.295
Sycp2	-0.992	0.503	0.00969497	2.351	4.652
Syn2	0.866	1.823	4.0697E-05	10.701	5.897
Synrg	0.269	1.205	0.01977443	56.291	46.692
Syt11	0.8	1.741	4.5122E-06	21.597	12.384
Szt2	0.591	1.506	0.04373997	6.585	4.345
Taf1a	-0.779	0.583	0.03286075	2.039	3.503
Tars	0.326	1.253	0.02541733	34.704	27.633
Tasor	-0.44	0.737	0.00053965	19.802	26.901
Tbpl1	0.838	1.787	0.00029547	11.742	6.587
Tcta	-0.504	0.705	0.0052991	11.723	16.594
Tfcp2	-0.507	0.704	0.03000001	6.872	9.769
Tfr2	1.232	2.348	0.00018302	4.317	1.834
Thap4	0.478	1.393	0.0065398	18.535	13.286
Thoc2l	-0.274	0.827	0.01387536	42.505	51.392
Thoc5	0.39	1.31	0.03434372	12.33	9.391
Timm8a1	2.125	4.362	0.01051029	1.332	0.302
Tmc6	0.778	1.714	0.00333751	6.634	3.898
Tmem160	0.303	1.233	0.01938079	66.834	54.186
Tmem178b	-1.415	0.375	0.04705141	0.518	1.406
Tmem204	0.367	1.29	0.01800099	24.417	18.929
Tmem222	-0.326	0.798	0.02736184	17.475	21.896
Tmem25	-0.976	0.508	0.03933485	1.153	2.282
Tmem74b	-1.485	0.357	0.04672526	0.471	1.319
Tmem87a	-0.542	0.687	0.01218917	10.046	14.585
Tmem88b	0.979	1.97	0.00410276	4.708	2.397
Tmem94	0.369	1.291	0.0029466	29.776	23.031
Tmtc2	1.593	3.016	0.00157749	2.171	0.721
Tmx1	0.262	1.2	0.03168868	32.434	27.007
Tnfaip6	-3.104	0.116	0.0392765	0.059	0.526
Tnfrsf1a	0.221	1.165	0.04893437	66.033	56.701
Tnpo3	0.246	1.186	0.04340709	51.409	43.349
Tom1l2	0.38	1.301	0.00473117	50.094	38.544
Tomm20	0.445	1.362	0.03773286	10.695	7.874
Top3b	0.431	1.348	0.00550342	23.984	17.801
Topors	-0.426	0.744	0.0023718	25.756	34.608
Tor4a	-1.182	0.441	0.01421931	1.185	2.701
Tpcn1	0.35	1.274	0.00879693	71.961	56.525
Trbc2	-1.776	0.292	0.01273935	0.409	1.418
Trim80	1.449	2.731	0.03658273	1.405	0.513

Trip4	-0.445	0.735	0.0171298	12.002	16.379
Trp53	-0.976	0.508	0.02178285	1.502	2.965
Trp53rka	-0.535	0.69	0.00924474	6.68	9.683
Tsc22d2	-0.44	0.737	0.02015714	15.291	20.676
Tssc4	0.442	1.359	0.02799383	14.824	10.922
Ttc14	-0.396	0.76	9.9874E-05	40.386	53.141
Ttc22	4.963	31.18	0.00011589	0.736	0
Ttc28	0.626	1.543	1.8236E-05	157.706	102.284
Ttc33	0.413	1.331	0.04895943	15.043	11.268
Ttll12	0.617	1.534	0.01326049	7.255	4.735
Tubd1	-0.952	0.517	0.01201628	1.786	3.456
Tut4	-0.469	0.723	0.00169386	18.534	25.603
Txndc16	-0.959	0.515	0.0171298	1.481	2.869
Txndc9	0.397	1.316	0.00098248	37.719	28.611
Ubap2l	-0.324	0.799	0.008147	52.787	66.114
Ube2n	0.82	1.766	0.00016534	9.909	5.598
Uimc1	-0.398	0.759	0.00313845	16.743	22.056
Umps	-0.524	0.695	0.03649948	6.257	8.966
Utp25	-0.56	0.678	0.02370466	5.193	7.647
Vkorc1l1	-0.458	0.728	0.04756623	11.243	15.413
Vps26c	0.678	1.6	0.00078344	10.26	6.413
Vps35l	0.38	1.301	0.02674171	17.565	13.481
Vrk1	-0.542	0.687	0.01291164	5.671	8.251
Vti1a	-0.378	0.769	0.02205893	13.595	17.675
Wdr46	0.53	1.444	0.04784185	7.126	4.92
Wdr55	0.7	1.625	0.01618918	6.329	3.922
Wdr74	0.47	1.385	0.01278999	14.945	10.771
Wdr75	-0.513	0.701	0.03222319	9.237	13.134
Wdr76	-0.742	0.598	0.01600304	2.96	4.957
Wee1	-1.024	0.492	0.00063299	2.757	5.591
Wiz	0.427	1.344	0.01869091	13.016	9.694
Wnt5a	-0.524	0.695	0.03085935	8.37	11.99
Wrn	-0.528	0.693	0.01192761	8.331	12.002
Wscd2	1.523	2.873	0.00450712	2.053	0.709
Wwc2	0.197	1.147	0.02653908	72.941	63.651
Xlr3a	-1.951	0.259	0.04239291	0.211	0.798
Xntrpc	-2.283	0.205	0.03189497	0.146	0.721
Ybx2	0.634	1.552	0.00737695	35.502	22.9
Zbtb10	-0.491	0.711	0.03021778	6.01	8.454
Zc3h6	-0.963	0.513	3.6217E-05	6.708	13.085
Zdhhc13	1.538	2.904	0.01083348	1.49	0.51
Zdhhc21	-0.443	0.735	0.01963822	9.959	13.506
Zdhhc6	-0.479	0.717	0.01398222	9.052	12.626
Zdhhc7	0.322	1.25	0.01940666	23.439	18.786
Zeb1	-0.34	0.79	0.00777818	44.892	56.724
Zfand3	0.298	1.229	0.02916104	42.419	34.549
Zfp101	0.581	1.496	0.04848949	5.696	3.776
Zfp280d	-0.576	0.671	0.00030659	14.236	21.207

Zfp318	-0.305	0.81	0.00529846	32.582	40.289
Zfp324	-0.752	0.594	0.02951889	2.754	4.618
Zfp326	-0.339	0.79	0.0285858	37.849	47.96
Zfp329	-0.506	0.704	0.03065631	7.082	10.075
Zfp330	-0.746	0.596	0.00045971	7.058	11.776
Zfp385a	0.836	1.785	0.00505051	5.964	3.348
Zfp420	-0.87	0.547	0.02364172	1.915	3.48
Zfp428	0.583	1.498	0.03743223	5.465	3.648
Zfp451	-0.378	0.769	0.01218536	14.664	19.074
Zfp583	-1.816	0.284	0.02163729	0.332	1.156
Zfp651	-0.559	0.679	0.03072756	5.162	7.606
Zfp655	0.46	1.376	0.01069448	24.238	17.667
Zfp710	0.568	1.482	0.00718115	13.263	8.971
Zfp800	-0.33	0.795	0.01844773	22.97	28.915
Zfp870	-0.767	0.587	0.02303994	2.458	4.175
Zfp871	-0.405	0.755	0.00312795	28.853	38.225
Zfp933	-0.7	0.616	0.04232608	3.12	5.102
Zfp945	-0.703	0.614	0.0013776	5.89	9.574
Zfp974	-0.679	0.624	0.01073375	4.05	6.488
Zic1	0.496	1.41	0.02653908	12.275	8.7
Zkscan8	-0.672	0.628	0.0015292	7.612	12.049
Zmym2	-0.516	0.699	0.00065378	13.258	18.922
Zrsr1	-0.324	0.799	0.00886397	31.798	39.76
Zxdc	-0.719	0.607	0.02241958	3.986	6.609

Table 8. Cold-responsive protein-coding genes (also predicted), and lncRNA genes found in BAT but not in PVAT, WATg, or WATi

Cold-responsive protein-coding genes (also predicted), and lncRNA genes found in PVAT but not in BAT, WATg, or WATi:

Symbol	log2(fold change)	Ratio	padj	Mean FPM PVAT 4°C	Mean FPM PVAT 23°C
0610009B22Rik	0.371	1.293	0.01176801	25.138	19.402
1500002F19Rik	1.329	2.512	0.01798638	1.979	0.786
1500026H17Rik	0.623	1.54	0.01416349	8.095	5.256
1700007K13Rik	2.48	5.581	0.02120498	0.931	0.162
1810026B05Rik	-0.512	0.701	0.00561875	8.789	12.417
2010007H06Rik	-0.757	0.592	0.00084511	5.572	9.534
2310002L09Rik	1.949	3.86	0.00361756	2.839	0.753
2700097O09Rik	-0.454	0.73	0.00916327	12.253	16.819
3425401B19Rik	2.862	7.269	0.00124375	5.803	0.802
3830406C13Rik	-0.29	0.818	0.03878038	24.876	30.51
3830408C21Rik	-1.424	0.373	0.0335605	0.546	1.617
4430402I18Rik	-0.414	0.751	0.03612099	7.387	9.897
4833438C02Rik	-0.712	0.611	0.02576711	2.769	4.594
4930412C18Rik	-0.855	0.553	0.00658228	2.807	4.953
4931428L18Rik	-1.595	0.331	0.04565137	0.341	0.997
5430405H02Rik	-0.554	0.681	0.00251243	7.53	11.043

6530402F18Rik	1.478	2.785	0.00056369	3.027	1.085
9330159F19Rik	-1.004	0.499	0.02517293	1.303	2.662
A430018G15Rik	0.904	1.871	0.00416037	4.049	2.178
A430035B10Rik	0.607	1.523	0.01549586	7.756	5.091
A730063M14Rik	-0.566	0.675	0.0376206	4.358	6.463
A930019D19Rik	-0.847	0.556	0.00490426	2.746	4.955
AA986860	-1.366	0.388	0.01375667	0.847	2.08
Aar2	0.505	1.419	0.0347561	8.669	6.098
Aasdh	-0.532	0.692	0.00948864	6.517	9.367
Abcb7	0.472	1.387	0.01965669	15.301	10.956
Abhd8	0.751	1.683	0.00989213	5.446	3.191
Abra	2.048	4.135	0.0009084	4.281	1.048
Acsm5	-1.303	0.405	0.0409412	0.657	1.574
Actg2	-2.012	0.248	0.00649203	0.428	1.69
Actr3	0.314	1.244	0.02762778	29.54	23.611
Adal	0.9	1.866	0.00032476	8.548	4.563
Adam11	-0.978	0.508	0.00237325	2.136	4.177
Adam17	0.367	1.29	0.03184158	28.539	22.079
Adamts9	0.503	1.418	0.00355215	21.056	14.933
Adgrl1	-0.58	0.669	0.00050799	12.732	19.175
Agfg1	0.472	1.387	6.7402E-05	40.685	29.433
Akr1c14	1.686	3.218	0.01202426	1.51	0.468
Alkbh5	0.35	1.274	0.00039196	47.255	37.214
Alkbh6	0.34	1.265	0.0362628	17.86	14.125
Alox12	1.009	2.012	0.02092704	3.081	1.541
Alpk3	1.691	3.228	0.00156852	4.005	1.257
Amfr	0.209	1.156	0.04453752	55.301	47.802
Ampd1	1.976	3.933	0.01553384	2.586	0.671
Amz2	-0.267	0.831	0.02845164	28.961	34.723
Ankrd2	3.912	15.06	1.7579E-07	10.899	0.727
Ankrd33b	1.081	2.115	0.02369413	2.232	1.08
Aox1	-0.308	0.808	0.02202339	40.195	49.754
Apbb1ip	0.547	1.461	0.03783105	7.351	4.974
Arfip1	0.458	1.374	0.00848688	14.331	10.489
Arhgap44	-1.119	0.46	0.02057023	0.947	2.108
Arhgef18	0.37	1.293	0.04531658	20.6	15.778
Arid1a	-0.389	0.764	0.01757481	20.686	27.209
Arl4c	0.872	1.831	0.00438866	4.546	2.473
Arsg	-1.067	0.477	0.02628748	1.195	2.46
Asf1b	0.752	1.684	0.02611011	5.081	2.973
Aspm	2.059	4.168	6.4205E-05	2.569	0.613
Asxl2	-0.321	0.801	0.00762967	25.754	32.383
Atl2	-0.592	0.663	0.04144857	55.703	83.975
Atmin	0.507	1.421	0.00099027	19.919	13.953
Atoh8	-0.862	0.55	0.00375113	2.877	5.244
Atp2a1	2.116	4.336	0.02879346	4.609	1.069
Atp5g1	1.008	2.011	0.02622743	4.694	2.367
Atp6v1c2	-2.501	0.177	0.00771432	0.182	1.031

Atp6v1g2	-0.778	0.583	0.04271546	2.205	3.806
Atr	-0.398	0.759	0.02062587	11.224	14.694
Atxn10	-0.348	0.786	0.01830146	30.085	38.33
Atxn1l	0.482	1.397	0.0123078	11.986	8.518
B230206L02Rik	-0.87	0.547	0.00915426	2.332	4.166
B230217C12Rik	-1.547	0.342	0.01100192	0.489	1.421
B330016D10Rik	-0.503	0.705	0.02269117	6.722	9.512
Bace1	-0.315	0.804	0.01624866	28.155	35.125
BC017158	-0.6	0.66	0.00570186	5.628	8.607
Bcl7b	0.506	1.42	8.2089E-06	36.994	26.014
Birc5	1.263	2.401	0.01084621	2.821	1.175
Bloc1s6	0.392	1.313	0.02836145	16.55	12.692
Bpifa1	5.503	45.34	1.3505E-05	10.011	0.221
Brd2	-0.466	0.724	1.5917E-08	106.037	146.552
Brip1	1.568	2.964	0.00882291	1.6	0.538
Brpf1	-0.341	0.789	0.01000485	20.702	26.152
Bzw1	0.464	1.379	0.0002167	44.97	32.549
C030013C21Rik	-1.002	0.499	0.04337751	0.991	1.958
C130023A14Rik	-1.001	0.5	0.00119674	2.303	4.563
C1galt1	0.443	1.359	0.01939095	15.077	11.144
C430014B12Rik	1.249	2.376	0.01002189	2.544	1.071
Cab39l	-0.302	0.811	0.03367737	28.972	35.426
Cacng4	-1.347	0.393	0.04269066	0.608	1.584
Cant1	-0.332	0.794	0.04871906	15.877	20.227
Capg	0.642	1.56	0.03199668	5.73	3.619
Capza2	0.227	1.17	0.02110231	63.576	54.168
Casp1	-0.561	0.678	0.00898411	5.924	8.7
Casq1	1.818	3.525	0.02859832	7.903	2.25
Cavin2	-0.192	0.875	0.01638826	369.129	421.701
Cavin4	1.32	2.497	0.00738885	3.418	1.391
Ccdc157	-0.906	0.534	0.0033675	2.732	5.142
Ccdc69	-0.365	0.776	0.02201271	24.243	31.078
Ccl12	1.667	3.175	0.02268027	1.619	0.499
Ccl7	1.627	3.088	0.04747562	1.023	0.324
Ccna2	1.365	2.577	0.01391203	2.318	0.885
Ccser2	-0.346	0.787	0.00065158	81.764	103.89
Cd22	1.82	3.53	0.01443679	1.731	0.488
Cd300ld	0.809	1.752	0.0028699	7.803	4.408
Cd68	0.718	1.644	0.00264377	10.235	6.147
Cdadc1	-0.366	0.776	0.00076055	27.765	35.898
Cdc42se1	0.371	1.293	0.01443804	25.461	19.576
Cdca2	1.85	3.606	0.00311833	1.657	0.449
Cdkl5	-0.774	0.585	0.0123078	2.919	5.011
Cdyl2	-0.704	0.614	0.01335986	3.724	6.223
Cenpo	-0.935	0.523	0.02820645	1.281	2.469
Cep104	0.344	1.269	0.0409412	18.18	14.301
Cep128	-0.858	0.552	0.0387089	1.63	2.953
Cep55	1.388	2.617	0.0212722	1.519	0.58

Chga	-1.165	0.446	0.01731539	1.769	4.118
Chm	0.404	1.324	0.0056351	19.499	14.838
Chn1os3	-1.64	0.321	0.03454004	0.322	1.006
Chrm2	-1.183	0.441	0.0408536	1.406	3.251
Chuk	0.332	1.258	0.00389575	33.288	26.554
Ciita	0.927	1.902	0.03435459	3.98	2.076
Cilp	0.905	1.872	0.00412879	11.279	6.049
Ckap2	2.284	4.87	0.00284894	1.363	0.278
Ckap2l	2.4	5.278	9.8771E-05	1.933	0.366
Ckm	2.134	4.39	0.00443854	44.352	10.108
Ckmt2	1.867	3.647	0.01452381	52.171	14.314
Cldn12	0.481	1.395	0.00145658	18.296	13.166
Clec16a	0.59	1.505	0.0002295	17.21	11.361
Clec1a	0.634	1.551	0.00191196	15.365	9.91
Clec4n	2.072	4.205	0.00324232	1.643	0.382
Clic1	0.373	1.295	0.04455952	14.262	11.03
Clip1	0.342	1.267	0.00085961	78.156	61.788
Clip3	-0.645	0.64	0.03139475	5.777	9.069
Clspn	1.59	3.011	0.03163548	1.342	0.435
Cmc1	-0.335	0.793	0.00037152	57.486	72.287
Cnih1	-0.239	0.847	0.02723654	43.44	51.16
Col20a1	-1.777	0.292	0.00534839	0.525	1.889
Col5a3	0.749	1.681	1.1083E-06	51.156	30.424
Coro1a	0.806	1.749	0.02945193	4.884	2.8
Cox15	0.401	1.32	0.00030006	58.163	44.123
Crk	0.443	1.359	0.00082261	27.696	20.338
Crmp1	-2.109	0.232	0.00444813	0.285	1.263
Crtc3	-0.32	0.801	0.03660366	15.608	19.463
Csgalnact2	0.551	1.465	0.0302705	7.404	5.063
Csnk1g3	0.356	1.28	0.02945193	17.047	13.354
Ctsa	0.307	1.237	0.04509729	17.601	14.235
Cx3cl1	1.018	2.025	0.0177663	3.222	1.595
Cystm1	1.2	2.297	3.0682E-07	17.991	7.863
Cyth2	0.379	1.3	0.01341538	26.101	20.126
D030056L22Rik	-0.801	0.574	0.00292509	4.116	7.25
D10Wsu102e	-0.517	0.699	0.0190988	7.34	10.655
D130062J10Rik	-0.981	0.506	0.03128139	1.184	2.304
D16Ertd472e	-0.6	0.66	1.1802E-06	16.112	24.337
Dcbld2	-0.811	0.57	0.00697508	3.054	5.302
Dctn4	0.261	1.198	0.00881899	59.667	49.715
Dcun1d4	0.435	1.352	0.03306573	13.307	9.783
Dcun1d5	0.342	1.267	0.01416349	30.871	24.284
Ddit4l	1.59	3.01	0.0164722	3.557	1.197
Det1	0.594	1.509	0.02424098	7.994	5.262
Dgke	-0.427	0.744	0.04159031	7.993	10.615
Dhodh	-0.388	0.764	0.01512322	13.182	17.12
Dhtkd1	-1.201	0.435	0.04500101	0.945	2.255
Dhx37	0.958	1.942	0.02253031	2.604	1.327

Dnaja1	0.492	1.407	0.00017215	29.937	21.23
Dnaja4	2.398	5.269	0.0058643	1.021	0.193
Dnajc12	-1.215	0.431	0.00018865	1.598	3.762
Dnajc19	-0.328	0.797	0.00512119	34.633	43.375
Dnmbp	-0.625	0.648	0.0079759	5.361	8.173
Doc2g	-0.858	0.552	0.03200818	1.976	3.569
Dock4	-0.378	0.769	0.04218473	11.471	14.954
Drd2	-1.92	0.264	0.03882479	0.242	0.981
Dsp	-1.105	0.465	0.03658179	1.614	3.531
Dtd1	-0.422	0.746	0.00868964	13.219	17.708
Dtl	1.299	2.46	0.00130448	3.324	1.345
Dtymk	-0.425	0.745	0.04993573	11.208	14.902
Dus4l	-0.809	0.571	0.04842293	1.655	2.977
Dusp12	-0.648	0.638	0.0202703	5.029	7.836
E030030I06Rik	-0.91	0.532	0.01186762	1.66	3.145
E130307A14Rik	-1.099	0.467	0.00204625	2.041	4.452
E130309D02Rik	0.637	1.555	0.00082583	11.296	7.276
E2f5	-0.452	0.731	0.04602301	6.154	8.427
Ebna1bp2	0.41	1.329	0.00068755	30.19	22.696
Eda2r	2.897	7.446	0.00050547	1.408	0.189
Ednra	-0.69	0.62	0.0228604	3.795	6.115
Efcab12	1.976	3.934	0.01254484	1.37	0.339
Ehmt1	-0.262	0.834	0.01200014	34.846	41.833
Eif2b3	0.436	1.353	0.00883149	17.561	12.935
Elmo2	0.396	1.316	0.01785034	18.147	13.668
Elp2	-0.271	0.829	0.02953174	26.201	31.508
Emd	-0.351	0.784	0.03874727	20.961	26.841
Ensa	0.624	1.541	2.0962E-05	24.41	15.853
Epb41l3	-0.683	0.623	0.02884712	2.689	4.342
Epb41l4a	-0.668	0.629	0.02859832	3.436	5.568
Ercc6l2	0.466	1.381	0.03142278	10.547	7.689
Erg28	0.34	1.266	0.03145641	19.866	15.626
Eya4	-1.578	0.335	0.00600344	0.512	1.563
F2r	0.846	1.797	4.1151E-06	21.055	11.752
F3	-0.907	0.533	0.00025605	4.531	8.429
Fads6	1.058	2.083	0.04335006	2.182	1.059
Fam149a	-0.919	0.529	0.00045596	3.88	7.241
Fam160a1	1.199	2.296	0.02340703	2.01	0.888
Fam172a	-0.405	0.755	0.02953174	10.855	14.548
Fam181b	0.913	1.884	0.00783381	4.864	2.525
Fam214b	0.381	1.303	0.0029126	27.695	21.318
Fbh1	0.314	1.243	0.02381242	28.891	23.408
Fbp1	1.626	3.087	0.00672918	1.716	0.547
Fbxo27	2.364	5.149	0.01661934	0.879	0.17
Fbxo3	0.203	1.151	0.02763579	66.081	57.371
Fbxo34	0.479	1.394	0.03638303	10.123	7.328
Fbxo7	-0.575	0.671	5.8545E-05	12.79	18.835
Fbxw8	0.707	1.633	0.04434848	4.652	2.79

Fcsk	-0.764	0.589	0.00592383	4.435	7.498
Fgf10	-1.098	0.467	0.02503127	1.54	3.201
Fignl2	-0.552	0.682	0.03835476	6.884	10.048
Filip1	0.687	1.61	0.01047645	7.554	4.715
Fitm1	1.731	3.318	0.03091928	2.625	0.809
Flnb	0.348	1.273	0.00355006	36.929	28.936
Flnc	1.282	2.432	0.01448177	5.056	2.093
Flot1	-0.36	0.779	0.00587505	30.138	38.7
Fntb	-0.673	0.627	0.00065084	6.591	10.515
Fos	-0.967	0.512	0.02280573	1.53	2.976
Fus	-0.419	0.748	0.00347609	289.907	387.996
Fxr2	-0.344	0.788	0.00663788	42.594	54.197
Fxyd5	0.472	1.387	0.01088721	12.047	8.613
Fyn	0.437	1.354	0.0258116	13.628	10.119
Gabarapl2	0.543	1.457	0.00017199	26.339	18.053
Gas1	0.393	1.313	0.01022264	36.982	28.17
Gcat	0.417	1.335	0.01744068	14.619	10.933
Gcc1	-0.486	0.714	0.04496746	5.832	8.26
Gck	-1.334	0.397	0.03038398	0.798	2.078
Get1	-0.43	0.742	0.04932949	7.726	10.391
Ggact	0.978	1.97	0.02817495	2.383	1.212
Glrx	0.517	1.431	0.02704113	14.062	9.741
Glt28d2	1.377	2.597	0.00521034	2.11	0.814
Glyr1	0.246	1.186	0.04539258	46.632	39.586
Gm11520	1.608	3.048	0.00103496	2.616	0.858
Gm11716	1.596	3.023	0.00741479	2.286	0.769
Gm12795	-0.917	0.529	0.03786138	1.274	2.353
Gm12940	-0.882	0.543	0.04159426	1.433	2.629
Gm15261	-1.675	0.313	0.00381707	0.54	1.67
Gm19514	0.872	1.83	2.2956E-05	21.277	11.639
Gm20219	-2.24	0.212	0.00574135	0.246	1.307
Gm20379	-1.121	0.46	0.04262723	0.757	1.707
Gm20594	2.15	4.438	0.00722566	1.193	0.278
Gm21992	-1.491	0.356	0.04975695	0.344	0.97
Gm25930	-1.73	0.302	0.01190685	0.395	1.433
Gm26594	1.97	3.917	0.03244727	0.847	0.221
Gm26944	-0.825	0.565	0.04572597	1.491	2.619
Gm29560	4.013	16.15	0.00147891	0.934	0.053
Gm30015	2.05	4.141	0.02128575	0.904	0.218
Gm31251	-2.162	0.223	0.01993432	0.371	1.742
Gm3235	-1.722	0.303	0.0470562	0.337	1.041
Gm34474	-1.276	0.413	0.03571706	0.641	1.595
Gm36371	0.683	1.605	0.00468771	10.286	6.443
Gm36608	-1.527	0.347	0.0409412	0.391	1.129
Gm36963	-0.996	0.501	8.264E-07	4.396	8.786
Gm37090	-1.206	0.434	0.02225112	0.842	1.907
Gm37274	-0.647	0.639	0.00035949	7.07	10.993
Gm37474	-0.34	0.79	0.04469283	15.385	19.506

Gm37709	1.689	3.224	0.03809537	1.278	0.409
Gm38042	-0.498	0.708	0.00858492	9.125	12.766
Gm42515	-0.839	0.559	0.0129687	2.217	3.911
Gm42633	-0.888	0.54	0.00628595	2.977	5.379
Gm42639	-1.266	0.416	0.01251193	0.926	2.363
Gm42659	-0.533	0.691	0.00148987	10.449	15.177
Gm42979	-0.573	0.672	0.04046299	5.476	8.224
Gm43410	-1.733	0.301	0.01005755	0.395	1.478
Gm43482	-1.907	0.267	0.00420864	0.559	2.029
Gm43588	-1.394	0.381	0.03981067	0.619	1.534
Gm43605	-1.054	0.482	0.04844615	2.595	5.288
Gm43727	-1.022	0.493	0.04815381	0.858	1.709
Gm44829	-0.622	0.65	0.0177663	4.684	7.225
Gm45120	-1.694	0.309	0.04025565	0.261	0.927
Gm45222	-1.177	0.442	0.03977857	0.664	1.569
Gm45413	-0.91	0.532	0.03401282	1.641	3.031
Gm45449	-1.912	0.266	0.00400549	0.422	1.522
Gm45572	-1.646	0.32	0.01219524	0.42	1.304
Gm45698	-1.296	0.407	0.02434026	0.848	2.109
Gm45838	1.14	2.203	0.02102358	2.033	0.919
Gm47138	-0.964	0.513	0.0190484	1.764	3.442
Gm47601	-1.094	0.468	0.00883984	1.561	3.255
Gm47817	-0.708	0.612	0.01789308	4.098	6.738
Gm49123	0.802	1.744	0.02280573	4.451	2.512
Gm49307	-1.169	0.445	0.00263044	1.439	3.222
Gm5144	0.791	1.73	0.03709973	3.365	1.947
Gm6658	0.955	1.938	0.04230191	2.148	1.12
Gm7607	1.013	2.018	0.03328442	2.753	1.373
Gm9885	-0.499	0.708	0.02350396	9.117	12.881
Gmeb1	0.762	1.696	0.00033643	8.98	5.329
Gna12	0.324	1.252	0.04825324	23.6	18.778
Gnai3	0.433	1.35	0.00842407	19.324	14.214
Gorasp2	0.223	1.167	0.03190992	43.949	37.554
Gpbp1	-0.271	0.829	0.03422962	31.165	37.763
Gpkow	-0.491	0.711	0.01887367	8.796	12.33
Gpsm3	0.904	1.871	0.00565225	5.641	2.958
Gramd1b	-0.46	0.727	0.0180539	18.162	25.013
Gramd3	0.471	1.386	0.03540249	11	8.05
Grid2	-0.982	0.506	0.00968163	1.595	3.226
Gtf2h1	0.434	1.351	0.00013492	40.554	30.019
Gtf2i	-0.246	0.843	0.03312795	70.137	83.132
Gusb	0.32	1.248	0.04335006	20.414	16.388
H19	2.651	6.28	9.5583E-05	56.724	9.036
H1f0	0.252	1.191	0.02545987	123.803	103.975
Hace1	-0.844	0.557	0.04402132	1.494	2.8
Hamp	-2.935	0.131	6.9113E-05	0.415	3.319
Haus1	-1.608	0.328	0.01830146	0.395	1.198
Hcls1	0.562	1.476	0.01627904	9.647	6.475

Hcn4	-1.848	0.278	0.00027711	0.669	2.299
Hdac6	-0.573	0.672	0.03257136	7.94	11.992
Hlf	-0.415	0.75	0.0490839	27.235	36.257
Hlx	-0.438	0.738	0.00598917	14.716	19.891
Hmmr	2.065	4.183	0.00166567	1.493	0.369
Hnrnpa2b1	-0.221	0.858	0.0032674	118.613	137.952
Hnrnpl	-0.239	0.847	0.04702956	45.724	53.904
Hotairm1	-0.665	0.631	0.00535621	4.579	7.226
Hoxa7	-0.359	0.78	0.04341826	19.06	24.386
Hoxa9	-1.43	0.371	2.5402E-05	2.042	5.486
Hps4	-0.52	0.697	0.01602048	7.023	10.11
Hps5	-0.442	0.736	0.04300871	9.353	12.61
Hrh2	-1.353	0.392	0.00190342	1.085	2.824
I830077J02Rik	1.117	2.169	0.04429714	1.806	0.831
Ift20	-0.372	0.773	1.8277E-05	115.516	149.438
Ift74	0.496	1.411	0.00488406	11.998	8.517
Ighg2c	-3.82	0.071	0.03315621	0.297	4.181
Il2rb	-0.985	0.505	0.01856585	1.303	2.578
Insl6	1.106	2.152	0.01769048	2.531	1.15
Insyn1	1.064	2.091	0.01872142	2.633	1.26
Irak3	0.614	1.531	0.00823476	10.83	7.086
Irs2	-1.222	0.429	0.01490476	34.003	79.334
Irx3	0.733	1.663	0.00842195	8.283	4.995
Ist1	0.283	1.216	0.0020851	57.587	47.385
Itgae	1.314	2.487	0.0031973	2.912	1.152
Itgam	0.745	1.676	0.04746378	4.528	2.739
Itgb1	0.237	1.179	0.00047999	124.028	105.315
Itm2c	-0.243	0.845	0.03770402	34.981	41.45
Jak1	0.19	1.141	0.04832621	131.977	115.458
Jmjd6	0.245	1.185	0.04288134	34.961	29.554
Jsrp1	2.249	4.755	0.00071763	3.968	0.854
Junb	-0.523	0.696	0.00638871	11.823	17.185
Kansl3	-0.329	0.796	0.00504942	62.732	78.845
Kat8	0.539	1.453	0.02945337	6.79	4.678
Kcna1	-0.631	0.646	0.00893342	5.635	8.756
Kcnab3	-0.967	0.512	0.04358966	1.42	2.693
Kctd14	-1.615	0.327	0.00160992	0.894	2.745
Kdsr	0.234	1.176	0.0491119	43.673	37.105
Khdc4	-0.312	0.805	0.00523564	37.86	46.803
Khk	-0.514	0.7	0.01079294	7.539	10.664
Klhl25	-0.788	0.579	0.00242982	5.214	8.911
Klhl30	2.16	4.469	0.01794935	0.967	0.223
Klhl31	1.742	3.344	0.02030748	6.672	2.011
Klhl40	2.614	6.121	0.01673807	3.661	0.598
Klhl41	1.817	3.522	0.01186762	7.189	2.055
Kmt5c	-0.456	0.729	0.04008001	8.548	11.759
Laptm5	0.531	1.445	0.01798638	19.567	13.476
Las1l	-0.232	0.852	0.04794618	31.688	36.988

Lbx1	2.433	5.4	0.0335605	0.871	0.165
Lclat1	0.396	1.316	0.00695603	19.974	15.28
Lcmt2	0.718	1.644	0.00030936	11.95	7.218
Lgmn	0.35	1.275	0.02170525	19.489	15.411
Limd1	0.368	1.29	0.00800304	72.717	56.366
Lin9	-0.692	0.619	0.0424973	3.497	5.545
Llgl2	1.156	2.228	0.00995192	3.502	1.563
Lmo4	-0.248	0.842	0.00811585	85.927	102.248
Lmod3	1.594	3.019	0.00064537	6.666	2.244
Lrp6	-0.255	0.838	0.03328098	42.824	51.427
Lrrc28	0.502	1.417	0.01615956	11.976	8.455
Lrrc30	2.091	4.261	0.04344621	1.628	0.388
Lrrc9	-1.435	0.37	0.00851772	0.724	2.011
Lrrfip1	0.431	1.348	0.00211757	29.208	21.701
Lst1	0.807	1.749	0.02259713	3.736	2.127
Lyst	-0.418	0.749	0.03212435	12.208	16.322
Lyz2	0.706	1.631	5.6243E-08	91.526	55.992
Magi2	-0.913	0.531	8.6827E-05	3.671	6.866
Magix	0.877	1.836	0.04577099	2.595	1.416
Man1a	0.773	1.709	0.00083554	9.838	5.789
Man2a2	-0.449	0.733	6.9627E-06	51.199	70.01
Map1lc3a	-0.218	0.86	0.025176	195.542	227.358
Map3k20	0.335	1.262	0.00838227	37.683	29.95
Map3k8	1.013	2.018	0.04197541	2.057	1.036
Map7	0.62	1.537	0.03200818	6.754	4.353
Mapk1	0.264	1.201	0.02296337	47.017	39.076
Matn4	-1.24	0.423	0.01299673	0.82	2.036
Mboat2	-0.934	0.523	0.01277865	1.696	3.266
Mcm3ap	-0.409	0.753	0.01472638	12.703	16.82
Mcm5	1.006	2.008	0.0321825	2.958	1.464
Med11	0.525	1.439	0.00332688	12.214	8.42
Med17	-0.5	0.707	0.00709293	9.037	12.932
Med23	-0.501	0.706	0.03244727	7.62	10.815
Med4	-0.422	0.746	0.00575244	17.038	22.63
Mettl15	-1.064	0.478	0.00261037	1.734	3.63
Mettl21e	2.186	4.55	0.01926079	0.98	0.215
Mettl24	-1.733	0.301	0.03330375	0.355	1.282
Mettl27	-0.422	0.746	0.02747404	9.989	13.333
Mga	0.238	1.179	0.00732345	71.615	60.75
Micu2	0.342	1.267	0.00568679	26.641	20.966
Mis18bp1	1.754	3.373	0.00103496	2.589	0.761
Mllt1	0.444	1.36	0.03328442	9.368	6.906
Mmp12	3.553	11.73	4.204E-05	1.679	0.142
Mob1a	0.263	1.2	0.02632429	38.561	32.15
Morc4	0.507	1.421	0.00687925	12.868	9.079
Mpeg1	0.796	1.736	0.01119776	5.546	3.153
Mpp3	-1.242	0.423	0.01080956	1.476	3.461
Mrgbp	0.395	1.315	0.025145	14.704	11.265

Mrln	2.821	7.067	0.04678711	0.957	0.137
Ms4a6d	0.951	1.933	0.03014882	2.928	1.508
Msln	1.235	2.354	0.01109178	3.135	1.315
Msx1	0.63	1.548	0.04107645	5.404	3.468
Mta3	0.556	1.47	0.02352319	9.729	6.642
Mtfmt	-0.67	0.628	0.01241879	5.267	8.336
Mtmr3	0.422	1.34	0.00381347	23.528	17.531
Mtpn	0.231	1.173	0.0094437	71.82	61.165
Mtr	-0.931	0.524	6.173E-06	5.677	11.119
Mup11	2.861	7.265	0.00128129	1.205	0.161
Mvb12b	-0.462	0.726	0.03509981	7.451	10.423
Mvp	-0.413	0.751	0.00217383	16.148	21.406
Mxi1	0.547	1.461	0.00037152	24.816	17.013
Myadml2	2.772	6.83	0.04517748	0.912	0.134
Mybpc1	2.756	6.756	0.00064173	15.099	2.241
Myc	-1.807	0.286	0.00732297	0.437	1.58
Mycn	2.395	5.259	8.492E-05	2.005	0.386
Myg1	-0.391	0.762	0.02073703	12.134	15.8
Myh1	2.357	5.123	0.00042205	8.539	1.677
Myh2	2.962	7.79	0.00015119	26.255	3.381
Myl2	2.301	4.928	0.0152449	14.334	2.914
Myl6	-0.318	0.802	0.01345153	33.011	41.226
Myl7	-2.481	0.179	0.03772662	11.923	66.647
Mylk2	2.767	6.807	0.00292778	1.504	0.233
Mylpf	2.627	6.179	0.00042992	96.157	15.569
Myom3	0.855	1.809	0.02213512	11.439	6.389
Myot	2.648	6.266	0.00106046	9.192	1.477
Myoz1	2.368	5.164	0.0173974	8.043	1.562
Mzf1	-1.845	0.278	0.03544073	0.227	0.925
Nab1	0.311	1.241	0.01300102	33.444	27.025
Nbr1	0.28	1.214	0.0057194	64.596	53.218
Ncapg	1.977	3.937	0.01022291	1.345	0.341
Ncf1	0.994	1.991	0.0022355	4.862	2.48
Nctc1	2.9	7.464	0.00357764	3.8	0.519
Neb	2.308	4.95	0.00278128	85.529	17.286
Nes	0.674	1.596	0.00018565	21.133	13.209
Nfe2l2	0.28	1.214	0.03863581	80.767	66.651
Ngfr	-1.157	0.448	0.04366365	8.582	19.189
Ngly1	0.43	1.347	0.00415589	29.263	21.62
Nicn1	-0.321	0.801	0.02840397	19.29	23.992
Nin	0.505	1.419	0.02597221	9.756	6.887
Nipsnap3b	-0.42	0.747	0.0484855	7.376	9.834
Nmrk2	2.764	6.791	0.00289371	1.659	0.25
Nox4	0.875	1.834	0.03975965	2.446	1.334
Nprl2	-0.429	0.743	0.01728559	14.221	18.814
Nrap	2.475	5.56	0.00953965	1.678	0.31
Nrg2	1.578	2.985	0.03773805	0.992	0.338
Ntng1	-0.943	0.52	0.04747562	1.702	3.182

Ntpcr	-0.975	0.509	0.00018001	4.031	7.957
Numa1	-0.47	0.722	0.00036512	20.618	28.468
Numb	1.361	2.569	1.1318E-08	11.555	4.52
Orai1	0.638	1.556	0.00060144	15.526	9.946
Orai3	0.36	1.283	0.02918345	30.648	23.968
Ormdl1	-0.574	0.672	0.02143584	5.353	7.855
Osr2	0.934	1.911	0.01391791	2.949	1.565
Pabpn1	-0.373	0.772	0.00244589	23.765	30.939
Pafah1b3	0.754	1.687	0.0499719	4.268	2.541
Pank3	-0.302	0.811	0.02948073	68.751	85.035
Parn	-0.496	0.709	0.00168435	12.027	16.963
Pcdhb20	-1.332	0.397	0.04050664	0.498	1.239
Pdcl	0.413	1.331	0.04366145	11.495	8.665
Pde4b	0.419	1.337	0.02071802	22.43	16.803
Per3	-0.843	0.557	0.03106148	36.376	65.3
Pf4	0.57	1.485	1.6129E-06	34.643	23.198
Pfas	-0.479	0.717	0.02971426	8.174	11.486
Pfn1	0.562	1.476	0.0166834	15.861	10.763
Pgf	1.255	2.386	0.01088595	2.029	0.866
Phax	0.321	1.249	0.03647178	29.351	23.461
Phgdh	-1.679	0.312	0.02802018	0.346	1.145
Phka2	-0.368	0.775	0.00212765	24.434	31.52
Phyhip	-2.124	0.229	0.00406734	0.289	1.227
Pigp	-0.445	0.735	0.03757221	9.81	13.269
Pik3ca	0.25	1.189	0.03097068	60.428	50.738
Pim3	-0.707	0.612	2.8103E-05	82.937	135.614
Pir	0.539	1.453	0.03292958	7.86	5.353
Pirt	-0.941	0.521	0.03577614	3.164	6.154
Pithd1	-0.365	0.777	0.04040514	18.984	24.296
Plat	0.617	1.534	0.04852323	5.152	3.32
Plk1	1.293	2.45	0.03956748	1.624	0.665
Plk3	1.193	2.286	0.00673178	2.42	1.063
Pln	-1.788	0.29	0.04614717	1.908	6.689
Plod1	0.283	1.217	0.00370975	53.998	44.278
Plpp1	1.889	3.703	0.01887367	1.118	0.309
Plxna1	-0.412	0.752	0.01422091	18.587	24.827
Pnkd	-0.528	0.693	0.00013441	31.01	44.466
Poc1b	-0.504	0.705	0.01324204	6.896	9.835
Pold3	0.56	1.474	0.04468714	6.023	4.102
Polg	-0.334	0.793	0.03203118	15.35	19.545
Polk	-0.525	0.695	0.0382476	4.544	6.515
Ppan	-0.483	0.716	0.04197541	7.102	9.831
Ppip5k2	-0.442	0.736	0.02124158	10.648	14.554
Ppox	-0.43	0.742	0.04231074	8.763	11.851
Ppp1r27	3.039	8.221	1.0568E-05	3.849	0.476
Ppp6c	0.259	1.196	0.01189004	53.299	44.521
Prcc	0.751	1.683	0.02843926	4.483	2.604
Preb	-0.365	0.777	0.01329935	24.315	31.286

Prg4	0.895	1.859	0.04704216	3.5	1.864
Prkab2	-0.458	0.728	0.02902241	9.798	13.487
Prkca	-0.54	0.688	0.00753508	7.385	10.792
Proser1	-0.342	0.789	0.03066277	13.825	17.632
Prpf18	0.385	1.306	0.01472638	17.712	13.577
Prrc2b	-0.267	0.831	0.03999083	21.676	26.186
Prrg2	-0.384	0.766	9.533E-05	33.195	43.08
Psmc3ip	1.357	2.561	0.0348539	1.347	0.524
Psmd13	0.322	1.25	0.00388776	70.041	56.126
Psmd9	0.395	1.315	0.03084727	17.504	13.24
Psmg4	-0.584	0.667	4.2446E-05	12.584	18.913
Ptdss1	-0.295	0.815	0.04196369	28.75	35.148
Pttg1	-0.285	0.821	0.00901712	104.675	127.543
Pttg1ip	-0.182	0.882	0.02784015	122.119	138.299
R3hdm4	-0.487	0.714	7.2643E-06	40.126	56.38
Rab12	0.222	1.167	0.03353663	109.743	94.138
Rab18	0.179	1.132	0.04539219	70.164	62.003
Rabep2	-0.63	0.646	0.02225112	3.704	5.744
Rabgap1	-0.301	0.812	0.02099959	23.373	29.116
Rabgef1	0.569	1.484	0.00670051	10.682	7.252
Rabif	0.327	1.255	0.03323249	19.412	15.422
Rad51	2	3.999	0.02297163	1.041	0.264
Rad51b	-0.935	0.523	0.0484855	1.174	2.235
Rap2c	0.412	1.331	0.0074266	25.361	18.909
Rasa1	0.275	1.21	0.00800001	70.742	58.519
Rassf9	0.665	1.586	0.00114917	17.078	10.709
Rbfox2	-0.353	0.783	0.01088197	25.805	33.134
Rbm14	-0.597	0.661	0.0202638	6.566	9.919
Rbm17	0.446	1.362	0.00202064	31.99	23.512
Rbmx	-0.561	0.678	0.00243288	8.579	12.77
Rce1	0.612	1.528	0.01160265	9.981	6.552
Rdh16	3.646	12.52	3.4272E-11	4.521	0.345
Relb	-0.569	0.674	0.00869555	5.521	8.191
Rem1	-1.19	0.438	0.03947316	0.71	1.687
Rgs12	1.006	2.009	0.0009306	4.685	2.316
Rhoq	0.2	1.149	0.02030748	160.783	140.013
Rilpl1	0.538	1.452	0.019014	11.26	7.755
Ripk3	1.509	2.847	0.00058527	2.741	0.944
Rnf115	0.362	1.285	0.00766893	23.61	18.316
Rnf122	-0.895	0.538	0.01833884	1.886	3.441
Rnf123	-1.788	0.29	0.00258191	0.476	1.609
Rnf216	-0.341	0.79	0.0173974	17.624	22.257
Rp9	-0.186	0.879	0.02551053	88.37	100.488
Rpap2	-0.402	0.757	0.0366858	8.66	11.451
Rpl3l	2.35	5.099	0.00278128	8.163	1.612
Rpl9	-0.662	0.632	0.04917609	3.122	4.966
Rplp0	-0.347	0.786	0.00034332	81.233	103.163
Rps11-ps1	-1.266	0.416	0.00881607	1.046	2.44

Rps16	-1.071	0.476	0.04262723	0.919	1.954
Rrm1	0.48	1.395	0.00916327	15.979	11.43
Rtn2	1.16	2.234	0.00890857	6.549	2.968
Ryr1	2	4	0.01046752	11.702	2.938
S100a11	0.278	1.212	0.01046102	83.896	69.096
S100g	1.962	3.895	0.00119948	1.863	0.472
Sac3d1	-0.468	0.723	0.01471723	8.86	12.125
Sacs	0.732	1.661	0.00064967	8.706	5.265
Safb2	-0.275	0.826	0.00714533	41.933	50.938
Sap30	1.961	3.894	0.00309064	1.414	0.363
Sat1	0.717	1.644	0.01309404	7.03	4.289
Sat2	-0.906	0.534	0.00788732	2.481	4.506
Sbk3	-1.549	0.342	0.02761803	0.955	2.882
Scgb1a1	4.796	27.79	4.4471E-05	17.812	0.642
Scn4b	1.829	3.554	8.3199E-05	4.081	1.169
Sdhaf2	0.251	1.19	0.04258539	43.263	36.336
Secisbp2l	0.322	1.25	0.00161203	60.803	48.792
Sel1l3	1.543	2.913	0.0429773	1.839	0.641
Selenof	0.458	1.374	6.7402E-05	123.453	89.809
Senp2	0.348	1.273	0.01323273	24.259	19.101
Serf1	-0.674	0.627	0.00011576	10.105	15.947
Serinc2	3.454	10.96	1.4383E-05	2.099	0.191
Sertad1	-0.448	0.733	0.04186906	11.512	15.692
Sertad2	-0.508	0.703	0.00037965	12.856	18.351
Sestd1	0.548	1.462	0.03612099	7.539	5.191
Sfswap	-0.259	0.836	0.01452381	40.93	48.932
Sgcb	0.444	1.36	0.00081315	25.883	19.026
Sh3bgr	1.23	2.345	6.9093E-05	10.663	4.604
Sh3tc1	0.661	1.581	0.04137589	5.304	3.356
Shank1	-1.442	0.368	0.04466046	0.393	1.176
Siah1a	0.558	1.472	0.00652261	9.631	6.582
Sin3b	-0.202	0.869	0.04907926	51.063	58.459
Sirt1	-0.688	0.621	0.00019089	7.282	11.639
Slc20a2	0.732	1.661	0.00021297	21.759	13.19
Slc35b2	-0.377	0.77	0.04495857	21.483	28.057
Slc43a3	0.377	1.298	0.04390113	20.202	15.704
Slc4a11	-1.647	0.319	0.00166229	0.594	1.867
Slc9a3r1	0.642	1.56	0.01783023	6.338	4.042
Slit2	-1.35	0.392	0.0065597	0.799	2.012
Smap2	0.469	1.384	0.00788732	15.153	10.916
Smim27	-0.461	0.727	0.00771346	17.281	23.462
Smtnl1	3.255	9.548	0.00107304	5.786	0.607
Smurf2	0.28	1.215	0.04874966	22.937	18.835
Smyd3	-0.631	0.646	0.04167525	3.695	5.692
Snhg12	-0.688	0.621	0.01309404	5.859	9.424
Snhg4	-0.599	0.66	0.00959814	5.77	8.767
Snrnp200	-0.292	0.817	0.00461042	39.037	47.79
Sntb2	0.45	1.366	0.01746604	21.222	15.543

Snx15	0.596	1.512	0.0057194	9.226	6.071
Snx3	0.227	1.171	0.00189885	154.772	132.31
Socs6	0.404	1.323	0.01522772	19.276	14.587
Sox7	0.637	1.555	0.00536465	9.895	6.327
Spast	-0.354	0.783	0.01813466	18.443	23.797
Spata6	-0.785	0.58	0.00213079	4.047	6.903
Specc1l	-0.344	0.788	0.00914455	18.712	23.703
Sppl2a	0.411	1.329	0.00013058	83.551	62.956
Spred2	0.607	1.523	0.04712744	7.159	4.735
Sptssa	-0.289	0.818	0.03033938	23.499	28.845
Ss18	-0.348	0.786	0.02717563	23.883	30.381
Ssu2	1.164	2.24	0.01653771	2.323	1.029
Stat3	-0.397	0.759	1.8587E-08	78.814	103.619
Stk38l	-0.497	0.708	0.00934665	10.163	14.317
Sumf2	-0.585	0.667	0.02368423	5.224	7.797
Suox	-0.332	0.794	0.02806548	16.334	20.622
Synj2bp	0.215	1.161	0.03486451	67.465	57.841
Sypl2	1.942	3.842	0.00039818	3.922	1.037
Tango6	-0.636	0.643	0.01118502	4.567	7.118
Tbx15	1.741	3.344	0.02859832	1.844	0.568
Tbx5	-0.576	0.671	0.01431492	6.952	10.461
Tbxa2r	1.422	2.679	0.0275907	1.679	0.621
Tcaf1	-0.493	0.711	0.01102943	12.385	17.589
Tceal5	1.718	3.29	0.03385933	1.076	0.335
Tceal7	6.541	93.15	0.0021406	2.386	0
Tead1	0.32	1.248	0.01249881	31.757	25.402
Thap12	0.273	1.209	0.03106148	46.723	38.702
Tk2	-0.363	0.777	0.03976189	11.115	14.405
Tmem129	-0.507	0.704	0.00804271	8.902	12.564
Tmem139	2.545	5.838	0.00212003	1.336	0.228
Tmem164	-0.526	0.694	0.01820878	6.205	9.032
Tmem17	-1.377	0.385	0.01261447	0.698	1.731
Tmem175	-0.556	0.68	0.02352319	4.752	7.072
Tmem189	0.557	1.471	0.00044201	18.97	12.999
Tmem234	-0.225	0.856	0.03596431	68.878	80.003
Tmem245	-0.267	0.831	0.020603	33.283	40.108
Tmem251	0.611	1.527	0.00323599	10.742	7.009
Tmem52	2.406	5.3	0.00635195	2.16	0.412
Tmem9	-0.448	0.733	0.00883348	10.566	14.38
Tmod4	2.335	5.044	0.00023771	4.852	0.973
Tnfaip2	0.952	1.934	0.00475448	5.157	2.699
Tnnc2	2.479	5.573	0.01088721	7.458	1.344
Tnni2	2.664	6.336	0.00050799	162.624	25.673
Tnnt1	2.045	4.127	0.00322579	15.124	3.679
Tnnt3	2.496	5.642	0.00134118	153.018	27.128
Tob2	-0.578	0.67	1.8226E-07	138.481	206.91
Tollip	0.357	1.281	0.00990397	27.941	21.883
Tpcn2	1.267	2.406	8.7263E-05	4.161	1.729

Tpm2	1.76	3.387	0.00900158	116.433	34.394
Tpm3	0.537	1.451	0.02030748	31.239	21.66
Tpx2	1.542	2.912	0.0049521	2.204	0.742
Trappc10	0.318	1.247	0.01779621	31.491	25.277
Trdn	1.499	2.826	0.04720358	60.738	21.506
Tshr	-1.025	0.491	0.01400443	4.123	8.324
Ttc21b	-0.826	0.564	0.02265337	2.055	3.661
Ttk	2.099	4.283	0.0145281	0.941	0.218
Ttyh1	-0.763	0.589	0.01656112	3.134	5.31
Tubb6	0.433	1.35	0.0330367	13.071	9.653
Twist2	-1.222	0.429	0.01658312	1.148	2.588
Txn1	-0.265	0.832	0.00028276	154.326	185.444
Uaca	0.382	1.304	0.00688437	28.286	21.747
Uba5	-0.28	0.824	0.02457522	32.334	39.279
Ube2c	1.13	2.189	0.04476115	1.911	0.867
Ube2q1	0.351	1.275	0.00320616	47.563	37.301
Ube2r2	-0.185	0.879	0.01472638	136.649	155.222
Ucp2	0.311	1.241	0.04738909	20.674	16.573
Unc50	-0.394	0.761	0.0005006	32.168	42.034
Unk	-0.521	0.697	0.03758557	5.027	7.304
Upk3b	0.75	1.681	0.04712229	5.603	3.334
Usp24	0.32	1.248	0.01202426	43.57	34.821
Usp36	-0.279	0.824	0.00519107	40.78	49.624
Usp4	0.279	1.213	0.00327708	49.34	40.596
Uty	-0.31	0.807	0.036665	17.682	21.779
Uxs1	-0.503	0.705	0.00800001	9.522	13.646
Vapa	0.437	1.354	2.0086E-06	84.423	62.309
Vcpip1	-0.381	0.768	0.01712847	13.898	18.153
Vgll2	2.431	5.392	0.0197902	3.535	0.658
Vip	1.128	2.186	0.0329929	3.682	1.673
Vps39	0.503	1.417	0.00825357	13.257	9.292
Vps51	0.666	1.587	0.02847184	4.676	2.938
Vps54	0.357	1.281	0.04974597	18.185	14.217
Wdr13	-0.289	0.818	0.03296517	26.68	32.706
Wdr33	0.23	1.173	0.02531488	48.773	41.65
Wfdc2	3.72	13.18	0.01149487	1.062	0.082
Wfs1	0.557	1.471	0.01986167	9.593	6.51
Wnt11	-1.539	0.344	0.00136464	0.757	2.289
Wwox	-0.444	0.735	0.01244679	9.042	12.191
Xirp1	1.832	3.561	0.01180201	1.964	0.569
Xirp2	1.466	2.764	0.03038398	43.132	15.619
Xkr6	1.432	2.697	0.00645259	1.883	0.695
Xpr1	0.466	1.382	0.00011727	30.438	21.994
Xrcc1	-0.509	0.703	0.02531488	8.457	11.94
Xylt2	-0.613	0.654	0.00095885	8.621	13.132
Yipf7	1.748	3.358	0.04619007	2.002	0.607
Zbtb6	-0.48	0.717	0.03271341	6.798	9.311
Zbtb8os	0.444	1.36	0.00874633	16.899	12.325

Zdhhc23	1.021	2.029	0.00326254	4.369	2.147
Zfp27	0.735	1.664	0.00946429	6.246	3.761
Zfp3	-0.713	0.61	0.040336	2.401	3.897
Zfp346	0.716	1.642	0.02624154	6.453	3.957
Zfp422	0.684	1.607	0.00933037	6.388	3.977
Zfp438	-1.478	0.359	0.00164625	1.233	3.457
Zfp579	-0.573	0.672	0.04335006	4.964	7.427
Zfp592	-0.419	0.748	0.00916327	11.862	15.77
Zfp653	-0.514	0.7	0.04411212	4.878	6.84
Zfp869	-0.484	0.715	0.00122042	11.933	16.767
Zfp949	-0.826	0.564	0.02397246	1.964	3.476
Zim1	-1.469	0.361	0.02137516	0.473	1.408
Zkscan17	-0.593	0.663	0.02459704	5.011	7.508

Table 9. Cold-responsive protein-coding genes (also predicted), and lncRNA genes found in PVAT but not in PBAT, WATg, or WATi

Cold-responsive protein-coding genes (also predicted), and lncRNA genes found in WATg but not in BAT, PVAT, or WATi:

Symbol	log2(fold change)	Ratio	padj	Mean WATg 4°C	Mean WATg 23°C
1700066M21Rik	0.936	1.913	0.01143634	6.315	3.31
1810013L24Rik	0.413	1.332	0.00688784	78.042	58.597
1810058I24Rik	0.393	1.313	1.6779E-05	176.639	134.54
2310068J16Rik	1.026	2.037	0.02800749	3.683	1.801
2610016A17Rik	0.684	1.607	0.0439776	47.094	29.298
4930578M01Rik	-0.759	0.591	0.00741061	8.285	14.033
4932438A13Rik	-0.32	0.801	0.02618292	70.631	88.162
8030487O14Rik	-0.659	0.633	0.02220637	5.617	8.881
A130048G24Rik	-0.68	0.624	0.02807089	9.475	15.153
A330076H08Rik	-1.877	0.272	0.00056374	0.846	3.139
A830052D11Rik	2.077	4.221	9.8252E-05	3.241	0.767
A930007A09Rik	-1.234	0.425	0.02205169	1.269	3.011
Abca9	-0.62	0.651	0.03522776	9.907	15.257
Abcb9	0.535	1.449	0.00557485	16.377	11.282
Abhd14a	0.793	1.732	0.00085069	19.178	11.05
Abhd17a	0.478	1.393	0.0010505	49.415	35.499
Abhd4	0.515	1.429	0.0052064	56.975	39.892
Acp6	0.667	1.588	3.4429E-06	49.218	30.952
Adam22	-0.895	0.538	0.02562893	3.687	6.88
Adh5	0.307	1.237	0.00977637	119.497	96.558
Adpgk	0.521	1.435	0.01513053	22.748	15.799
Adrm1	0.683	1.606	0.01602753	10.599	6.59
Aff3	-0.857	0.552	0.02451167	5.509	10.021
Ahi1	-0.549	0.683	0.02084766	12.833	18.766
Akap13	-0.265	0.832	0.00999077	167.646	201.447
Akap8	-0.27	0.829	0.01549335	45.199	54.554
Akr1a1	0.333	1.26	0.00931572	398.368	316.227

Akr1e1	0.416	1.334	0.00366317	41.783	31.327
Aldh3b1	-0.754	0.593	0.02743205	4.51	7.641
Aldh7a1	0.311	1.241	0.03161901	48.81	39.334
Alg2	0.581	1.496	0.03033376	19.098	12.766
Alg5	0.556	1.47	1.188E-06	65.515	44.562
Amdhd2	0.607	1.523	0.00700934	22.452	14.733
Amn1	-0.329	0.796	0.00227857	53.296	66.962
Anapc5	-0.192	0.875	0.03467781	98.278	112.291
Angptl8	1.827	3.547	0.02507919	39.945	11.274
Ankrd26	-0.568	0.675	0.00094261	15.963	23.705
Anxa1	-0.618	0.652	0.01357297	141.265	216.819
Anxa5	-0.211	0.864	0.02520141	288.232	333.831
Ap2s1	0.359	1.283	0.00753498	68.182	53.105
Apeh	0.51	1.425	0.01085376	37.243	26.148
Aph1b	-0.406	0.755	0.03304818	17.718	23.483
Arhgap17	-0.408	0.754	0.015523	25.728	34.156
Arhgap21	-0.39	0.763	0.00857296	46.952	61.496
Arhgap32	-0.577	0.67	0.01331552	13.678	20.444
Arhgdib	-0.415	0.75	0.02185653	16.869	22.454
Arid3a	-0.586	0.666	0.03094544	9.606	14.45
Arl6ip4	0.321	1.249	0.03874271	58.653	46.988
Arrb2	0.639	1.557	0.00023641	43.54	27.948
Arsk	-0.517	0.699	0.04427468	15.011	21.455
Asap1	-0.278	0.825	0.02578833	80.932	98.096
Asap3	-0.875	0.545	0.0333439	3.62	6.636
Asb8	0.322	1.25	0.02488039	36.296	29.014
Atg7	0.371	1.293	0.01400594	56.541	43.727
Atp10a	-0.774	0.585	0.00859027	5.452	9.363
Atp13a2	0.462	1.377	0.04587858	24.873	18.086
Atp2b1	-0.453	0.731	3.7696E-05	202.221	276.686
Atp5j	1.096	2.138	4.1255E-06	162.286	75.939
AU022252	0.656	1.575	0.00226841	21.103	13.401
AU041133	-1.074	0.475	0.00573363	2.402	5.034
Axin2	-1.179	0.442	4.8797E-05	12.377	28.023
B130024G19Rik	-0.884	0.542	0.00433847	7.905	14.628
B3galt1	1.48	2.79	4.4562E-05	5.871	2.093
B3gnt8	-1.19	0.438	3.2197E-05	6.99	15.919
B430010I23Rik	0.343	1.268	0.03993299	104.327	82.245
Bad	0.393	1.313	0.04544578	53.861	41.005
Bcat1	-1.565	0.338	0.00732544	2.379	7.044
Bcl2	-0.648	0.638	9.9358E-09	38.608	60.514
Blmh	0.556	1.47	0.00031758	94.682	64.395
Bola1	0.471	1.386	0.01085376	32.019	23.083
Borcs8	0.602	1.518	0.0050965	18.567	12.226
Bpgm	0.563	1.478	0.00091295	27.633	18.699
Btd	0.523	1.437	0.02649326	25.641	17.85
C2cd2l	1.432	2.699	3.8287E-15	95.569	35.385
C530043K16Rik	-0.42	0.748	0.03954562	12.667	16.892

C6	-1.051	0.483	0.00113247	23.42	48.51
C7	-1.186	0.439	0.0045575	2.439	5.603
C920021L13Rik	0.616	1.532	0.01802649	13.411	8.738
Cacna1e	-1.822	0.283	0.00028683	1.138	4.019
Camp	1.399	2.637	0.00358872	4.105	1.552
Capzb	0.315	1.244	0.0394558	192.874	155.017
Car11	0.991	1.987	0.01180308	7.326	3.699
Casq2	-1.474	0.36	0.00636526	1.815	5.062
Ccdc107	0.52	1.434	0.00707184	20.062	13.987
Ccdc66	-0.604	0.658	0.00487227	9.928	15.124
Ccdc71l	-0.59	0.664	0.01054077	15.055	22.654
Ccdc73	0.447	1.363	0.02690301	18.537	13.622
Ccdc88b	-1.127	0.458	0.02989177	1.431	3.117
Ccm2	0.594	1.509	0.00600052	34.393	22.802
Ccn4	-3.165	0.111	0.00181701	1.143	10.291
Ccng1	0.499	1.414	0.00289488	114.938	81.278
Cct7	0.413	1.331	0.02411543	169.451	127.24
Cd180	-0.726	0.605	0.03874271	3.602	5.952
Cd44	-0.663	0.632	0.02854525	21.598	34.224
Cd53	-0.667	0.63	0.01337769	10.757	17.125
Cdc42bpb	-0.449	0.733	0.04967791	11.913	16.306
Cdc42se2	-0.377	0.77	0.03200396	29.098	37.716
Cdk17	-0.393	0.762	0.04256007	19.638	25.78
Cdk5r1	-1.037	0.487	0.0079981	4.696	9.641
Cenpx	0.342	1.268	0.02886888	33.35	26.288
Cep112	-0.648	0.638	0.00694505	10.384	16.338
Cep126	-1.146	0.452	0.03858391	3.593	7.975
Cep170	-0.484	0.715	0.00872532	23.17	32.427
Cep290	-0.497	0.709	0.03336222	25.733	36.385
Cept1	0.63	1.547	0.00010276	61.158	39.515
Chmp2a	0.287	1.22	0.03020092	115.791	94.851
Chmp7	0.326	1.254	0.02902485	36.93	29.422
Ciart	0.908	1.877	0.02527964	10.745	5.727
Cidec	0.496	1.41	0.0079981	2707.786	1920.483
Clmp	1.034	2.048	1.3149E-13	182.213	88.985
Cmtm4	0.437	1.354	0.02256106	25.361	18.737
Cnih4	0.301	1.232	0.02649251	55.465	45.018
Cntln	-0.558	0.679	0.00056152	44.941	66.181
Cntrl	-0.438	0.738	0.00553839	32.716	44.338
Cog4	0.608	1.525	0.00033025	97.75	64.109
Cog8	0.438	1.354	0.01118509	59.56	43.95
Commd4	0.527	1.441	0.00060734	43.567	30.235
Copz1	0.494	1.408	0.00058016	143.935	102.178
Coq2	0.777	1.714	0.00201917	15.982	9.329
Cox16	1.658	3.156	0.01976186	3.964	1.263
Cplane1	-0.599	0.66	0.03215108	11.806	17.915
Cpsf1	0.365	1.288	0.02079603	52.631	40.89
Cpsf3	0.374	1.296	0.01815518	77.131	59.538

Cpxm1	-1.143	0.453	0.001823	3.023	6.726
Creld1	0.431	1.349	0.03621904	53.043	39.324
Cry2	-0.308	0.808	0.00986495	41.322	51.144
Cryzl2	0.748	1.679	0.00584074	12.871	7.675
Csnk2b	0.349	1.274	0.0073344	107.438	84.307
Ctif	0.7	1.625	0.00539761	21.875	13.47
Cttnbp2	-1.379	0.384	0.00250427	1.674	4.321
Cuta	0.498	1.412	0.00999077	66.438	47.018
Cxcl13	-2.081	0.236	0.00719403	1.459	6.167
Cyb5d2	0.652	1.571	0.00746224	16.836	10.751
Cyp27a1	-0.541	0.687	0.0066268	35.37	51.448
Cysltr1	-0.797	0.576	0.01694237	3.885	6.778
Cyth4	-0.441	0.736	0.02694074	17.08	23.216
D230025D16Rik	0.798	1.739	0.02231508	5.504	3.16
Dap	0.331	1.258	0.00212761	133.388	106.005
Dcst1	-0.596	0.662	0.01300129	7.345	11.068
Dctn2	0.234	1.176	0.04160321	145.135	123.411
Ddit4	-0.925	0.527	0.00072605	50.43	95.766
Ddx41	0.517	1.431	0.01201327	20.287	14.18
Ddx5	-0.375	0.771	0.00172025	216.978	281.331
Ddx60	-0.665	0.631	0.01762295	11.828	18.787
Dedd2	0.517	1.431	0.04150503	10.043	7.017
Derl2	0.269	1.205	0.04101288	61.887	51.382
Dhcr7	0.941	1.92	0.00286432	18.41	9.601
Dipk2b	-1.017	0.494	0.02419779	1.593	3.215
Disp1	-0.763	0.589	0.00330321	6.752	11.482
Dmtf1	-0.454	0.73	0.00797469	27.569	37.846
Dock10	-0.511	0.702	0.0133157	21.796	31.067
Dock2	-0.566	0.675	0.02413795	9.971	14.819
Dohh	0.356	1.28	0.01002019	35.204	27.536
Dok7	-1.222	0.429	0.02512611	1.885	4.398
Dpagt1	0.299	1.23	0.0358693	38.002	30.911
Dpf3	0.593	1.509	0.04894884	7.056	4.675
Dpm2	0.406	1.325	0.02276566	34.366	25.959
Dpm3	0.369	1.292	0.00092194	112.76	87.288
Dst	-0.423	0.746	0.00508843	234.223	314.08
Dtx3l	0.43	1.347	0.01278798	36.835	27.357
Dynlrb1	0.453	1.369	0.00487046	181.355	132.499
Egfros	-1.072	0.476	0.00094914	3.147	6.584
Ehd3	-0.95	0.518	7.2638E-08	17.424	33.643
Eif2b1	0.521	1.435	0.00753498	35.688	24.818
Eif3i	0.258	1.195	0.04711364	145.589	121.787
Elmod3	0.623	1.54	0.00121195	39.945	25.884
Elp3	0.45	1.366	0.00894496	42.684	31.251
Ep400	-0.229	0.853	0.04315946	67.929	79.623
Epb41	0.32	1.249	0.00651126	92.773	74.26
Epc2	-0.319	0.801	0.03172355	37.813	47.232
Ephb1	-1.284	0.411	0.00819563	2.147	5.175

Eps15	-0.385	0.766	0.00088538	41.663	54.376
Epsti1	-0.475	0.72	0.04106326	10.177	14.171
Ergic3	0.573	1.487	0.0089079	89.58	60.247
Etv1	-1.204	0.434	0.02269418	3.743	8.651
Exd1	0.73	1.658	0.01645983	13.873	8.351
Exoc6	-0.535	0.69	0.03242708	18.461	26.775
F830016B08Rik	-1.354	0.391	0.00524291	1.141	2.93
Fadd	0.502	1.416	0.01001947	17.115	12.075
Faf1	0.329	1.256	0.01573875	47.02	37.446
Fam117a	0.74	1.67	0.00107287	32.356	19.357
Fam120a	0.401	1.32	0.0216691	163.492	123.836
Fam120c	-0.842	0.558	0.01326384	4.601	8.227
Fam49a	-0.499	0.708	0.03142145	10.659	15.07
Fam76a	-0.458	0.728	0.01814401	15.993	22.019
Fam81a	-2.289	0.205	0.0359794	0.933	4.598
Fancl	0.655	1.574	0.00749528	15.368	9.779
Fastkd3	0.574	1.488	0.03044752	9.334	6.265
Fbxl20	0.412	1.33	0.0184848	27.578	20.701
Fbxl6	0.864	1.82	0.00149063	16.919	9.309
Fbxo4	0.374	1.296	0.00645001	61.271	47.262
Fbxo8	0.358	1.282	0.03662477	42.287	32.981
Fcgrt	0.515	1.429	0.0024876	205.945	144.141
Fchsd2	-0.481	0.716	0.00582311	19.483	27.273
Filip1l	-0.396	0.76	0.02339163	60.732	79.969
Fkbp14	-0.463	0.725	0.02488597	12.018	16.57
Fkbp1a	0.387	1.307	0.03044752	323.341	247.313
Fkbp1b	-1.212	0.432	0.01975586	1.319	3.086
Fkbp2	0.447	1.363	0.00023496	84.886	62.322
Fkbp5	-0.716	0.609	0.00097779	59.097	97.056
Fli1	-0.651	0.637	0.0014126	48.819	76.649
Fmnl1	-0.585	0.667	0.03521731	6.466	9.694
Fmnl3	-0.568	0.675	0.02105288	7.823	11.568
Fndc3b	-0.454	0.73	0.00228687	83.231	114.013
Fnta	0.348	1.273	0.03106081	122.964	96.606
Folh1	-1.148	0.451	0.03029247	3.494	7.786
Foxp1	-0.302	0.811	0.00914763	121.975	150.361
Foxs1	-0.784	0.581	0.0255137	3.739	6.463
Fyb	-0.705	0.613	0.00066406	20.02	32.701
Gab3	-0.543	0.686	0.03808282	7.764	11.305
Gbp9	-0.807	0.571	0.0018849	6.963	12.183
Gid4	0.46	1.375	0.00886066	44.086	32.025
Gimap8	-0.8	0.574	0.00222393	12.212	21.261
Git2	-0.315	0.804	0.01244589	79.182	98.555
Glo1	0.56	1.475	2.8925E-06	74.648	50.62
Gm10115	-0.726	0.604	8.5907E-05	23.926	39.595
Gm10419	1.031	2.044	0.0002689	13.726	6.699
Gm11773	2.262	4.797	0.03904336	2.991	0.636
Gm13340	1.243	2.366	0.02600675	3.229	1.373

Gm13594	-0.838	0.559	0.01273333	3.366	5.993
Gm14049	0.968	1.956	0.00793587	5.396	2.752
Gm15635	0.968	1.957	0.03215108	5.474	2.802
Gm16124	0.516	1.43	0.01901949	11.879	8.28
Gm16235	1.043	2.061	0.02981709	2.967	1.451
Gm16731	1.939	3.834	0.00024151	3.863	1.009
Gm17018	0.477	1.392	0.01428968	20.133	14.451
Gm1966	-1.007	0.498	0.02393756	2.9	5.878
Gm22482	-0.679	0.625	0.04596832	5.323	8.506
Gm26569	-1.553	0.341	0.00010666	1.635	4.816
Gm26588	0.66	1.58	0.0460412	9.746	6.167
Gm26881	0.574	1.488	0.0335239	18.658	12.561
Gm28119	-0.736	0.6	0.04570192	5.362	8.959
Gm33432	1.704	3.257	0.002467	6.185	1.904
Gm34294	-0.73	0.603	0.00234004	7.924	13.097
Gm34907	-2.001	0.25	0.00040692	0.915	3.664
Gm37060	-0.801	0.574	0.00025438	10.039	17.499
Gm37333	-0.571	0.673	0.02938615	10.826	16.097
Gm37423	-0.666	0.63	0.00784854	6.622	10.524
Gm38104	-0.739	0.599	0.00642767	6.421	10.737
Gm4117	-0.645	0.64	0.01546106	5.996	9.367
Gm42517	1.044	2.062	0.01087812	7.511	3.627
Gm42778	-0.751	0.594	0.0449883	5.164	8.709
Gm42946	0.618	1.535	0.03528841	14.334	9.355
Gm43527	1.057	2.08	0.03444432	3.536	1.689
Gm43528	1.219	2.328	0.0216691	2.819	1.213
Gm43627	-1.117	0.461	0.03545373	1.293	2.776
Gm43793	-0.82	0.566	0.00319523	5.263	9.335
Gm43813	-0.691	0.62	0.04151983	5.539	8.958
Gm44432	-0.846	0.556	0.0449883	3.332	5.962
Gm44674	-1.156	0.449	0.04544578	1.199	2.675
Gm44956	0.957	1.942	0.04698127	4.488	2.314
Gm44996	-0.808	0.571	0.01440044	5.02	8.759
Gm45338	1.107	2.154	0.02940182	5.096	2.352
Gm45343	-0.703	0.614	0.01660579	5.086	8.291
Gm454	1.649	3.136	0.0087574	3.174	1.02
Gm45407	-0.822	0.566	0.02834622	4.001	7.058
Gm47000	1.029	2.04	0.04688788	4.619	2.263
Gm47583	-1.284	0.411	0.02419779	1.511	3.708
Gm48768	-0.635	0.644	0.03939478	4.676	7.243
Gm48878	-2.132	0.228	9.6828E-06	0.883	3.87
Gm48972	-1.522	0.348	0.00591377	0.951	2.727
Gm49041	0.786	1.724	0.03807166	6.036	3.481
Gm49226	-0.643	0.64	0.04106326	3.95	6.162
Gm50010	-1.046	0.484	0.0106464	2.381	4.901
Gm960	1.33	2.514	2.2729E-07	20.655	8.214
Gna11	0.415	1.333	0.00058862	132.132	99.186
Gnb4	-1.165	0.446	3.5874E-13	27.736	62.148

Gne	0.556	1.47	0.00331785	24.731	16.8
Gnpat	0.374	1.296	0.01326384	160.861	124.132
Gps1	0.862	1.817	0.04167043	4.581	2.501
Gpx4-ps2	0.61	1.527	0.01731181	9.515	6.23
Grwd1	0.605	1.521	0.03533372	9.846	6.489
Gsr	0.433	1.35	0.01064226	25.156	18.626
Gt(ROSA)26Sor	-0.506	0.704	0.0014631	17.359	24.67
Gtpbp1	0.645	1.564	0.03411468	28.096	17.969
H1f10	1.246	2.373	3.3301E-08	30.941	13.043
H2-T24	-0.587	0.666	0.04394756	7.095	10.629
H2aj	0.318	1.247	0.00651126	62.169	49.763
Halr1	-1.721	0.303	0.00077727	0.975	3.159
Haus7	0.601	1.517	0.01904931	10.437	6.863
Hectd3	0.389	1.31	0.01514636	37.178	28.411
Hecw2	-0.84	0.559	0.00148867	5.463	9.756
Hexa	0.687	1.61	1.0883E-07	80.237	49.835
Hfe	0.416	1.335	0.00642767	84.467	63.334
Hip1	-0.646	0.639	9.4223E-06	40.828	63.911
Hmgb1-ps8	-0.8	0.574	0.03334313	2.708	4.702
Hnrnpu	0.333	1.26	0.0361013	33.357	26.473
Hpca	-2.883	0.136	1.3136E-05	0.573	4.219
Hprt	0.409	1.328	0.01481808	142.988	107.596
Hps3	-0.447	0.733	0.0462655	18.604	25.439
Hsbp1	0.505	1.419	0.00766877	239.556	168.845
Hspa2	-0.987	0.504	0.00414258	7.63	15.173
Hspb7	-1.518	0.349	0.03116432	2.029	5.837
Htra4	-1.061	0.479	0.00808663	3.053	6.381
Ice1	-0.562	0.677	0.00030158	24.593	36.272
Icmt	0.541	1.455	0.01365093	13.312	9.135
Ide	1.303	2.468	0.02916861	2.707	1.106
Idh1	0.429	1.346	0.02260595	422.368	313.642
Idnk	0.641	1.559	0.02577085	47.017	30.176
Ifi203-ps	-0.829	0.563	0.00704678	6.554	11.646
Ifi205	-0.673	0.627	0.02303435	7.492	11.891
Ikbkb	-0.275	0.826	0.02242096	50.796	61.41
Il15ra	0.556	1.47	0.007971	43.574	29.621
Imp3	0.258	1.196	0.04868439	57.851	48.314
Inmt	-1.082	0.472	0.0001347	87.278	184.78
Ino80	-0.321	0.801	0.04420671	34.998	43.715
Ints9	0.411	1.33	0.02220637	19.203	14.443
Ipo5	0.296	1.228	0.02762215	55.909	45.535
Iqgap1	-0.291	0.818	0.00298579	156.697	191.664
Irf8	-0.676	0.626	0.00199036	20.68	33.111
Iscu	1.163	2.238	9.8958E-05	20.053	8.941
Itgal	-0.927	0.526	0.03594463	2.138	4.086
Itgb1bp1	0.393	1.313	0.01942164	120.633	91.832
Itpripl1	-0.411	0.752	0.03044752	13.515	17.959
Itsn1	-0.321	0.8	0.04972561	51.586	64.464

Itsn2	-0.391	0.762	0.00470607	100.607	131.923
Jcad	-0.383	0.767	0.01077802	61.923	80.739
Jchain	-1.509	0.351	0.0077815	4.341	12.318
Jkamp	0.53	1.444	1.3891E-05	69.629	48.202
Josd1	0.579	1.494	0.02572328	30.632	20.511
Josd2	0.655	1.575	0.01989735	22.137	14.065
Jpt1	0.532	1.445	0.02854525	37.291	25.773
Jpt2	-0.887	0.541	0.0018849	4.875	9.065
Kcnc2	-1.089	0.47	0.03792639	1.911	4.081
Kcnq1ot1	-0.472	0.721	1.5097E-05	204.142	283.139
Kiz	-0.327	0.797	0.04156476	24.065	30.207
Klhl5	-0.471	0.722	1.6352E-05	57.924	80.313
Kmt2b	0.565	1.479	0.04892816	14.984	10.134
Kmt2d	-0.364	0.777	0.033259	30.946	39.952
Kptn	0.539	1.453	0.04763112	9.577	6.613
Kremen1	-0.46	0.727	0.04021438	16.231	22.307
L3hypdh	0.438	1.355	0.01399415	38.236	28.176
Lage3	0.39	1.311	0.02689842	48.16	36.713
Larp1b	0.528	1.442	1.0505E-05	133.439	92.545
Lbh	-0.649	0.638	0.00774407	19.542	30.709
Ldb3	0.972	1.961	0.0041003	7.735	3.908
Ldhd	1.144	2.209	6.1161E-05	21.948	9.961
Ldlrad3	0.481	1.396	0.01054981	22.238	15.931
Lhfpl2	-0.489	0.712	0.00029657	48.725	68.415
Lima1	-0.474	0.72	0.00376886	85.229	118.379
Lipg	2.369	5.164	2.0156E-05	6.402	1.244
Lman2l	0.417	1.335	0.04515262	39.392	29.509
Lpar4	-0.596	0.662	0.01110298	16.934	25.597
Lrch1	-0.574	0.672	0.01194809	12.013	17.911
Lrif1	-0.465	0.725	0.01572051	28.474	39.316
Lrrc29	0.967	1.954	0.01010423	4.547	2.323
Lrrn4cl	0.663	1.583	0.04833254	12.358	7.828
Lxn	-0.507	0.704	0.03497191	9.219	13.169
Ly6h	-1.259	0.418	0.01275086	1.558	3.719
Lyn	-0.422	0.746	0.0033443	32.579	43.61
Lzts2	0.795	1.735	0.04006796	11.606	6.683
Maf1	0.319	1.248	0.02070983	50.481	40.436
Map1a	-0.739	0.599	0.00522562	12.092	20.221
Map3k5	0.402	1.322	0.01654336	52.084	39.423
Map4	-0.486	0.714	4.657E-05	55.755	78.21
Map6	1.108	2.155	6.9138E-05	31.514	14.651
Mark1	-0.872	0.546	0.0200473	4.675	8.572
Masp1	1.159	2.234	0.00023473	15.746	7.025
Mast4	-0.345	0.787	0.00298483	54.476	69.225
Mbd4	-0.903	0.535	0.01443456	3.11	5.797
Mbnl1	-0.503	0.706	0.00096701	380.545	539.215
Mccc1	0.61	1.526	0.00033858	186.407	122.145
Me2	0.721	1.648	1.8075E-05	24.245	14.682

Mecom	-0.601	0.659	0.01569368	16.867	25.579
Mest	-2.009	0.248	8.8155E-06	2.345	9.428
Mettl7b	0.764	1.698	0.02821383	10.536	6.166
Mfsd6	-0.45	0.732	0.04387844	11.907	16.283
Mgat5	0.638	1.556	0.00058179	27.023	17.39
Mgst1	0.651	1.57	0.00017697	1371.56	873.72
Mical2	-0.731	0.603	0.00256489	10.479	17.406
Micall1	-0.608	0.656	0.00131509	24.325	37.177
Mier1	-0.275	0.826	0.03764465	95.957	116.163
Mindy1	0.411	1.329	0.02878421	37.375	28.096
Mir100hg	-0.571	0.673	0.00132096	37.417	55.614
Mir703	-0.482	0.716	0.02618292	20.926	29.225
Mob4	0.376	1.298	0.01738303	58.437	44.988
Mocs1	0.373	1.295	0.02371907	45.214	34.842
Mogat2	2.088	4.253	2.9636E-05	4.673	1.104
Mospd3	0.459	1.375	0.03767113	24.874	18.122
Mpzl1	-0.539	0.688	0.01546106	12.605	18.306
Mrm2	0.64	1.559	0.01458139	11.856	7.603
Mrpl10	0.372	1.294	0.01275086	28.629	22.083
Mrpl22	0.585	1.5	0.02937452	9.56	6.348
Mrpl33	0.265	1.202	0.01389736	124.984	104.019
Mrpl41	0.504	1.418	0.0017145	43.275	30.537
Mrpl49	0.38	1.301	0.01672357	47.497	36.488
Mrps24	0.482	1.396	0.00022575	58.582	41.957
Mrps26	0.391	1.312	0.00504259	47.989	36.527
Ms4a1	-1.241	0.423	0.04150238	1.458	3.454
Mthfr	-1.085	0.471	8.1227E-05	8.195	17.404
Mthfsl	0.733	1.662	0.00078005	13.978	8.406
Mtmr4	0.436	1.353	0.0067924	35.121	25.986
Mvk	0.509	1.423	0.04864237	25.858	18.171
Mydgf	0.318	1.247	0.04575497	41.618	33.325
Myh14	0.776	1.712	0.01092558	7.92	4.628
Myo9b	-0.67	0.628	0.00190145	11.371	18.039
N4bp2l1	0.464	1.38	0.02735264	73.541	53.31
Nabp2	0.463	1.378	0.01911666	36.271	26.297
Nadk	0.334	1.261	0.0061594	193.947	153.829
Natd1	0.718	1.644	0.00017032	35.203	21.434
Nav1	-0.225	0.855	0.0343258	94.599	110.646
Naxe	0.332	1.259	0.02017638	91.461	72.677
Ncbp2	0.451	1.367	0.00191529	57.629	42.1
Nckap5l	-0.938	0.522	0.0373423	1.628	3.111
Ncoa2	-0.321	0.801	0.04950451	29.608	37.017
Ncs1	-1.172	0.444	0.04519942	1.508	3.408
Ndufaf3	0.545	1.459	0.00102389	35.908	24.595
Nepn	-1.088	0.47	0.00577332	2.414	5.13
Nexn	-0.601	0.659	0.02413474	37.538	56.984
Nfs1	0.457	1.372	0.00080284	56.517	41.187
Nfxl1	-0.6	0.66	0.02711937	6.924	10.542

Nit2	0.605	1.521	0.00107658	23.715	15.612
Nkiras1	0.382	1.303	0.02466142	24.083	18.478
Nlrx1	0.657	1.576	0.00025602	21.773	13.831
Nmnat3	0.883	1.844	3.1357E-05	18.926	10.266
Nol12	0.539	1.453	0.01156163	19.248	13.221
Nol6	0.347	1.272	0.03653275	49.815	39.098
Nomo1	0.493	1.407	0.00028715	67.827	48.199
Nop9	0.472	1.387	0.04040227	17.445	12.589
Npepl1	0.294	1.226	0.03627807	49.425	40.346
Nr1d1	0.691	1.615	0.01383953	85.008	52.658
Nsun2	0.37	1.292	0.03653275	59.638	46.104
Ntan1	0.628	1.546	0.00751951	15.712	10.163
Nudcd3	0.385	1.306	0.00996702	81.628	62.507
Nup160	-0.679	0.625	0.02944292	4.425	7.087
Oaf	0.51	1.424	0.03209601	33.847	23.813
Oas1c	-1.376	0.385	0.00552016	1.279	3.356
Ormdl3	0.988	1.984	7.6675E-05	139.339	70.275
Osbpl8	-0.382	0.768	0.02190796	33.255	43.412
Osgepl1	0.645	1.563	0.0373423	6.759	4.311
Pank2	0.424	1.342	0.01546106	35	26.065
Park7	0.498	1.412	1.1867E-05	243.919	172.668
Parl	0.345	1.27	0.0060905	40.079	31.525
Pcbp1	0.348	1.273	0.00503425	97.925	76.959
Pcdh12	-1.041	0.486	0.00698805	5.423	11.155
Pde4dip	0.636	1.555	2.5497E-06	69.05	44.348
Pex7	0.468	1.383	0.00615904	30.656	22.126
Pfdn2	0.453	1.369	0.01042913	39.067	28.509
Pfkm	0.599	1.515	0.01609471	19.464	12.863
Pgam5	0.481	1.396	0.00364566	32.154	23.022
Pgm2l1	-0.507	0.704	0.04191758	16.072	22.793
Pi4k2a	0.471	1.386	0.00876164	43.985	31.734
Pigk	0.345	1.27	0.03874688	56.585	44.503
Pigo	0.661	1.581	0.0114321	11.211	7.092
Pigx	0.383	1.304	0.04698612	19.006	14.567
Pigyl	0.387	1.307	0.019881	34.649	26.468
Pinx1	0.385	1.306	0.04905174	22.253	17.021
Pip4k2a	-0.562	0.677	0.00175353	14.047	20.731
Pitpnm3	-0.818	0.567	0.03879627	2.49	4.396
Plbd2	0.566	1.48	0.00038083	63.893	43.144
Plekha2	-0.558	0.679	4.0975E-05	22.666	33.414
Plekha7	-1.222	0.429	0.0120095	3.304	7.731
Pnpo	0.585	1.5	0.00269051	28.331	18.872
Polr2g	0.513	1.427	0.00331785	41.841	29.327
Pomt1	0.67	1.591	0.0060775	34.147	21.472
Pou2f2	-0.612	0.654	0.01491604	11.012	16.832
Ppp1r16b	-0.563	0.677	0.04539257	11.968	17.665
Pqlc2	0.552	1.466	0.04299295	10.63	7.23
Prdm11	-0.857	0.552	0.04490244	2.546	4.62

Prdm2	-0.439	0.737	0.00127327	32.692	44.363
Prickle3	-0.495	0.709	0.02185653	10.925	15.41
Prkag3	-2.661	0.158	6.095E-09	1.198	7.479
Prpf19	0.696	1.62	0.0343258	27.475	16.965
Prrx2	-1.732	0.301	0.01149055	0.889	2.953
Prtg	-1.06	0.48	0.02651166	1.633	3.422
Prxl2b	0.317	1.246	0.04314115	79.635	63.939
Psat1	0.809	1.753	1.0474E-06	173.817	99.141
Psma5	0.612	1.528	0.00088457	20.097	13.124
Psmb1	0.436	1.353	0.00010216	183.461	135.557
Psmd5	0.508	1.422	0.00039105	49.01	34.397
Pth1r	1.024	2.034	0.00113247	62.452	30.733
Ptpa	0.487	1.401	0.02070983	120.573	86.063
Ptpre	-0.572	0.673	0.00267026	27.077	40.289
Ptx3	-2.271	0.207	0.00045503	1.113	5.41
Pxmp4	0.656	1.575	2.5152E-05	174.448	110.719
Qpct	-0.894	0.538	0.00346551	4.196	7.843
Qrich1	-0.36	0.779	0.03545373	32.386	41.475
Rab15	-1.206	0.434	0.0104547	2.722	6.292
Rab26os	0.721	1.649	0.00340835	19.029	11.532
Rabac1	0.601	1.517	0.0016826	131.048	86.403
Rad18	-0.671	0.628	0.00013146	18.265	29.116
Raph1	-0.297	0.814	0.0303222	71.899	88.337
Rasal2	-0.458	0.728	0.0186929	30.071	41.282
Rassf2	0.488	1.403	0.0335239	34.541	24.599
Rassf5	-0.809	0.571	0.01272718	5.395	9.514
Rassf6	1.74	3.341	0.00029731	4.933	1.464
Rbm15	-0.525	0.695	0.00227415	21.114	30.379
Rcbtb2	0.454	1.37	0.00610203	76.269	55.701
Rfng	0.627	1.544	0.00451746	25.481	16.512
Rhbdd3	0.554	1.468	0.00165068	28.998	19.764
Rhbdl3	-0.735	0.601	0.01673608	7.012	11.653
Rhoh	-0.936	0.523	0.00529438	3.028	5.768
Rin2	0.33	1.257	0.01917879	67.989	54.111
Rnasel	-0.55	0.683	0.0076838	17.462	25.525
Rnf150	-0.398	0.759	0.01143634	19.151	25.275
Rnf217	0.769	1.704	2.1127E-05	22.167	13.005
Rnpep	0.393	1.313	0.01762295	63.675	48.418
Rock1	-0.331	0.795	0.00404827	343.976	432.54
Rock2	-0.707	0.612	5.8523E-07	324.174	529.286
Rorc	1.159	2.234	0.00048535	13.077	5.876
Rpl22l1	0.974	1.964	0.04075476	8.652	4.394
Rpp40	0.528	1.442	0.04343344	9.335	6.495
Rrs1	0.552	1.466	0.00831174	31.677	21.614
Rtl5	-1.01	0.497	0.00518764	2.422	4.871
Rufy2	-0.308	0.808	0.0462323	24.81	30.698
S1pr3	-0.798	0.575	0.01057616	9.252	16.066
Sag	-1.278	0.412	0.02618292	1.153	2.773

Samd9l	-0.535	0.69	0.00752917	16.433	23.89
Sap30l	0.334	1.261	0.02632188	32.312	25.589
Sardh	0.656	1.575	0.00202818	18.913	11.968
Scara5	-0.777	0.584	3.2022E-05	37.296	63.903
Sdccag8	-0.348	0.786	0.04905174	24.539	31.267
Sdr42e1	0.566	1.48	0.04653326	19.514	13.145
Selenop	1.104	2.149	0.04021438	7.736	3.61
Septin11	-0.637	0.643	0.00021477	44.658	69.531
Serpina3b	1.334	2.521	0.029535	14.228	5.627
Serpina3j	3.142	8.826	1.6557E-14	9.569	1.076
Serpina3k	2.301	4.929	4.9228E-10	33.887	6.854
Serpina3m	1.242	2.365	1.0838E-05	8.328	3.514
Sf3a3	-0.276	0.826	0.04087455	27.582	33.383
Sgk3	0.391	1.311	0.02263835	23.861	18.182
Sgms1	-0.304	0.81	0.00721932	60.146	74.239
Sharpin	0.41	1.328	0.0329666	27.655	20.811
Sidt2	0.429	1.346	0.00032412	76.643	56.861
Sirt6	0.728	1.657	0.03390175	4.748	2.868
Skil	-0.44	0.737	0.03447249	15.732	21.34
Slc15a2	-0.804	0.573	0.01823331	5.448	9.508
Slc16a10	-0.586	0.666	0.00480017	17.95	26.917
Slc17a5	0.471	1.386	0.02384274	15.334	11.046
Slc19a1	0.551	1.466	0.00474332	29.197	19.956
Slc25a22	0.953	1.937	3.5424E-09	68.514	35.337
Slc25a24	-0.474	0.72	0.02623592	24.304	33.804
Slc25a30	-0.618	0.652	0.00044337	24.482	37.629
Slc30a6	0.538	1.452	0.01890126	12.657	8.726
Slc35b4	0.746	1.677	2.4805E-07	55.467	33.053
Slc35f6	0.707	1.632	0.00168779	15.352	9.414
Slc39a11	0.666	1.587	0.0052064	30.448	19.193
Slc48a1	0.695	1.619	5.5438E-05	239.144	147.774
Slc5a3	-0.446	0.734	0.02002272	76.153	103.762
Slc5a6	1.387	2.616	9.2372E-07	119.544	45.68
Slc8a1	-0.91	0.532	0.00232476	9.753	18.365
Slc9a6	1.032	2.045	6.9222E-10	108.603	53.066
Slc9a9	-0.654	0.636	0.00359381	7.885	12.392
Smarce1	-0.484	0.715	0.01360102	20.156	28.111
Smim1	0.26	1.197	0.0373423	46.624	38.916
Smim26	0.689	1.612	0.00028768	45.942	28.472
Snca	1.381	2.604	0.00096989	9.86	3.771
Sncaip	-0.711	0.611	0.02041478	4.403	7.2
Snf8	0.502	1.416	0.00172833	44.118	31.146
Snn	0.427	1.345	0.04763112	27.153	20.203
Sorbs1	0.363	1.286	0.01295872	1064.861	828.177
Sox6os	0.666	1.587	0.01764585	32.046	20.201
Spcs1	0.354	1.278	0.0359794	96.34	75.352
Spcs2	0.327	1.255	0.02299417	80.701	64.269
Spg21	0.49	1.404	0.00116344	151.404	107.834

Spred1	-0.608	0.656	0.0018849	25.806	39.371
Spsb1	-0.526	0.694	0.03025618	25.585	36.789
Sptbn1	-0.558	0.679	4.1532E-09	1010.49	1487.387
Srgap2	-0.475	0.72	0.0004069	32.911	45.715
Srpr	0.604	1.52	0.0023291	21.355	14.034
Srr	0.762	1.696	8.3615E-05	29.881	17.659
Ss18l1	0.931	1.906	0.00405078	8.906	4.666
Ssr2	0.321	1.249	0.01605205	74.421	59.542
St3gal2	-0.763	0.589	9.1997E-11	28.769	48.788
St8sia4	-0.442	0.736	0.04124245	16.776	22.846
Steap2	-0.836	0.56	0.00781384	11.233	20.03
Stk11ip	-0.598	0.661	0.04515855	7.003	10.613
Strap	0.308	1.238	0.00865693	92.785	74.928
Stt3b	0.435	1.352	0.00132154	212.388	157.182
Stx18	0.629	1.546	0.00014429	27.327	17.666
Stx2	-0.451	0.732	0.00114896	32.717	44.693
Stx8	0.386	1.307	0.01975128	33.853	25.869
Surf1	0.286	1.219	0.03805316	62.939	51.653
Swsap1	0.629	1.547	0.04633056	10.33	6.663
Sys1	0.365	1.287	0.00299375	65.092	50.539
Tab3	0.478	1.393	0.00604808	27.206	19.552
Taf10	0.482	1.396	0.00447891	25.912	18.521
Taf3	-0.278	0.825	0.03673301	54.795	66.415
Tafa5	1.115	2.167	1.5824E-05	9.616	4.434
Taok3	-0.323	0.8	0.00364702	51.847	64.828
Tatdn3	-0.685	0.622	0.0032165	8.122	13.034
Tbc1d31	0.48	1.395	0.02857542	14.065	10.051
Tbc1d32	-0.449	0.732	0.03554811	12.022	16.399
Tbc1d7	0.614	1.53	0.00789276	13.114	8.576
Tbl3	0.606	1.522	0.02249649	18.077	11.872
Tfb1m	1.571	2.971	0.002002	4.336	1.475
Tgm3	5.181	36.27	1.3278E-06	6.471	0.181
Thsd7a	-0.431	0.742	0.01313786	23.055	31.052
Timm17b	0.395	1.315	0.0114321	37.729	28.674
Timp3	-0.458	0.728	0.01933157	31.791	43.672
Tle4	-0.456	0.729	0.00931572	21.53	29.533
Tm7sf2	1.378	2.599	1.4419E-05	10.095	3.89
Tmem104	0.538	1.452	0.01365168	15.242	10.489
Tmem115	0.75	1.681	5.9718E-05	19.163	11.407
Tmem134	1.929	3.807	0.02242096	4.898	1.292
Tmem161a	0.397	1.317	0.04778444	27.384	20.788
Tmem179b	0.466	1.382	0.00971874	51.645	37.403
Tmem182	0.474	1.389	0.01778266	96.361	69.409
Tmem199	0.458	1.374	0.02651166	20.071	14.618
Tmem205	0.443	1.359	0.00933028	127.183	93.551
Tmem216	0.412	1.331	0.00926535	50.322	37.819
Tmem238	0.539	1.453	0.04087829	13.369	9.196
Tmem263	-0.502	0.706	1.3553E-05	36.6	51.784

Tmem80	0.33	1.257	0.03215108	34.032	27.053
Tor1aip2	0.318	1.247	0.01977839	68.97	55.347
Tor2a	0.918	1.889	0.00553839	14.659	7.761
Tpmt	0.569	1.483	0.00126024	35.66	23.996
Trak1	0.376	1.297	0.00642767	114.271	88.054
Trappc2l	0.545	1.459	0.01323889	56.961	39.036
Trhde	0.83	1.777	0.01738303	8.963	5.047
Tril	-0.565	0.676	0.02762215	10.955	16.189
Trim39	-0.517	0.699	0.01694237	9.799	14.016
Trmt9b	0.92	1.892	0.00498412	9.441	4.968
Trpc4ap	0.352	1.276	0.01331552	64.178	50.289
Tsc1	-0.363	0.777	0.00504122	29.805	38.293
Tsc2	0.455	1.37	0.0303312	26.737	19.493
Tspan13	-0.452	0.731	0.00160892	74.064	101.289
Tspan4	1.156	2.229	0.04490244	2.824	1.266
Tsta3	0.633	1.551	0.0042418	23.122	14.905
Ttc39c	0.524	1.438	0.00359995	22.913	15.922
Ttyh2	0.669	1.59	3.8614E-06	50.562	31.781
Txnl4a	0.629	1.547	0.00645792	32.438	20.969
Uba1	0.447	1.363	0.00866717	290.563	213.075
Ubac2	0.43	1.347	0.00286432	38.772	28.784
Ube2d2a	-0.322	0.8	0.00266939	50.438	63.017
Ubr1	-0.269	0.83	0.0222846	49.147	59.215
Uchl5	0.326	1.253	0.03983501	34.953	27.921
Ugcg	-0.557	0.68	0.00085069	29.353	43.152
Uhrf1bp1l	0.307	1.237	0.00846644	107.79	87.117
Uhrf2	-0.37	0.774	0.03505415	33.034	42.735
Unc45b	-0.665	0.631	0.01227911	8.382	13.345
Unc5a	1.266	2.404	6.4758E-05	13.706	5.711
Upf2	-0.297	0.814	0.0222163	74.738	91.766
Usp20	0.6	1.516	0.00069049	20.939	13.817
Usp35	-0.475	0.719	0.01156163	19.517	27.146
Vcam1	-0.672	0.628	0.00169318	21.338	34.001
Vcp	0.322	1.25	0.00698686	168.363	134.637
Vps25	1.151	2.221	0.01995047	3.194	1.444
Vps28	0.444	1.36	0.00396961	119.457	87.845
Vps45	0.472	1.387	0.04361897	18.884	13.619
Vstm4	-0.633	0.645	0.00339572	9.286	14.405
Wbp1	0.528	1.442	0.01010423	31.8	22.079
Wdfy1	-0.597	0.661	0.00942861	10.204	15.399
Wdr18	0.357	1.281	0.03764212	32.441	25.289
Wdr35	-0.507	0.704	0.04308854	10.773	15.284
Wdr70	0.355	1.279	0.03815628	25.18	19.638
Wdr83	1.363	2.572	0.02442753	3.547	1.378
Wdr83os	0.762	1.695	0.0165105	15.364	9.082
Wdsub1	-0.329	0.796	0.03554811	31.068	38.948
Wipf1	-0.441	0.737	0.01448057	21.574	29.329
Wsb1	-0.639	0.642	0.00819563	15.071	23.469

Yif1a	0.653	1.572	0.00332954	49.453	31.477
Ykt6	0.31	1.239	0.03850247	84.376	68.084
Ypel5	0.334	1.261	0.02386059	195.009	154.675
Ythdc1	-0.29	0.818	0.03898375	50.982	62.326
Zbtb1	-0.49	0.712	0.01520093	16.047	22.561
Zbtb11os1	0.686	1.608	0.00056761	21.403	13.278
Zbtb37	-0.633	0.645	0.01481808	6.9	10.731
Zbtb5	0.505	1.419	0.0158983	20.362	14.333
Zc3h10	-0.625	0.648	0.0243365	8.263	12.724
Zcchc10	-0.411	0.752	0.03070859	16.696	22.177
Zdhhc4	0.543	1.457	0.00074113	68.843	47.25
Zfas1	0.419	1.337	0.00338444	46.039	34.411
Zfp142	-0.896	0.537	0.01617255	2.87	5.396
Zfp2	0.546	1.46	0.04761283	9.153	6.244
Zfp462	-0.569	0.674	0.02527654	14.016	20.815
Zfp472	-0.678	0.625	0.04763112	4.07	6.51
Zfp608	-0.636	0.643	0.00456234	11.244	17.484
Zfp846	-0.476	0.719	0.02549568	13.043	18.121
Zfp90	-0.575	0.671	0.02404646	8.663	12.87
Zmiz1	-0.413	0.751	2.1098E-05	59.548	79.34

Table 10. Cold-responsive protein-coding genes (also predicted), and lncRNA genes found in WATg but not in BAT, PVAT, or WATi

Cold-responsive protein-coding genes (also predicted), and lncRNA genes found in WATi but not in BAT, PVAT, or WATg:

Symbol	log2(fold change)	Ratio	padj	Mean WATi 4°C	Mean WATi 23°C
0610010F05Rik	0.729	1.657	4.0521E-06	38.624	23.268
1110004F10Rik	0.615	1.532	0.00064835	38.203	24.967
1300002E11Rik	-0.341	0.79	0.04563813	27.196	34.473
1700086O06Rik	0.656	1.575	0.01309564	14.197	9.014
1810034E14Rik	1.034	2.047	0.02326089	4.944	2.444
2010016I18Rik	-0.857	0.552	0.00628645	6.052	10.991
2310010J17Rik	-0.494	0.71	0.00464302	40.694	57.136
2310011J03Rik	0.566	1.481	0.00342953	33.225	22.376
2310022B05Rik	-0.455	0.73	0.01635834	22.359	30.641
2610002M06Rik	-0.589	0.665	0.02090878	8.37	12.566
2900052L18Rik	-0.915	0.53	0.04205319	3.558	6.727
3222401L13Rik	-0.81	0.57	0.02298811	3.868	6.785
4632404H12Rik	0.707	1.633	0.03860963	7.967	4.903
4633401B06Rik	0.857	1.811	0.03240547	6.682	3.732
4921524J17Rik	0.688	1.612	0.02148507	12.63	7.809
4930599N24Rik	2.05	4.141	0.01691738	3.228	0.784
5430431A17Rik	-1.613	0.327	0.03532702	1.026	3.173
5730408A14Rik	0.916	1.887	0.01429691	8.688	4.634
5730455P16Rik	0.626	1.543	0.00068574	38.054	24.64
5730507A11Rik	1.221	2.331	0.04917158	3.111	1.351

5830448L01Rik	0.878	1.838	0.02535265	5.777	3.165
6330562C20Rik	-1.121	0.46	0.02835184	2.192	4.789
6430571L13Rik	1.738	3.336	0.00211596	5.583	1.693
9130002K18Rik	-0.925	0.527	0.00993785	3.658	6.918
9130023H24Rik	0.911	1.88	0.04203958	5.622	3.003
9330162G02Rik	0.998	1.997	0.00233159	9.493	4.777
9430025C20Rik	-0.964	0.513	0.04590684	3.609	7.051
9530068E07Rik	-0.443	0.735	0.00056907	49.021	66.669
A230020J21Rik	3.116	8.671	0.01372756	1.208	0.147
A430110C17Rik	2.572	5.948	0.02996936	0.997	0.168
A530017D24Rik	-1.287	0.41	0.04783352	1.121	2.703
A730020M07Rik	1.789	3.457	0.00251154	3.038	0.88
A930001M01Rik	1.198	2.294	0.01522885	4.046	1.76
Abcb1a	-0.793	0.577	5.2033E-05	12.732	21.968
Abcb1b	-0.571	0.673	0.04838575	7.241	10.761
Abcg2	-0.451	0.731	0.02769518	29.07	39.798
Abhd2	-0.541	0.687	0.001603	20.611	29.926
AC154200.1	-0.72	0.607	0.00298005	11.089	18.224
Acaa1b	3.68	12.818	9.5602E-06	3.036	0.238
Acad9	0.813	1.757	0.04753107	5.895	3.353
Ackr1	-1.229	0.427	0.00277483	4.328	10.074
Ackr4	0.802	1.743	0.02597532	7.427	4.258
Acp1	0.439	1.356	0.02410226	38.417	28.301
Acrbp	-0.559	0.679	0.01216284	10.911	16.091
Acss3	0.96	1.945	1.3893E-06	22.346	11.491
Actc1	-2.392	0.191	0.01382226	0.427	2.202
Acvr1b	-1.133	0.456	0.00033457	7.245	15.822
Adam19	-0.501	0.707	0.03344466	13.609	19.31
Adam33	-1.165	0.446	8.2384E-10	21.901	49.02
Adam9	-1.256	0.419	0.00466517	5.414	12.9
Adamtsl1	-1.082	0.472	5.2078E-05	8.892	18.872
Adap2	0.66	1.58	0.02329792	16.51	10.476
Adarb1	-0.606	0.657	0.00951385	14.326	21.723
Adgrd1	-0.834	0.561	0.00287417	17.329	30.772
Adgre5	-0.461	0.726	0.00839163	40.419	55.608
Adra1a	1.369	2.583	1.2679E-07	39.621	15.381
Adrb3	-0.663	0.632	2.0418E-08	486.637	770.053
Aebp1	-1.056	0.481	2.3889E-06	26.068	54.159
Afap1l2	-1.386	0.383	0.00184303	2.14	5.626
Aff1	-0.536	0.69	0.01616108	20.197	29.214
Agrn	-0.756	0.592	5.0759E-05	21.234	35.829
Agtr1a	-0.544	0.686	0.04857122	8.658	12.683
Ahcyl1	1.343	2.537	1.5197E-25	254.303	100.276
Ahsa1	0.79	1.729	0.01180817	10.667	6.152
AI838599	-2.316	0.201	0.0021358	0.584	2.954
Aida	-0.442	0.736	0.03096535	15.875	21.616
Aimp1	0.449	1.365	0.00275493	64.726	47.327
Aip	4.736	26.657	0.00175373	1.092	0.038

Akap7	0.459	1.375	0.00024958	129.124	93.918
Alkbh7	0.859	1.814	3.5824E-05	29.477	16.316
Alkbh8	0.532	1.446	0.01502699	22.984	15.931
Amigo2	-1.27	0.415	1.7904E-05	7.419	17.833
Ammecr1l	0.572	1.486	0.00096649	37.991	25.544
Amt	-1.305	0.405	0.00023015	2.936	7.262
Anapc2	-0.374	0.771	0.00928112	38.248	49.558
Angptl7	1.487	2.804	0.02806597	2.644	0.946
Ankhd1	0.332	1.259	0.02086949	147.205	116.972
Ankrd11	0.325	1.253	0.00011249	289.18	230.843
Ankrd13d	-2.225	0.214	0.04779405	0.262	1.27
Ankrd49	0.457	1.373	0.01836836	30.238	22.029
Ankrd52	1.007	2.01	0.01686198	5.12	2.542
Ano1	-1.004	0.499	6.8083E-05	14.649	29.306
Anp32b	0.48	1.395	4.8797E-05	115.437	82.811
Anpep	-1.692	0.31	1.7949E-08	7.869	25.383
Anxa4	-0.389	0.764	0.04954881	18.235	23.834
Anxa6	-0.53	0.692	7.7833E-08	294.073	424.531
Ap1g1	0.316	1.245	0.04533288	58.958	47.36
Ap5s1	0.372	1.294	0.03728508	29.399	22.655
Apba1	-1.376	0.385	0.00088907	2.316	5.99
Apc	0.373	1.295	0.01112425	51.661	39.837
Apobec1	-0.588	0.665	0.00890852	12.009	18.037
Apool	0.575	1.49	0.00012524	38.034	25.523
Arap3	-0.73	0.603	2.5292E-05	39.295	65.167
Arglu1	0.321	1.249	0.00163958	273.952	219.41
Arhgap33	-2.127	0.229	0.01812343	0.375	1.615
Arhgap39	-1.318	0.401	0.00035722	3.403	8.462
Arhgef1	-0.782	0.581	0.00014019	49.965	86.122
Arhgef10l	-1.331	0.397	0.00791221	2.668	6.695
Arl6ip1	0.37	1.292	0.00227991	266.168	205.902
Armt1	0.663	1.583	0.00175661	19.207	12.152
Arpin	-0.869	0.548	0.02666093	3.878	7.044
Arsa	-0.52	0.697	0.04115587	13.27	19.037
Arsi	-1.651	0.318	1.434E-05	2.775	8.662
Arxes1	0.355	1.279	0.04815529	93.847	73.282
Asgr2	-1.307	0.404	0.0458664	1.247	3.06
Aste1	0.791	1.731	0.01097392	12.413	7.185
Asxl1	-0.583	0.668	0.0393009	9.953	14.95
Atf2	0.41	1.328	0.0151621	46.337	34.837
Atg10	0.666	1.587	0.00018992	34.006	21.449
Atg101	0.669	1.59	1.7912E-05	47.671	30.008
Atn1	-0.665	0.631	0.0002732	16.029	25.375
Atp11a	-1.026	0.491	3.3754E-10	22.194	45.007
Atp6ap1	-0.301	0.812	0.04166515	145.175	178.686
Atp6v0e2	-1.28	0.412	0.00031793	4.428	10.734
Atpif1	-0.359	0.78	0.04115739	40.054	51.255
Atrnl1	-0.504	0.705	0.03208904	17.604	24.895

Atxn2	0.598	1.513	4.616E-07	105.086	69.392
AU021092	-2.537	0.172	0.00853586	0.308	1.839
Axl	-0.453	0.731	0.03096535	37.56	51.266
B230206H07Rik	-1.977	0.254	0.00891978	0.786	3.101
Bag2	0.892	1.855	0.04156933	4.375	2.35
Bag6	0.262	1.199	0.04364222	69.594	57.974
Banf1	0.397	1.316	0.0303461	70.779	53.753
Banp	-0.646	0.639	0.00721427	18.073	28.444
Baz2a	0.494	1.408	3.6393E-05	93.552	66.42
Bbs1	-1.225	0.428	0.02721108	1.402	3.25
Bbs2	-0.691	0.619	0.03971676	5.042	8.131
BC035044	-1.818	0.284	0.01629059	0.584	2.086
Bcam	-1.013	0.496	0.00131247	13.987	28.179
Bcap29	0.698	1.622	0.00064981	30.073	18.512
Bccip	0.787	1.726	0.00892323	10.184	5.917
Bcl9	-0.515	0.7	0.01302347	12.872	18.379
Bdh2	-1.428	0.372	0.01442727	1.504	3.986
Bet1	0.495	1.409	0.0145682	37.938	27.003
Bicc1	-0.482	0.716	0.04203958	21.853	30.444
Bid	-0.793	0.577	0.00437501	7.005	12.099
Birc6	0.52	1.434	2.9727E-05	149.242	104.137
Bmp1	-0.918	0.529	5.4699E-06	13.913	26.126
Bmp2	-1.06	0.48	0.00468944	3.419	7.134
Bmp4	-1.325	0.399	0.00110808	9.416	23.619
Bms1	0.323	1.251	0.04177181	43.267	34.667
Brd1	0.415	1.333	0.0254262	50.447	37.904
Brd7	0.6	1.515	1.434E-08	85.074	56.201
Brd9	-0.375	0.771	0.0035825	49.555	64.232
Bri3bp	0.957	1.941	2.2326E-08	31.192	16.068
Brwd3	0.668	1.589	0.01209326	13.462	8.456
Btrc	-0.527	0.694	0.01738937	12.381	17.771
Bzw2	0.405	1.324	0.00511868	63.114	47.689
C330011M18Rik	1.954	3.874	0.02248361	1.552	0.397
C430039J01Rik	-0.957	0.515	0.01288846	3.521	6.796
Cab39	0.424	1.341	0.00407324	46.383	34.611
Cabp1	-1.765	0.294	0.03532702	0.796	2.689
Cacybp	0.466	1.382	0.00630566	58.555	42.437
Cadm1	-0.732	0.602	0.02858865	7.874	13.128
Cadm4	-1.624	0.324	0.01064693	1.354	4.222
Calca	-3.036	0.122	0.00016503	0.328	2.646
Calcrl	-0.968	0.511	2.9605E-05	9.956	19.576
Calhm5	-2.307	0.202	0.00144495	0.691	3.414
Calm2	0.288	1.221	0.0238141	115.867	94.92
Camk2g	-0.516	0.699	0.01172995	19.44	27.758
Camk2n1	-0.776	0.584	0.00576501	24.033	41.05
Car13	0.637	1.555	0.00146502	23.788	15.301
Car2	0.979	1.971	0.0119884	5.617	2.846
Car7	-0.852	0.554	0.02579615	5.215	9.489

Card10	-0.875	0.545	2.1476E-07	18.838	34.539
Casc3	-0.453	0.731	0.02167351	22.303	30.548
Casp4	-0.681	0.624	0.03096825	6.711	10.81
Casp9	-0.573	0.672	0.00919833	13.417	19.955
Casz1	-0.586	0.666	0.00418024	19.726	29.573
Cavin3	-1.079	0.473	0.00813658	91.206	192.647
Cbs	-1.038	0.487	0.00655465	3.353	6.833
Ccdc127	0.427	1.344	0.01946425	30.922	23.028
Ccdc25	0.453	1.369	0.00016702	95.016	69.521
Ccdc50	0.317	1.246	0.03714494	100.186	80.349
Ccdc58	0.682	1.604	0.01075302	12.498	7.77
Ccdc86	0.551	1.465	0.03610596	12.882	8.794
Ccdc93	-0.545	0.685	0.03456303	10.715	15.651
Ccl11	-0.927	0.526	0.00111016	17.41	32.979
Ccm2l	-0.864	0.55	0.00033457	12.328	22.508
Ccn1	-1.503	0.353	0.00021487	4.326	12.155
Ccnl2	-0.463	0.726	0.00131639	144.893	199.818
Cct4	0.289	1.222	0.04961781	63.939	52.241
Cd163	-0.636	0.643	0.0407531	19.289	29.875
Cd209c	-2.242	0.211	0.02591833	0.313	1.503
Cd209g	-1.388	0.382	0.00073166	4.465	11.749
Cd3e	1.969	3.916	0.02396794	4.618	1.19
Cd47	-0.662	0.632	2.3672E-07	99.395	157.193
Cd7	-1.267	0.416	0.03593612	1.498	3.662
Cd81	-0.501	0.707	2.7095E-05	291.39	412.177
Cd8b1	2.3	4.925	0.03517117	2.732	0.568
Cdan1	-0.816	0.568	0.0002869	9.006	15.879
Cdc25a	1.19	2.282	2.1478E-06	14.155	6.195
Cdc37	0.353	1.277	0.00543861	87.554	68.585
Cdc42bpa	0.403	1.323	0.02605842	31.042	23.496
Cdc42ep2	-0.559	0.679	0.00468944	22.472	33.033
Cdc42ep3	-0.717	0.608	0.00305771	12.222	20.14
Cdc42ep4	-0.729	0.603	1.0627E-08	68.588	113.564
Cdk15	-1.63	0.323	0.03946274	0.688	2.134
Cdk19	-0.538	0.689	0.00840313	28.128	40.87
Cdk6	0.568	1.483	0.0026282	37.503	25.298
Cdon	-0.78	0.582	0.01442727	10.604	18.141
Cds2	-0.734	0.601	6.6851E-07	33.777	56.097
Cebpd	-0.887	0.541	0.00406731	11.348	20.933
Celf2	-0.248	0.842	0.03873608	511.117	606.605
Cenpq	1.3	2.462	0.04394253	2.653	1.078
Cep63	0.481	1.396	0.03257895	22.248	16.024
Cers5	-0.366	0.776	0.01327137	41.699	53.667
Cers6	-1.427	0.372	0.00025227	3.14	8.39
Cetn4	-1.331	0.398	0.01356507	1.453	3.62
Cfap20	-0.642	0.641	0.01735467	11.93	18.63
Cfap74	-2.23	0.213	0.042599	0.318	1.49
Cfb	-0.744	0.597	0.04380037	4.402	7.385

Cfdp1	0.383	1.304	0.01778585	67.946	52.037
Cfh	-0.784	0.581	0.00328789	16.23	27.84
Cfl1	-0.41	0.753	0.00302524	61.062	80.996
Chchd7	0.427	1.344	0.01812343	52.823	39.206
Chd2	0.462	1.377	0.00017658	97.495	70.803
Chek2	-0.996	0.502	0.00337567	5.172	10.311
Chic1	-0.948	0.518	0.03928087	2.962	5.653
Chml	-0.549	0.683	0.01910582	12.282	17.974
Chmp6	0.551	1.465	0.04196341	17.443	11.903
Chpf2	-1.054	0.482	0.00045905	4.91	10.251
Chrd	-0.984	0.505	0.00262745	4.364	8.657
Chrnb1	-1.298	0.407	0.04196341	2.173	5.417
Chst7	-1.029	0.49	0.04415339	2.663	5.497
Ciao3	0.659	1.579	0.00095841	26.174	16.593
Cilk1	-0.446	0.734	0.04100378	19.536	26.54
Cisd2	0.411	1.33	0.00644726	55.422	41.74
Ciz1	0.834	1.783	0.02425771	9.952	5.624
Cldn19	-1.383	0.384	0.00209491	2.924	7.555
Cldn5	-0.747	0.596	0.01908107	21.892	36.749
Clec10a	-1.151	0.45	3.8279E-05	35.375	78.488
Clec4a1	-0.83	0.562	0.0369003	7.817	13.904
Clk2	-0.794	0.577	0.00025795	14.148	24.607
Clpx	0.787	1.725	1.1316E-10	60.743	35.2
Clstn1	-0.803	0.573	2.6331E-05	33.459	58.214
Cmtm3	-0.785	0.58	0.00042128	13.898	23.835
Cmtm5	-1.991	0.252	0.01748404	0.463	1.834
Cmtm6	-0.761	0.59	8.4113E-06	36.253	61.445
Cnot8	-0.377	0.77	0.01426839	30.688	39.919
Cnp	-0.681	0.624	0.00166969	17.037	27.318
Cnpy4	-0.681	0.624	0.00218945	13.272	21.269
Cobll1	-0.427	0.744	0.00929117	24.867	33.411
Col4a4	-1.117	0.461	0.0004699	5.522	11.909
Colgalt1	0.851	1.804	0.00107548	12.74	7.077
Coq10b	1.128	2.185	0.00018542	18.656	8.501
Coro2b	-0.671	0.628	0.0001229	18.41	29.293
Cpn2	1.692	3.23	0.02174634	6.725	2.093
Cpne2	-0.926	0.526	3.6278E-08	25.887	49.067
Cpped1	0.52	1.434	0.0113293	48.923	34.038
Cpsf2	0.652	1.572	0.00118999	38.395	24.451
Cpsf4	-0.521	0.697	0.04931455	10.381	14.921
Cpsf7	-0.406	0.755	0.02577016	20.077	26.657
Cpxm2	-1.585	0.333	0.00406882	2.389	7.13
Cpz	-2.073	0.238	0.01081184	0.55	2.307
Cracr2b	-0.697	0.617	0.02308342	9.406	15.262
Crip1	-0.52	0.697	8.6697E-06	73.173	104.963
Crtc1	-0.915	0.53	0.00836555	5.052	9.63
Crtc2	-1.84	0.279	0.00126503	2.261	8.172
Csf1r	-0.828	0.564	0.00050612	47.964	85.028

Csf2ra	-0.569	0.674	0.00917607	35.485	52.683
Csf2rb	-0.622	0.65	5.4843E-05	27.749	42.719
Csnk2a1	0.787	1.726	4.057E-13	139.585	80.858
Csnk2a2	0.284	1.218	0.02934291	70.407	57.741
Csrp1	-0.894	0.538	5.3489E-05	28.266	52.491
Cstf2t	-0.528	0.694	0.00971195	16.938	24.528
CT010467.1	1.174	2.256	3.2354E-09	42751.197	18946.863
Ctdsp2	-0.556	0.68	3.4893E-05	68.276	100.218
Ctnnd1	-0.864	0.549	2.4063E-08	50.687	92.051
Ctsc	-0.559	0.679	0.00209004	64.722	95.274
Ctsh	-0.73	0.603	0.00217358	44.759	74.317
Cul4a	0.399	1.318	0.03872544	25.359	19.178
Cul5	0.729	1.658	1.0514E-09	85.172	51.336
Cxadr	1.614	3.062	1.9421E-06	16.8	5.51
Cyfip1	-0.307	0.808	0.04348411	46.782	57.82
Cygb	-0.396	0.76	0.03926361	123.222	162.037
Cyp4f16	-0.8	0.574	0.02988043	4.26	7.449
Cys1	-1.225	0.428	0.01888082	1.629	3.784
Cytl1	-1.032	0.489	0.02408831	5.328	10.899
Cyyr1	0.998	1.997	0.00427693	19.239	9.659
D930048N14Rik	-1.951	0.259	9.7744E-06	1.651	6.484
Dact3	-1.701	0.308	0.02448052	0.924	3.01
Dapk1	-0.849	0.555	0.0026905	49.997	90.114
Dbf4	1.123	2.178	0.04406252	5.304	2.451
Dbndd2	-0.727	0.604	0.04090384	5.325	8.88
Dbp	1.927	3.803	0.00310074	3.045	0.796
Dcaf1	0.97	1.959	0.00099198	15.211	7.806
Dcaf12l1	2.948	7.717	0.00223834	1.86	0.252
Dcun1d1	0.327	1.254	0.04975257	45.611	36.4
Ddx10	0.458	1.374	0.00217358	35.982	26.17
Ddx39b	-0.827	0.564	6.9166E-12	81.033	143.798
Ddx52	0.382	1.303	0.0197893	38.314	29.432
Def8	0.401	1.321	0.04197592	29.425	22.298
Dgkb	-1.781	0.291	0.02205958	0.888	3.036
Dhps	0.817	1.762	0.01430924	7.322	4.153
Dhrs1	0.544	1.458	1.7795E-05	89.74	61.539
Dixdc1	0.519	1.433	0.02061345	18.3	12.793
Dlg5	-0.561	0.678	0.04289942	10.557	15.54
Dll4	-0.899	0.536	0.0090782	8.301	15.448
Dmd	-0.671	0.628	0.01176184	22.846	36.36
Dmwd	-0.515	0.7	0.01949459	19.179	27.334
Dnajb14	0.745	1.676	1.0062E-07	66.543	39.742
Dnajb6	0.651	1.57	0.01458666	11.926	7.61
Dnajc2	0.526	1.439	0.0004003	47.472	33.027
Dnajc21	0.835	1.783	8.278E-11	74.302	41.68
Dnttip2	0.403	1.323	0.01665843	44.761	33.784
Dok1	-0.951	0.517	0.02159226	4.157	8.113
Dok2	-0.926	0.526	0.01395688	4.159	7.852

Dolpp1	-0.737	0.6	0.02153489	10.531	17.553
Dop1b	-0.655	0.635	0.00434737	11.538	18.203
Dpf2	-0.502	0.706	0.0141497	17.587	24.916
Dpysl3	-0.856	0.552	0.00042749	12.32	22.286
Drp2	-1.597	0.331	0.00072328	3.711	11.198
Dse	-0.692	0.619	0.01236571	12.914	20.824
Dtd2	0.838	1.787	0.00098278	13.542	7.576
Dtna	-1.012	0.496	0.02163656	4.186	8.426
Dtx3	-1.793	0.288	6.6002E-13	11.339	39.396
Dusp22	0.323	1.251	0.0296949	39.165	31.274
E230001N04Rik	-1.906	0.267	0.02135358	0.631	2.386
E230020A03Rik	-1.431	0.371	0.00765675	1.459	3.874
Ebag9	0.737	1.667	8.3621E-05	23.045	13.808
Echdc1	1.713	3.278	0.02561958	1.892	0.58
Ecscr	-0.673	0.627	0.00872235	11.766	18.85
Eef1akmt1	0.586	1.501	0.00853298	23.45	15.687
Egfl7	-0.35	0.785	0.04627461	109.143	139.188
Ehmt2	-0.633	0.645	0.00021705	34.277	53.07
Eif2ak3	-1.09	0.47	0.00498836	4.149	8.797
Eif2s2	0.527	1.441	0.00010772	73.578	51.063
Eif3a	0.545	1.459	2.9108E-10	433.165	296.931
Eif3j1	0.572	1.486	0.03939824	14.292	9.619
Eif4a1	0.488	1.403	0.00148271	65.013	46.306
Eif6	0.38	1.301	0.01935155	49.646	38.063
Elovl1	-0.529	0.693	0.00046335	28.693	41.394
Emc2	0.429	1.347	0.00872235	118.693	88.179
Eml1	-0.822	0.566	0.02369628	3.776	6.651
Emp3	-0.734	0.601	0.00017846	21.422	35.7
En1	-0.933	0.524	0.01349371	4.589	8.777
Enah	-0.785	0.58	8.1251E-05	20.615	35.513
Endod1	-0.598	0.66	0.00889529	10.634	16.099
Entpd1	-0.799	0.575	0.02765121	4.457	7.785
Eny2	0.527	1.44	0.00205553	47.59	32.999
Eogt	-0.971	0.51	0.0023165	6.354	12.413
Epb41l4aos	-0.591	0.664	0.01448987	14.997	22.598
Epcam	4.611	24.439	0.02976416	1.013	0.038
Epha3	-1.273	0.414	0.04896223	1.495	3.574
Ephb4	-0.851	0.554	0.00826992	6.872	12.35
Ephb6	-1.752	0.297	5.1736E-05	2.074	6.973
Ephx3	-1.621	0.325	0.00861981	1.178	3.644
Epm2a	-0.834	0.561	0.0161928	5.759	10.236
Eprs	0.381	1.302	0.00158381	196.286	150.676
Erbin	0.931	1.907	1.1865E-07	30.662	16.029
Erc1	0.441	1.357	0.01935155	77.281	56.877
Erlec1	0.295	1.227	0.04924703	41.2	33.574
Esrrg	2.347	5.086	0.00027709	3.826	0.761
Etnk2	-2.514	0.175	0.03931551	0.185	1.054
Ets2	-0.549	0.684	0.00351269	60.814	89.006

Evc	-1.249	0.421	5.3414E-05	4.247	10.059
Exosc9	1.599	3.03	0.00018992	5.536	1.836
Ext2	-0.488	0.713	0.0023915	26.482	37.045
Eya2	-1.555	0.34	0.00576467	1.142	3.364
Fa2h	-1.508	0.352	0.01510503	1.355	3.829
Fads2	0.85	1.803	0.00047488	29.001	16.078
Fads3	-0.544	0.686	0.02228331	113.604	165.587
Faf2	0.43	1.348	0.01322839	41.956	31.199
Fam124a	-0.906	0.534	0.00365468	5.428	10.144
Fam129a	-0.423	0.746	0.04172698	19.958	26.763
Fam129b	-0.91	0.532	0.00013152	9.215	17.316
Fam160b1	0.559	1.474	0.01054062	24.738	16.821
Fam174a	-0.406	0.755	0.04560944	20.488	27.136
Fam178b	-1.4	0.379	0.00143572	3.336	8.781
Fam204a	0.712	1.638	0.00086772	35.699	21.772
Fam219a	-0.653	0.636	0.03356829	9.768	15.359
Fap	-0.921	0.528	0.00102577	9.199	17.434
Fastkd1	1.017	2.024	0.00069046	12.229	6.048
Fastkd5	0.844	1.795	0.04566526	5.981	3.304
Fat1	-0.948	0.518	0.000135	7.006	13.483
Fbf1	-1.251	0.42	0.00033327	3.446	8.187
Fblim1	-0.675	0.627	0.01465297	9.045	14.417
Fbln2	-0.645	0.64	0.00878308	15.969	24.899
Fbln7	-1.395	0.38	0.00106006	3.637	9.572
Fbxo45	-0.49	0.712	0.01502699	29.268	40.999
Fcrls	-0.987	0.504	0.01032252	6.752	13.417
Fem1c	-0.586	0.666	0.045905	7.998	11.974
Fermt2	-0.367	0.775	0.00296198	113.554	146.453
Fes	-0.991	0.503	0.00047529	6.667	13.354
Fgd2	-0.927	0.526	0.00398564	8.122	15.544
Fhl2	-2.181	0.221	0.00695418	0.514	2.298
Fkbp3	0.765	1.699	1.7641E-05	31.843	18.758
Fktn	0.568	1.483	0.00420889	23.703	16.012
Fn1	-0.758	0.591	0.00076336	39.579	66.871
Fndc1	-0.727	0.604	0.04408386	9.964	16.409
Fnip2	-0.769	0.587	0.04357081	5.342	9.037
Fopnl	0.296	1.228	0.01848298	73.373	59.77
Foxk1	-0.646	0.639	0.00177378	21.923	34.252
Foxo3	-0.784	0.581	0.00026415	13.778	23.649
Fsbp	1.645	3.128	0.04135894	1.773	0.553
Fstl1	-0.842	0.558	4.0895E-07	79.486	142.256
Ftsj3	0.296	1.228	0.04001107	53.283	43.411
Fuca1	0.279	1.213	0.01777356	121.83	100.437
Fut11	-0.894	0.538	0.0002288	9.095	16.789
Fxyd6	-1.189	0.439	0.02189397	4.366	9.934
Fyco1	0.418	1.336	0.00051006	82.212	61.609
Fzd1	-0.787	0.58	0.01064258	8.868	15.192
Fzd2	-1.09	0.47	0.00403673	3.478	7.343

Galnt1	0.347	1.272	0.0100024	67.71	53.241
Galnt17	-1.376	0.385	0.0322584	1.081	2.763
Galnt4	-0.77	0.586	0.0087059	7.365	12.581
Ganc	0.403	1.322	0.00056231	90.478	68.489
Gbp5	-1.034	0.489	0.00823773	7.127	14.555
Gcc2	0.632	1.55	0.00309244	18.037	11.629
Gclc	0.567	1.481	0.00522263	29.406	19.9
Gem	-1.541	0.344	0.02935644	0.912	2.662
Get4	1.502	2.833	0.00736134	3.524	1.235
Gfod1	-0.467	0.724	0.01201785	22.566	31.126
Gfra2	-1.108	0.464	0.00538268	3.768	8.19
Ggh	-0.55	0.683	0.02641747	22.944	33.48
Ggt5	-0.589	0.665	0.01554332	18.408	27.611
Ggta1	-0.48	0.717	0.02914691	14.384	20.021
Gigyf1	-0.606	0.657	0.00010704	31.651	48.27
Gigyf2	0.432	1.349	0.01321358	54.601	40.505
Gipr	-0.898	0.537	0.0145316	4.887	9.147
Gja4	-0.56	0.678	0.04404952	9.786	14.475
Gjc3	-1.464	0.363	0.01720807	1.31	3.578
Gkn3	-1.711	0.305	0.00852457	1.406	4.622
Glce	-0.709	0.612	0.00108344	10.718	17.47
Glg1	0.29	1.223	0.0165055	93.571	76.535
Gli1	-3.202	0.109	0.02238559	0.132	1.253
Glipr2	-1.043	0.485	0.00125972	6.658	13.781
Gm10441	-1.308	0.404	0.00100166	3.186	7.853
Gm10717	1.503	2.834	0.00742226	3.636	1.266
Gm10722	4.795	27.759	0.00242591	1.138	0.032
Gm10762	1.043	2.061	0.0150731	8.329	4.047
Gm10801	1.952	3.869	4.1041E-05	5.356	1.377
Gm12155	1.428	2.691	0.02470971	7.487	2.77
Gm13423	-1.027	0.491	0.00293879	3.762	7.683
Gm13470	-1.614	0.327	0.0103383	0.902	2.801
Gm15327	-1.123	0.459	0.04356629	2.047	4.467
Gm15408	1.422	2.679	0.00437435	4.264	1.597
Gm15609	0.823	1.769	0.00417919	10.323	5.816
Gm16153	0.647	1.566	0.0377644	8.125	5.186
Gm16201	-1.621	0.325	0.02933927	0.746	2.281
Gm17029	1.412	2.661	0.00988682	4.914	1.878
Gm17110	-0.746	0.596	0.02619339	5.627	9.418
Gm17251	-0.982	0.506	0.03266552	3.856	7.589
Gm19705	-2.036	0.244	0.00031737	1.016	4.268
Gm19938	-1.708	0.306	0.03899901	0.56	1.811
Gm20337	1.382	2.607	0.04534879	2.551	0.984
Gm22613	-2.774	0.146	0.02181146	0.196	1.281
Gm26532	-0.601	0.659	0.04896591	14.013	21.224
Gm26575	-4.418	0.047	0.00286041	0.049	1.192
Gm26648	1.514	2.856	0.01967469	2.808	0.977
Gm26805	4.722	26.395	0.00339435	1.091	0.035

Gm28151	-1.078	0.474	0.02608719	2.19	4.685
Gm28320	-1.187	0.439	0.03771913	1.759	3.935
Gm29107	-1.206	0.434	0.0166598	2.123	4.897
Gm30211	4.488	22.44	0.00568414	1.521	0.074
Gm32036	2.005	4.015	0.01448987	1.87	0.467
Gm32817	1.529	2.886	0.01487612	3.092	1.09
Gm36423	-1.227	0.427	0.02364051	1.431	3.342
Gm36988	-2.292	0.204	0.02364531	0.343	1.747
Gm37033	-0.378	0.769	0.04649273	30.868	40
Gm37391	2.788	6.907	0.02013573	1.184	0.178
Gm37726	3.186	9.099	0.01520224	1.216	0.133
Gm37860	3.283	9.735	5.958E-05	2.62	0.264
Gm37949	2.812	7.024	0.02563127	1.224	0.18
Gm38082	1.3	2.462	0.0331424	3.815	1.548
Gm38162	1.192	2.285	0.00828691	8.381	3.689
Gm38230	2.899	7.46	4.0895E-07	5.132	0.709
Gm38319	4.919	30.252	0.00074437	1.244	0.031
Gm39121	-1.317	0.401	0.04436425	1.029	2.528
Gm40761	-2.069	0.238	1.6833E-06	2.036	8.508
Gm4129	2.132	4.382	0.04961781	1.179	0.263
Gm42507	0.563	1.477	0.00551337	28.08	19.04
Gm42547	-1.137	0.455	0.02635787	1.67	3.643
Gm42613	1.407	2.652	0.03736144	3.355	1.25
Gm42640	-1.517	0.349	0.00071239	1.702	4.869
Gm42710	-1.363	0.389	0.00346292	3.294	8.412
Gm43072	4.085	16.977	0.00082896	1.716	0.102
Gm43526	0.993	1.99	0.03118434	4.503	2.251
Gm43570	-2.656	0.159	0.04210089	0.174	1.139
Gm43611	1.151	2.221	0.00035885	10.816	4.881
Gm43637	-1.327	0.399	0.00181795	2.615	6.548
Gm43672	1.713	3.279	4.2924E-10	14.415	4.409
Gm43728	-0.868	0.548	0.02396776	3.464	6.305
Gm43775	-0.721	0.607	0.00023486	16.712	27.661
Gm43792	-1.004	0.499	0.01283975	4.454	8.884
Gm43795	0.842	1.792	0.03589517	6.119	3.43
Gm44130	3.067	8.38	0.0268323	1.13	0.133
Gm44250	0.633	1.55	0.0001452	41.135	26.573
Gm44633	-1.805	0.286	0.00324958	0.906	3.094
Gm44834	1.26	2.395	0.0385064	3.036	1.255
Gm44836	-0.824	0.565	0.01028751	9.718	17.145
Gm44967	2.853	7.223	0.04322615	0.971	0.133
Gm45012	4.279	19.409	0.00379803	1.306	0.066
Gm45206	1.577	2.984	0.00451822	3.303	1.101
Gm45221	2.63	6.192	0.02418052	1.055	0.174
Gm45555	3.844	14.356	0.02737232	0.976	0.07
Gm45762	1.734	3.326	0.01912024	2.127	0.636
Gm45909	1.404	2.646	0.03051762	2.503	0.952
Gm4707	1.359	2.565	0.03281671	2.886	1.145

Gm48673	2.788	6.908	0.014379	1.406	0.207
Gm48727	-1.775	0.292	0.02011318	0.696	2.384
Gm4876	-1.44	0.368	7.9188E-05	5.027	13.485
Gm49544	2.88	7.362	0.01984034	1.253	0.175
Gm49940	1.473	2.777	0.00448197	4.044	1.444
Gm50008	1.461	2.753	0.02383044	3.461	1.24
Gm7265	1.244	2.369	0.00227991	7.98	3.387
Gm867	1.893	3.713	0.00020746	5.226	1.391
Gmds	-0.732	0.602	0.033673	5.198	8.604
Gmnn	1.802	3.486	1.207E-05	7.765	2.242
Gmps	1.083	2.119	7.3344E-12	31.116	14.686
Gnal	-0.924	0.527	0.02791998	7.97	15.165
Gnl3	0.723	1.65	1.0293E-05	56.663	34.316
Golga1	0.427	1.345	0.04525494	22.001	16.392
Golph3l	-0.643	0.64	0.03389543	6.829	10.634
Gpatch11	0.472	1.387	0.00751517	35.294	25.475
Gpc3	-0.929	0.525	0.02402401	3.648	6.895
Gphn	0.375	1.297	0.03177308	48.638	37.492
Gpm6a	-1.707	0.306	0.0135302	1.007	3.353
Gpn3	-0.822	0.566	0.02597532	3.985	7.003
Gpnmb	-1.241	0.423	2.4523E-05	14.215	33.618
Gpr156	-2.031	0.245	0.01502699	0.463	1.88
Gpr160	-0.669	0.629	0.02739953	8.476	13.427
Gpr4	-0.805	0.572	0.0020387	11.217	19.506
Gps2	-0.292	0.817	0.02167691	54.038	66.17
Gpx8	0.477	1.392	0.01950936	189.661	136.292
Gramd4	-0.973	0.51	0.00310774	7.069	13.839
Grasp	-0.805	0.572	0.02820333	6.665	11.627
Grb2	-0.479	0.717	7.7941E-05	59.609	83.027
Grina	-0.344	0.788	0.00788915	342.63	434.85
Grip2	-1.465	0.362	0.04133823	0.865	2.399
Grk3	0.889	1.852	0.0070939	45.497	24.607
Grpel2	0.746	1.677	0.00836555	12.061	7.192
Gsk3b	0.442	1.358	1.4273E-05	150.684	110.898
Gss	0.796	1.736	0.00054029	20.638	11.958
Gstm1	-0.416	0.749	0.00063798	206.962	275.943
Gstt3	-1.108	0.464	9.554E-06	14.836	31.821
Gtf2ird1	0.818	1.763	0.00125937	26.818	15.249
Gtpbp2	-0.524	0.696	0.01405445	35.415	50.908
Gtpbp4	0.678	1.6	2.4943E-08	98.734	61.679
Gucy1a2	-1.291	0.409	0.03229583	1.256	3.046
Guf1	0.673	1.595	1.4391E-05	32.628	20.499
Gxylt2	-1.178	0.442	0.00374598	3.361	7.657
Gzma	-1.156	0.449	0.00099456	3.471	7.765
H2-Eb1	-0.801	0.574	0.001327	111.039	193.472
H2-M3	-0.856	0.552	0.01932423	4.214	7.565
H2-M9	-1.344	0.394	0.00627982	1.967	4.957
H4c1	-2.844	0.139	0.01617797	0.188	1.32

Hacd4	-1.276	0.413	8.0725E-06	5.879	14.166
Hbp1	0.788	1.727	3.4452E-05	25.457	14.75
Hccs	0.828	1.775	9.7665E-06	26.785	15.071
Hdac4	-0.473	0.72	0.03203922	16.288	22.602
Hdac5	-0.761	0.59	1.9284E-06	28.138	47.566
Hdac7	-0.701	0.615	8.6003E-06	90.975	147.999
Hdhd3	1.105	2.15	0.00174952	8.663	4.024
Hectd1	0.361	1.284	0.00102632	141.753	110.346
Helz2	-0.608	0.656	0.0169502	14.865	22.729
Herc3	1.059	2.084	0.00269013	9.274	4.473
Herc6	-0.638	0.643	0.01568514	9.282	14.482
Hexim1	0.266	1.202	0.03807685	64.622	53.771
Heyl	-1.04	0.486	0.0008955	7.89	16.179
Hic2	-0.537	0.689	0.04369371	8.91	12.864
Hipk2	0.965	1.952	5.5637E-10	107.074	54.896
Hmbox1	-0.578	0.67	0.02459278	13.48	20.06
Hmgcs2	-1.016	0.494	2.5092E-05	9.893	20.049
Hnrnpa0	-0.256	0.838	0.0377644	100.382	119.835
Homer1	0.672	1.593	0.00861981	16.129	10.175
Hoxc5	-0.66	0.633	0.01141278	9.519	14.985
Hoxc9	-0.426	0.744	0.03116158	95.202	127.857
Hoxd4	-0.716	0.609	0.00217046	11.532	18.95
Hoxd8	-0.598	0.661	0.02514936	12.05	18.194
Hoxd9	-1.17	0.445	0.04463508	1.445	3.246
Hpcal1	-0.486	0.714	0.0057079	20.673	29.021
Hrk	-2.012	0.248	0.03578217	0.495	1.926
Hs3st1	-1.655	0.317	0.0111419	0.866	2.745
Hsf1	-0.615	0.653	0.01186037	12.311	18.854
Hspb2	-1.105	0.465	0.04264874	2.226	4.831
Hspg2	-0.441	0.737	8.0694E-06	158.757	215.4
Htatsf1	0.691	1.615	3.1057E-09	73.006	45.206
Htra3	-0.857	0.552	1.5398E-06	108.572	196.631
Huwe1	0.475	1.39	2.0369E-07	167.577	120.531
Hyou1	-0.953	0.516	0.02549474	3.441	6.586
Id3	-0.567	0.675	5.203E-05	65.114	96.525
Id4	-1.534	0.345	1.3166E-06	4.08	11.888
Idua	-0.682	0.623	0.00047652	14.422	23.073
Ier5l	-1.052	0.482	0.00058931	4.833	10.055
Iffo2	-0.575	0.671	0.00989134	12.806	19.15
Ifi204	-0.851	0.554	0.00342953	9.414	16.867
Ifi44	-0.846	0.556	0.01070984	8.113	14.66
Ifit1	-0.967	0.511	0.00079032	9.257	18.073
Ifit3b	-0.969	0.511	0.04885969	4.351	8.601
Ifitm3	-0.922	0.528	8.1781E-14	149.293	282.604
Ifitm6	-1.171	0.444	0.02055917	1.738	3.862
Igbp1	0.55	1.464	1.0645E-05	55.439	37.905
Igfbp6	-0.701	0.615	0.0078009	26.23	42.533
Igfbp7	-0.704	0.614	9.1021E-07	248.326	404.281

Igsf3	-0.891	0.539	0.02705147	3.88	7.176
Ik	0.419	1.337	0.00033925	105.713	78.991
Ikzf4	-1.494	0.355	0.0078668	1.152	3.239
Il10rb	-0.676	0.626	1.0716E-05	24.09	38.367
Il11ra1	-0.665	0.631	4.1047E-06	71.414	113.106
Il15	-0.987	0.505	0.0038234	4.382	8.753
Il17rd	-1.011	0.496	0.01391866	3.716	7.505
Il1r2	-0.963	0.513	0.0308422	3.618	7.03
Il1rl2	-0.996	0.501	0.00567514	5.986	11.828
Inhbb	-1.502	0.353	1.0805E-09	7.466	21.087
Insyn2a	-1.103	0.466	6.2296E-06	7.908	16.938
Ints3	-0.618	0.652	0.0011577	15.151	23.259
Ipo8	0.35	1.275	0.03322229	32.286	25.307
Irf2bp2	-0.462	0.726	0.02882363	17.377	23.91
Irf7	-0.979	0.507	1.3491E-07	14.951	29.429
Irf9	-0.62	0.651	0.0001027	23.814	36.522
Irgq	0.531	1.445	0.00104473	39.311	27.239
Isca2	0.639	1.557	1.6115E-07	91.561	58.876
Islr	-1.341	0.395	0.00786083	2.298	5.855
Itga5	-1.472	0.36	0.01668128	0.967	2.685
Itga8	-2.993	0.126	0.00111488	0.33	2.581
Itgb5	-0.639	0.642	0.00091968	23.833	37.076
Itgbl1	-1.091	0.47	0.00532076	2.831	6.064
Iws1	0.634	1.552	0.00167377	29.374	18.956
Jdp2	-0.705	0.614	0.00539602	10.468	17.018
Kank1	-0.565	0.676	0.00916948	46.143	68.173
Kank3	-0.657	0.634	8.663E-05	31.189	49.286
Katnal2	0.661	1.581	0.04193032	9.714	6.14
Kbtbd11	0.463	1.379	0.02383348	38.254	27.796
Kcnb1	0.947	1.928	2.0011E-05	149.63	77.684
Kcne4	-1.266	0.416	0.00263634	2.324	5.54
Kcnj2	-2.382	0.192	0.01470568	0.345	1.874
Kcnk4	2.218	4.653	0.04166515	1.108	0.24
Kcnk6	-1.214	0.431	0.00108692	3.189	7.486
Kcnmb1	-2.289	0.205	0.03691882	0.362	1.781
Kctd12	-0.471	0.722	0.00322758	34.129	47.307
Kdm4a	-0.335	0.793	0.02960596	36.739	46.338
Kdm6b	-0.804	0.573	0.00033732	17.094	29.77
Kif1a	-2.049	0.242	0.00165428	0.877	3.619
Kif2a	0.824	1.77	1.373E-08	60.414	34.064
Kif7	-1.145	0.452	0.0310903	1.978	4.312
Klc1	-0.55	0.683	0.00034556	50.242	73.526
Klf11	-0.85	0.555	0.03589862	3.345	6.036
Klf3	0.446	1.362	0.01358419	78.282	57.488
Klrg1	-2.327	0.199	0.04338366	0.296	1.563
Knstrn	1.517	2.862	0.01810665	2.615	0.917
Kpna3	0.69	1.613	0.00010785	47.721	29.524
Krba1	-0.884	0.542	0.0377852	4.669	8.68

Krt7	3.091	8.522	0.02061345	1.159	0.133
Ksr1	-0.635	0.644	0.00464787	11.843	18.434
Kyat3	0.431	1.348	0.03191012	34.874	25.825
L1cam	-1.309	0.404	0.00620681	2.994	7.534
Lamc1	-0.902	0.535	7.1545E-09	81.484	152.146
Lap3	0.387	1.308	0.003462	95.157	72.745
Larp1	0.411	1.329	0.01123747	37.549	28.17
Larp4	0.985	1.979	1.2811E-07	24.876	12.568
Larp4b	0.399	1.319	0.00346292	150.312	113.983
Lars2	0.414	1.333	0.03954629	27.129	20.33
Lats2	-0.454	0.73	0.01426839	26.586	36.447
Lbhd1	0.643	1.562	0.03174533	10.93	6.997
Lcor	0.574	1.489	0.00403541	22.274	14.956
Lcorl	0.421	1.339	0.04469989	21.542	16.083
Ldb1	-0.91	0.532	3.3397E-06	19.956	37.543
Lgi2	-1.45	0.366	8.4214E-06	4.151	11.288
Lhfp	-0.63	0.646	0.0403506	7.544	11.694
Lig4	0.717	1.643	0.02002618	13.422	8.122
Lipf	4.134	17.559	0.00696751	1.2	0.074
Lmo2	-0.592	0.663	0.03162344	15.839	24.001
Lmod1	-1.207	0.433	0.01379457	7.401	17.07
Lncbate10	7.506	181.81	1.0017E-08	4.52	0
Lnx2	-0.753	0.593	0.0003956	17.683	29.732
Loxl2	-0.967	0.511	2.979E-07	26.229	51.195
Lpar6	0.633	1.55	7.6026E-05	55.239	35.667
Lrfn2	-3.094	0.117	0.00742181	0.181	1.556
Lrrc32	-0.783	0.581	0.00638438	10.939	18.807
Lrrc39	0.9	1.865	0.00022662	23.942	12.797
Lrrc45	-0.59	0.664	0.01481472	11.429	17.271
Lrrc47	1.611	3.056	0.00018245	6.111	1.988
Lrrc8a	-0.582	0.668	0.00269224	33.316	49.849
Lrrk1	-0.508	0.703	0.02563127	18.132	25.77
Lrrn2	-1.831	0.281	0.01968666	0.562	1.984
Lrwd1	-0.643	0.641	0.04776992	7.509	11.83
Lsm14a	-0.451	0.731	0.00847737	35.988	49.298
Lsm3	1.05	2.07	0.00044347	10.519	5.072
Ltv1	0.607	1.523	0.0005132	32.712	21.496
Lurap1	0.7	1.624	0.01645368	9.72	5.979
Ly6e	-0.913	0.531	5.8014E-18	207.597	391.164
Lyl1	-1.113	0.462	0.00406774	3.638	7.878
Lypla2	-0.447	0.734	0.00700873	34.13	46.483
Mab21l2	3.568	11.856	0.00995934	1.195	0.1
Madcam1	3.232	9.397	0.00895578	1.248	0.131
Mafb	-0.549	0.684	0.01508359	26.265	38.381
Mafg	0.581	1.496	0.0001662	73.331	49.017
Magt1	0.283	1.217	0.01742737	136.867	112.493
Mal	-1.536	0.345	1.3099E-05	6.736	19.483
Maml1	-0.65	0.637	0.02194134	8.458	13.285

Man1b1	-0.533	0.691	0.00451822	22.877	33.083
Man1c1	-0.921	0.528	1.1837E-05	15.691	29.605
Mapk1ip1	-0.442	0.736	0.00616759	34.251	46.526
Mapk7	-0.991	0.503	0.02238559	3.532	7.019
Mapkapk3	0.601	1.517	0.04804532	18.733	12.39
Marchf8	-0.497	0.709	0.00022156	34.17	48.217
Mau2	0.477	1.392	0.00786083	35.106	25.196
Mbp	-1.103	0.465	3.4749E-05	62.817	134.87
Mcpt4	-1.507	0.352	0.01054062	2.42	6.858
Mcts1	0.601	1.517	1.2537E-07	96.663	63.625
Mcub	-1.296	0.407	0.0262542	1.338	3.278
Mcur1	0.456	1.372	9.7101E-08	341.506	248.781
Mdk	-1.015	0.495	0.0308422	3.322	6.646
Mdn1	0.473	1.388	0.01739433	37.558	27.153
Me3	1.266	2.405	0.04169032	3.7	1.521
Mea1	0.804	1.746	0.00207653	19.112	10.915
Med24	0.648	1.567	0.01727552	12.049	7.666
Med28	-0.38	0.768	0.00777593	80.297	104.385
Med30	-0.891	0.539	0.03598837	3.612	6.643
Med31	-0.671	0.628	0.04698078	5.948	9.466
Megf8	-0.634	0.645	0.00238817	17.74	27.538
Meis3	-1.258	0.418	0.0087813	2.739	6.455
Mertk	-0.731	0.603	0.00054988	26.184	43.56
Metap2	0.445	1.361	8.6524E-05	146.826	107.822
Mex3d	-1.538	0.344	0.00032235	1.85	5.359
Mfap1b	-0.606	0.657	0.00477762	12.529	19.082
Mfap2	-1.113	0.462	0.02329792	3.687	7.989
Mff	0.431	1.349	0.00019762	82.248	60.964
Mfsd10	-1	0.5	0.00059425	5.919	11.904
Mia2	0.47	1.385	7.4348E-05	94.287	67.987
Mid2	-0.523	0.696	0.04853767	12.582	18.052
Midn	0.434	1.351	0.04129792	113.799	84.224
Mief1	0.582	1.497	0.0013005	24.037	16.072
Mier2	-0.6	0.66	0.04478968	7.117	10.767
Miga2	0.427	1.344	0.00105843	82.121	61.185
Mir6236	4.265	19.226	1.2533E-05	2.607	0.14
Mirg	-1.637	0.321	0.00131639	1.737	5.411
Mmp23	-1.338	0.396	3.6698E-05	5.004	12.53
Mmp27	-1.594	0.331	0.03669888	0.793	2.38
Mmp28	1.681	3.206	0.04329599	2.013	0.612
Mmp3	-1.121	0.46	2.5299E-07	11.314	24.521
Mmp9	-1.063	0.479	0.00596541	8.253	17.214
Morf4l1	0.585	1.5	0.04277184	14.969	9.977
Mov10	-0.974	0.509	0.00149387	5.294	10.316
Mphosph10	0.544	1.459	0.00218826	31.196	21.363
Mpp2	-0.799	0.575	0.00819942	7.493	12.973
Mpzl2	1.98	3.946	0.00126837	3.208	0.804
Mrc2	-0.927	0.526	0.00131247	6.646	12.572

Mrm3	1.003	2.004	0.00068835	14.937	7.472
Mrpl14	0.313	1.242	0.04506866	71.802	57.768
Mrpl19	0.764	1.699	0.00251429	15.908	9.392
Mrpl21	0.487	1.402	0.01011196	39.825	28.472
Mrpl28	0.507	1.422	0.00108296	47.681	33.536
Mrpl3	0.369	1.291	0.004728	53.23	41.259
Mrpl9	0.694	1.618	0.0135302	11.756	7.242
Mrps18c	0.47	1.386	0.00257344	36.255	26.13
Mrps31	0.642	1.561	1.7508E-05	46.872	30.046
Mrps9	0.517	1.43	0.00121972	49.27	34.445
Mrvi1	-1.34	0.395	0.00183236	3.698	9.397
Mst1r	-1.534	0.345	2.3426E-06	6.711	19.336
Mtif2	1.214	2.32	1.7588E-12	42.258	18.278
Mtrex	0.658	1.578	0.00015197	44.123	28.037
Mustn1	-1.146	0.452	0.00015559	11.612	25.69
Myd88	-0.573	0.672	0.00034293	24.322	36.273
Myl12b	-0.52	0.697	0.01340482	15.998	22.931
Myo1b	-0.583	0.668	0.0001229	24.783	37.047
Myo5b	1.434	2.702	0.02110344	4.973	1.858
Naa20	0.642	1.561	0.01028751	14.15	9.031
Nampt	0.442	1.359	0.0095086	119.748	88.146
Nans	-0.545	0.685	0.03111348	11.457	16.664
Napg	0.299	1.231	0.04847089	41.845	34.039
Nbeal1	0.505	1.42	0.00236171	114.513	80.7
Nbl1	-1.117	0.461	0.0077591	6.244	13.564
Ncald	-0.96	0.514	0.0352751	2.716	5.222
Ncam1	-1.346	0.393	0.00056881	3.661	9.27
Ncapg2	1.228	2.342	0.02966545	3.781	1.626
Ncf2	-1.194	0.437	0.00935007	2.248	5.126
Ncl	0.673	1.594	1.238E-06	342.317	214.693
Ncmap	-1.254	0.419	0.00228827	4.555	10.883
Ncoa5	-0.77	0.587	0.00012139	13.135	22.462
Ndufaf5	0.552	1.466	0.04729268	21.498	14.688
Neat1	-0.446	0.734	0.00232337	1303.965	1776.989
Nectin1	-0.678	0.625	0.04277184	4.694	7.514
Nek4	0.532	1.446	0.01425917	16.974	11.749
Nek6	-0.631	0.646	0.01352952	20.975	32.426
Nelfb	-0.416	0.75	0.04899784	22.928	30.556
Nfatc3	0.441	1.358	0.00357424	69.597	51.188
Nfu1	0.377	1.299	0.01868258	40.515	31.195
Nfyb	0.491	1.405	0.00521486	32.776	23.355
Nkd1	-1.033	0.489	0.04172245	3.183	6.494
Nlgn2	-1.062	0.479	0.00217115	4.38	9.089
Nod1	-1.002	0.499	6.5206E-12	22.809	45.731
Nol11	0.538	1.452	0.03264434	16.005	11.009
Nol3	0.957	1.941	6.9378E-05	35.584	18.362
Nol8	0.53	1.443	0.00329757	43.801	30.364
Nolc1	0.761	1.694	3.0599E-07	50.624	29.967

Nova1	-1	0.5	4.444E-08	28.347	56.635
Npdc1	-0.587	0.666	0.00187851	50.033	75.014
Nphp1	0.484	1.398	0.03728508	28.064	20.069
Npr1	-0.555	0.681	0.01335539	29.445	43.264
Nr3c1	-0.45	0.732	0.00152908	105.937	144.625
Nrd1	0.324	1.252	0.00344385	124.887	99.847
Nrip2	-2.09	0.235	0.00131831	1.069	4.54
Nt5m	0.756	1.689	0.00257466	20.092	11.973
Nubp2	0.81	1.754	4.7585E-05	28.848	16.473
Nucks1	0.363	1.286	0.00098447	267.571	208.059
Nudt13	0.53	1.444	0.0005358	69.901	48.441
Nup85	-0.61	0.655	0.00141352	17.546	26.897
Nvl	0.546	1.46	0.00207869	29.216	20.041
Oas2	-1.717	0.304	0.00025795	2.082	6.883
Oasl2	-0.781	0.582	0.00664044	8.079	13.961
Ogfod2	0.684	1.606	1.8896E-05	38.815	24.124
Olfm2	-1.122	0.459	0.03114303	1.917	4.167
Olfml3	-1.358	0.39	3.8653E-05	3.315	8.474
Olfr78	-2.296	0.204	0.00151119	0.735	3.619
Orc2	0.796	1.737	0.00518065	12.36	7.096
Orc3	0.549	1.463	0.00087268	31.591	21.549
Osbpl1a	0.389	1.309	0.01882847	108.525	82.953
Osmr	-0.906	0.534	5.3732E-05	10.518	19.713
Oxtr	1.715	3.283	8.0694E-06	23.915	7.302
P2rx1	-1.459	0.364	0.04837254	1.023	2.797
P2rx7	-1.086	0.471	0.01420127	2.412	5.126
P3h1	-0.636	0.644	0.00092247	13.924	21.624
P4hb	-0.651	0.637	5.8489E-07	100.978	158.488
Pabpc4	-0.322	0.8	0.04892817	100.378	125.469
Pak2	0.33	1.257	0.0190706	94.792	75.471
Pakap	1.265	2.404	0.00446418	0	0.067
Pakap	1.265	2.404	0.00446418	4.652	1.956
Palm	-1.653	0.318	1.0687E-14	11.987	37.464
Parp14	-0.483	0.715	0.01992469	37.43	52.374
Parp3	-0.435	0.74	0.00294178	69.37	93.793
Pbxip1	-0.395	0.76	0.00405221	74.048	97.53
Pcdhga6	-1.483	0.358	0.00894967	1.718	4.735
Pcgf5	0.461	1.376	0.04351412	17.248	12.53
Pcp4l1	-1.533	0.346	0.02554991	1.857	5.404
Pcyt1a	1.101	2.145	0.00036264	12.146	5.659
Pde1c	2.09	4.257	0.04899776	1.146	0.268
Pde4d	1.1	2.143	0.00522263	10.408	4.878
Pde8a	0.764	1.698	0.001305	32.098	18.919
Pdgfra	-0.849	0.555	0.00019298	17.767	31.898
Pdgfrl	-1.203	0.434	0.03598837	1.355	3.14
Pdlim4	-0.773	0.585	0.0036408	12.722	21.697
Pdzk1ip1	1.69	3.227	0.04597596	4.37	1.364
Pes1	0.446	1.362	0.04846337	21.522	15.793

Pex11b	0.541	1.455	0.005069	25.562	17.582
Pfkfb2	-1.649	0.319	0.01225522	0.865	2.714
Phc2	-0.603	0.658	0.00339365	21.213	32.269
Phf13	-0.52	0.697	0.02574546	10.209	14.615
Phf2	-0.467	0.723	0.03200909	24.997	34.567
Phf21a	-0.373	0.772	0.02551814	36.596	47.492
Phf3	0.326	1.253	0.03433634	113.032	90.169
Phkg1	-0.921	0.528	0.03022106	6.358	12.008
Phrf1	-0.317	0.803	0.0459232	37.702	46.967
Phykpl	0.476	1.391	0.01598843	21.053	15.158
Pias1	-0.439	0.737	0.01394421	21.261	28.77
Pias3	-0.652	0.637	0.00438229	13.2	20.709
Pias4	-0.661	0.633	0.00016002	18.403	29.139
Pik3r6	-0.903	0.535	0.0008253	7.62	14.28
Pipox	-2.622	0.162	0.03551989	0.183	1.135
Pirb	-0.83	0.563	0.02700587	6.015	10.748
Pitpnc1	-0.437	0.739	0.0240866	33.579	45.486
Pitrm1	0.751	1.683	0.01324652	11.618	6.909
Pja2	0.557	1.471	0.00023504	65.339	44.396
Pkdcc	-0.799	0.575	0.00539026	7.641	13.359
Pkn2	0.42	1.338	0.00303291	105.85	79.117
Pkp2	-1.091	0.47	3.6641E-06	8.231	17.474
Pla1a	-0.657	0.634	0.00889529	13.192	20.764
Plau	-0.966	0.512	0.00030626	6.625	12.92
Pld2	-0.609	0.656	0.03863982	6.449	9.807
Plekha5	-0.441	0.736	0.04832476	15.139	20.55
Plekha8	-0.933	0.524	0.04739167	2.666	5.108
Plekhg5	-0.808	0.571	6.8994E-06	22.417	39.285
Plekho1	-0.853	0.553	0.0004702	17.604	31.876
Plet1os	4.083	16.943	0.00030755	2.339	0.147
Plk2	-0.567	0.675	0.04917158	9.337	13.735
Pllp	-1.107	0.464	0.0028749	6.212	13.333
Plod2	-0.635	0.644	0.04722933	9.279	14.332
Plscr4	-0.626	0.648	0.00151539	17.74	27.407
Plxna3	-1.498	0.354	0.02784919	0.941	2.612
Pm20d1	1.213	2.318	0.00213421	8.255	3.562
Pmp22	-0.412	0.752	0.03899901	189.546	252.003
Pmpca	0.454	1.37	0.03355999	29.114	21.248
Poc1a	0.748	1.679	0.04041262	6.603	3.95
Pola2	-0.509	0.703	0.01652726	15.667	22.313
Polr2a	-0.316	0.803	0.03532702	50.951	63.359
Polr3g	1.159	2.233	2.7272E-05	18.114	8.159
Pomgnt1	0.502	1.417	0.01075302	36.319	25.647
Pon3	0.262	1.199	0.02439839	98.574	82.142
Pou2af1	2.065	4.185	0.03461759	4.313	1.043
Pou3f1	-2.492	0.178	0.01294084	0.275	1.55
Ppara	2.659	6.315	1.7118E-22	58.033	9.216
Ppargc1a	1.37	2.584	6.3668E-12	53.628	20.753

Ppargc1b	1.45	2.733	1.4219E-13	124.665	45.638
Ppfia2	-1.153	0.45	0.02597532	2.26	4.954
Ppfibp1	0.535	1.449	4.0315E-05	72.063	49.782
Pphln1	0.857	1.811	0.00478445	9.189	5.081
Ppid	-0.585	0.666	0.00234714	17.407	26.218
Ppip5k1	0.477	1.392	0.00882722	31.229	22.496
Ppl	-1.275	0.413	0.00103819	3.536	8.525
Ppm1h	-0.859	0.551	0.02329792	3.867	7.065
Ppp1ca	4.749	26.893	0.00048366	1.829	0.067
Ppp1r14b	1.364	2.574	1.1478E-07	14.559	5.685
Ppp1r3b	1.773	3.418	0.00786083	210.347	61.554
Ppp4c	-0.761	0.59	0.045358	5.614	9.557
Ppp4r3b	0.704	1.629	4.1783E-07	118.899	72.99
Ppt1	-0.344	0.788	0.0210017	37.941	48.17
Prcp	-0.626	0.648	0.01128839	10.273	15.827
Prkacb	0.303	1.234	0.0239407	69.723	56.481
Prkch	-0.664	0.631	0.00905261	11.367	18.041
Prkrip1	0.486	1.401	0.02579615	20.647	14.761
Prom1	-1.429	0.371	0.04931455	0.893	2.371
Pros1	-0.885	0.542	9.8966E-05	15.148	27.84
Prpf6	0.42	1.338	0.00035378	83.94	62.695
Prr14	-0.639	0.642	0.0102341	14.501	22.621
Prr16	-1.434	0.37	3.4749E-05	5.105	13.642
Prrt1	-1.781	0.291	0.00030431	1.645	5.643
Prss23	-0.835	0.561	5.4699E-06	17.923	31.925
Prss53	-4.202	0.054	0.00662416	0.04	1.035
Prx	-1.88	0.272	0.00010781	2.996	10.959
Psmb3	0.42	1.338	0.0215682	26.346	19.688
Psmb7	2.517	5.725	0.0001816	3.088	0.532
Pstk	0.533	1.447	0.02970702	19.035	13.191
Ptcd1	0.515	1.429	0.04310957	16.164	11.258
Ptger4	-0.966	0.512	0.00292043	8.44	16.512
Ptk2	-0.316	0.803	0.04163481	36.572	45.578
Ptma	-0.39	0.763	0.00945242	36.756	48.118
Ptp4a2	0.571	1.486	2.7137E-10	310.601	209.02
Ptpdc1	-0.767	0.588	0.01428441	5.668	9.579
Ptpn2	0.49	1.405	0.0322584	18.63	13.213
Ptpra	-0.354	0.782	0.02777815	62.929	80.429
Pum1	0.393	1.313	0.0038419	111.972	85.299
Pura	-0.283	0.822	0.02209241	350.093	426.004
Pus7	0.626	1.543	0.02860633	12.376	8.044
Pxn	-0.507	0.704	0.01298962	17.909	25.471
Pycr1	-1.587	0.333	0.01322764	1.012	3.028
Pygo2	-0.5	0.707	0.00667315	22.35	31.672
Qk	0.33	1.257	0.00063168	280.965	223.651
Qrsl1	1.018	2.025	5.4214E-07	25.426	12.57
Rab3il1	-1.118	0.461	0.00102703	3.92	8.465
Rab5b	-0.493	0.711	0.00857129	21.603	30.404

Rab7b	-0.816	0.568	0.00086272	15.477	27.128
Rab9b	-2.588	0.166	0.01869035	0.279	1.654
Rabep1	0.656	1.576	1.434E-08	91.328	57.923
Rad23a	1.475	2.779	0.01554332	2.706	0.958
Rala	0.378	1.3	0.0019436	196.517	151.2
Ramp2	-0.648	0.638	0.00105882	46.853	73.364
Ranbp1	0.865	1.822	0.03924472	8.184	4.51
Rap1a	-0.333	0.794	0.03473353	38.015	47.874
Rap1gap2	-0.898	0.537	0.01448987	4.554	8.481
Rapgef1	-0.423	0.746	0.00661352	129.942	174.217
Rapgef3	-0.5	0.707	0.00998304	27.65	39.123
Rara	-1.037	0.487	5.7391E-05	6.539	13.472
Rasgef1a	-1.972	0.255	0.02428136	0.523	2.117
Rasgrp4	-1.177	0.442	0.0491505	1.657	3.773
Rasip1	-0.654	0.635	0.00053416	74.632	117.405
Rbl2	1.333	2.52	9.9977E-05	8.258	3.275
Rbm43	-0.914	0.531	0.01392451	3.855	7.304
Rbp1	-0.942	0.521	0.00619021	5.078	9.76
Rbpj	-0.476	0.719	0.03708346	16.948	23.579
Rc3h2	0.287	1.22	0.02909637	64.967	53.265
Rcn1	-0.857	0.552	8.5686E-06	16.672	30.097
Rcn2	-0.617	0.652	0.00268185	13.385	20.48
Rdh5	-0.891	0.539	0.0188258	3.722	6.915
Reln	-1.681	0.312	0.0006451	1.442	4.583
Repin1	-0.453	0.731	0.02567746	20.759	28.344
Reps2	-1.059	0.48	0.01946374	2.367	4.99
Rergl	-2.631	0.161	0.0313964	0.227	1.418
Ret	-1.041	0.486	0.03191012	3.34	6.799
Retreg3	0.986	1.981	0.00147908	10.339	5.231
Rft1	1.161	2.236	7.5949E-05	9.502	4.267
Rgcc	-0.532	0.691	4.6639E-06	275.078	397.656
Rgs10	-1.058	0.48	0.0018659	4.857	10.18
Rgs3	-0.952	0.517	0.00140964	5.373	10.442
Rhbdf2	-0.937	0.522	0.04153159	2.459	4.774
Rhebl1	-0.909	0.532	0.04558844	3.179	5.971
Rhoa	-0.246	0.843	0.03301103	94.156	111.599
Rhoj	-0.731	0.603	1.8626E-06	56.814	94.152
Ric8a	-0.414	0.751	0.0096632	25.342	33.778
Rims4	0.743	1.673	0.01623274	26.603	15.913
Ripor1	-0.653	0.636	1.7998E-07	41.092	64.537
Rita1	0.84	1.79	0.00247623	9.882	5.536
Rmdn2	0.764	1.698	0.00196158	14.453	8.519
Rmnd1	1.11	2.158	2.5198E-05	20.474	9.539
Rnase4	-0.563	0.677	0.03537612	58.947	86.997
Rnf114	-0.524	0.696	0.00233059	21.741	31.236
Rnf13	-0.325	0.798	0.03847536	58.164	72.844
Rnf130	-0.611	0.655	0.00484417	20.518	31.243
Rnf149	1.075	2.106	2.4105E-05	20.328	9.662

Rnf213	-0.689	0.62	0.00096508	21.48	34.774
Rnf24	1.516	2.86	7.1045E-05	6.754	2.369
Rnf38	-0.471	0.721	0.03344466	14.794	20.496
Rnf6	0.659	1.579	0.00042781	42.136	26.627
Rny3	1.77	3.411	0.02135044	1.832	0.535
Rp2	-0.714	0.609	0.03941941	5.717	9.455
Rpf2	0.561	1.475	0.00893478	19.757	13.346
Rpl36	1.509	2.846	0.01198714	3.151	1.105
Rpl7l1	0.517	1.431	0.00096842	49.93	34.921
Rpn2	-0.335	0.793	0.0249783	120.637	152.021
Rps11	0.658	1.578	0.00094581	32.146	20.357
Rps2	0.41	1.329	0.00272352	98.496	74.139
Rps6kb1	0.402	1.321	0.00097284	132.392	100.107
Rras	-0.401	0.757	0.00356198	80.191	105.733
Rrm2	1.305	2.471	0.0254262	3.366	1.369
Rrp1	0.33	1.257	0.01990643	67.8	53.882
Rrp12	0.723	1.651	0.03745942	7.189	4.346
Rrp8	0.822	1.768	0.00055448	15.174	8.589
Rsad1	0.661	1.581	0.00305626	22.127	14.016
Rsad2	-0.612	0.654	0.03740694	30.067	46.012
Rsph9	-0.878	0.544	0.04042317	3.315	6.042
Rsu1	-0.426	0.744	0.00155233	46.332	62.231
Rtl6	-1.53	0.346	0.02904546	0.893	2.542
Rtp3	-1.204	0.434	0.01248692	1.792	4.132
Rtp4	-1.052	0.482	1.2558E-07	22.89	47.478
Rubcn	-0.474	0.72	0.02657332	22.359	31.085
Rufy4	-1.16	0.447	0.0169502	1.89	4.204
Rwdd1	0.795	1.735	0.01093201	12.115	7.01
Rwdd4a	0.735	1.665	3.4235E-08	50.322	30.233
Rxra	-0.377	0.77	0.04379035	88.206	114.427
Rxylt1	0.484	1.399	0.02687244	34.415	24.566
S100a4	-0.687	0.621	0.01621901	20.493	33.028
S100a6	-0.676	0.626	3.8403E-06	205.256	327.624
Sacm1l	2.526	5.759	0.0009122	2.526	0.434
Sae1	-0.369	0.775	0.03294812	55.409	71.596
Safb	0.47	1.385	0.00528066	40.381	29.159
Samd1	-0.766	0.588	0.00649928	6.645	11.328
Sav1	1.982	3.952	0.00882722	2.481	0.615
Scaf11	0.376	1.298	0.00643037	92.743	71.459
Scaf4	0.743	1.674	7.4213E-05	34.909	20.894
Scmh1	-0.547	0.685	0.00140428	21.158	30.926
Scrn1	-1.222	0.429	0.0280548	1.82	4.212
Sdc1	-1.387	0.382	0.00144495	2.538	6.605
Sdf2l1	-0.933	0.524	0.03608763	3.757	7.126
Sdsl	1.444	2.721	5.9872E-06	13.86	5.121
Sec14l4	2.146	4.427	5.6872E-09	8.399	1.911
Sec61g	1.364	2.574	0.02253095	4.414	1.717
Selenom	-0.45	0.732	0.0310903	14.707	20.046

Selenon	-0.956	0.516	1.1889E-05	10.02	19.421
Selenos	0.477	1.392	0.00277483	115.125	82.666
Selenot	0.353	1.278	0.02131427	48.651	38.043
Selp	-1.332	0.397	0.01637932	1.886	4.794
Sema5b	-1.488	0.357	0.01911263	1.298	3.672
Senp5	0.428	1.345	0.04403994	26.459	19.706
Senp6	0.564	1.478	1.9697E-06	79.011	53.476
Septin10	0.686	1.609	2.2774E-05	49.78	30.913
Septin3	-1.627	0.324	0.00219794	2.022	6.367
Septin4	-0.694	0.618	0.00121958	33.346	54.077
Septin7	0.757	1.69	1.7159E-09	242.211	143.358
Septin8	-0.566	0.675	0.00035107	33.339	49.249
Serbp1	0.445	1.361	4.624E-10	540.528	397.205
Serinc3	-0.397	0.76	1.7926E-06	386.285	508.451
Serpinb6a	-0.601	0.659	0.02422848	59.815	90.658
Serpinb8	-1.294	0.408	0.00260319	2.483	6.071
Serpinf1	-0.728	0.604	0.00102703	57.311	94.797
Serping1	-0.886	0.541	5.7327E-06	95.83	176.962
Sertad4	-1.373	0.386	0.0103954	1.713	4.477
Set	0.65	1.569	0.00083796	21.631	13.786
Setx	0.622	1.539	0.00102106	36.254	23.598
Sf3b2	0.265	1.201	0.01963573	169.386	140.954
Sfmbt1	0.744	1.675	0.00010788	33.003	19.74
Sfr1	0.32	1.248	0.04410588	117.525	94.051
Sfrp2	-1.515	0.35	0.01736108	1.059	3.009
Sgip1	-1.103	0.466	9.9881E-05	5.783	12.397
Sgpp1	-0.707	0.613	0.00482045	16.745	27.361
Sgtb	1.598	3.028	0.00021197	5.534	1.839
Sh2b3	-0.413	0.751	0.03728508	16.73	22.265
Sh2d3c	-0.994	0.502	0.00195781	11.429	22.694
Sh3bgrl3	0.938	1.916	0.0085519	20.77	10.834
Sh3bp2	-0.975	0.509	0.0269978	3.873	7.644
Sh3gl1	-1.117	0.461	3.4532E-06	20.998	45.521
Sh3glb1	0.357	1.281	0.00242591	635.475	496.227
Sh3kbp1	0.846	1.798	4.5989E-09	94.335	52.465
Shb	0.816	1.76	0.00223421	21.255	12.068
Shc4	-1.757	0.296	0.00959968	0.972	3.289
Shisa4	-1.314	0.402	0.00714097	2.266	5.683
Shld2	0.585	1.5	0.02288338	12.781	8.565
Shoc2	0.552	1.466	0.00048764	33.053	22.546
Sipa1	-0.533	0.691	0.01671552	32.437	47.092
Sirt2	-0.27	0.829	0.0376297	62.943	76.01
Sirt5	0.877	1.837	4.242E-05	21.585	11.737
Skiv2l	-0.393	0.762	0.00448189	43.382	57.009
Slc10a6	-1.539	0.344	0.00475658	1.415	4.132
Slc11a1	-1.641	0.321	1.1474E-05	2.338	7.215
Slc16a6	-1.393	0.381	0.0033541	4.214	11.191
Slc24a1	2.203	4.605	0.02433894	1.426	0.311

Slc25a42	1.195	2.29	8.7573E-06	31.828	13.891
Slc27a2	3.015	8.085	7.2437E-11	13.022	1.603
Slc27a3	-1.258	0.418	0.00363325	2.092	4.975
Slc29a3	-0.787	0.58	9.28E-07	22.434	38.639
Slc2a13	-1.97	0.255	2.0507E-08	3.474	13.472
Slc2a3	-1.146	0.452	0.01262339	2.8	6.272
Slc37a4	0.536	1.45	0.04473121	22.828	15.779
Slc45a3	-2.348	0.196	0.02201915	0.347	1.821
Slc52a2	0.596	1.512	0.04517108	12.774	8.472
Slc6a8	-1.238	0.424	0.00038757	3.96	9.322
Slco2a1	-0.75	0.595	0.01815071	6.927	11.651
Slco3a1	-0.776	0.584	0.00906094	12.246	20.946
Slk	0.41	1.328	0.0033382	95.891	72.168
Slmap	0.906	1.873	5.0873E-09	94.703	50.547
Smarcd2	-0.317	0.803	0.04872353	45.15	56.375
Smc2	0.492	1.406	0.03835139	20.603	14.654
Smim10l2a	-2.582	0.167	0.02791998	0.254	1.421
Smim14	-0.316	0.803	0.01394421	93.709	116.557
Smim20	0.632	1.549	0.00013983	47.094	30.399
Smpd3	-1.567	0.338	1.6507E-08	9.264	27.369
Smtn	-0.54	0.688	0.02238559	22.306	32.45
Snhg8	-0.46	0.727	0.00296815	43.352	59.538
Snrnp25	0.766	1.7	0.00451844	13.438	7.937
Snrpd3	0.662	1.583	7.8598E-06	65.666	41.539
Sntb1	-0.288	0.819	0.04566526	50.193	61.138
Sntg2	-2.433	0.185	0.0044678	0.508	2.745
Snx1	-0.411	0.752	0.02739953	48.216	64.07
Snx21	-0.446	0.734	0.03916083	17.09	23.271
Snx33	-0.593	0.663	0.03277815	13.204	19.798
Socs2	-0.63	0.646	0.0052893	22.105	34.29
Socs3	-1.325	0.399	0.00019732	3.538	8.903
Son	-0.212	0.863	0.04781337	587.123	679.762
Sorbs2	-1.192	0.438	0.00499346	10.693	24.401
Sos1	0.686	1.609	0.00010727	31.114	19.342
Sox10	-1.221	0.429	0.02636267	3.378	7.863
Sox13	-0.926	0.526	0.01308656	6.134	11.647
Sp2	-0.887	0.541	0.00232036	7.866	14.594
Spaar	-0.603	0.658	0.00310588	17.11	25.985
Spag5	1.709	3.268	0.04315094	1.638	0.499
Spc24	1.222	2.332	0.04139164	2.524	1.086
Spc25	1.434	2.703	0.00648973	4.15	1.545
Spg7	0.507	1.421	7.5721E-06	98.386	69.209
Spindoc	-0.835	0.56	0.00792585	4.684	8.402
Spock2	-1.039	0.487	0.01144368	3.879	7.997
Spon2	-0.974	0.509	0.01438181	3.112	6.073
Sppl3	-0.574	0.672	0.00066524	21.805	32.436
Sptbn2	3.372	10.352	0.01371957	1.074	0.109
Srf	-1.314	0.402	0.00834002	2.154	5.347

Sri	-0.332	0.795	0.01946374	77.567	97.515
Srp19	0.466	1.381	0.00072541	76.932	55.628
Srsf10	0.332	1.259	0.0359512	52.709	41.888
Ssb	0.74	1.67	1.3426E-08	204.825	122.606
Ssc5d	-0.977	0.508	0.0077591	5.116	10.051
Ssr1	-0.317	0.803	0.02587366	86.085	107.104
St6galnac2	-0.658	0.634	0.02136297	7.656	12.045
St6galnac6	0.602	1.518	0.01840561	15.187	10.021
Stab1	-0.668	0.629	0.02873701	10.566	16.786
Stac	-2.566	0.169	0.00472507	0.393	2.233
Stam2	0.442	1.359	0.01605332	32.878	24.192
Stard9	-0.612	0.654	0.03174533	10.579	16.262
Steap3	-0.848	0.556	0.00059018	14.052	25.218
Strn3	0.354	1.278	0.00532076	107.711	84.227
Stx16	-0.486	0.714	0.00015028	59.436	83.212
Stx4a	-0.589	0.665	3.4639E-05	56.853	85.397
Stxbp1	-0.666	0.63	0.01812343	8.759	13.918
Stxbp3	-0.794	0.577	2.0572E-05	16.801	29.142
Stxbp4	-0.844	0.557	0.03057469	3.831	6.901
Sub1	0.698	1.622	9.3517E-09	289	178.145
Supt16	1.095	2.136	4.6119E-09	32.65	15.261
Supt5	0.724	1.652	0.01292447	16.103	9.768
Susd5	-2.711	0.153	0.01323655	0.283	1.824
Suz12	1.022	2.031	2.6487E-09	37.282	18.365
Sycp3	0.499	1.413	0.01053301	23.546	16.685
Syde1	-0.396	0.76	0.04892817	20.234	26.634
Syne1	0.588	1.503	0.00154026	54.129	35.971
Syt7	-0.807	0.572	0.00063414	15.791	27.553
Sytl2	-1.563	0.338	0.00264351	1.387	4.073
Tacc2	-0.606	0.657	0.00740073	29.947	45.586
Taf2	0.714	1.64	0.0091783	14.501	8.899
Taf9b	-0.995	0.502	0.00107548	7.155	14.185
Tagln	-1.773	0.293	0.00488485	2.968	10.121
Tars2	0.427	1.345	0.02142676	25.182	18.73
Tatdn1	0.565	1.479	0.0218182	14.602	9.871
Tbc1d10a	-1.056	0.481	0.0285982	3.402	7.091
Tbc1d15	0.592	1.508	0.04271328	15.496	10.269
Tbc1d17	-0.391	0.762	0.02579615	22.891	29.992
Tbca	0.278	1.213	0.0144573	151.838	125.189
Tbcd	1.555	2.939	0.0407034	1.863	0.631
Tbl1xr1	0.571	1.486	9.7659E-05	42.005	28.213
Tbp	-0.517	0.699	0.0475081	10.007	14.342
Tbrg1	0.614	1.53	0.03543292	10.922	7.115
Tbx18	-0.753	0.593	0.00440023	8.3	13.896
Tbx2	-1.048	0.484	0.0071718	4.131	8.505
Tcerg1	0.543	1.457	2.2162E-06	108.205	74.292
Tcf15	-0.596	0.662	0.0055607	36.554	55.244
Tcf25	0.238	1.179	0.01195416	251.944	213.72

Tcp1	0.565	1.479	0.00046948	30.634	20.665
Tcp11l2	-0.63	0.646	0.01968666	9.669	15.01
Tdrd7	-0.621	0.65	0.01000432	12.438	19.041
Tefm	1.146	2.213	9.1434E-05	14.436	6.521
Tfam	0.77	1.705	1.4791E-05	41.802	24.537
Tfg	0.281	1.215	0.0305089	66.922	55.12
Tgfb1i1	-0.665	0.631	0.00257783	13.64	21.591
Thap3	-0.453	0.731	0.0285982	17.02	23.35
Thbs1	-1.323	0.4	0.02135015	1.568	3.865
Thoc7	1.321	2.498	6.6631E-18	45.224	18.18
Thrap3	0.377	1.299	0.01880077	40.015	30.804
Tie1	-0.598	0.661	0.00561742	33.411	50.609
Timeless	-0.919	0.529	0.04292014	4.148	7.913
Timm10b	0.411	1.33	0.00047325	79.369	59.712
Tinag	1.066	2.093	0.01673405	7.143	3.417
Tjap1	-0.645	0.64	0.02313655	10.597	16.642
Tlr4	-0.652	0.637	0.02167193	7.32	11.543
Tm9sf4	0.586	1.501	3.7142E-06	64.271	42.838
Tma7	1.062	2.088	0.01561891	5.14	2.45
Tmbim1	-0.369	0.774	0.01784482	80.854	104.277
Tmbim4	0.295	1.227	0.01369334	111.552	90.835
Tmcc3	-0.504	0.705	1.0132E-06	136.747	193.783
Tmem106a	-0.432	0.741	0.04271328	33.111	44.586
Tmem106c	-0.634	0.644	0.00051017	16.435	25.46
Tmem119	-1.14	0.454	0.000761	7.615	16.795
Tmem126b	0.553	1.467	0.00104603	55.734	38.043
Tmem158	-1.192	0.438	0.02418388	3.246	7.36
Tmem161b	0.688	1.611	0.00419488	21.294	13.229
Tmem176a	-0.674	0.627	0.00043843	27.296	43.593
Tmem176b	-0.83	0.563	3.6378E-09	65.569	116.472
Tmem184c	0.449	1.365	0.00469589	46.291	33.819
Tmem201	0.584	1.499	0.03586291	15.692	10.432
Tmem231	-1.281	0.412	0.00076336	2.599	6.328
Tmem250-ps	0.532	1.446	0.00022719	88.895	61.565
Tmem252	-1.323	0.4	0.00030431	3.146	7.848
Tmem253	2.903	7.481	0.02284354	0.992	0.129
Tmem255b	-1.484	0.358	0.01538856	1.129	3.202
Tmem39a	-0.663	0.632	0.02055917	7.061	11.158
Tmem39b	-1.023	0.492	0.0281228	2.381	4.866
Tmem44	-0.723	0.606	0.03714494	5.582	9.201
Tmem60	0.713	1.639	2.376E-05	37.824	23.019
Tmsb10	-0.996	0.501	0.0142847	3.792	7.619
Tnfrsf1b	-0.91	0.532	0.00171475	7.593	14.327
Tnfrsf25	-1.388	0.382	0.00324958	2.137	5.616
Tnfsf13b	-0.925	0.527	0.02324424	3.727	7.042
Tns3	-0.662	0.632	0.03548778	6.62	10.508
Tomm22	0.502	1.416	0.00029287	56.077	39.596
Tomm34	-0.5	0.707	0.02757005	17.325	24.58

Tor3a	-0.518	0.699	0.00885244	16.701	23.881
Tpp2	0.336	1.262	0.02543016	63.287	50.061
Tppp3	-0.926	0.526	2.4707E-07	19.313	36.583
Tpra1	-0.734	0.601	0.00205371	14.491	24.098
Tpst1	-0.686	0.622	2.5398E-05	28.353	45.498
Traf7	-0.613	0.654	0.00022907	33.224	50.804
Tram1	-0.342	0.789	0.01352026	65.6	82.997
Tram2	-0.807	0.572	0.0055523	7.967	13.83
Trappc8	0.539	1.453	0.03947625	12.916	8.881
Trappc9	0.514	1.428	0.00513129	32.605	22.827
Trim11	-0.432	0.741	0.0410262	21.007	28.379
Trim25	-0.535	0.69	0.00023386	28.181	40.803
Trim45	-1.819	0.283	0.00556932	0.865	3.068
Trim8	-0.603	0.659	4.0809E-05	34.588	52.455
Trip10	-0.933	0.524	0.00039258	11.089	21.169
Trip11	0.5	1.415	0.00021709	66.434	46.946
Trip12	0.333	1.259	0.00793484	110.698	87.912
Trmt2b	0.735	1.664	0.00069089	28.318	17.08
Trmt6	0.539	1.453	0.00218598	40.226	27.651
Trmu	0.569	1.484	0.02313655	13.799	9.292
Trp53i11	-0.882	0.542	0.00092777	21.43	39.591
Trp53i13	-0.98	0.507	0.00048622	6.602	12.913
Trpv2	-0.896	0.537	0.01889873	3.602	6.717
Tsc22d4	-0.4	0.758	0.04166515	40.943	53.935
Tspan11	-1.642	0.32	0.01080827	1.134	3.561
Tspan18	0.847	1.799	1.0168E-06	241.011	133.972
Ttll11	2.424	5.368	0.01032812	1.63	0.301
Tulp3	-0.995	0.502	0.00045668	5.087	10.166
Tusc2	0.426	1.343	0.00533308	43.995	32.805
Txlng	0.882	1.843	0.00031294	20.18	10.964
Txndc5	-0.524	0.696	0.00188438	33.977	48.709
Txnrd2	2.287	4.882	0.03203166	1.634	0.327
Tyk2	-0.642	0.641	0.00166288	12.237	19.124
U2surp	0.296	1.228	0.00389749	144.983	118.033
Uba3	0.831	1.779	4.7128E-07	27.692	15.592
Uba52	4.212	18.529	8.7624E-06	3.101	0.166
Uba7	-0.808	0.571	1.6734E-05	25.301	44.465
Ubb	-0.515	0.7	0.01180744	100.92	144.126
Ube4a	0.593	1.509	0.03111348	15.811	10.491
Ublcp1	1.597	3.025	0.00027496	5.732	1.878
Ubp1	0.999	1.998	3.4795E-07	25.481	12.728
Ubqln2	-0.622	0.65	0.00257666	18.807	28.877
Ubr5	0.313	1.242	0.01566096	106.745	85.907
Ubxn7	-0.48	0.717	0.01461002	19.222	26.851
Ufsp1	0.917	1.889	0.01314338	9.044	4.765
Unc13b	-0.757	0.592	0.01652604	6.595	11.133
Unc45bos	-1.544	0.343	0.01451678	2.047	5.97
Unc93a2	-1.515	0.35	0.01888082	1.144	3.268

Unc93b1	-0.522	0.697	0.00416464	27.959	40.106
Upf1	0.753	1.685	0.02451705	10.51	6.264
Upp2	-0.866	0.549	0.01043244	4.778	8.67
Uqcc1	0.965	1.952	2.4087E-13	71.46	36.641
Ushbp1	-0.755	0.593	0.00038902	56.507	95.38
Usp18	-0.627	0.648	0.03256779	7.061	10.93
Usp33	1.589	3.009	0.00414705	4.51	1.485
Usp47	0.279	1.213	0.0377119	84.089	69.293
Usp48	-0.27	0.829	0.02872247	92.461	111.478
Uspl1	0.55	1.464	0.03301103	17.909	12.233
Uxt	0.937	1.914	0.01314338	11.263	5.86
Vars2	0.621	1.538	0.00043657	25.838	16.825
Vldlr	0.853	1.807	2.4882E-10	166.619	92.253
Vmp1	-0.284	0.821	0.04571365	80.215	97.594
Vps13c	0.923	1.897	2.4769E-09	45.809	24.132
Vps36	0.422	1.34	0.00109781	64.387	48.061
Vsig10	-0.853	0.553	0.04535783	3.691	6.663
Vsig2	-0.852	0.554	0.01078433	5.582	10.135
Vsir	-0.797	0.575	1.9638E-09	47.826	83.001
Vtn	-0.681	0.624	0.01453475	9.645	15.5
Wapl	0.49	1.404	0.00010781	83.618	59.508
Washc2	0.452	1.368	0.02156957	21.136	15.439
Wbp11	0.423	1.34	0.01031224	38.346	28.565
Wbp4	0.574	1.488	5.3986E-05	59.172	39.749
Wdr1	-0.342	0.789	0.00874035	54.69	69.198
Wdr43	0.583	1.498	6.134E-05	74.617	49.797
Wdr62	-0.765	0.589	0.01385557	6.371	10.753
Wipi2	0.468	1.384	2.1211E-05	78.369	56.631
Wrnip1	-0.674	0.627	0.02716279	7.941	12.645
Xdh	-0.647	0.639	1.0633E-06	89.046	139.361
Xpnpep2	-1.687	0.31	0.02005116	1.009	3.24
Xpnpep3	0.735	1.665	1.3872E-05	46.674	28.053
Yap1	-0.542	0.687	0.00084365	39.707	57.764
Yif1b	3.471	11.086	4.593E-06	3.374	0.308
Yipf3	-0.363	0.777	0.01512215	41.472	53.356
Ypel2	0.494	1.408	0.03293177	21.854	15.55
Ypel4	-1.171	0.444	0.00965198	2.137	4.794
Ythdf2	0.339	1.265	0.03193957	47.219	37.284
Zbp1	-0.825	0.564	0.01330741	5.267	9.403
Zbtb18	1.22	2.33	0.01028751	5.212	2.223
Zbtb43	0.599	1.515	0.00720419	19.029	12.514
Zbtb46	-0.593	0.663	0.00133716	24.157	36.338
Zbtb8a	-1.074	0.475	0.01280223	2.594	5.445
Zc3h7b	-0.318	0.802	0.0382701	39.696	49.422
Zc3h8	1.111	2.16	0.0007073	11.46	5.333
Zcchc17	0.328	1.255	0.01769532	67.308	53.599
Zcwpw1	1.249	2.376	0.04412891	2.482	1.042
Zdhhc18	-0.568	0.674	0.01309564	16.955	25.181

Zfp131	0.793	1.733	1.3018E-09	53.156	30.704
Zfp14	-1.029	0.49	0.02289608	3.045	6.242
Zfp219	1.357	2.562	0.0359046	2.558	1.009
Zfp26	-0.602	0.659	0.00715725	10.534	15.971
Zfp281	-0.552	0.682	0.00821373	13.437	19.727
Zfp362	-0.687	0.621	0.01026186	11.278	18.136
Zfp383	-1.056	0.481	0.03194928	2.442	5.074
Zfp449	-0.985	0.505	0.0242645	2.855	5.647
Zfp512	-0.634	0.644	0.00819942	14.026	21.711
Zfp516	0.584	1.499	0.01875614	15.618	10.379
Zfp521	-1.333	0.397	0.00161101	2.72	6.794
Zfp536	-1.563	0.338	0.01740645	1.101	3.263
Zfp58	-1.177	0.442	0.01778952	1.818	4.13
Zfp644	0.303	1.234	0.00940736	83.022	67.307
Zfp664	0.398	1.317	0.01290944	38.804	29.479
Zfp672	0.605	1.521	8.1565E-05	37.407	24.634
Zfp748	-1.031	0.489	0.04271328	2.359	4.822
Zfp760	-0.875	0.545	0.02030175	3.731	6.82
Zfp788	-0.72	0.607	0.03968614	5.751	9.485
Zfp874b	-0.687	0.621	0.03714494	5.261	8.464
Zfpm1	-0.717	0.608	0.03714494	6.679	11.041
Zmat2	0.459	1.374	0.00018705	123.848	90.08
Zmiz2	0.58	1.494	0.0050654	23.172	15.488
Znrd1	-0.47	0.722	0.02832636	16.985	23.427
Zpr1	0.383	1.304	0.04776992	24.522	18.848
Zranb2	0.563	1.478	3.7462E-05	110.396	74.781
Zscan26	-0.454	0.73	0.01214339	23.668	32.354
Zswim6	-0.675	0.626	0.0040666	14.418	23.142
Zyg11b	0.397	1.317	0.02087386	65.686	49.807

Table 11. Cold-responsive protein-coding genes (also predicted), and lncRNA genes found in WATi but not in BAT, PVAT, or WATg

7.2 COLD-RESPONSIVE MIRNAS FOUND ONLY IN ONE ADIPOSE TISSUE

miRNAs found in cold-exposed BAT but not in PVAT, WATg, or WATi

SYMBOL	log2(fold change)	Ratio	padj	Mean FPM BAT 4°C	Mean FPM BAT 23°C
mmu-miR-1249-3p	0.714	1.64	0.04305121	77.938	47.552
mmu-miR-148a-5p	-0.856	0.55	0.0072438	26.505	48.046
mmu-miR-149-5p	1.008	2.01	9.4246E-05	80.273	39.92
mmu-miR-16-5p	-0.626	0.65	0.00177842	262.761	404.938
mmu-miR-181a-1-3p	-1.006	0.5	0.04776981	9.044	18.01
mmu-miR-190a-5p	-0.976	0.51	0.00015486	56.691	111.727

mmu-miR-193a-5p	0.563	1.48	0.02176171	370.885	251.304
mmu-miR-199b-5p	-0.825	0.57	0.00161125	53.494	95.041
mmu-miR-3073a-3p	2.439	5.42	0.0072438	8.692	1.495
mmu-miR-30c-1-3p	0.729	1.66	0.0168685	72.974	43.85
mmu-miR-30c-2-3p	0.633	1.55	0.00177842	384.416	247.925
mmu-miR-30c-5p	-0.571	0.67	0.0194562	109.998	163.319
mmu-miR-322-3p	-0.329	0.8	0.04956973	1297.801	1630.547
mmu-miR-326-3p	0.694	1.62	0.04184283	133.192	82.734
mmu-miR-369-3p	0.577	1.49	0.0072438	182.522	122.572
mmu-miR-423-5p	0.631	1.55	0.00444666	356.032	229.777
mmu-miR-450a-1-3p	-0.81	0.57	0.04777438	16.314	28.502
mmu-miR-450b-5p	-0.629	0.65	0.03617672	42.104	64.906
mmu-miR-495-3p	0.55	1.46	0.04305121	96.486	65.584
mmu-miR-5121	-0.695	0.62	0.00528862	1017.755	1647.036
mmu-miR-615-3p	0.618	1.53	0.01667481	117.333	76.222
mmu-miR-99b-3p	0.815	1.76	0.0141544	66.194	37.894

Table 12. Cold-responsive miRNA genes found in BAT but not in PVAT, WATg, or WATi

miRNAs found in cold-exposed PVAT but not in BAT, WATg, or WATi

Symbol	log2(fold change)	Ratio	padj	Mean FPM PVAT 4°C	Mean FPM PVAT 23°C
mmu-let-7a-5p	-0.503	0.71	0.01814399	144.195	204.099
mmu-let-7c-5p	-0.761	0.59	1.232E-07	296.045	501.278
mmu-let-7d-5p	-0.552	0.68	0.00010332	3173.302	4650.581
mmu-miR-130b-3p	1.032	2.05	0.04742605	13.424	6.547
mmu-miR-144-5p	0.583	1.5	0.00321125	515.641	344.019
mmu-miR-1839-3p	0.744	1.68	0.01958364	26.321	15.687
mmu-miR-18a-5p	0.732	1.66	0.00703454	48.558	29.207
mmu-miR-204-5p	-0.313	0.81	0.03324379	237.23	294.347
mmu-miR-210-3p	0.941	1.92	0.01502444	35.01	18.283
mmu-miR-21a-5p	0.471	1.39	0.00432448	39069.586	28185.504
mmu-miR-26b-5p	-0.26	0.84	0.01551307	14359.356	17198.783
mmu-miR-340-5p	0.736	1.67	1.2823E-05	754.686	453.39
mmu-miR-365-2-5p	-0.944	0.52	0.03861299	8.017	15.36

mmu-miR-423-3p	0.262	1.2	0.00937824	846.963	706.096
mmu-miR-500-3p	0.78	1.72	0.00175512	52.15	30.367
mmu-miR-501-3p	0.474	1.39	0.01780654	81.692	58.827
mmu-miR-5099	0.589	1.5	0.02975516	40.205	26.753
mmu-miR-652-3p	-0.322	0.8	0.0109291	895.205	1118.762
mmu-miR-708-5p	-0.503	0.71	0.00331713	375.206	531.525
mmu-miR-744-5p	-0.869	0.55	0.00321125	36.065	66.077
mmu-miR-92a-3p	-0.283	0.82	0.00442236	2263.958	2754.75

Table 13. Cold-responsive miRNA genes found in PVAT but not in BAT, WATg, or WATi

miRNAs found in cold-exposed WATg but not in BAT, PVAT, or WATi

Symbol	log2(fold change)	Ratio	padj	Mean FPM WATg 4°C	Mean FPM WATg 23°C
mmu-let-7i-3p	-0.934	0.52	0.00202938	49.83	95.921
mmu-miR-101b-3p	0.485	1.4	0.02168246	3197.302	2285.108
mmu-miR-103-3p	0.848	1.8	0.00033452	217.685	119.904
mmu-miR-106b-5p	0.411	1.33	0.02471905	880.588	661.831
mmu-miR-125b-1-3p	-0.628	0.65	0.00657613	30.962	48.495
mmu-miR-126a-3p	-0.553	0.68	0.00090585	44833.295	65792.59
mmu-miR-140-5p	-0.689	0.62	0.00838438	211.809	341.55
mmu-miR-142a-3p	-0.764	0.59	0.04177117	275.596	467.83
mmu-miR-142a-5p	-0.814	0.57	0.00019421	821.176	1443.412
mmu-miR-146a-5p	-1.153	0.45	4.8115E-08	832.694	1852.057
mmu-miR-148b-5p	-1.172	0.44	0.00327787	10.19	23.139
mmu-miR-17-5p	0.564	1.48	0.00838438	186.859	124.517
mmu-miR-181c-5p	-1.105	0.47	0.00746426	116.433	252.423
mmu-miR-1843a-5p	-0.769	0.59	0.00010575	153.079	260.642
mmu-miR-203-3p	0.728	1.66	0.00838438	4091.376	2469.127
mmu-miR-218-5p	-1.096	0.47	1.6285E-06	37.527	80.067
mmu-miR-24-2-5p	-0.344	0.79	0.03725914	1090.687	1383.05
mmu-miR-27a-3p	-0.404	0.76	0.01354115	6119.105	8098.124
mmu-miR-29b-1-5p	0.96	1.95	0.02856744	18.736	9.202

mmu-miR-29b-2-5p	1.081	2.12	0.02168246	15.916	7.896
mmu-miR-300-3p	-0.537	0.69	0.01432123	56.946	84.102
mmu-miR-3076-3p	2.155	4.46	0.00412538	7.612	1.473
mmu-miR-30b-3p	-0.769	0.59	0.01545909	13.394	22.389
mmu-miR-32-3p	0.885	1.85	0.01623303	22.872	11.984
mmu-miR-32-5p	-1.228	0.43	8.9668E-05	97.866	230.23
mmu-miR-320-3p	0.572	1.49	0.00058886	501.346	335.439
mmu-miR-335-3p	-1.401	0.38	4.8115E-08	137.27	364.261
mmu-miR-338-3p	-1.067	0.48	0.02051353	35.002	72.725
mmu-miR-374b-5p	-0.692	0.62	4.3855E-06	167.991	273.752
mmu-miR-376b-3p	-0.794	0.58	0.00327787	19.744	34.939
mmu-miR-376b-5p	-1.269	0.42	3.381E-06	25.568	61.983
mmu-miR-484	0.417	1.34	0.04177117	268.336	200.245
mmu-miR-542-5p	-0.957	0.52	0.02911005	7.585	15.313
mmu-miR-6236	-2.538	0.17	0.04710606	0.679	4.445
mmu-miR-6240	-3.293	0.1	1.7756E-05	3.228	31.94
mmu-miR-679-5p	-1.446	0.37	0.02822734	2.37	6.281
mmu-miR-872-5p	-0.894	0.54	2.8751E-06	311.751	581.809

Table 14. Cold-responsive miRNA genes found in WATg but not in BAT, PVAT, or WATi

miRNAs found in cold-exposed WATi but not in BAT, PVAT, or WATg

Symbol	log2(fold change)	Ratio	padj	Mean FPM WATi 4°C	Mean FPM WATi 23°C
mmu-miR-223-5p	-0.955	0.52	0.03528813	40.338	78.237
mmu-miR-224-5p	-0.876	0.55	0.019928	185.472	339.927
mmu-miR-30e-5p	0.883	1.85	0.02494246	18286.361	9912.776
mmu-miR-378a-3p	1.12	2.17	6.8786E-06	17929.019	8251.896
mmu-miR-378a-5p	1.016	2.02	0.01487659	266.389	132.378
mmu-miR-379-3p	-1.212	0.43	0.02097143	29.53	67.565
mmu-miR-382-3p	-1.093	0.47	0.04710507	23.707	50.7
mmu-miR-574-3p	-0.692	0.62	0.04710507	152.683	246.617

Table 15. Cold-responsive miRNA genes found in WATi but not in PVAT, or WATg

7.3 Delayed differentiation of PVAi in comparison to BAi

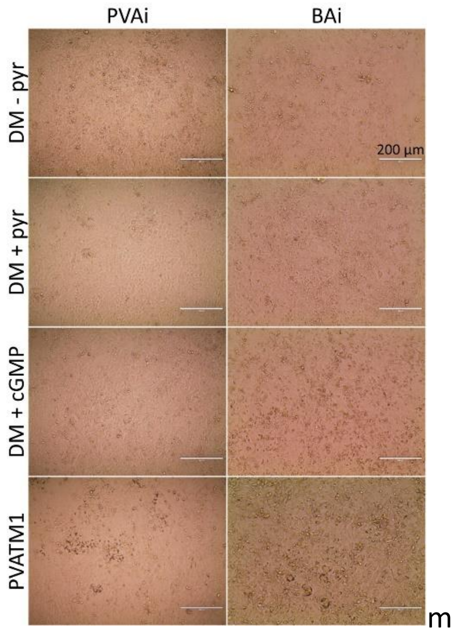

Figure 42. Microscopic comparison of immortalized perivascular adipocytes (PVAi) and immortalized brown adipocytes (BAi) cultured in media as indicated after two days of induction (D2)

7.4 Deletion of Pparg in Sm22-a positive cells results in PVAT KO

To analyse the impact of PVAT and its secreted factors on the whole organism, I breed the *Pparg* floxed and *Sm22-α* Cre strains to prevent the formation of PVAT, as described in a publication of Chang et. al. This mouse strain was to be used to investigate influence the lack of PVAT on secretory profile, and diseases development. Since the animal protocol was not approved in time (submitted to responsible veterinarian in Animal Facility of University of Bonn on April 2020, which was approved in October 2021), I focused on the activation of PVAT, BAT, WATg, and WATi by cold exposure. The resulting mice were not distinguishable from WT mice besides lacking PVAT around aorta (*Figure 43*). BAT and WAT were visually unaffected by the tissue-selective Knock-Out of *Pparg*.

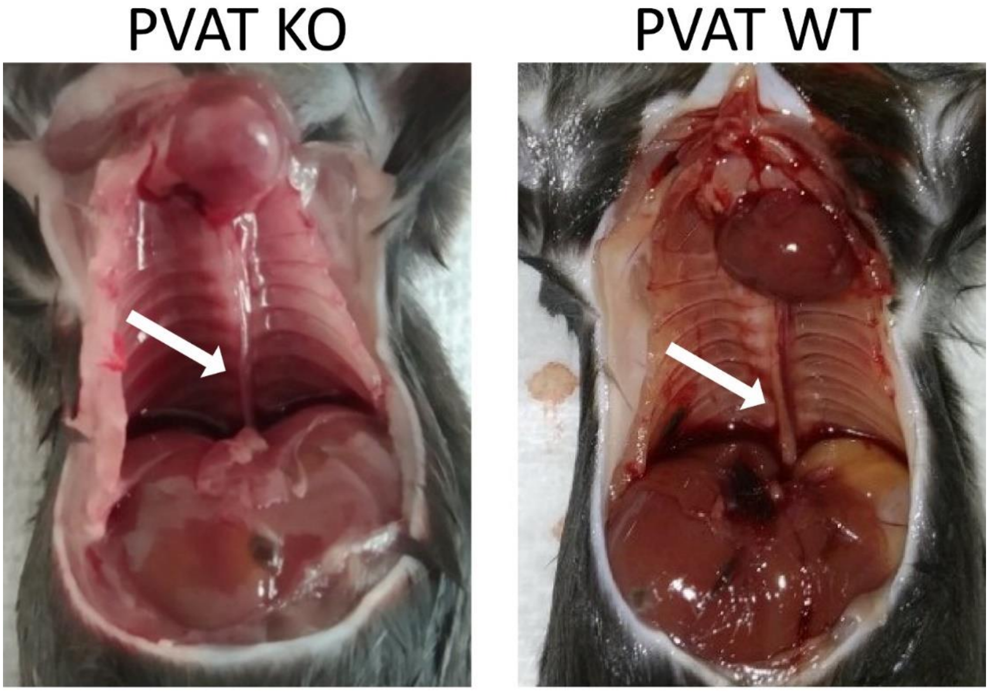

Figure 43. Knock out of Pparg in SM22-α positive cells results in missing PVAT.

7.5 Top enriched GOBP terms for cold-exposed PVAT

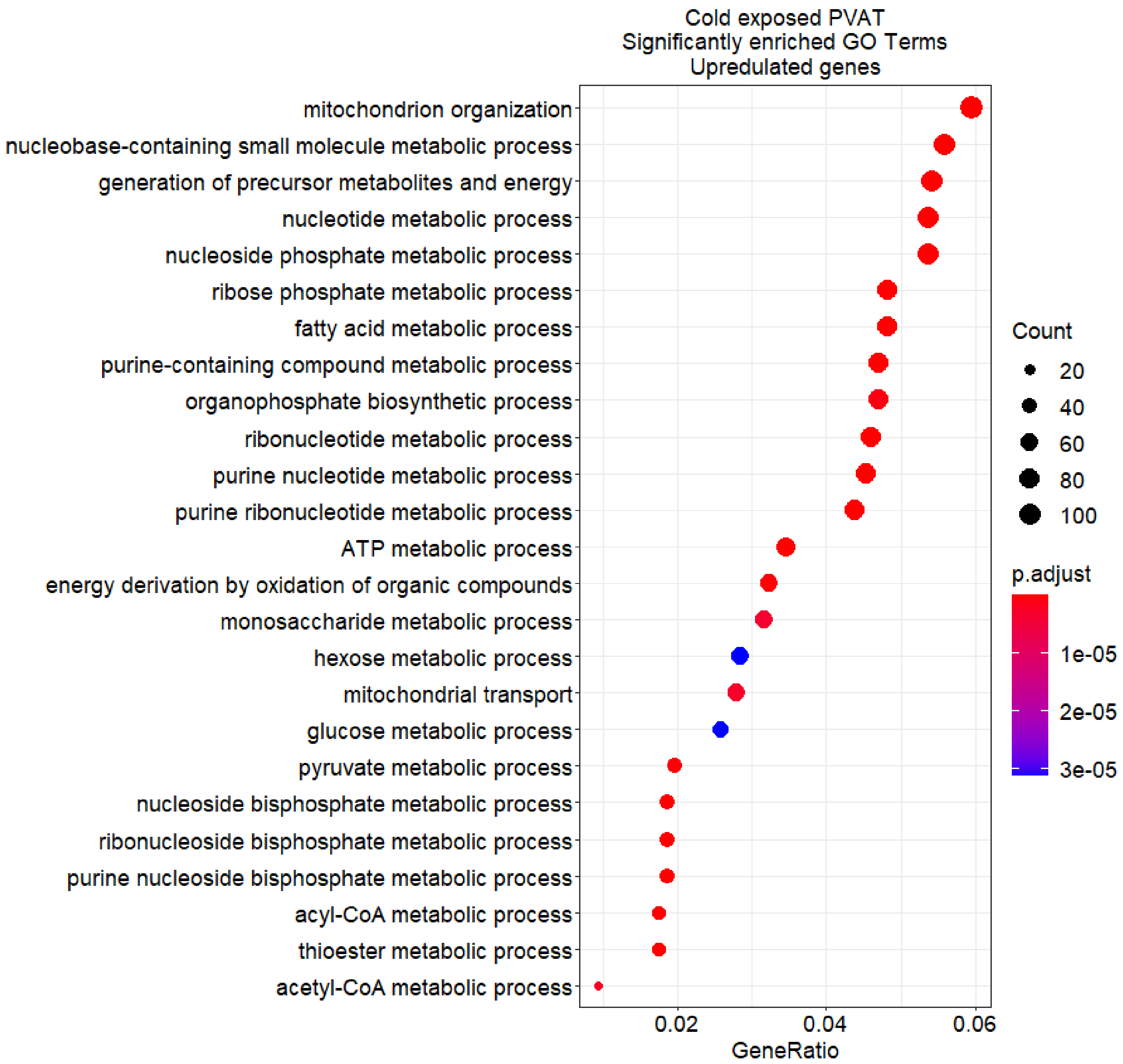

Figure 44. Fast Gene Ontology Analysis[287] from domain Biological Process of upregulated, cold-responsive genes in PVAT

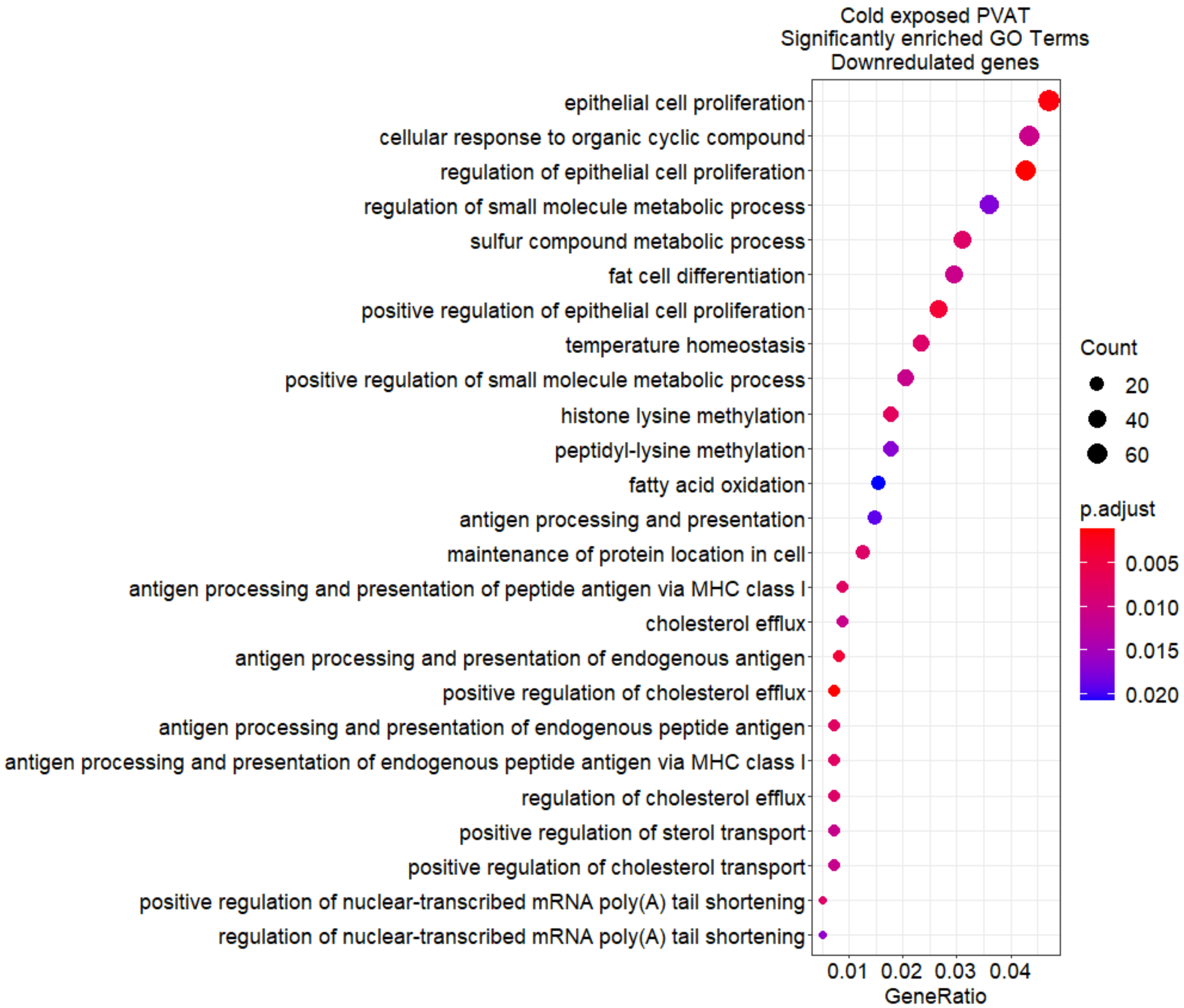

Figure 45. Fast Gene Ontology Analysis[287] *from domain Biological Process of downregulated, cold-responsive genes in PVAT*

7.6 Most enriched GOBP terms of cold-responsive adipo-miRNAs

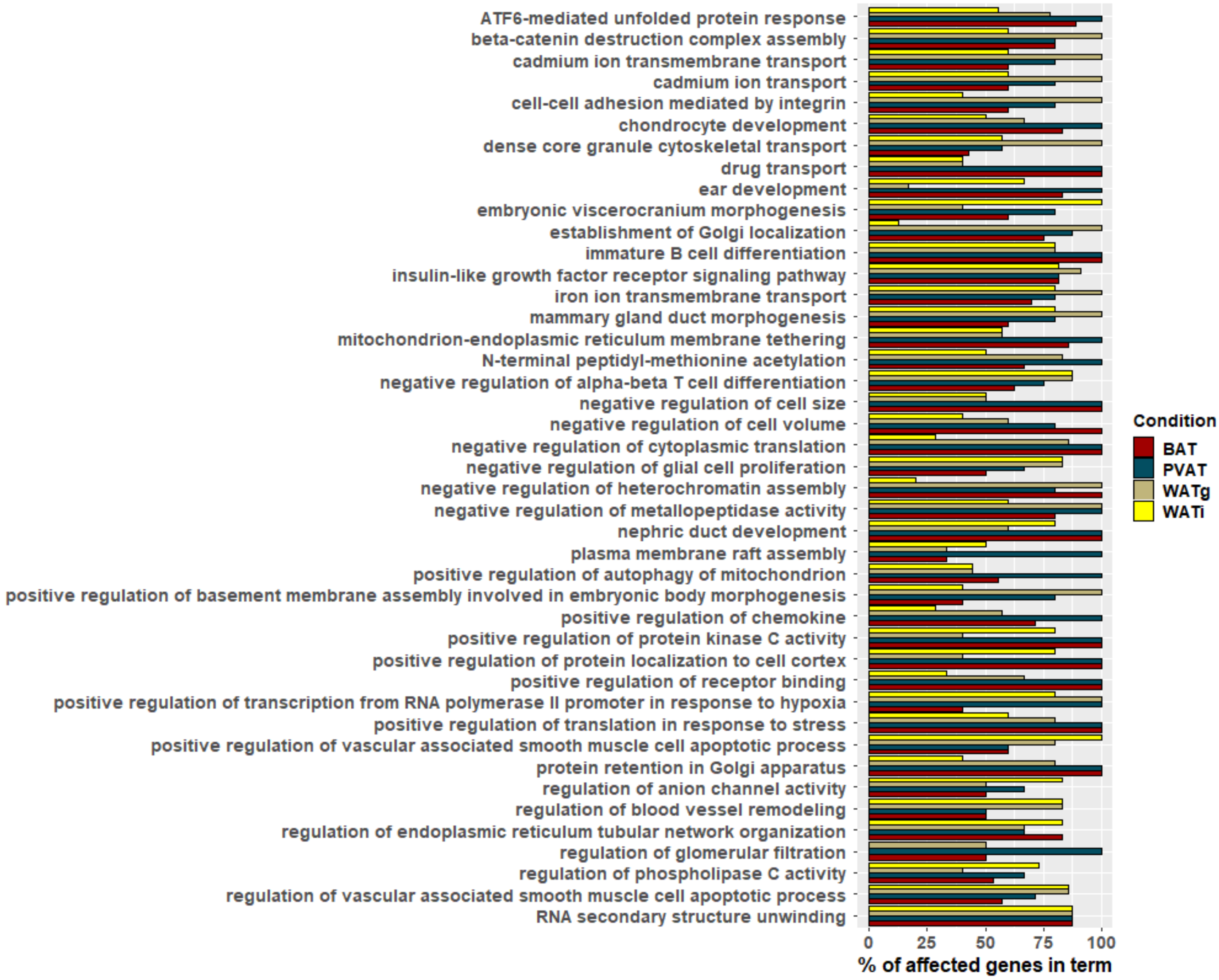

Figure 46. Gene Ontology analysis of target genes of upregulated in cold-exposed BAT (red), PVAT (green), WATi (yellow), and WATg (brown). Results show 12 most affected terms from each analysed adipose tissue.

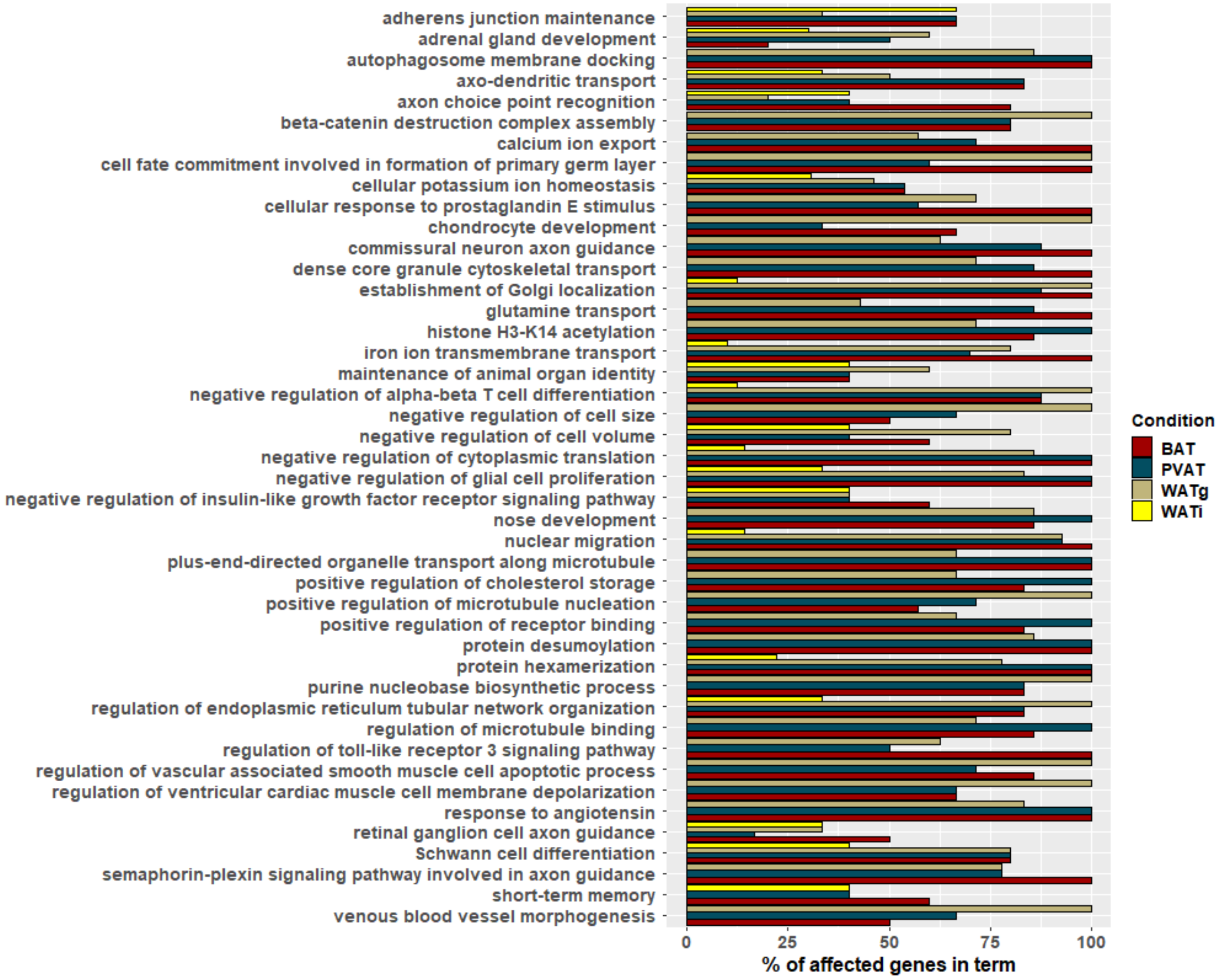

Figure 47. Gene Ontology analysis of target genes of downregulated miRNAs in cold-exposed BAT (red), PVAT (green), WATi (yellow), and WATg (brown). Results show 12 most affected terms from each analysed adipose tissue.

8 PUBLICATIONS

Freyter, B.M.; Al-razaq, M.A.; Isermann, A.; Dietz, A.; Azimzadeh, O.;Hekking, L.; Gomolka, M.; Rübe, C.E. Nuclear Fragility in Radiation-Induced Senescence: Blebs and Tubes Visualized by 3D Electron Microscopy. Cells 2022, 11, 273. https://doi.org/10.3390/cells11020273

9 REFERENCES

1. Kassab, G. S. Biomechanics of the cardiovascular system: the aorta as an illustratory example. *J R Soc Interface* **3**, 719–740 (2006).

2. Davis, F. M., Rateri, D. L. & Daugherty, A. Mechanisms of aortic aneurysm formation: translating preclinical studies into clinical therapies. *Heart* **100**, 1498–1505 (2014).

3. Landenhed, M. *et al.* Risk Profiles for Aortic Dissection and Ruptured or Surgically Treated Aneurysms: A Prospective Cohort Study. *Journal of the American Heart Association: Cardiovascular and Cerebrovascular Disease* **4**, e001513 (2015).

4. Rylski, B., Desjardins, B., Moser, W., Bavaria, J. E. & Milewski, R. K. Gender-related changes in aortic geometry throughout life. *European Journal of Cardio-Thoracic Surgery* **45**, 805–811 (2014).

5. REDHEUIL, A. *et al.* Age-Related Changes in Aortic Arch Geometry: Relationship with Proximal Aortic Function and Left Ventricular Mass and Remodeling. *J Am Coll Cardiol* **58**, 1262 (2011).

6. Stackelberg, O. *et al.* Lifestyle and Risk of Screening-Detected Abdominal Aortic Aneurysm in Men. *Journal of the American Heart Association: Cardiovascular and Cerebrovascular Disease* **6**, (2017).

7. Boileau, C. *et al.* 2014 ESCGuidelines on the diagnosis and treatment ofaortic diseases. *Jeroen J. Bax (Netherlands)* doi:10.1093/eurheartj/ehu281.

8. Quast, C. *et al.* Erkrankungen der Aorta: von der Aortenklappe bis zur Aortenbifurkation. *DMW - Deutsche Medizinische Wochenschrift* **144**, 734–738 (2019).

9. Rutkovskiy, A. *et al.* Valve interstitial cells: The key to understanding the pathophysiology of heart valve calcification. *J Am Heart Assoc* **6**, 1–23 (2017).

10. Lindsay, M. E. & Dietz, H. C. Lessons on the pathogenesis of aneurysm from heritable conditions. *Nature* **473**, 308 (2011).

11. Bonow, R. O. & Greenland, P. Population-Wide Trends in Aortic Stenosis Incidence and Outcomes. *Circulation* **131**, 969–971 (2015).

12. McClure, R. S. *et al.* Economic Burden and Healthcare Resource Use for Thoracic Aortic Dissections and Thoracic Aortic Aneurysms—A Population-Based Cost-of-Illness Analysis. *J Am Heart Assoc* **9**, 14981 (2020).

13. Rozeik, M. M., Wheatley, D. J. & Gourlay, T. The aortic valve: Structure, complications and implications for transcatheter aortic valve replacement. *Perfusion (United Kingdom)* **29**, 285–300 (2014).

14. El-Hamamsy, I., Chester, A. H. & Yacoub, M. H. Cellular regulation of the structure and function of aortic valves. *J Adv Res* **1**, 5–12 (2010).

15. TC, F. & A, P. Living artificial heart valve alternatives: a review. *Eur Cell Mater* **6**, 28–45 (2003).

16. DA, F., A, R. & M, S. Interstitial cells of the heart valves possess characteristics similar to smooth muscle cells. *Circ Res* **59**, 310–320 (1986).

17. Chester, A. H. & Taylor, P. M. Molecular and functional characteristics of heart-valve interstitial cells. *Philosophical Transactions of the Royal Society B: Biological Sciences* **362**, 1437 (2007).

18. Aikawa, E. & Libby, P. A Rock and a Hard Place. *Circulation* **135**, 1951–1955 (2017).

19. Goody, P. R. *et al.* Aortic valve stenosis: From basic mechanisms to novel therapeutic targets. *Arteriosclerosis, Thrombosis, and Vascular Biology* vol. 40 885–900 Preprint at https://doi.org/10.1161/ATVBAHA.119.313067 (2020).

20. Hoffman, J. I. E. & Kaplan, S. The incidence of congenital heart disease. *Journal of the American College of Cardiology* vol. 39 1890–1900 Preprint at https://doi.org/10.1016/S0735-1097(02)01886-7 (2002).

21. Cripe, L., Andelfinger, G., Martin, L. J., Shooner, K. & Benson, D. W. Bicuspid aortic valve is heritable. *J Am Coll Cardiol* **44**, 138–143 (2004).

22. Garg, V. *et al.* Mutations in NOTCH1 cause aortic valve disease. *Nature* **437**, 270–274 (2005).

23. Yang, B. *et al.* Protein-altering and regulatory genetic variants near GATA4 implicated in bicuspid aortic valve. *Nat Commun* **8**, (2017).

24. Padang, R., Bagnall, R. D., Richmond, D. R., Bannon, P. G. & Semsarian, C. Rare non-synonymous variations in the transcriptional activation domains of GATA5 in bicuspid aortic valve disease. *J Mol Cell Cardiol* **53**, 277–81 (2012).

25. Rajamannan, N. M. *et al.* Calcific aortic valve disease: Not simply a degenerative process: A review and agenda for research from the national heart and lung and blood institute aortic stenosis working group. *Circulation* **124**, 1783–1791 (2011).

26. Czarny, M. J. & Resar, J. R. Diagnosis and management of valvular aortic stenosis. *Clinical Medicine Insights: Cardiology* vol. 8 15–24 Preprint at https://doi.org/10.4137/CMC.S15716 (2014).

27. Aortic valve disease - Symptoms and causes - Mayo Clinic. https://www.mayoclinic.org/diseases-conditions/aortic-valve-disease/symptoms-causes/syc-20355117.

28. Otto, C. M., Lind, B. K., Kitzman, D. W., Gersh, B. J. & Siscovick, D. S. Association of Aortic-Valve Sclerosis with Cardiovascular Mortality and Morbidity in the Elderly. *New England Journal of Medicine* **341**, 142–147 (1999).

29. Stewart, B. F. *et al.* Clinical factors associated with calcific aortic valve disease. *J Am Coll Cardiol* **29**, 630–634 (1997).

30. Ferreira-González, I. *et al.* Prevalence of calcific aortic valve disease in the elderly and associated risk factors: A population-based study in a Mediterranean area. *Eur J Prev Cardiol* **20**, 1022–1030 (2013).

31. Braunwald, E. Aortic Stenosis: Then and Now. *Circulation* **137**, 2099–2100 (2018).

32. O'Brien, K. D. *et al.* Apolipoproteins B, (a), and E Accumulate in the Morphologically Early Lesion of 'Degenerative' Valvular Aortic Stenosis. *Arterioscler Thromb Vasc Biol* **16**, 523–532 (1996).

33. Olsson, M., Thyberg, J. & Nilsson, J. Presence of oxidized low density lipoprotein in nonrheumatic stenotic aortic valves. *Arterioscler Thromb Vasc Biol* **19**, 1218–1222 (1999).

34. Knott, T. J. *et al.* Complete protein sequence and identification of structural domains of human apolipoprotein B. *Nature 1986 323:6090* **323**, 734–738 (1986).

35. Goldstein, J. L. & Brown, M. S. The LDL Receptor. *Arterioscler Thromb Vasc Biol* **29**, 431–438 (2009).

36. Brown, M. S. & Goldstein, J. L. Receptor-mediated endocytosis: insights from the lipoprotein receptor system. *Proc Natl Acad Sci U S A* **76**, 3330 (1979).

37. Yancey, P. G. & Jerome, W. G. Lysosomal sequestration of free and esterified cholesterol from oxidized low density lipoprotein in macrophages of different species. *J Lipid Res* **39**, 1349–1361 (1998).

38. Brunzell, J. D. *et al.* Lipoprotein Management in Patients With Cardiometabolic Risk. *Diabetes Care* **31**, 811–822 (2008).

39. Trpkovic, A. *et al.* Oxidized low-density lipoprotein as a biomarker of cardiovascular diseases. *Crit Rev Clin Lab Sci* **52**, 70–85 (2015).

40. Stewart, B. F. *et al.* Clinical factors associated with calcific aortic valve disease. *J Am Coll Cardiol* **29**, 630–634 (1997).

41. Steinberg, D. Low Density Lipoprotein Oxidation and Its Pathobiological Significance *. *Journal of Biological Chemistry* **272**, 20963–20966 (1997).

42. Wang, Y. *et al.* Smooth Muscle Cells Contribute the Majority of Foam Cells in ApoE (Apolipoprotein E)-Deficient Mouse Atherosclerosis. *Arterioscler Thromb Vasc Biol* **39**, 876–887 (2019).

43. Ollikainen, E. *et al.* Smooth Muscle Cell Foam Cell Formation, Apolipoproteins, and ABCA1 in Intracranial Aneurysms: Implications for Lipid Accumulation as a Promoter of Aneurysm Wall Rupture. *J Neuropathol Exp Neurol* **75**, 689 (2016).

44. Lee, S. H. & Choi, J. H. Involvement of inflammatory responses in the early development of calcific aortic valve disease: lessons from statin therapy. *Animal Cells and Systems* vol. 22 390–399 Preprint at https://doi.org/10.1080/19768354.2018.1528175 (2018).

45. Kostyunin, A. *et al.* Ultrastructural Pathology of Atherosclerosis, Calcific Aortic Valve Disease, and Bioprosthetic Heart Valve Degeneration: Commonalities and Differences. *Int J Mol Sci* **21**, 1–17 (2020).

46. Wada, Y. *et al.* Lipid Accumulation in Smooth Muscle Cells Under LDL Loading Is Independent of LDL Receptor Pathway and Enhanced by Hypoxic Conditions. *Arterioscler Thromb Vasc Biol* **22**, 1712–1719 (2002).

47. Kunjathoor, V. V *et al.* Scavenger Receptors Class A-I/II and CD36 Are the Principal Receptors Responsible for the Uptake of Modified Low Density Lipoprotein Leading to Lipid Loading in Macrophages*. *Journal of Biological Chemistry* **277**, 49982–49988 (2002).

48. Steinbrechers, U. P., Lougheed, M., Kwans, W.-C. & Dirks, M. Recognition of Oxidized Low Density Lipoprotein by the Scavenger Receptor of Macrophages Results from Derivatization of Apolipoprotein B by Products of Fatty Acid Peroxidation". *J Biol Chem* **264**, 15216–15223 (1989).

49. Yoshida, H. & Kisugi, R. Mechanisms of LDL oxidation. *Clinica Chimica Acta* **411**, 1875–1882 (2010).

50. Cushing, S. D. *et al.* Minimally modified low density lipoprotein induces monocyte chemotactic protein 1 in human endothelial cells and smooth muscle cells. *Proc Natl Acad Sci U S A* **87**, 5134 (1990).

51. Liao, F. *et al.* Minimally modified low density lipoprotein is biologically active in vivo in mice. *Journal of Clinical Investigation* **87**, 2253 (1991).

52. Brown, M. S., Basu, S. K., Falck, J. R., Ho, Y. K. & Goldstein, J. L. The scavenger cell pathway for lipoprotein degradation: Specificity of the binding site that mediates the uptake of negatively-charged LDL by macrophages. *Journal of Supramolecular and Cellular Biochemistry* **13**, 67–81 (1980).

53. Ross, R. The pathogenesis of atherosclerosis: A perspective for the 1990s. *Nature* vol. 362 801–809 Preprint at https://doi.org/10.1038/362801a0 (1993).

54. Li, F., Zhao, Z., Cai, Z., Dong, N. & Liu, Y. Oxidized low-density lipoprotein promotes osteoblastic differentiation of valvular interstitial cells through RAGE/MAPK. *Cardiology (Switzerland)* **130**, 55–61 (2015).

55. Paranya, G. *et al.* Aortic valve endothelial cells undergo transforming growth factor-β-mediated and non-transforming growth factor-β-mediated transdifferentiation in Vitro. *American Journal of Pathology* **159**, 1335–1343 (2001).

56. Tanaka, K. *et al.* Age-associated aortic stenosis in apolipoprotein E-deficient mice. *J Am Coll Cardiol* **46**, 134–141 (2005).

57. Chen, J. H., Yip, C. Y. Y., Sone, E. D. & Simmons, C. A. Identification and characterization of aortic valve mesenchymal progenitor cells with robust osteogenic calcification potential. *American Journal of Pathology* **174**, 1109–1119 (2009).

58. Xing, Y., Warnock, J. N., Zhaoming, H., Hilbert, S. L. & Yoganathan, A. P. Cyclic pressure affects the biological properties of porcine aortic valve leaflets in a magnitude and frequency dependent manner. *Ann Biomed Eng* **32**, 1461–1470 (2004).

59. Yip, C. Y. Y., Chen, J. H., Zhao, R. & Simmons, C. A. Calcification by valve interstitial cells is regulated by the stiffness of the extracellular matrix. *Arterioscler Thromb Vasc Biol* **29**, 936–942 (2009).

60. Kaden, J. J. *et al.* Tumor necrosis factor alpha promotes an osteoblast-like phenotype in human aortic valve myofibroblasts: a potential regulatory mechanism of valvular calcification. *Int J Mol Med* **16**, 869–872 (2005).

61. Kaden, J. J. *et al.* Interleukin-1 beta promotes matrix metalloproteinase expression and cell proliferation in calcific aortic valve stenosis. *Atherosclerosis* **170**, 205–211 (2003).

62. Kaden, J. J. *et al.* Inflammatory regulation of extracellular matrix remodeling in calcific aortic valve stenosis. *Cardiovascular Pathology* **14**, 80–87 (2005).

63. Kaden, J. J. *et al.* Influence of receptor activator of nuclear factor kappa B on human aortic valve myofibroblasts. *Exp Mol Pathol* **78**, 36–40 (2005).

64. Jian, B., Narula, N., Li, Q. Y., Mohler, E. R. & Levy, R. J. Progression of aortic valve stenosis: TGF-β1 is present in calcified aortic valve cusps and promotes aortic valve interstitial cell calcification via apoptosis. *Annals of Thoracic Surgery* **75**, 457–465 (2003).

65. Keidar, S., Kaplan, M. & Aviram, M. Angiotensin II–Modified LDL Is Taken Up by Macrophages Via the Scavenger Receptor, Leading to Cellular Cholesterol Accumulation. *Arterioscler Thromb Vasc Biol* **16**, 97–105 (1996).

66. Fóris, G., Dezsö, B., Medgyesi, G. A. & Füst, G. Effect of angiotensin II on macrophage functions. *Immunology* **48**, 529 (1983).

67. Chen, X.-L., Tummala, P. E., Olbrych, M. T., Alexander, R. W. & Medford, R. M. Angiotensin II Induces Monocyte Chemoattractant Protein-1 Gene Expression in Rat Vascular Smooth Muscle Cells. *Circ Res* **83**, 952–959 (1998).

68. O'Brien, K. D. *et al.* Association of angiotensin-converting enzyme with low-density lipoprotein in aortic valvular lesions and in human plasma. *Circulation* **106**, 2224–2230 (2002).

69. Investigators, T. H. O. P. E. S. Effects of an Angiotensin-Converting–Enzyme Inhibitor, Ramipril, on Cardiovascular Events in High-Risk Patients. *New England Journal of Medicine* **342**, 145–153 (2000).

70. Lonn, E. M. *et al.* Emerging Role of Angiotensin-Converting Enzyme Inhibitors in Cardiac and Vascular Protection.

71. Bridgewater, B. *et al.* Sixth National Adult Cardiac Surgical Database Report 2008 Demonstrating quality Cardiac Surgery.

72. Paxton, S. *et al.* The Leeds Histology Guide. Preprint at (2003).

73. Norman, P. E., Muller, J. & Golledge, J. The cardiovascular and prognostic significance of the infrarenal aortic diameter. *J Vasc Surg* **54**, 1817–1820 (2011).

74. Johnston, K. W. *et al.* Suggested standards for reporting on arterial aneurysms. *J Vasc Surg* **13**, 452–458 (1991).

75. Mathur, A., Mohan, V., Ameta, D., Gaurav, B. & Haranahalli, P. Aortic aneurysm. *J Transl Int Med* **4**, 35–41 (2016).

76. Lederle, F. A. *et al.* The Aneurysm Detection and Management study screening program: Validation cohort and final results. *Arch Intern Med* **160**, 1425–1430 (2000).

77. Silverberg, E., Boring, C. C. & Squires, T. S. Cancer statistics, 1990. *CA Cancer J Clin* **40**, 9–26 (1990).

78. Guo, D. C., Papke, C. L., He, R. & Milewicz, D. M. Pathogenesis of thoracic and abdominal aortic aneurysms. in *Annals of the New York Academy of Sciences* vol. 1085 339–352 (Blackwell Publishing Inc., 2006).

79. Koch, A. E. *et al.* Human abdominal aortic aneurysms. Immunophenotypic analysis suggesting an immune-mediated response. *American Journal of Pathology* **137**, 1199–1213 (1990).

80. Tang, P. C. Y. *et al.* Hyperplastic cellular remodeling of the media in ascending thoracic aortic aneurysms. *Circulation* **112**, 1098–1105 (2005).

81. Lesauskaite, V. *et al.* Smooth muscle cells of the media in the dilatative pathology of ascending thoracic aorta: Morphology, immunoreactivity for osteopontin, matrix metalloproteinases, and their inhibitors. *Hum Pathol* **32**, 1003–1011 (2001).

82. Szekanecz, Z., Shah, M. R., Pearce, W. H. & Koch, A. E. Human atherosclerotic abdominal aortic aneurysms produce interleukin (IL)-6 and interferon-gamma but not IL-2 and IL-4: The possible role for IL-6 and interferon-gamma in vascular inflammation. *Agents Actions* **42**, 159–162 (1994).

83. Koch, A. E. *et al.* Enhanced production of the chemotactic cytokines interleukin-8 and monocyte chemoattractant protein-1 in human abdominal aortic aneurysms. *American Journal of Pathology* **142**, 1423–1431 (1993).

84. Pearce, W. H., Sweis, I., Yao, J. S. T., McCarthy, W. J. & Koch, A. E. Interleukin-1β and tumor necrosis factor-α release in normal and diseased human infrarenal aortas. *J Vasc Surg* **16**, 784–789 (1992).

85. Juvonen, J. *et al.* Elevated circulating levels of inflammatory cytokines in patients with abdominal aortic aneurysm. *Arterioscler Thromb Vasc Biol* **17**, 2843–2847 (1997).

86. Shimizu, K., Shichiri, M., Libby, P., Lee, R. T. & Mitchell, R. N. Erratum: Th2-predominant inflammation and blockade of IFN-γ signaling induce aneurysms in allografted aortas (Journal of Clinical Investigation (2004) 114 (300-308) doi:10.1172/JCI200419855). *Journal of Clinical Investigation* **114**, 739 (2004).

87. Abdominal aortic aneurysm - Symptoms and causes - Mayo Clinic. https://www.mayoclinic.org/diseases-conditions/abdominal-aortic-aneurysm/symptoms-causes/syc-20350688.

88. Rurali, E. *et al.* Precise Therapy for Thoracic Aortic Aneurysm in Marfan Syndrome: A Puzzle Nearing Its Solution. *Progress in Cardiovascular Diseases* vol. 61 328–335 Preprint at https://doi.org/10.1016/j.pcad.2018.07.020 (2018).

89. Calero, A. & Illig, K. A. Overview of aortic aneurysm management in the endovascular era. *Seminars in Vascular Surgery* vol. 29 3–17 Preprint at https://doi.org/10.1053/j.semvascsurg.2016.07.003 (2016).

90. Erbel, Raimund, Aboyans Victor, Boileau Catherine, Bosson Eduardo, Di Bartolomeo Roberto, Eggebrecht Holger, Evangelista Arturo, Falk Volkmar, Frank Herbert, Gaemperli Oliver, Grabenwöger Martin, Haverich Axel, Iung Bernard, Manolis Athanasios John, Meijb, V. C. J. M. 2014 ESC Guidelines on the diagnosis andtreatment of aortic diseases. *Eur Heart J* **35**, 2873–2926 (2014).

91. Chaikof, E. L. *et al.* The Society for Vascular Surgery practice guidelines on the care of patients with an abdominal aortic aneurysm. *J Vasc Surg* **67**, 2-77.e2 (2018).

92. Hiratzka, L. F. *et al. Guidelines for the Diagnosis and Management of Patients With Thoracic Aortic Disease Writing Committee*. (2010).

93. Brady, A. R., Fowkes, F. G. R., Thompson, S. G. & Powell, J. T. Aortic Aneurysm Diameter and Risk of Cardiovascular Mortality. *Arterioscler Thromb Vasc Biol* **21**, 1203–1207 (2001).

94. Roux, P. P. & Blenis, J. ERK and p38 MAPK-Activated Protein Kinases: a Family of Protein Kinases with Diverse Biological Functions. *Microbiology and Molecular Biology Reviews* **68**, 320 (2004).

95. Franceschi, R. T., Ge, C., Xiao, G., Roca, H. & Jiang, D. Transcriptional Regulation of Osteoblasts. *Cells Tissues Organs* **189**, 144 (2008).

96. Ge, C., Xiao, G., Jiang, D. & Franceschi, R. T. Critical role of the extracellular signal–regulated kinase–MAPK pathway in osteoblast differentiation and skeletal development. *J Cell Biol* **176**, 709 (2007).

97. Gu, X. & Masters, K. S. Role of the MAPK/ERK pathway in valvular interstitial cell calcification. *Am J Physiol Heart Circ Physiol* **296**, 1748–1757 (2009).

98. Ding, H.-T., Wang, C.-G., Zhang, T.-L. & Wang, K. Fibronectin enhances in vitro vascular calcification by promoting osteoblastic differentiation of vascular smooth muscle cells via ERK pathway. *J Cell Biochem* **99**, 1343–1352 (2006).

99. Simmons, C. A., Nikolovski, J., Thornton, A. J., Matlis, S. & Mooney, D. J. Mechanical stimulation and mitogen-activated protein kinase signaling independently regulate osteogenic differentiation and mineralization by calcifying vascular cells. *J Biomech* **37**, 1531–1541 (2004).

100. Roy, J., Kazi, M., Hedin, U. & Thyberg, J. Phenotypic modulation of arterial smooth muscle cells is associated with prolonged activation of ERK1/2. *Differentiation* **67**, 50–58 (2001).

101. Reustle, A. & Torzewski, M. Role of p38 MAPK in atherosclerosis and aortic valve sclerosis. *International Journal of Molecular Sciences* vol. 19 3761 Preprint at https://doi.org/10.3390/ijms19123761 (2018).

102. Reustle, A. & Torzewski, M. Role of p38 MAPK in atherosclerosis and aortic valve sclerosis. *International Journal of Molecular Sciences* vol. 19 Preprint at https://doi.org/10.3390/ijms19123761 (2018).

103. Calcinotto, A. *et al.* Cellular Senescence: Aging, Cancer, and Injury. *https://doi.org/10.1152/physrev.00020.2018* **99**, 1047–1078 (2019).

104. Oh, K. S. *et al.* Cellular senescence evaluated by P16INK4a immunohistochemistry is a prevalent phenomenon in advanced calcific aortic valve disease. *Cardiovascular Pathology* **52**, 107318 (2021).

105. Balint, B. *et al.* Seno-destructive smooth muscle cells in the ascending aorta of patients with bicuspid aortic valve disease. *EBioMedicine* **43**, 54–66 (2019).

106. Li, F. *et al.* Pioglitazone attenuates progression of aortic valve calcification via down-regulating receptor for advanced glycation end products. *Basic Res Cardiol* **107**, (2012).

107. Murphy, D. J. The biogenesis and functions of lipid bodies in animals, plants and microorganisms. *Prog Lipid Res* **40**, 325–438 (2001).

108. Hildebrand, S., Stümer, J. & Pfeifer, A. PVAT and its relation to brown, beige, and white adipose tissue in development and function. *Front Physiol* **9**, 1–10 (2018).

109. Sanchez-Gurmaches, J. & Guertin, D. A. Adipocyte lineages: Tracing back the origins of fat. *Biochimica et Biophysica Acta (BBA) - Molecular Basis of Disease* **1842**, 340–351 (2014).

110. Pfeifer, A. & Hoffmann, L. S. Brown, beige, and white: The new color code of fat and its pharmacological implications. *Annu Rev Pharmacol Toxicol* **55**, 207–227 (2015).

111. Bjørndal, B., Burri, L., Staalesen, V., Skorve, J. & Berge, R. K. Different Adipose Depots: Their Role in the Development of Metabolic Syndrome and Mitochondrial Response to Hypolipidemic Agents. *J Obes* **2011**, 15 (2011).

112. Richard, A. J., White, U., Elks, C. M. & Stephens, J. M. *Adipose Tissue: Physiology to Metabolic Dysfunction*. *Endotext* (MDText.com, Inc., 2020).

113. Richard, A. J., White, U., Elks, C. M. & Stephens, J. M. Adipose Tissue: Physiology to Metabolic Dysfunction. *Endotext* (2020).

114. Zhang, F. *et al.* An Adipose Tissue Atlas: An Image-Guided Identification of Human-like BAT and Beige Depots in Rodents Cell Metabolism Resource An Adipose Tissue Atlas: An Image-Guided Identification of Human-like BAT and Beige Depots in Rodents. *Cell Metab* **27**, 252–262 (2018).

115. Cypess, A. M. *et al.* Identification and Importance of Brown Adipose Tissue in Adult Humans. *N Engl J Med* **360**, 1509 (2009).

116. Mirbolooki, M. R., Constantinescu, C. C., Pan, M.-L. & Mukherjee, J. Quantitative assessment of brown adipose tissue metabolic activity and volume using 18F-FDG PET/CT and β3-adrenergic receptor activation. *EJNMMI Research 2011 1:1* **1**, 1–11 (2011).

117. Chait, A. & den Hartigh, L. J. Adipose Tissue Distribution, Inflammation and Its Metabolic Consequences, Including Diabetes and Cardiovascular Disease. *Front Cardiovasc Med* **7**, 22 (2020).

118. Kajimura, S., Spiegelman, B. M. & Seale, P. Brown and beige fat: Physiological roles beyond heat generation. *Cell Metabolism* vol. 22 546–559 Preprint at https://doi.org/10.1016/j.cmet.2015.09.007 (2015).

119. Nedergaard, J. *et al.* UCP1: The only protein able to mediate adaptive non-shivering thermogenesis and metabolic inefficiency. *Biochimica et Biophysica Acta - Bioenergetics* vol. 1504 82–106 Preprint at https://doi.org/10.1016/S0005-2728(00)00247-4 (2001).

120. Okamatsu-Ogura, Y. *et al.* Thermogenic Ability of Uncoupling Protein 1 in Beige Adipocytes in Mice. *PLoS One* **8**, 84229 (2013).

121. Thalmann, S. & Meier, C. A. Local adipose tissue depots as cardiovascular risk factors. (2007) doi:10.1016/j.cardiores.2007.03.008.

122. Fitzgibbons, T. P. *et al.* Similarity of mouse perivascular and brown adipose tissues and their resistance to diet-induced inflammation. *Am J Physiol Heart Circ Physiol* **301**, H1425 (2011).

123. Chang, L. *et al.* Loss of perivascular adipose tissue on peroxisome proliferator-activated receptor-γ deletion in smooth muscle cells impairs intravascular thermoregulation and enhances atherosclerosis. *Circulation* **126**, 1067–1078 (2012).

124. Tabuchi, C. & Sul, H. S. Signaling Pathways Regulating Thermogenesis. *Front Endocrinol (Lausanne)* **0**, 243 (2021).

125. Angueira, A. R. *et al.* Defining the lineage of thermogenic perivascular adipose tissue. *Nature Metabolism 2021 3:4* **3**, 469–484 (2021).

126. Solway, J. *et al.* Structure and Expression of a Smooth Muscle Cell-specific Gene, SM22α ∗. *Journal of Biological Chemistry* **270**, 13460–13469 (1995).

127. Lowell, B. B. & Spiegelman, B. M. Towards a molecular understanding of adaptive thermogenesis. *Nature* **404**, 652–660 (2000).

128. Tchivileva, I. E. *et al.* Signaling Pathways Mediating Beta 3 Adrenergic Receptor-induced Production of Interleukin-6 in Adipocytes. *Mol Immunol* **46**, 2256 (2009).

129. Cao, W. *et al.* Direct Binding of Activated c-Src to the β3-Adrenergic Receptor Is Required for MAP Kinase Activation *. *Journal of Biological Chemistry* **275**, 38131–38134 (2000).

130. Komai, A. M. *et al.* White Adipocyte Adiponectin Exocytosis Is Stimulated via β3-Adrenergic Signaling and Activation of Epac1: Catecholamine Resistance in Obesity and Type 2 Diabetes. *Diabetes* **65**, 3301–3313 (2016).

131. Gettys, T. W., Harkness, P. J. & Watson, P. M. The beta 3-adrenergic receptor inhibits insulin-stimulated leptin secretion from isolated rat adipocytes. *Endocrinology* **137**, 4054–4057 (1996).

132. Moss, G. P., Smith, P. A. S. & Tavernier, D. Glossary of class names of organic compounds and reactive intermediates based on structure (IUPAC recommendations 1995). *Pure and Applied Chemistry* **67**, 1307–1375 (1995).

133. Fahy, E. *et al.* Update of the LIPID MAPS comprehensive classification system for lipids. *Journal of Lipid Research* vol. 50 S9 Preprint at https://doi.org/10.1194/jlr.R800095-JLR200 (2009).

134. Subramaniam, S. *et al.* Bioinformatics and systems biology of the lipidome. *Chemical Reviews* vol. 111 6452–6490 Preprint at https://doi.org/10.1021/cr200295k (2011).

135. Drewnowski, A. Sensory Properties of Fats and Fat Replacements. *Nutr Rev* **50**, 17–20 (1992).

136. Gluchowski, N. L., Becuwe, M., Walther, T. C. & Farese, R. V. Lipid droplets and liver disease: From basic biology to clinical implications. *Nature Reviews Gastroenterology and Hepatology* vol. 14 343–355 Preprint at https://doi.org/10.1038/nrgastro.2017.32 (2017).

137. Birsoy, K., Festuccia, W. T. & Laplante, M. A comparative perspective on lipid storage in animals. *Journal of Cell Science* vol. 126 1541–1552 Preprint at https://doi.org/10.1242/jcs.104992 (2013).

138. Chen, Y., Pan, R. & Pfeifer, A. Fat tissues, the brite and the dark sides. *Pflugers Archiv European Journal of Physiology* vol. 468 1803–1807 Preprint at https://doi.org/10.1007/s00424-016-1884-8 (2016).

139. Gálvez-Prieto, B. *et al.* Comparative expression analysis of the renin - Angiotensin system components between white and brown perivascular adipose tissue. *Journal of Endocrinology* **197**, 55–64 (2008).

140. Fitzgibbons, T. P. & Czech, M. P. Epicardial and perivascular adipose tissues and their influence on cardiovascular disease: Basic mechanisms and clinical associations. *Journal of the American Heart Association* vol. 3 Preprint at https://doi.org/10.1161/JAHA.113.000582 (2014).

141. Lass, A., Zimmermann, R., Oberer, M. & Zechner, R. Lipolysis - A highly regulated multi-enzyme complex mediates the catabolism of cellular fat stores. *Prog Lipid Res* **50**, 14–27 (2011).

142. Berg, J., Tymoczko, J. & Stryer, L. *Biochemistry*. *Biochemistry* (W H Freeman, 2002).

143. Cannon, B. & Nedergaard, J. Brown Adipose Tissue: Function and Physiological Significance. (2004) doi:10.1152/physrev.00015.2003.-The.

144. Jones, G. Fifty shades of brown. *Tunnels and Tunnelling International* **126**, 43–47 (2012).

145. Mills, E. L. *et al.* Accumulation of succinate controls activation of adipose tissue thermogenesis. *Nature* **560**, 102 (2018).

146. Betz, M. J. & Enerbäck, S. Targeting thermogenesis in brown fat and muscle to treat obesity and metabolic disease. *Nat Rev Endocrinol* **14**, 77–87 (2018).

147. Fedorenko, A., Lishko, P. V. & Kirichok, Y. Mechanism of fatty-acid-dependent UCP1 uncoupling in brown fat mitochondria. *Cell* **151**, 400–413 (2012).

148. Boon, R. *et al.* Brown fat activation reduces hypercholesterolaemia and protects from atherosclerosis development. (2015) doi:10.1038/ncomms7356.

149. Lehr, S., Hartwig, S. & Sell, H. Adipokines: A treasure trove for the discovery of biomarkers for metabolic disorders. *Proteomics Clin Appl* **6**, 91–101 (2012).

150. Zhang, J. M. & An, J. Cytokines, inflammation, and pain. *International Anesthesiology Clinics* vol. 45 27–37 Preprint at https://doi.org/10.1097/AIA.0b013e318034194e (2007).

151. Liu, W. *et al.* Association of adipokines with blood pressure, arterial elasticity and cardiac markers in dialysis patients: cross-sectional analysis of baseline data from a cohort study. *Nutr Metab (Lond)* **14**, 1–8 (2017).

152. Ahima, R. S. & Lazar, M. A. Adipokines and the peripheral and neural control of energy balance. *Molecular Endocrinology* vol. 22 1023–1031 Preprint at https://doi.org/10.1210/me.2007-0529 (2008).

153. Ahima, R. S., Saper, C. B., Flier, J. S. & Elmquist, J. K. Leptin regulation of neuroendocrine systems. *Front Neuroendocrinol* **21**, 263–307 (2000).

154. Ingalls, A. M., Dickie, M. M. & Snell, G. D. Obese, a new mutation in the house mouse. *Obes Res* **4**, 101 (1950).

155. Friedman, J. M., Leibel, R. L., Siegel, D. S., Walsh, J. & Bahary, N. Molecular mapping of the mouse ob mutation. *Genomics* **11**, 1054–1062 (1991).

156. Morris, D. L. & Rui, L. Recent advances in understanding leptin signaling and leptin resistance. *American Journal of Physiology - Endocrinology and Metabolism* vol. 297 E1247 Preprint at https://doi.org/10.1152/ajpendo.00274.2009 (2009).

157. Raman, P. & Khanal, S. Leptin in atherosclerosis: Focus on macrophages, endothelial and smooth muscle cells. *Int J Mol Sci* **22**, (2021).

158. Taleb, S. *et al.* Defective leptin/leptin receptor signaling improves regulatory T cell immune response and protects mice from atherosclerosis. *Arterioscler Thromb Vasc Biol* **27**, 2691–2698 (2007).

159. Kadowaki, T. & Yamauchi, T. Adiponectin and adiponectin receptors. *Endocrine Reviews* vol. 26 439–451 Preprint at https://doi.org/10.1210/er.2005-0005 (2005).

160. Maeda, N. *et al.* Diet-induced insulin resistance in mice lacking adiponectin/ACRP30. *Nat Med* **8**, 731–737 (2002).

161. Kubota, N. *et al.* Disruption of adiponectin causes insulin resistance and neointimal formation. *Journal of Biological Chemistry* **277**, 25863–25866 (2002).

162. Scheja, L. & Heeren, J. The endocrine function of adipose tissues in health and cardiometabolic disease. *Nat Rev Endocrinol* **15**, 507–524 (2019).

163. Wang, G. X., Zhao, X. Y. & Lin, J. D. The brown fat secretome: Metabolic functions beyond thermogenesis. *Trends in Endocrinology and Metabolism* **26**, 231–237 (2015).

164. Rome, S., Blandin, A. & Lay, S. le. Adipocyte-Derived Extracellular Vesicles: State of the Art. *Int J Mol Sci* **22**, 1–19 (2021).

165. Bond, S. T., Calkin, A. C. & Drew, B. G. Adipose-Derived Extracellular Vesicles: Systemic Messengers and Metabolic Regulators in Health and Disease. *Front Physiol* **0**, 286 (2022).

166. Słomka, A., Urban, S. K., Lukacs-Kornek, V., Żekanowska, E. & Kornek, M. Large Extracellular Vesicles: Have We Found the Holy Grail of Inflammation? *Front Immunol* **9**, 2723 (2018).

167. van Niel, G., D'Angelo, G. & Raposo, G. Shedding light on the cell biology of extracellular vesicles. *Nature Reviews Molecular Cell Biology 2018 19:4* **19**, 213–228 (2018).

168. Coelho, M., Oliveira, T. & Fernandes, R. Biochemistry of adipose tissue: an endocrine organ. *Arch Med Sci* **9**, 191 (2013).

169. Hartwig, S. *et al.* Exosomal proteins constitute an essential part of the human adipose tissue secretome. *Biochimica et Biophysica Acta (BBA) - Proteins and Proteomics* **1867**, 140172 (2019).

170. Tysoe, O. Adipocyte-derived exosomes drive cancer metastasis. *Nature Reviews Endocrinology 2021 18:2* **18**, 68–68 (2021).

171. Bartel, D. P. Metazoan MicroRNAs. *Cell* vol. 173 20–51 Preprint at https://doi.org/10.1016/j.cell.2018.03.006 (2018).

172. Sohel, M. H. Extracellular/Circulating MicroRNAs: Release Mechanisms, Functions and Challenges. *Achievements in the Life Sciences* **10**, 175–186 (2016).

173. Cai, X., Hagedorn, C. H. & Cullen, B. R. Human microRNAs are processed from capped, polyadenylated transcripts that can also function as mRNAs. *RNA* **10**, 1957–1966 (2004).

174. Lee, Y. *et al.* MicroRNA genes are transcribed by RNA polymerase II. *EMBO Journal* **23**, 4051–4060 (2004).

175. Lee, Y., Jeon, K., Lee, J. T., Kim, S. & Kim, V. N. MicroRNA maturation: Stepwise processing and subcellular localization. *EMBO Journal* **21**, 4663–4670 (2002).

176. Lee, Y. *et al.* The nuclear RNase III Drosha initiates microRNA processing. *Nature* **425**, 415–419 (2003).

177. Murchison, E. P. & Hannon, G. J. miRNAs on the move: miRNA biogenesis and the RNAi machinery. *Curr Opin Cell Biol* **16**, 223–229 (2004).

178. Lund, E. & Dahlberg, J. E. Substrate selectivity of exportin 5 and Dicer in the biogenesis of microRNAs. *Cold Spring Harb Symp Quant Biol* **71**, 59–66 (2006).

179. Thomou, T. *et al.* Adipose-derived circulating miRNAs regulate gene expression in other tissues. *Nature* **542**, 450–455 (2017).

180. Hofmanis, J. *et al.* Prognostic Utility of Circulating Growth Factors in Aortic Valve Stenosis: A Pilot Study. *Medicina (B Aires)* **57**, 1–13 (2021).

181. Planavila, A., Redondo-Angulo, I. & Villarroya, F. FGF21 and Cardiac Physiopathology. *Front Endocrinol (Lausanne)* **6**, (2015).

182. Kozomara, A. & Griffiths-Jones, S. MiRBase: Annotating high confidence microRNAs using deep sequencing data. *Nucleic Acids Res* **42**, D68–D73 (2014).

183. Baek, D. *et al.* The impact of microRNAs on protein output. *Nature* **455**, 64–71 (2008).

184. Lim, L. P. *et al.* Microarray analysis shows that some microRNAs downregulate large numbers of target mRNAs. *Nature 2005 433:7027* **433**, 769–773 (2005).

185. Selbach, M. *et al.* Widespread changes in protein synthesis induced by microRNAs. *Nature* **455**, 58–63 (2008).

186. Liu, W. & Wang, X. Prediction of functional microRNA targets by integrative modeling of microRNA binding and target expression data. *Genome Biol* **20**, 1–10 (2019).

187. Van Rossum, G. *Python tutorial*. (1995).

188. R Core Team. R: A Language and Environment for Statistical Computing. Preprint at http://www.r-project.org (2008).

189. RStudio Team. RStudio: Integrated Development for R. RStudio. Preprint at (2020).

190. The Spyder Development Team. Spyder The Scientific Python Development Environment. Preprint at (2020).

191. Morgan M., S. L. AnnotationHub: Client to access AnnotationHub resources. Preprint at (2021).

192. Durinck, S., Spellman, P. T., Birney, E. & Huber, W. Mapping identifiers for the integration of genomic datasets with the R/ Bioconductor package biomaRt. *Nat Protoc* **4**, 1184–1191 (2009).

193. Bokeh Development Team. Bokeh: Python library for interactive visualization. Preprint at (2020).

194. Wu, T. *et al.* clusterProfiler 4.0: A universal enrichment tool for interpreting omics data. *The Innovation* **2**, (2021).

195. Martin, M. Cutadapt removes adapter sequences from high-throughput sequencing reads. *EMBnet J* **17**, 10 (2011).

196. Love, M. I., Huber, W. & Anders, S. Moderated estimation of fold change and dispersion for RNA-seq data with DESeq2. *Genome Biol* **15**, 550 (2014).

197. Kuleshov, M. v. *et al.* Enrichr: a comprehensive gene set enrichment analysis web server 2016 update. *Nucleic Acids Res* **44**, W90–W97 (2016).

198. Korotkevich, G. *et al.* Fast gene set enrichment analysis. *bioRxiv* 060012 (2021) doi:10.1101/060012.

199. Sergushichev, A. A. An algorithm for fast preranked gene set enrichment analysis using cumulative statistic calculation. *bioRxiv* 060012 (2016) doi:10.1101/060012.

200. Anders, S., Pyl, P. T. & Huber, W. HTSeq—a Python framework to work with high-throughput sequencing data. *Bioinformatics* **31**, 166–169 (2015).

201. Ru, Y. *et al.* The multiMiR R package and database: Integration of microRNA-target interactions along with their disease and drug associations. *Nucleic Acids Res* **42**, e133 (2014).

202. Carlson, M. org.Mm.eg.db: Genome wide annotation for Mouse. R. Preprint at (2019).

203. Mckinney, W. *Data Structures for Statistical Computing in Python*. (2010) doi:10.25080/Majora-92bf1922-00a.

204. Kolde, R. Pheatmap: pretty heatmaps. Preprint at (2012).

205. Slenter, D. N. *et al.* WikiPathways: a multifaceted pathway database bridging metabolomics to other omics research. *Nucleic Acids Res* **46**, D661 (2018).

206. Dobin, A. *et al.* STAR: Ultrafast universal RNA-seq aligner. *Bioinformatics* **29**, 15–21 (2013).

207. Wickham, H. *et al.* Welcome to the Tidyverse. *J Open Source Softw* **4**, 1686 (2019).

208. Chen, H. & Boutros, P. C. VennDiagram: A package for the generation of highly-customizable Venn and Euler diagrams in R. *BMC Bioinformatics* **12**, 35 (2011).

209. Jassal, B. *et al.* The reactome pathway knowledgebase. *Nucleic Acids Res* **48**, D498–D503 (2020).

210. Frankish, A. *et al.* GENCODE reference annotation for the human and mouse genomes. *Nucleic Acids Res* **47**, D766–D773 (2019).

211. Sobell, M. G. A practical guide to Ubuntu Linux. Preprint at (2015).

212. GNU, P. Free Software Foundation. Bash (3.2. 48)[Unix shell program]. Preprint at (2007).

213. Hadley Wickham, Romain François, Lionel Henry, Kirill Müller, Rs. dplyr: A Grammar of Data Manipulation. Preprint at (2021).

214. Bult, C. J. *et al.* Mouse Genome Database (MGD) 2019. *Nucleic Acids Res* **47**, D801–D806 (2019).

215. Yu, G., Wang, L. G., Han, Y. & He, Q. Y. ClusterProfiler: An R package for comparing biological themes among gene clusters. *OMICS* **16**, 284–287 (2012).

216. HGNC Guidelines | HUGO Gene Nomenclature Committee. https://www.genenames.org/about/guidelines/.

217. Piñero, J. *et al.* The DisGeNET knowledge platform for disease genomics: 2019 update. *Nucleic Acids Res* **48**, D845–D855 (2020).

218. Park, A. Distinction of white, beige and brown adipocytes derived from mesenchymal stem cells. *World J Stem Cells* **6**, 33 (2014).

219. Balkow, A. *et al.* A novel crosstalk between Alk7 and cGMP signaling differentially regulates brown adipocyte function. *Mol Metab* **4**, 576–583 (2015).

220. Lefterova, M. I., Haakonsson, A. K., Lazar, M. A. & Mandrup, S. PPARγ and the global map of adipogenesis and beyond. *Trends in Endocrinology and Metabolism* **25**, 293–302 (2014).

221. Bengtsson, T., Cannon, B. & Nedergaard, J. Differential adrenergic regulation of the gene expression of the β-adrenoceptor subtypes β1, β2 and β3 in brown adipocytes. *Biochemical Journal* **347**, 643–651 (2000).

222. Eva M. LINDGREN, R. N. N. P. A. J. S. M. B. C. and J. N. Noradrenaline represses PPARG2 gene expression in brown adipocytes intracellular signalling and effects on PPARG2 and PPARG1 protein levels.

223. Chu, D.-T., Malinowska, E., Gawronska-Kozak, B. & Kozak, L. P. Expression of Adipocyte Biomarkers in a Primary Cell Culture Models Reflects Preweaning Adipobiology *. (2014) doi:10.1074/jbc.M114.555821.

224. Reverte-Salisa, L., Sanyal, A. & Pfeifer, A. Role of cAMP and cGMP signaling in brown fat. *Handb Exp Pharmacol* **251**, 161–182 (2019).

225. Zhang, P., Konja, D. & Wang, Y. Adipose tissue secretory profile and cardiometabolic risk in obesity. *Endocrine and Metabolic Science* **1**, 100061 (2020).

226. Kolishovski, G. *et al.* The JAX Synteny Browser for mouse-human comparative genomics. *Mammalian Genome* **30**, 353–361 (2019).

227. Fu, Y., Luo, N., Klein, R. L. & Timothy Garvey, W. Adiponectin promotes adipocyte differentiation, insulin sensitivity, and lipid accumulation. *J Lipid Res* **46**, 1369–1379 (2005).

228. Ferrand, N. *et al.* WISP1/CCN4 inhibits adipocyte differentiation through repression of PPARγ activity. *Scientific Reports 2017 7:1* **7**, 1–12 (2017).

229. Mukherjee, S., Aseer, K. R. & Yun, J. W. Roles of Macrophage Colony Stimulating Factor in White and Brown Adipocytes. *Biotechnology and Bioprocess Engineering 2020 25:1* **25**, 29–38 (2020).

230. Espina, Á. G. *et al.* Induction of Dlk1 by PTTG1 Inhibits Adipocyte Differentiation and Correlates with Malignant Transformation. *Mol Biol Cell* **20**, 3353 (2009).

231. Mitterberger, M. C. *et al.* DLK1(PREF1) is a negative regulator of adipogenesis in CD105+/CD90+/CD34+/CD31−/FABP4− adipose-derived stromal cells from subcutaneous abdominal fat pats of adult women. *Stem Cell Res* **9**, 35–48 (2012).

232. Goralski, K. B. *et al.* Chemerin, a Novel Adipokine That Regulates Adipogenesis and Adipocyte Metabolism * □ S. (2007) doi:10.1074/jbc.M700793200.

233. Kim, K. H., Lee, K., Moon, Y. S. & Sul, H. S. A Cysteine-rich Adipose Tissue-specific Secretory Factor Inhibits Adipocyte Differentiation *. *Journal of Biological Chemistry* **276**, 11252–11256 (2001).

234. Yoshida, S., Fuster, J. J. & Walsh, K. Adiponectin attenuates abdominal aortic aneurysm formation in hyperlipidemic mice. *Atherosclerosis* **235**, 339 (2014).

235. Yu, H. *et al.* Angiopoietin-2 attenuates angiotensin II-induced aortic aneurysm and atherosclerosis in apolipoprotein E-deficient mice. *Scientific Reports 2016 6:1* **6**, 1–11 (2016).

236. Wang, Q. *et al.* Monocyte Chemoattractant Protein-1 (MCP-1) Regulates Macrophage Cytotoxicity in Abdominal Aortic Aneurysm. *PLoS One* **9**, (2014).

237. Aoki, T. *et al.* Impact of monocyte chemoattractant protein-1 deficiency on cerebral aneurysm formation. *Stroke* **40**, 942–951 (2009).

238. Moehle, C. W. *et al.* Bone marrow–derived MCP1 required for experimental aortic aneurysm formation and smooth muscle phenotypic modulation. *J Thorac Cardiovasc Surg* **142**, 1567–1574 (2011).

239. Tieu, B. C. *et al.* An adventitial IL-6/MCP1 amplification loop accelerates macrophage-mediated vascular inflammation leading to aortic dissection in mice. *J Clin Invest* **119**, 3637–3651 (2009).

240. Li, X. F. *et al.* M1 macrophages promote aortic valve calcification mediated by microRNA-214/TWIST1 pathway in valvular interstitial cells. *Am J Transl Res* **8**, 5773 (2016).

241. Lee, S. H. & Choi, J. H. Involvement of inflammatory responses in the early development of calcific aortic valve disease: lessons from statin therapy. *Anim Cells Syst (Seoul)* **22**, 390 (2018).

242. Wenzel, D. *et al.* Endostatin, the proteolytic fragment of collagen XVIII, induces vasorelaxation. *Circ Res* **98**, 1203–1211 (2006).

243. Lindholt, J. S., Erlandsen, E. J. & Henneberg, E. W. Cystatin C deficiency is associated with the progression of small abdominal aortic aneurysms. *British Journal of Surgery* **88**, 1472–1475 (2002).

244. Schulte, S. *et al.* Cystatin C Deficiency Promotes Inflammation in Angiotensin II–Induced Abdominal Aortic Aneurisms in Atherosclerotic Mice. *Am J Pathol* **177**, 456–463 (2010).

245. Helske, S. *et al.* Increased expression of elastolytic cathepsins S, K, and V and their inhibitor cystatin C in stenotic aortic valves. *Arterioscler Thromb Vasc Biol* **26**, 1791–1798 (2006).

246. Patel, A., Jagadesham, V. P., Porter, K. E., Scott, D. J. A. & Carding, S. R. Characterisation of Fractalkine/CX3CL1 and Fractalkine Receptor (CX3CR1) Expression in Abdominal Aortic Aneurysm Disease. (2008) doi:10.1016/j.ejvs.2008.01.014.

247. Cheng, Z. *et al.* Diverse roles of macrophage polarization in aortic aneurysm: Destruction and repair. *J Transl Med* **16**, 1–8 (2018).

248. Shimizu, K., Shichiri, M., Libby, P., Lee, R. T. & Mitchell, R. N. Th2-predominant inflammation and blockade of IFN-γ signaling induce aneurysms in allografted aortas. *Journal of Clinical Investigation* **114**, 300 (2004).

249. Shen, M. *et al.* Divergent roles of matrix metalloproteinase 2 in pathogenesis of thoracic aortic aneurysm. *Arterioscler Thromb Vasc Biol* **35**, 888–898 (2015).

250. Sakalihasan, N., Delvenne, P., Nusgens, B. v., Limet, R. & Lapiere, C. M. Activated forms of MMP2 and MMP9 in abdominal aortic aneurysms. *J Vasc Surg* **24**, 127–133 (1996).

251. Kaden, J. J. *et al.* Expression and activity of matrix metalloproteinase-2 in calcific aortic stenosis. *Zeitschrift für Kardiologie 2004 93:2* **93**, 124–130 (2004).

252. Tengiz, I. *et al.* Elevated levels of matrix metalloprotein-3 in patients with coronary aneurysm: A case control study. *Curr Control Trials Cardiovasc Med* **5**, 1–6 (2004).

253. Silence, J., Lupu, F., Collen, D. & Lijnen, H. R. Persistence of Atherosclerotic Plaque but Reduced Aneurysm Formation in Mice With Stromelysin-1 (MMP-3) Gene Inactivation. *Arterioscler Thromb Vasc Biol* **21**, 1440–1445 (2001).

254. Maguire, E. M., Pearce, S. W. A., Xiao, R., Oo, A. Y. & Xiao, Q. Matrix Metalloproteinase in Abdominal Aortic Aneurysm and Aortic Dissection. *Pharmaceuticals* **12**, (2019).

255. Hadi, T. *et al.* Macrophage-derived netrin-1 promotes abdominal aortic aneurysm formation by activating MMP3 in vascular smooth muscle cells. *Nature Communications 2018 9:1* **9**, 1–16 (2018).

256. Kim, H. W. *et al.* Role of myeloperoxidase in abdominal aortic aneurysm formation: Mitigation by taurine. *Am J Physiol Heart Circ Physiol* **313**, H1168–H1179 (2017).

257. Myeloperoxidase and progression of aortic valve stenosis in patients undergoing hemodialysis. | Sigma-Aldrich. https://www.sigmaaldrich.com/DE/de/tech-docs/paper/428893.

258. Yamashita, O. *et al.* Periostin Links Mechanical Strain to Inflammation in Abdominal Aortic Aneurysm. *PLoS One* **8**, e79753 (2013).

259. Tkatchenko, T. v. *et al.* Lack of periostin leads to suppression of Notch1 signaling and calcific aortic valve disease. *Physiol Genomics* **39**, 160 (2009).

260. Golledge, J., Clancy, P., Jamrozik, K. & Norman, P. E. Obesity, adipokines, and abdominal aortic aneurysm: Health in men study. *Circulation* **116**, 2275–2279 (2007).

261. Gao, F., Si, F., Feng, S., Yi, Q. & Liu, R. Resistin Enhances Inflammatory Cytokine Production in Coronary Artery Tissues by Activating the NF-κB Signaling. *Biomed Res Int* **2016**, (2016).

262. Arabian, M. SIRT1 and resistin as therapeutic targets of resveratrol in aortic stenosis. *Clinical & Experimental Cardiology* **09**, (2018).

263. Carter, S. *et al.* Sirt1 Inhibits Resistin Expression in Aortic Stenosis. *PLoS One* **7**, 35110 (2012).

264. Samiei, N. *et al.* Modulatory Role of SIRT1 and Resistin as Therapeutic Targets in Patients with Aortic Valve Stenosis. *Arch Med Res* **50**, 333–341 (2019).

265. Kochtebane, N., Alzahrani, A. M. M. & Bartegi, A. Expression of uPA, tPA, and PAI-1 in Calcified Aortic Valves. *Biochem Res Int* **2014**, (2014).

266. DiMusto, P. D. *et al.* Increased PAI-1 in females compared with males is protective for abdominal aortic aneurysm formation in a rodent model. *Am J Physiol Heart Circ Physiol* **302**, (2012).

267. Dua, M. M. *et al.* Plasminogen Activator Inhibitor-1 Attenuates Abdominal Aortic Aneurysm in Hyperglycemic Mice. *Journal of Surgical Research* **158**, 216 (2010).

268. Qian, H. S. *et al.* Overexpression of PAI-1 prevents the development of abdominal aortic aneurysm in mice. *Gene Therapy 2008 15:3* **15**, 224–232 (2007).

269. O'Brien, K. D. *et al.* Osteopontin Is Expressed in Human Aortic Valvular Lesions. *Circulation* **92**, 2163–2168 (1995).

270. Bruemmer, D. *et al.* Angiotensin II–accelerated atherosclerosis and aneurysm formation is attenuated in osteopontin-deficient mice. *Journal of Clinical Investigation* **112**, 1318 (2003).

271. Wang, S. K. *et al.* Osteopontin may be a driver of abdominal aortic aneurysm formation. *J Vasc Surg* **68**, 22S-29S (2018).

272. Sun, J. Y. *et al.* Identification of key genes in calcific aortic valve disease via weighted gene co-expression network analysis. *BMC Med Genomics* **14**, 1–12 (2021).

273. Vorkapic, E., Kunath, A. & Wågsäter, D. Effects of osteoprotegerin/TNFRSF11B in two models of abdominal aortic aneurysms. *Mol Med Rep* **18**, 41 (2018).

274. Miyata, T. *et al.* Osteoprotegerin prevents intracranial aneurysm progression by promoting collagen biosynthesis and vascular smooth muscle cell proliferation. *J Am Heart Assoc* **9**, (2020).

275. Elevated serum osteoprotegerin is associated with decreased osteoclastic differentiation in stenotic aortic valves - PubMed. https://pubmed.ncbi.nlm.nih.gov/24930509/.

276. Dahl, J. S. *et al.* Relation of Osteoprotegerin in Severe Aortic Valve Stenosis to Postoperative Outcome and Left Ventricular Function. *American Journal of Cardiology* **112**, 1433–1438 (2013).

277. Weiss, R. M. *et al.* Osteoprotegerin Inhibits Aortic Valve Calcification and Preserves Valve Function in Hypercholesterolemic Mice. *PLoS One* **8**, e65201 (2013).

278. Lis, G. J. *et al.* Influence of osteoclasts and osteoprotegerin on the mode of calcific degeneration of aortic valves. *Pol Arch Med Wewn* **126**, 149–158 (2016).

279. Linhartova, K. *et al.* Linking soluble vascular adhesion molecule-1 level to calcific aortic stenosis in patients with coronary artery disease. *Exp Clin Cardiol* **14**, e80 (2009).

280. Aoki, T. *et al.* NF-κB is a key mediator of cerebral aneurysm formation. *Circulation* **116**, 2830–2840 (2007).

281. Fan, J. *et al.* MCP-1, ICAM-1 and VCAM-1 are present in early aneurysmal dilatation in experimental rats. *Folia Histochem Cytobiol* **48**, 455–461 (2010).

282. Shore, A. M. *et al.* Cold-Induced Changes in Gene Expression in Brown Adipose Tissue, White Adipose Tissue and Liver. *PLoS One* **8**, 1–9 (2013).

283. Okamatsu-Ogura, Y. *et al.* UCP1-dependent and UCP1-independent metabolic changes induced by acute cold exposure in brown adipose tissue of mice. *Metabolism* **113**, 154396 (2020).

284. Tan, C. Y. Y. *et al.* Brown Adipose Tissue Thermogenic Capacity Is Regulated by Elovl6. *Cell Rep* **13**, 2039–2047 (2015).

285. Xu, Z. *et al.* Cold-induced lipid dynamics and transcriptional programs in white adipose tissue. *BMC Biol* **17**, 1–21 (2019).

286. Lu, X. *et al.* The early metabolomic response of adipose tissue during acute cold exposure in mice. *Scientific Reports 2017 7:1* **7**, 1–11 (2017).

287. Korotkevich, G. *et al.* Fast gene set enrichment analysis. *bioRxiv* 060012 (2021) doi:10.1101/060012.

288. Frühbeck, G., Méndez-Giménez, L., Fernández-Formoso, J. A., Fernández, S. & Rodríguez, A. Regulation of adipocyte lipolysis. *Nutr Res Rev* **27**, 63–93 (2014).

289. M., N., YeganehAzadeh, G., T., ZahradkaPeter & T., W. Adipokines and the cardiovascular system: mechanisms mediating health and disease. *https://doi.org/10.1139/y2012-053* **90**, 1029–1059 (2012).

290. Golledge, J., Clancy, P., Jamrozik, K. & Norman, P. E. Obesity, Adipokines, and Abdominal Aortic Aneurysm. *Circulation* **116**, 2275–2279 (2007).

291. Kaltoft, M., Langsted, A. & Nordestgaard, B. G. Obesity as a Causal Risk Factor for Aortic Valve Stenosis. *J Am Coll Cardiol* **75**, 163–176 (2020).

292. Kals, J. *et al.* β2-microglobulin, a novel biomarker of peripheral arterial disease, independently predicts aortic stiffness in these patients. *http://dx.doi.org/10.3109/00365513.2011.558108* **71**, 257–263 (2011).

293. You, L. *et al.* High levels of serum β2-microglobulin predict severity of coronary artery disease. *BMC Cardiovasc Disord* **17**, 1–8 (2017).

294. CFD complement factor D [Homo sapiens (human)] - Gene - NCBI. https://www.ncbi.nlm.nih.gov/gene/1675.

295. Nishimura, S. *et al.* ENPP2 Contributes to Adipose Tissue Expansion and Insulin Resistance in Diet-Induced Obesity. *Diabetes* **63**, 4154–4164 (2014).

296. Towler, D. A. Lipoprotein(a): A Taxi for Autotaxin Takes a Toll in Calcific Aortic Valve Disease ∗. *JACC Basic Transl Sci* **2**, 241–243 (2017).

297. Harrison, O. J. *et al.* Candidate plasma biomarkers for predicting ascending aortic aneurysm in bicuspid aortic valve disease. *J Cardiothorac Surg* **13**, 1–9 (2018).

298. Hauffe, R. *et al.* GPx3 dysregulation impacts adipose tissue insulin receptor expression and sensitivity. *JCI Insight* **5**, (2020).

299. Napolioni, V. Role of Haptoglobin in Abdominal Aortic Aneurysm. *Inflammatory Response in Cardiovascular Surgery* 51–55 (2013) doi:10.1007/978-1-4471-4429-8_8.

300. Ruzevick, J., Jackson, C., Pradilla, G., Garzon-Muvdi, T. & Tamargo, R. J. Aneurysm Formation in Proinflammatory, Transgenic Haptoglobin 2-2 Mice. *Neurosurgery* **72**, 70–76 (2013).

301. Asleh, R. & Levy, A. P. In Vivo and In Vitro Studies Establishing Haptoglobin as a Major Susceptibility Gene for Diabetic Vascular Disease. *Vasc Health Risk Manag* **1**, 19 (2005).

302. Choi, C. H. *et al.* LRG1 is an adipokine that promotes insulin sensitivity and suppresses inammation. (2021) doi:10.21203/rs.3.rs-656094/v1.

303. Pang, K. T. *et al.* Leucine-Rich α-2-Glycoprotein 1 Suppresses Endothelial Cell Activation Through ADAM10-Mediated Shedding of TNF-α Receptor. *Front Cell Dev Biol* **9**, 1743 (2021).

304. van Leent, M. M. T. *et al.* Prosaposin mediates inflammation in atherosclerosis. *Sci Transl Med* **13**, (2021).

305. Ojima, K. *et al.* Proteomic analysis of secreted proteins from skeletal muscle cells during differentiation. *EuPA Open Proteom* **5**, 1–9 (2014).

306. Kraus, B. J. *et al.* Novel role for retinol-binding protein 4 in the regulation of blood pressure. *FASEB Journal* **29**, 3133–3140 (2015).

307. Steinhoff, J. S., Lass, A. & Schupp, M. Biological Functions of RBP4 and Its Relevance for Human Diseases. *Front Physiol* **12**, 294 (2021).

308. Fenzl, A. *et al.* Intact vitamin A transport is critical for cold-mediated adipose tissue browning and thermogenesis. *Mol Metab* **42**, 101088 (2020).

309. Sánchez-Solana, B., Laborda, J. & Baladrón, V. Mouse Resistin Modulates Adipogenesis and Glucose Uptake in 3T3-L1 Preadipocytes Through the ROR1 Receptor. *Molecular Endocrinology* **26**, 110 (2012).

310. Tanaka, K. *et al.* Age-Associated Aortic Stenosis in Apolipoprotein E-Deficient Mice. *J Am Coll Cardiol* (2005) doi:10.1016/j.jacc.2005.03.058.

311. Choi, B. *et al.* Dipeptidyl Peptidase-4 Induces Aortic Valve Calcification by Inhibiting Insulin-Like Growth Factor-1 Signaling in Valvular Interstitial Cells. *Circulation* **135**, 1935–1950 (2017).

312. Poudel-Bochmann, B. *et al.* Insulin-like growth factor-1 in calcified human aortic valves. *Thorac Cardiovasc Surg* **61**, SC123 (2013).

313. Rosa, M. *et al.* Leptin induces osteoblast differentiation of human valvular interstitial cells via the Akt and ERK pathways. *Acta Diabetol* **54**, 551–560 (2017).

314. Tao, M. *et al.* Locally Applied Leptin Induces Regional Aortic Wall Degeneration Preceding Aneurysm Formation in ApoE Deficient Mice. *Arterioscler Thromb Vasc Biol* **33**, 311 (2013).

315. Ben-Zvi, D. *et al.* Local Application of Leptin Antagonist Attenuates Angiotensin II–Induced Ascending Aortic Aneurysm and Cardiac Remodeling. *J Am Heart Assoc* **5**, (2016).

316. Madjene, C., Boutigny, A., Bouton, M.-C., Arocas, V. & Richard, B. Protease Nexin-1 in the Cardiovascular System: Wherefore Art Thou? *Front Cardiovasc Med* **0**, 241 (2021).

317. Lai, C.-H. *et al.* Recombinant adeno-associated virus vector carrying the thrombomodulin lectin-like domain for the treatment of abdominal aortic aneurysm. *Atherosclerosis* **262**, 62–70 (2017).

318. Kaschina, E. *et al.* Genetic kininogen deficiency contributes to aortic aneurysm formation but not to atherosclerosis. *https://doi.org/10.1152/physiolgenomics.00035.2004* **19**, 41–49 (2004).

319. Lutshumba, J. *et al.* Deletion of BMAL1 in Smooth Muscle Cells Protects Mice from Abdominal Aortic Aneurysms. *Arterioscler Thromb Vasc Biol* **38**, 1063 (2018).

320. APOE apolipoprotein E [Homo sapiens (human)] - Gene - NCBI. https://www.ncbi.nlm.nih.gov/gene?Db=gene&Cmd=ShowDetailView&TermToSearch=348.

321. Sims, G. P., Rowe, D. C., Rietdijk, S. T., Herbst, R. & Coyle, A. J. HMGB1 and RAGE in Inflammation and Cancer. *http://dx.doi.org/10.1146/annurev.immunol.021908.132603* **28**, 367–388 (2010).

322. Yang, H., Wang, H. & Andersson, U. Targeting Inflammation Driven by HMGB1. *Front Immunol* **11**, 484 (2020).

323. Kim, C. W. *et al.* Prevention of abdominal aortic aneurysm by anti-miRNA-712 or anti-miR-205 in Angiotensin II infused mice. *Arterioscler Thromb Vasc Biol* **34**, 1412 (2014).

324. O'Brien, J., Hayder, H., Zayed, Y. & Peng, C. Overview of microRNA biogenesis, mechanisms of actions, and circulation. *Front Endocrinol (Lausanne)* **9**, 402 (2018).

325. Icli, B. & Feinberg, M. W. MicroRNAs in dysfunctional adipose tissue: cardiovascular implications. *Cardiovasc Res* **113**, 1024–1034 (2017).

326. Tao, C. *et al.* Changes in white and brown adipose tissue microRNA expression in cold-induced mice. *Biochem Biophys Res Commun* **463**, 193–199 (2015).

327. Martens, M. *et al.* WikiPathways: Connecting communities. *Nucleic Acids Res* **49**, D613–D621 (2021).

328. Flemming, J. P. *et al.* miRNA- and cytokine-associated extracellular vesicles mediate squamous cell carcinomas. *J Extracell Vesicles* **9**, (2020).

329. Ricquier, D. UCP1, the mitochondrial uncoupling protein of brown adipocyte: A personal contribution and a historical perspective. *Biochimie* **134**, 3–8 (2017).

330. Nicholls, D. G., Bernson, V. S. M. & Heaton, G. M. The Identification of the Component in the Inner Membrane of Brown Adipose Tissue Mitochondria Responsible for Regulating Energy Dissipation. *Experientia Suppl* **32**, 89–93 (1978).

331. Siiteri, P. K. Adipose tissue as a source of hormones. *Am J Clin Nutr* **45**, 277–282 (1987).

332. Mohamed-Ali, V., Pinkney, J. H. & Coppack, S. W. Adipose tissue as an endocrine and paracrine organ.

333. Ailhaud, G. Adipose tissue as a secretory organ: from adipogenesis to the metabolic syndrome. *C R Biol* **329**, 570–577 (2006).

334. Fernández-Alfonso, M. S. *et al.* Role of perivascular adipose tissue in health and disease. *Compr Physiol* **8**, 23–59 (2018).

335. Ghigliotti, G. *et al.* Adipose tissue immune response: Novel triggers and consequences for chronic inflammatory conditions. *Inflammation* vol. 37 1337–1353 Preprint at https://doi.org/10.1007/s10753-014-9914-1 (2014).

336. Eckstein, H. H. & Maegdefessel, L. Linking obesity with abdominal aortic aneurysm development. *Eur Heart J* **41**, 2469–2471 (2020).

337. Lin Chang, MD, PhD1, Luis Villacorta, PhD1, Rongxia Li, PhD2, Milton Hamblin, PhD1, Wei Xu, PhD2, Chunyan Dou, MD1, Jifeng Zhang, PhD, Jiarui Wu, PhD2, Rong Zeng, PhD, and Y. Eugene Chen, MD, P. Loss of Perivascular Adipose Tissue upon PPARγ Deletion in Smooth Muscle Cells Impairs Intravascular Thermoregulation and Enhances Atherosclerosis. Preprint at (2012).

338. Ayala-Lopez, N. & Watts, S. W. New actions of an old friend: perivascular adipose tissue's adrenergic mechanisms. *Br J Pharmacol* **174**, 3454 (2017).

339. Ahmad, M. F. *et al.* Perivascular Adipocytes Store Norepinephrine by Vesicular Transport. *Arterioscler Thromb Vasc Biol* **39**, 188–199 (2019).

340. Kwok, K. H. M., Lam, K. S. L. & Xu, A. Heterogeneity of white adipose tissue: molecular basis and clinical implications. *Experimental & Molecular Medicine 2016 48:3* **48**, e215–e215 (2016).

341. Bjørndal, B., Burri, L., Staalesen, V., Skorve, J. & Berge, R. K. Different adipose depots: Their role in the development of metabolic syndrome and mitochondrial response to hypolipidemic agents. *J Obes* **2011**, (2011).

342. Castellani, J. W. & Young, A. J. Human physiological responses to cold exposure: Acute responses and acclimatization to prolonged exposure. *Auton Neurosci* **196**, 63–74 (2016).

343. Watts, S. W., Flood, E. D., Garver, H., Fink, G. D. & Roccabianca, S. A New Function for Perivascular Adipose Tissue (PVAT): Assistance of Arterial Stress Relaxation. *Scientific Reports 2020 10:1* **10**, 1–11 (2020).

344. Orlov, S. N., Gusakova, S. V., Smaglii, L. V., Koltsova, S. V. & Sidorenko, S. V. Vasoconstriction triggered by hydrogen sulfide: Evidence for Na+,K+,2Cl-cotransport and L-type Ca2+ channel-mediated pathway. *Biochem Biophys Rep* **12**, 220–227 (2017).

345. Wang, C. *et al.* Differentiation of Adipose-Derived Stem Cells into Contractile Smooth Muscle Cells Induced by Transforming Growth Factor-β1 and Bone Morphogenetic Protein-4. *https://home.liebertpub.com/tea* **16**, 1201–1213 (2010).

346. Aji, K. *et al.* Differentiation of Human Adipose Derived Stem Cells into Smooth Muscle Cells Is Modulated by CaMKII γ. *Stem Cells Int* **2016**, (2016).

347. Marra, K. G., Brayfield, C. A. & Rubin, J. P. Adipose Stem Cell Differentiation into Smooth Muscle Cells. *Methods Mol Biol* **702**, 261–268 (2011).

348. Tsuji, W., Rubin, J. P. & Marra, K. G. Adipose-derived stem cells: Implications in tissue regeneration. *World J Stem Cells* **6**, 312 (2014).

349. Rafii, S. & Lyden, D. Therapeutic stem and progenitor cell transplantation for organ vascularization and regeneration. *Nature Medicine 2003 9:6* **9**, 702–712 (2003).

350. Ingram, D. A. *et al.* Vessel wall–derived endothelial cells rapidly proliferate because they contain a complete hierarchy of endothelial progenitor cells. *Blood* **105**, 2783–2786 (2005).

351. Xie, Y., Fan, Y. & Xu, Q. Vascular Regeneration by Stem/Progenitor Cells. *Arterioscler Thromb Vasc Biol* **36**, e33–e40 (2016).

352. Luan, X. *et al.* Crystal Structure of Human RANKL Complexed with Its Decoy Receptor Osteoprotegerin. *The Journal of Immunology* **189**, 245–252 (2012).

353. Tsuda, E. *et al.* Isolation of a Novel Cytokine from Human Fibroblasts That Specifically Inhibits Osteoclastogenesis. *Biochem Biophys Res Commun* **234**, 137–142 (1997).

354. Bergmann, K. & Sypniewska, G. Diabetes as a complication of adipose tissue dysfunction. Is there a role for potential new biomarkers? *Clin Chem Lab Med* **51**, 177–185 (2013).

355. Van Kruijsdijk, R. C. M., Van Der Wall, E. & Visseren, F. L. J. Obesity and cancer: The role of dysfunctional adipose tissue. *Cancer Epidemiology Biomarkers and Prevention* vol. 18 2569–2578 Preprint at https://doi.org/10.1158/1055-9965.EPI-09-0372 (2009).

356. Ha, E. E. & Bauer, R. C. Emerging Roles for Adipose Tissue in Cardiovascular Disease. *Arteriosclerosis, thrombosis, and vascular biology* vol. 38 e137–e144 Preprint at https://doi.org/10.1161/ATVBAHA.118.311421 (2018).

357. Thanigaimani, S. & Golledge, J. Role of Adipokines and Perivascular Adipose Tissue in Abdominal Aortic Aneurysm: A Systematic Review and Meta-Analysis of Animal and Human Observational Studies. *Front Endocrinol (Lausanne)* **12**, 52 (2021).

358. Tao, M. *et al.* Locally applied leptin induces regional aortic wall degeneration preceding aneurysm formation in apolipoprotein E-deficient mice. *Arterioscler Thromb Vasc Biol* **33**, 311–320 (2013).

359. Éva Sikura, K. *et al.* Hydrogen sulfide inhibits aortic valve calcification in heart via regulating RUNX2 by NF-κB, a link between inflammation and mineralization. *Journal of Advanced Research* vol. 27 165–176 Preprint at https://doi.org/10.1016/j.jare.2020.07.005 (2021).

360. Gomez-Stallons, M. V., Wirrig-Schwendeman, E. E., Hassel, K. R., Conway, S. J. & Yutzey, K. E. Bone Morphogenetic Protein Signaling Is Required for Aortic Valve Calcification. *Arterioscler Thromb Vasc Biol* **36**, 1398–1405 (2016).

361. Li, Z. *et al.* Runx2 (Runt-Related Transcription Factor 2)-Mediated Microcalcification Is a Novel Pathological Characteristic and Potential Mediator of Abdominal Aortic Aneurysm. *Arterioscler Thromb Vasc Biol* **40**, 1352–1369 (2020).

362. Kostina, A. *et al.* Notch, BMP and WNT/β-catenin network is impaired in endothelial cells of the patients with thoracic aortic aneurysm. *Atheroscler Suppl* **35**, e6–e13 (2018).

363. Lai, C. H. *et al.* Recombinant human thrombomodulin suppresses experimental abdominal aortic aneurysms induced by calcium chloride in mice. *Ann Surg* **258**, 1103–1110 (2013).

364. Wang, B., Lin, H. qing, Li, F., Mao, Z. fan & Dong, N. guo. Aβ40 Promotes the Osteoblastic Differentiation of Aortic Valve Interstitial Cells through the RAGE Pathway. *Curr Med Sci* **40**, 931–936 (2020).

365. Sarkar, A., Prasad, K., Ziganshin, B. A. & Elefteriades, J. A. Reasons to Investigate the Soluble Receptor for Advanced Glycation End-Product (sRAGE) Pathway in Aortic Disease. *AORTA* **1**, 210–217 (2013).

366. Munjal, C. *et al.* Inhibition of MAPK-Erk pathway in vivo attenuates aortic valve disease processes in Emilin1-deficient mouse model. *Physiol Rep* **5**, (2017).

367. Ghosh, A. *et al.* The Role of Extracellular Signal-Related Kinase During Abdominal Aortic Aneurysm Formation. *J Am Coll Surg* **215**, 668 (2012).

368. Zhang, F. *et al.* Anti-receptor for advanced glycation end products therapies as novel treatment for abdominal aortic aneurysm. *Ann Surg* **250**, 416 (2009).